PRESSUREMETER DESIGN METHOD FOR SINGLE PILES SUBJECTED TO STATIC LATERAL LOAD

Volume I

A Dissertation

by

TREVOR DAVID SMITH

Submitted to the Graduate College of
Texas A&M University
in partial fulfillment of the requirement
for the degree of

DOCTOR OF PHILOSOPHY

August 1983

Major Subject: Civil Engineering

PRESSUREMETER DESIGN METHOD FOR SINGLE PILES SUBJECTED TO STATIC LATERAL LOAD

Volume I

A Dissertation

by

TREVOR DAVID SMITH

Approved as to style and content by:

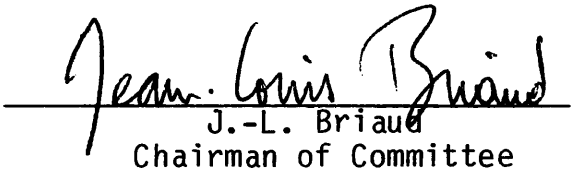

J.-L. Briaud
Chairman of Committee

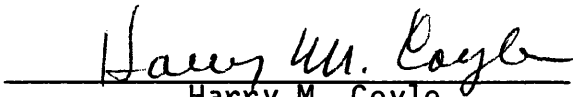

Harry M. Coyle
(Member)

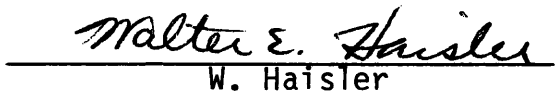

W. Haisler
(Member)

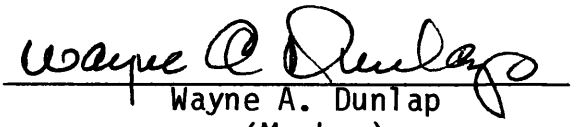

Wayne A. Dunlap
(Member)

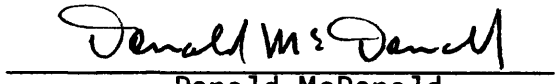

Donald McDonald
(Head of Department)

August 1983

ABSTRACT

Pressuremeter Design Method for Single Piles
Subjected to Static Lateral Load (August 1983)
Trevor David Smith,
B.Sc., University of Aston in Birmingham, England;
M.Sc., Imperial College, University of London, England
Chairman of Advisory Committee: Dr. J.-L. Briaud

A thorough review of the literature regarding design methods for lateral load behavior of foundation piles has been made. The most popular and versatile design technique is solution of the governing differential equation for the pile. The solution is obtained by the finite difference scheme using a high speed digital computer. Some dissatifaction is evident in the literature with the existing techniques available to describe the nonlinear spring representing the soil surrounding the pile which is expressed as a P-y curve. The theoretical and experimental basis for the soil P-y curves is presented, and the relationship between the lateral reaction mechanisms of pile and pressuremeter is explored in both elasticity and plasticity.

The P-y curve is shown to consist of two components: a frontal reaction, and a side shear reaction. It is shown that interpretation of a prebored pressuremeter test can measure both components. Using the theoretical stress distributions around a translating pile, a new method for the development of a lateral load P-y curve, based on plane strain, is proposed.

The reduction in mobilized soil reaction close to the free ground surface, termed the critical depth effect, is known to be of paramount importance for a laterally loaded pile. Based on interpretation of field instrumented pile test results, a new method of accounting for the pile critical depth which incorporates relative soil/pile rigidity is proposed. From a small strain finite element study of the expansion of a cylindrical cavity the critical depth effect for a pressuremeter is examined. A new approach to determine the pressuremeter critical depth is recommended.

A series of model pile and pressuremeter tests conducted under laboratory conditions confirmed the validity of the proposed P-y curve construction procedure. Two proposed tentative methods an Initial Criterion and Reload Criterion, were successfully applied to fourteen full scale laterally loaded piles at nine field sites where pressuremeter tests were conducted.

Based on the results from the tentative methods a final method is proposed to construct static lateral load P-y curves from a prebored pressuremeter test. A computer program, PYGEN, has been written to accomplish this task. Recommendations are given concerning the application of the method and pressuremeter testing procedures.

DEDICATION

To:

Elise, my wife, for all her understanding, my anchor in sanity, and Emma, my daughter, the future.

and

my Mother and Father

ACKNOWLEDGEMENTS

The financial support of the author's graduate studies at Texas A&M University, provided by the National Science Foundation under grant CME 8006727 monitored by Dr. C. A. Babendreier, and the Civil Engineering Department, is gratefully acknowledged.

Special thanks are extended to the author's Advisory Committee Chairman, Dr. Jean-Louis Briaud, for his continual guidance, patience, inspiration and friendship. Appreciation is also extended to the other members of the committee, including Dr. Harry Coyle, Dr. Wayne Dunlap, Dr. Walter Haisler and Dr. Joseph Newton.

Acknowledgement is given to Shell Development Company for the release of technical reports, to the staff of Texas A&M research annex, and to fellow, suffering, graduate students, Larry Tucker, Guy Felio and Pat Janicek for their physical and mental help.

The cooperation and advice of the staff of McClelland Engineers, including Mr. Barry Meyer, Mr. Lowell Babb and Mr. Robert Brunel, is acknowledged.

The excellent typing of Mrs. Vera Meador and Mrs. Joy Taylor is evident throughout the dissertation. Both are sincerely thanked for their perseverence and good 'humour' in converting English to American.

TABLE OF CONTENTS

Volume I

TABLE OF CONTENTS (Continued)

TABLE OF CONTENTS (Continued)

TABLE OF CONTENTS (Continued)

TABLE OF CONTENTS (Continued)

TABLE OF CONTENTS (Continued)

LIST OF TABLES

LIST OF FIGURES

LIST OF FIGURES (Continued)

LIST OF FIGURES (Continued)

LIST OF FIGURES (Continued)

LIST OF FIGURES (Continued)

LIST OF FIGURES (Continued)

LIST OF FIGURES (Continued)

LIST OF FIGURES (Continued)

LIST OF FIGURES (Continued)

LIST OF FIGURES (Continued)

LIST OF FIGURES (Continued)

INTRODUCTION

Problem Definition

Civil Engineers have for many years employed driven or bored piles as a solution to foundation problems. Frequently it is the only design available for the foundations of the rapidly growing number of offshore oil and gas production rigs. These structures are subjected to relatively high lateral loads from winds, wave action, ship collision and sea floor instability. The resultant of these forces is the application of high bending moments and shear forces at the mudline for the long slender pipe piles supporting these structures. Onshore, single short piers are increasingly being used to support power lines as reported by Vallabhan and Alikhanlou (97). These lines can run for several hundred miles across widely different soil conditions. This is one of the many examples of cases where onshore piers or piles have to resist significant lateral loads.

The prediction of the load deflection behavior of laterally loaded piles is a soil structure interaction problem. The most common and versatile technique employed to solve this problem is a finite difference formulation of the governing differential equation for an elastic beam on a "Winkler" soil model. This approach became a powerful analytical tool when it was generalized for application to high speed computes by Matlock and Reese (65).

The style and format of this dissertation follows that used by the Journal of the Geotechnical Engineering Division, American Society of Civil Engineers.

The program input requires characterization of the soil response by a set of independent, non-linear, springs described by P-y curves. P is the horizontal soil resistance in force per unit length of the pile and y is the horizontal deflection of the pile.

Many investigators including Azzouz, (5), Smith (89), amd St. John (88) have pointed out the empiricism involved in the current procedures used to obtain the soil P-y curves. This makes it difficult to extend the use of the current P-y curves to pile sizes and soil conditions different from those for which they were developed. Dissatisfaction is expressed in the literature by Bushan, Haley and Fong (24), Stevens and Audibert (93), Yegian and Wright (106), Legian and Hadley (58) and Lee and Gilbert (57), concerning the current procedures used to construct p-y curves.

Plan and Research Objectives

The purpose of this research is to develop a fundamentally and theoretically more satisfactory procedure to construct lateral load P-y curves at any depth, using preboring pressuremeter test results.

The pressuremeter is an expandable cylinder which is inserted into a tight fitting borehole and subsequently expanded. The lateral pressure required to inflate the probe and the increase in probe volume are recorded and the result is an in situ stress-strain curve in axisymmetric coordinates. A typical result is shown in Fig. 1(a). In Fig. 1(b) the idealization of a laterally loaded pile segment is shown,

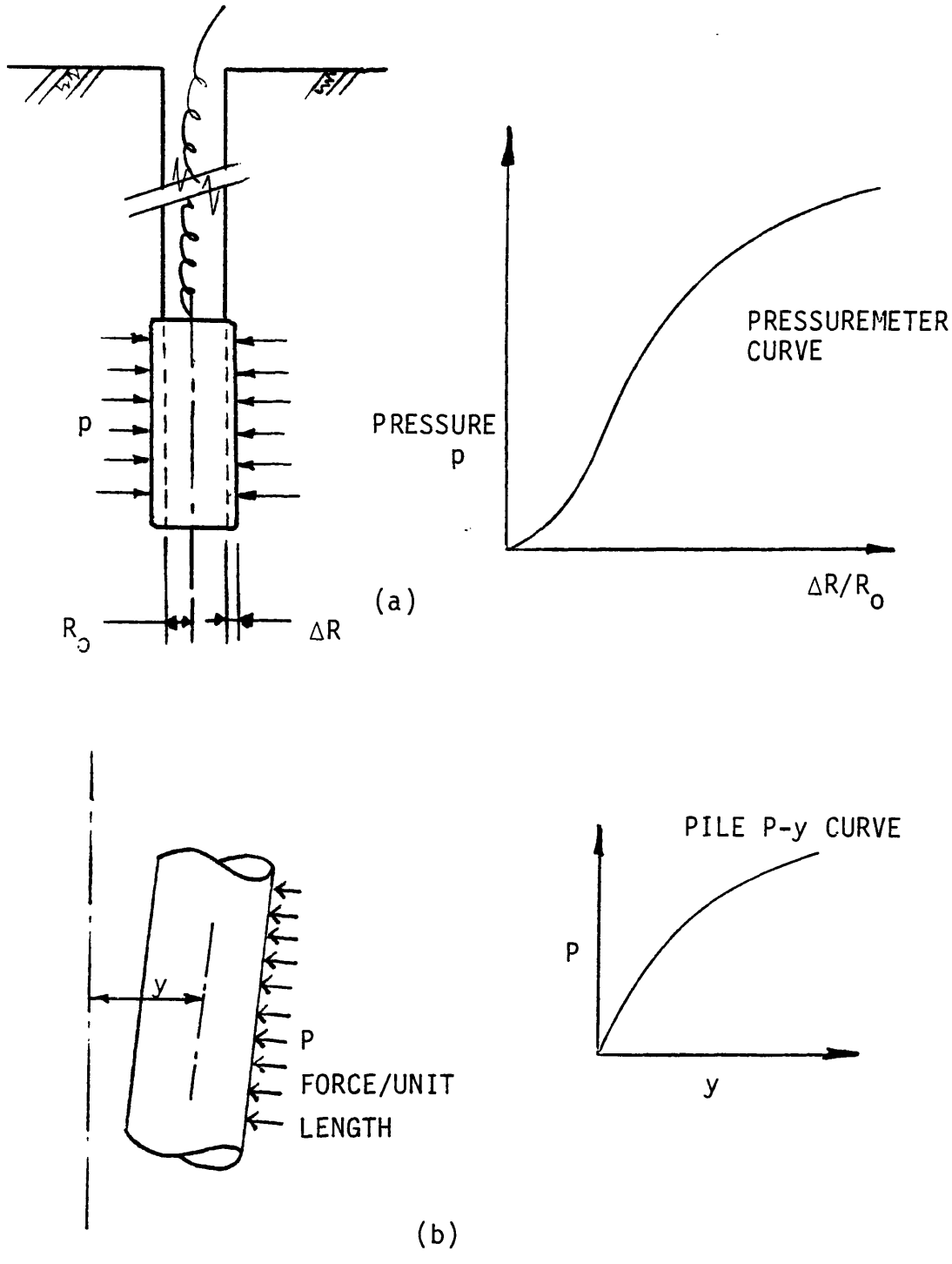

FIG. 1 - Comparison between a Typical Pressuremeter Curve and P-y Curve

together with a typical P-y curve response. The similarity between these two curves has been commented upon by Baguelin, Jezequel and Shields (11).

This research study will explore this similarity using theory, by laboratory data and field data from the results of instrumented test piles. Using theoretical considerations allied with laboratory tests, with model piles and a pressuremeter of equal size, a tentative procedure to construct P-y curves is developed. The procedure is then applied to full scale field load tests of laterally loaded piles and recommendations are made for design application.

Many researchers have been aware of the reduced soil resistance to the pile from the surface layers. The satisfactory prediction of this phenomenon has proved elusive. It is considered that the critical depth of reduced resistance is not only a function of pile diameter, but also of movement (i.e. displaced volume) and of the relative soil/pile stiffness.

BACKGROUND

Existing Design Methods

Flexible or Rigid Behavior

It is widely recognized that the behavior of a laterally loaded pile is controlled by the flexural stiffness of the shaft relative to the stiffness of the surrounding soil. In order to distinguish between these two cases, Broms (23) makes use of shaft and soil stiffness in a damping factor, β, defined as

$$\beta = \sqrt[4]{\frac{E_s}{4EI}} \quad \ldots\ldots\ldots\ldots\ldots\ldots\ldots\ldots\ldots\ldots \quad (1)$$

where: E_s = Soil Modulus (force/unit length/unit deflection),

E = Modulus of Elasticity of Pile,

I = Moment of Inertia of Pile Section

An alternate, but similar, expression is defined by Matlock and Reese (65), for constant soil modulus with depth. They define the relative stiffness as

$$R = \sqrt[4]{\frac{EI}{E_s}} \quad \ldots\ldots\ldots\ldots\ldots\ldots\ldots\ldots\ldots\ldots \quad (2)$$

Kasch, Coyle, Bartoskewitz and Sarver (49) report the comparison of the two approaches gives only 6% difference in deflection for the perfectly rigid and perfectly flexible behavior .

Fig. 2(a) and (b) shows the difference in deflected shape between

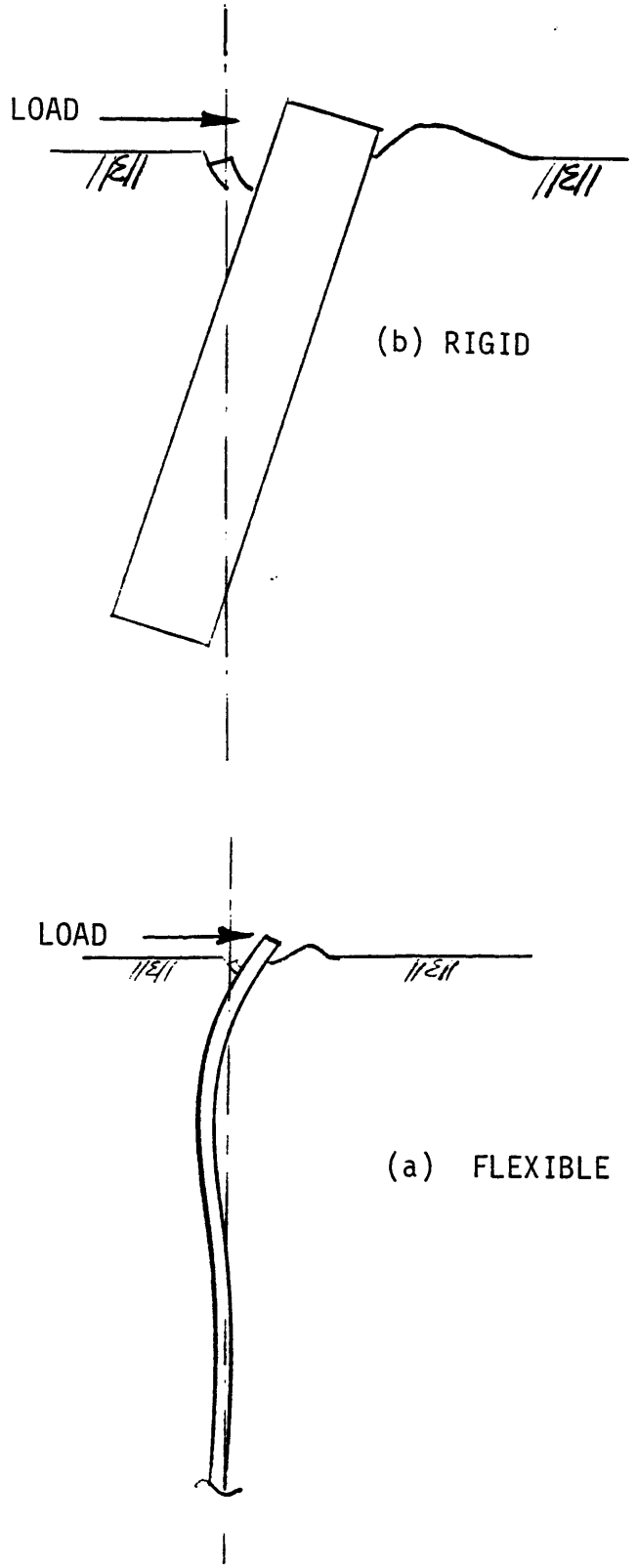

FIG. 2 - Comparison between Rigid and Flexible Behavior

flexible and a rigid pile. There is a definite difference in behavior between the two types of piles. For rigid piles the embedment length influences the pile behavior, while for flexible piles it does not. In both cases two criteria control the design: the safe load and the allowable deflection. The safe load is dictated by the ultimate resistance offered by the soil or by the ultimate bending moment that the pile can carry whereas the allowable deflection is dictated by the type of structure and its location.

Ultimate Load Approach

The majority of the early investigators developed ultimate lateral resistance approaches for rigid piles by assuming that the full passive Rankine earth pressures were mobilized. The method proposed by Hansen (38) is one of the earliest. The pile is assumed to rotate about a single point, the ultimate lateral load is calculated and the shearing force and bending moment diagrams are drawn.

Broms (21,22,23) presented methods to determine the ultimate lateral load in cohesive and cohesionless soils. For cohesive soils, Broms recommended ignoring the soil resistance for the top 1.5D, where D is the pile diameter, beyond this depth a maximum soil reaction of

$$P = 9\, C_u\, D \quad \ldots\ldots\ldots\ldots\ldots\ldots\ldots\ldots \quad (3)$$

where P = ultimate soil reaction

C_u = undrained shear strength

D = pile diameter

is used. This approach would be a conservative interpretation of what he considered to actually exist, which was 2 C_u D at the ground surface to between 8 C_u D to 12 C_u D at 3 pile diameters below ground level.

In cohesionless materials Broms makes the assumption that active pressures are mobilized very quickly at the back of the pile and can be neglected. Due to soil arching beyond one pile diameter below the ground level, Broms takes the total resistance available from beyond that depth as being

$$p = 3\ D\ \gamma' z\ K_p \quad \ldots\ldots\ldots\ldots\ldots\ldots\ldots\ldots\ldots\ldots (4)$$

where γ' = effective unit weight

K_p = Rankine passive earth pressure coefficient

z = depth below ground level

Kasch et al. (49) state that using Rankine's passive states will result in a very conservative solution. In reality they suggest the tilting of a cylindrical pile is resisted in part by friction along two planes tangential to the pile sides and parallel to the tilting plane. This failure mechanism is taken by Rowe (87), based on the earlier work of Terzaghi (95) and his treatment of anchor plates. In Terzaghi's work an attempt was made to rationalize the resistance by using a variable passive coefficient, K_{pm}, which is a function of the mobilized angle of shearing resistance, ϕ_m.

Load Deflection Approach

The methods available to predict lateral load deflection behavior fall into three broad categories.

The first category, Poulos (78) and Spillers and Stoll (91) consider the soil to be an ideal, elastic, homogeneous isotropic mass, having constant elastic parameters,Young's Modulus of Elasticity, E, and Poisson's ratio, ν. The work by Douglas and Davies (29) formed the earliest application of elasticity to lateral load/lateral movement problems. Their work concentrated on the movement of buried anchor plates and was based on Mindlin's (70) equations, In elasticity, continuity of the supporting material is fully maintained but only linear soil behavior is modeled. This model is most applicable to small lateral loads in overconsolidated clays. Furthermore, as Sogge (90) comments, if the pile is considered to be a thin rectangular vertical strip the horizontal shear stresses between the soil and the side of the pile are neglected.

Further extensions of this approach have been made in recent years by Banerjee and Davies (12) using a boundary element formulation. They produced an approximate elastic solution for working loads in a soil of linear increasing modulus with depth, approximating the case of normally consolidated clays and sands.

The second category is the characterization of the soil as a "Winkler" model of independent springs supporting an elastic continuous pile. This beam on elastic foundation approximation is often termed the "subgrade reaction method". The governing differential equation, Hetenyi (40), is

$$EI\frac{d^4y}{dz^4} + Q\frac{d^2y}{dz^2} - P = 0 \quad \ldots\ldots\ldots\ldots\ldots\ldots\ldots\ldots (5)$$

where E = Youngs modulus for the pile

I = Moment of inertia of section

Q = Axial load

y = Lateral deflection

z = Depth down the pile

P = Soil reaction

The solution of this equation allows calculation of bending moments, shearing forces, soil reactions and the deformed shape of the pile over its full depth at any load.

The generalized solutions produced by Matlock and Reese (65) are the first satisfactory treatment of the soil springs nonlinear force-deformation characterization. They further improved the understanding of the relationship between elastic pile and rigid pile theory.

Neglecting the generally small effects of the axial load, Eq. 5 can be solved in closed form for the case of constant soil modulus with depth. Using the notation from Eq. 5 , the soil modulus is defined as

$$E_s = \frac{-P}{y} \quad \ldots\ldots\ldots\ldots\ldots\ldots\ldots\ldots\ldots\ldots\ldots (6)$$

The negative sign indicates that the direction of the soil reaction is

opposite to the pile deflection.

McClelland and Focht (71) had recognized that E_s increases with depth and decreases with increased deflection. They further proposed a method of obtaining the nonlinear relationship between P and y from conventional laboratory triaxial tests.

The finite difference approximation to Eq. 5 , Reese and Desai (85), is the most practical and versatile solution scheme to design flexible laterally loaded piles. The computer program used, COM622, is documented by Reese (81). Violation of assumptions and increasing numerical error require that only piles with length to diameter ratios exceeding 6, Johnson, Sherman and Al-Hussaini (48), be designed by this technique.

A revised formulation employing four nonlinear spring models per pile node is available for rigid piles, DiGioia, Davidson and Donovan (28). Vallabhan and Alikhanlou (97) use two nonlinear springs per node and add additional springs for the base resistance, which, they show, is significant in short rigid piles.

In all subgrade reaction approaches the description of the soil resistance, variation of soil modulus, or nonlinear spring force-deformation response, must be available.

The third category employs the finite element method and makes use of the increased efficiency from high speed computers. The idealization of a laterally loaded pile in three dimensions,with pile and soil modeled as continua , presents a formidable formulation problem. The pioneering work of Desai and Appel (27) began the effort towards a working practical program, particularly for the interface elements

which allow relative slippage.

Kuhlemeyer (54) and Sogge (90) both used a finite element discretization of the pile with a subgrade reaction approach for the soil model. Kuhlemeyer claims, for the case of lateral translation, that the pile head response can be completely described in terms of functions of the ratio E_p/E_s, where E_p is the modulus of the pile and E_s is soil modulus.

Nordal, Grande and Janbu (72) employ a similar approach but the soil reaction is based on an effective stress approach combining stress and strain fields around the pile.

Existing Pressuremeter Design Methods

The similarity between the lateral resistance mobilized around a pile and that mobilized around the expanding pressuremeter has been noted by Baguelin et al. (11). Audibert and Nyman (4) further suggested, based on the work of Baguelin, that for cohesive soils the Menard method of using a soil modulus determined from pressuremeter tests is to be preferred to the Matlock method of using a modulus from undrained triaxial tests.

The beneficial use of in situ testing to offshore geotechnical engineering is recognized by many investigators, Smith (89), St. John (88) Johnson et al. (48), etc. For example, King, van Hoodydonk, Kolk and Windle (51) developed a crude pressuremeter with the specific purpose of obtaining P-y data at depth where samples of loose calcareous sediment could not be obtained. They further substantiated the

comments of Audibert and Nyman (4) "....conventional laboratory strength tests were again found to be an unreliable method of predicting pile load capacity...".

Menard, Bourdon and Gambin (68) pioneered the direct application of pressuremeter results to the design of laterally loaded piles. Gambin (36) summarized the comprehensive techniques which had been developed throughout the 1960's by Menard and his co-workers. The appropriate method for a given case is selected after comparing the pile embedded length, H, with the elastic length, l_o, given by

$$l_o = \sqrt[4]{\frac{4EI}{k_s(D)D}} \quad \ldots\ldots\ldots\ldots\ldots\ldots \quad (7)$$

where k_s (D) = Modulus of subgrade reaction.

For a homogeneous soil and for long piles (H/D > 10) the modulus of subgrade reaction is related to the pressuremeter modulus, E_m, by the following equations

$\underline{R > R_o}$

$$\frac{1}{k_s} = \frac{1.33R_o}{3\,E_m}\left(\frac{R}{R_o} \times 2.65\right)^{\alpha} + \frac{\alpha R}{3E_m} \quad \ldots\ldots\ldots \quad (8)$$

$\underline{R < R_o}$

$$\frac{1}{k_s} = R\left[\left(\frac{1.33}{3\,E_m} \times 2.65^{\alpha}\right) + \frac{\alpha}{3E_m}\right] \quad \ldots\ldots\ldots\ldots \quad (9)$$

where E_m = Pressuremeter modulus assuming linear elasticity and Poisson's ratio of 0.33

R_o = reference length of 0.30 m

R = radius of the pile

α = soil structure factor, ranging from 0 to 1.

The soil structure factor is a function of the soil type and the ratio E_m/P_L, where P_L is the limit pressure. Generally the stiffer and more cohesive the material is, the higher α becomes in the range of 0 to 1. Definitions are then made for the categories of infinitely rigid, relatively rigid, semi-flexible and flexible behavior. For the fully flexible condition the pile is considered infinitely long. Closed form solutions are available, expressed as trigonometrical functions, for a soil not stressed beyond its plasticity threshold.

For heavily loaded piles stressed beyond their pseudo-elastic range and embedded in variable soils, recommendations for constructing the appropriate P -y curves are given. This bi-linear elastic plastic model is shown in Figure 3(a). This curve, first proposed by Gambin (35), was simplified by Bourdon (16) to a single linear elastic plastic response shown in Figure 3(b).

Imai (43) proposed a procedure based on Chang's equation for an elastic pile (26) and using a modulus of subgrade reaction a function of the pile displacement.

Chang's equation for uniform soil as applied by Imai is as follows

$$H = \frac{12\ EI\ \beta^3 y}{(4-3f)(1+\beta h)^3+2} \quad \ldots\ldots\ldots\ldots\ldots\ldots\ldots\ldots\ldots\ldots\ (10)$$

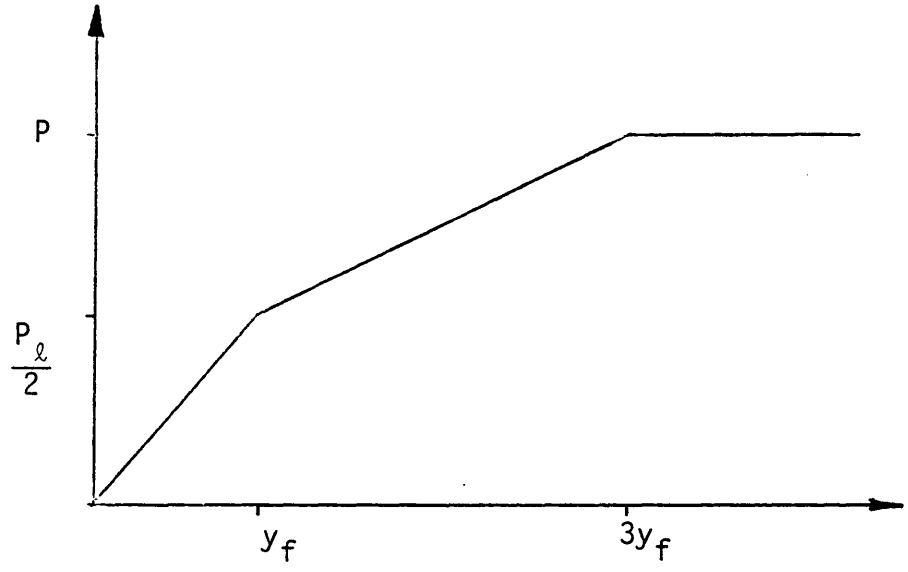

(a)

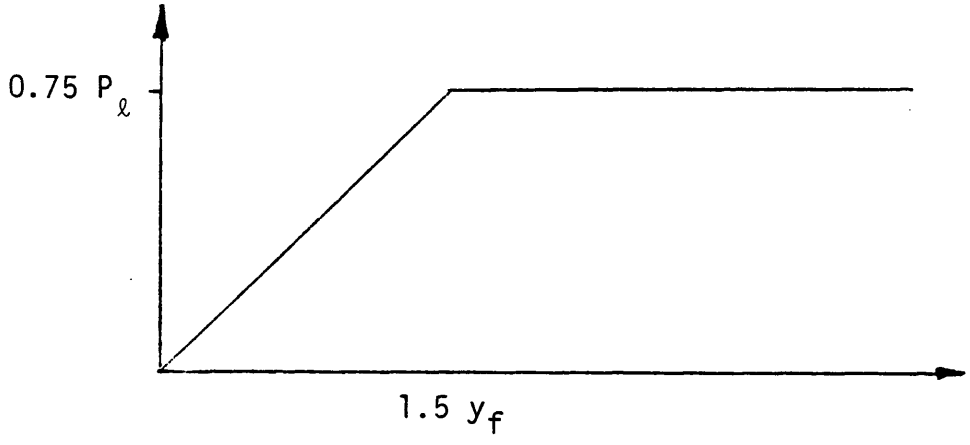

(b)

NOTE: P = pxD [after Gambin (35)]

FIG. 3 - Existing Recommendations for Pressure versus Displacement Curves from the Pressuremeter

$$\beta = \sqrt[4]{\frac{KD}{4EI}} \quad \ldots\ldots\ldots\ldots\ldots\ldots\ldots\ldots \quad (11)$$

where: H = horizontal force applied to pile

y = horizontal displacement at point of load application

f = constant representing degree of pile head fixity

(0 for free head,1 for head fully fixed)

h = height from ground surface to point of force application

K = design subgrade modulus value

Imai recognized that the load deflection behavior at the head of the pile is clearly nonlinear due to nonlinear soil resistance and changes in soil modulus with depth. Therefore, based on the results of full scale load tests, a semi-empirical procedure obtains an equivalent modulus, constant with depth, which includes nonlinearity by being a function of the pile head deflection The difference in the mechanism between pile and pressuremeter is taken into account by a factor of $\pi/2$.

Frydman, Sha'al and Mazurik (33) directly applied the expansion of the pressuremeter curve as a measured P-y curve. The assumption is made that the same pressure is applied to the soil from both pressuremeter and pile at equal circumferential strains. It then follows from Fig. 4

$$\frac{y_{pile}}{R_{pile}} = \frac{y_{pmt}}{R_{pmt}} \quad \ldots\ldots\ldots\ldots\ldots\ldots\ldots\ldots \quad (12)$$

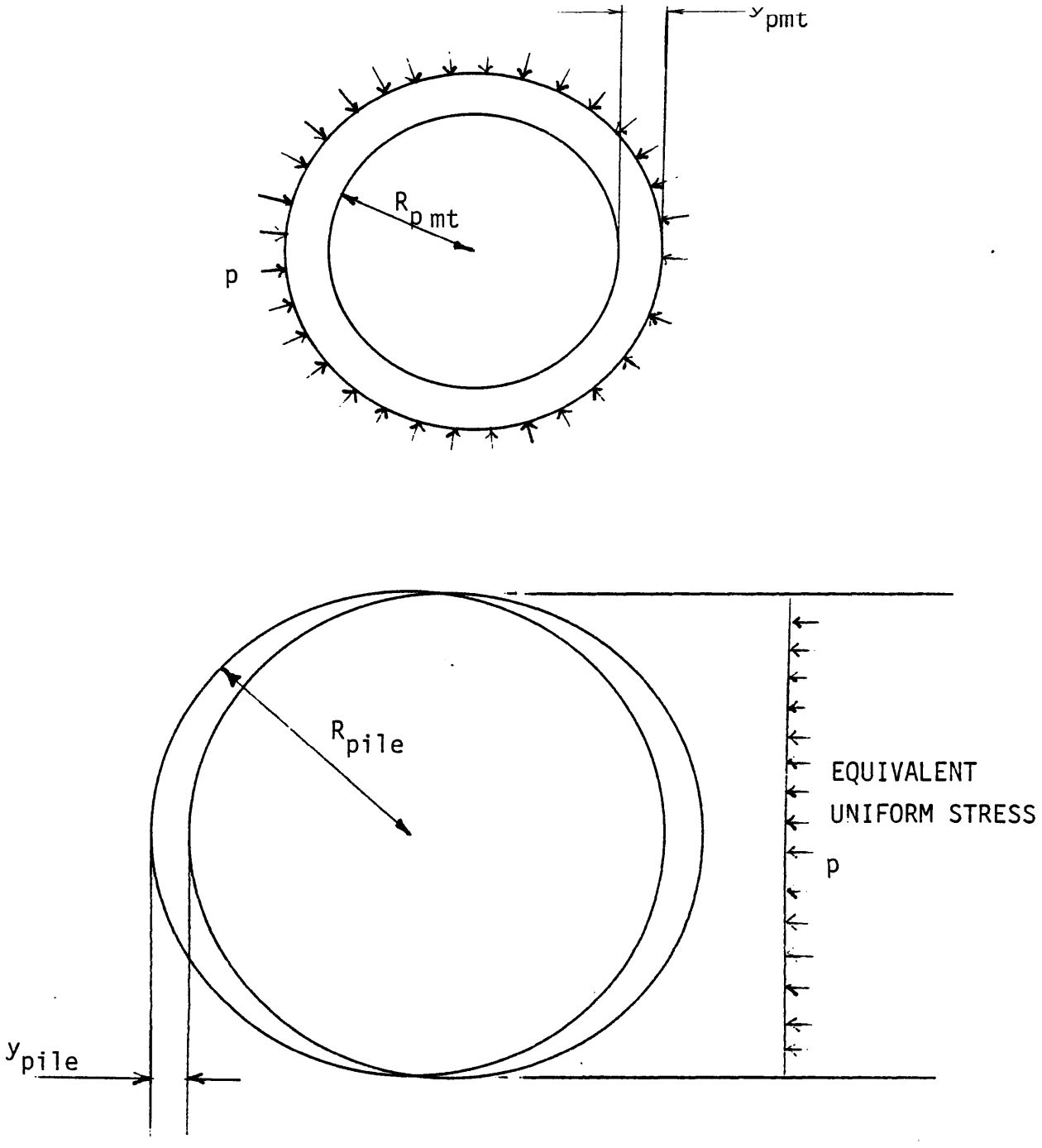

FIG. 4 - Radial Movements for the Pile and Pressuremeter

where y_{pmt} = increase in radius of the pressuremeter

R_{pmt} = initial radius of the pressuremeter.

Excellent agreement was obtained between measured and calculated deflections for a driven, square, precast concrete pile at a single working load.

Baguelin (11) proposed using the entire curve from a selfboring pressuremeter, up to the pressure corresponding to 20% volumetric strain. At this strain level only plastic behavior is considered. No recommendations were made for critical depth and no case histories were presented.

Comparisons between both the prebored and selfboring type of pressuremeters, and their corresponding P-y curves, were made by Hughes, Goldsmith and Fendall (42). In the procedure developed, at equal circumferential strains, the following relationship is suggested

$$P = 2p\ D \quad \ldots\ldots\ldots\ldots\ldots\ldots\ldots\ldots\ldots\ldots \quad (13)$$

where p = pressuremeter pressure

D = pile diameter

The factor of 2 is considered appropriate since the limiting pressure at which infinite expansion occurs for the pressuremeter test is approximately 5 times the cohesion, whereas, the limiting soil resistance to pushing a pile sideways is approximately 9 times the cohesion. In general, for the single load presented, the selfboring pressuremeter

gave a more appropriate modulus when compared to the prebored pressuremeter. Of interest is the investigation carried out to match the insertion disturbance for the pile with the pressuremeter by modifying the cutting shoe.

Dunand (30) employs the elastic plastic model for a front reaction pressure applied to the projected area and contests the existence of any side shear. The modulus of subgrade reaction is obtained from the pressuremeter modulus and elasticity theory. The plastic limit is obtained directly from the pressuremeter limit pressure.

DiGioia, Davidson and Donovan (28) correlate the spring responses to pressuremeter modulus for application to rigid piers. The front and shear resistance springs are parabolic in nature and the remainder are elastic-plastic. Georgiadis and Butterfield (37) constructed P-y curves from horizontal plate loading tests and attempted to incorporate shear coupling between the soil "springs". Marsland and Randolph (62) successfully correlated plate tests and pressuremeter tests in London clay.

THE P-y CURVE

The Theoretical and Experimental Basis

The P-y curve has previously been introduced as the nonlinear response of the soil surrounding a laterally loaded pile. From Fig. 5 it can be seen that P represents the load per unit depth, at a certain pile deflection y. It is therefore the total load resolved in the horizontal direction from the generated stress distribution.

From Fig.5 , and recalling Eq. 6, the secant modulus is

$$E_s = \frac{-P}{y} \quad \ldots\ldots\ldots\ldots\ldots\ldots\ldots\ldots \quad (6)$$

and is termed the Soil Modulus. The generated resistance to lateral movement from piles, retaining walls and anchor plates can also be expressed in terms of unit width.

$$k_s = \frac{P/D}{y} = \frac{p}{y} = \frac{E_s}{D} \quad \ldots\ldots\ldots\ldots\ldots\ldots \quad (14)$$

where p = uniform equivalent soil pressure

k_s = modulus of subgrade reaction

which has units of force per unit volume. It is often assumed that the modulus of subgrade reaction is inversely proportional to the width of the loaded area. Terzaghi (95) proposed for stiff clays

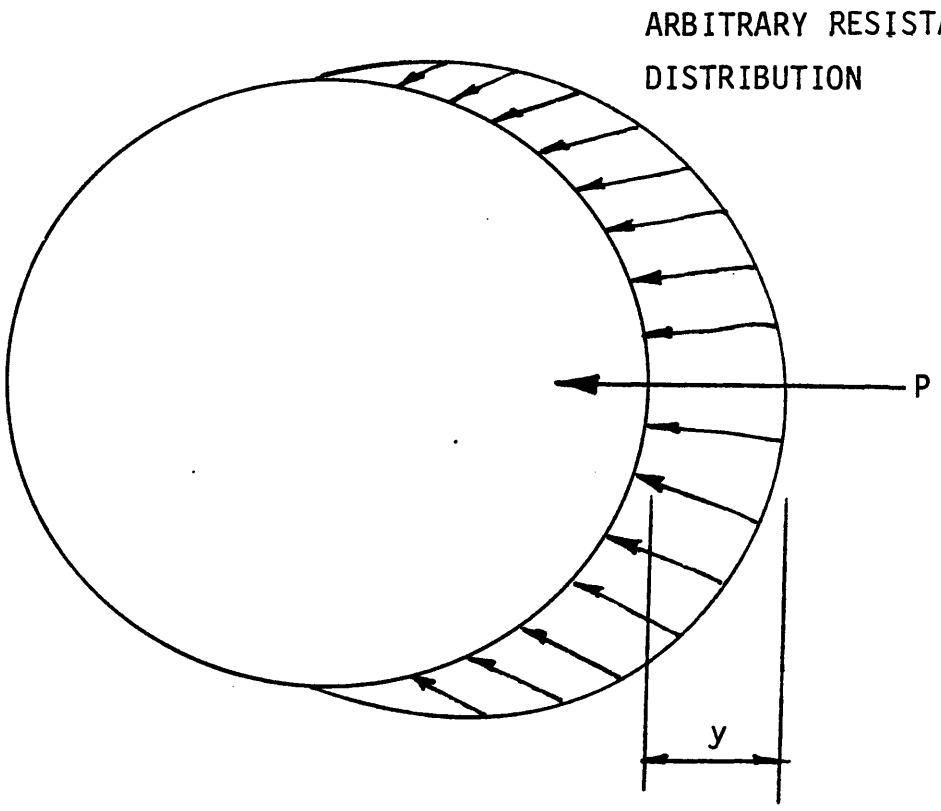

FIG. 5 - Net Resistance Distribution
Set Up Around Pile Circumference

$$k_s = \frac{k_{sq} \times 1}{1.5 \times D} \quad \ldots\ldots\ldots\ldots\ldots\ldots\ldots\ldots \quad (15)$$

where k_{sq} is the coefficient of subgrade reaction for a 1 ft (0.3m) square plate. The 1 in the numerator of Eq. 15 has units of feet. By combining Eqs. 14 and 15 and substituting for k_s it can be seen that

$$E_s = \frac{1}{1.5} k_{sq} \quad \ldots\ldots\ldots\ldots\ldots\ldots\ldots\ldots \quad (16)$$

and is therefore independent of pile width.

Yoshider and Yoshenka (107) performed a series of lateral plate load tests on sandy and clayey soils. With plate diameters ranging from 1.0 to 5.0 ft (0.3 to 1.5 m), for the same unit pressure on the plate, the penetration into the soil was proportional to the plate diameter raised to the 3/4 power.

Then for a circular plate

$$P = \frac{p\pi D^2}{4} \quad \ldots\ldots\ldots\ldots\ldots\ldots\ldots\ldots \quad (17)$$

and $$E_s = \frac{P}{y} = \frac{p\pi D^2}{4y(D^{3/4})} \quad \ldots\ldots\ldots\ldots\ldots\ldots\ldots \quad (18)$$

which indicates that for a circular plate the horizontal soil modulus is a function of diameter. Kubo (52) conducted 59 model pile tests in

sand with both fixed head and free head restraint conditions. The pile section was either rectangular or circular, and diameters (or width) ranged from 0.7 to 12 in. (17.5 to 300 mm.). The assumed relationship between soil pressure, p, and the lateral deflection was of the form

$$p = k\, x^m\, y^n \quad \ldots\ldots\ldots\ldots\ldots\ldots\ldots\ldots\ldots\ldots \quad (19)$$

where k = soil reaction coefficient

x = distance down the pile

y = lateral deflection

From the tests it was determined that the value of m would be unity and n would be 1/2. Of interest is the effect of pile diameter on the soil reaction coefficient, k. It was found that beyond pile diameters of 6 in. (150mm) the soil reaction coefficient is independent of pile diameter. Since,

$$E_s = \frac{P}{y} = \frac{pD}{y} \quad \ldots\ldots\ldots\ldots\ldots\ldots\ldots\ldots\ldots\ldots \quad (20)$$

then, substituting for p from Eq. 19, we have

$$E_s = \frac{kxy^{\frac{1}{2}}D}{y} = \frac{kxD}{y^{\frac{1}{2}}} \quad \ldots\ldots\ldots\ldots\ldots\ldots\ldots\ldots\ldots\ldots \quad (21)$$

which shows the soil modulus, E_s, to be a linear function of pile diameter and inversely proportional to the square root of deflection.

Combining Eq. 14 and Eq. 21 gives

$$k_s = \frac{E_s}{D} = \frac{kx}{y^{\frac{1}{2}}} \quad \ldots\ldots\ldots\ldots\ldots\ldots\ldots \quad (22)$$

and the modulus of subgrade reaction is therefore independent of pile diameter.

It has previously been indicated that the soil modulus, E_s, defined as the secant modulus of the P-y curve, is a function of pile diameter, lateral deflection and depth below the ground surface. Reese and Cox (81) pointed out that the soil modulus is not a property of the soil but is a fitting function to correlate the pile behavior with the soil properties as reflected by the P-y curves. They further used a graphical argument, shown in Fig. 6, to propose the following relationship for all soils

$$E_s = kx^n \quad \ldots\ldots\ldots\ldots\ldots\ldots\ldots \quad (23)$$

in which the exponent, n, would be less then 3. Fig. 6 shows a series of P-y curves with the P ordinate increasing with depth. Also shown is a dashed line which indicates the possible shape of a laterally loaded pile under load. The resulting soil moduli values are plotted on the right hand side of Fig. 6.

The previous argument can be used to develop the P-y curves from lateral load tests where only head deflection and rotation are measured under the applied loads. By assuming the variation of soil modulus

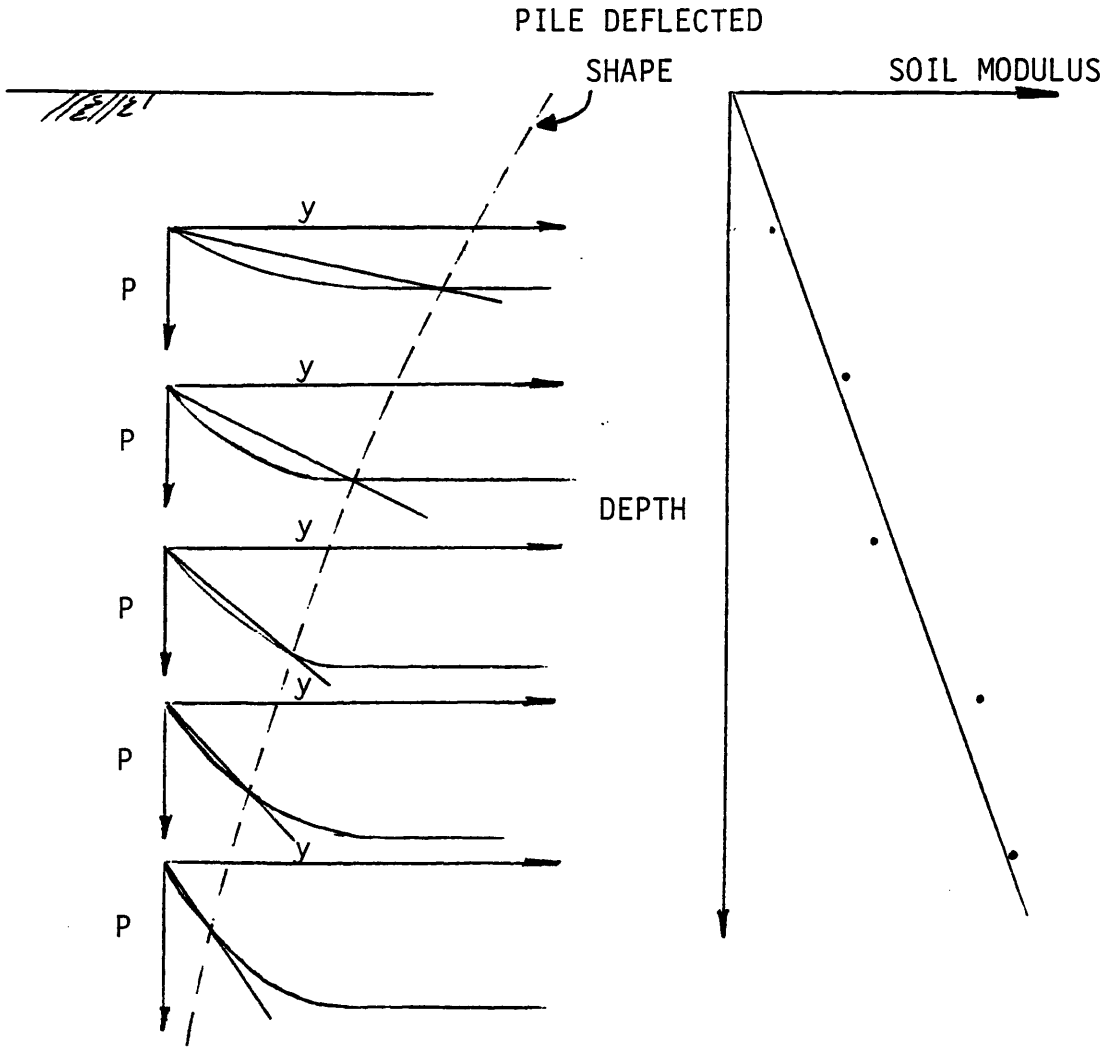

[after Reese and Cox (81)]

FIG. 6 - Graphical Argument to Substantiate the Variation of Soil Modulus with Depth

with depth and applying successive applications of a nondimensional solution (65) the governing P-y relationship can be constructed.

A more direct approach is to instrument a pile for a field load test with strain gages to measure bending strains. From the structural and material pile properties the distribution of bending moment, M, with depth is obtained. This technique was successfully applied to develop the current state of the art criteria for the construction of P-y curves (64,83,84,86,99). Using appropriate boundary conditions, P and y may be obtained at points along the pile by solving the following equations numerically

$$y = \iint \frac{M}{EI} dx \quad \ldots\ldots\ldots\ldots\ldots\ldots\ldots\ldots\ldots\ldots \quad (24)$$

$$P = \frac{d^2M}{dx^2} \quad \ldots\ldots\ldots\ldots\ldots\ldots\ldots\ldots\ldots\ldots\ldots \quad (25)$$

This technique yields the closest approximation to 'measured' field P-y curves, but P is sensitive to the double differentiation process. The shape of the resulting curve is semi-empirically correlated to measured soil properties and the strain, ε_{50}, corresponding to half of the maximum deviator stress in an undrained test.

The theoretical ultimate lateral resistance is calculated for the shallow surface layers from a failing wedge theory and for the plane

strain condition below the surface layers from a theory describing the flow of soil around the pile. By equating 'measured' and theoretical lateral resistance, an empirical adjustment factor is recommended.

Application in the Finite Difference Method

Since the soil P-y response is highly nonlinear and variable with depth an approximation to Eq.5,by the finite difference technique,is forced to iterate to an acceptable solution. This operation has been incorporated into a design oriented computer program, title COM622, by Reese (81) specifically for laterally loaded piles. The finite difference model is developed by dividing the pile into N equally spaced nodes. Writing Eq. 5 in finite difference form for a typical node, m, shown on Fig. 7, gives the following

$$y_{m-2}\,(R_{m-1}) + y_{m-1}(2R_{m-1} - 2R_m + P_x h^2) +$$

$$y_m(R_{m-1} + 4R_m + R_{m-1} - 2P_x h^2 + E_{sm} h4) +$$

$$y_{m+1}(-2R_m - 2R_{m+1} + P_x h^2) + y_{m+2}(R_{m+1}) = 0 \quad \ldots\ldots \quad (26)$$

where R_m = EI (pile flexural stiffness) at node m

h = distance between nodes

P_x = axial load

E_{sm} = soil modulus at node m.

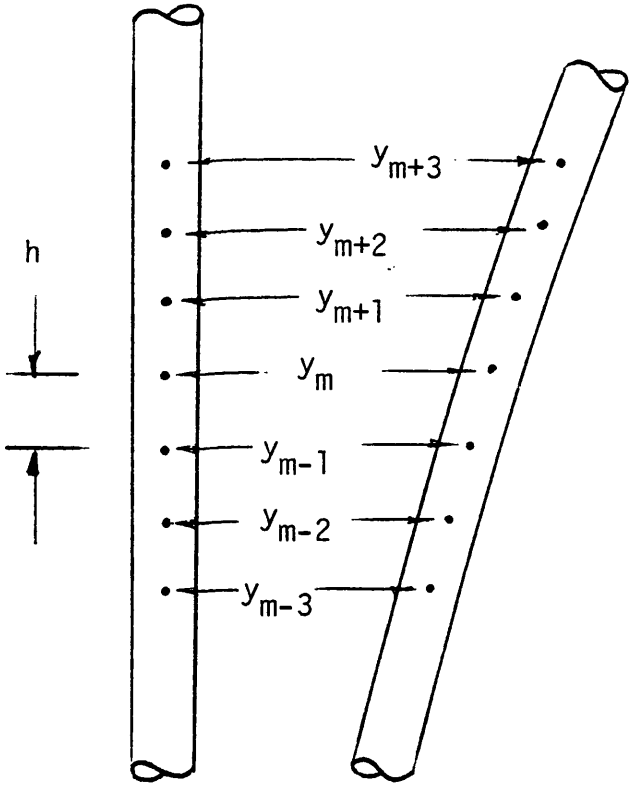

FIG. 7 - Representation of the Pile by Discrete Nodes

This gives N Equations with N+4 unknowns;the solution proceeds by writing the boundary conditions for the 4 imaginary nodes at the top and bottom of the pile.

Clearly the response of each soil spring, expressed in P-y form, is independent of the response of all remaining springs. This represents the most serious limiting assumption for all the methods of subgrade reaction.

The Theoretical Relationship to the Pressuremeter

Introduction

It is usual to express the material properties of an elastic isotropic continuum as the Young's Modulus, E, and Poisson's ratio, ν. However the pressuremeter test is an axisymetric shear test which, if analyzed according to the theory of linear elasticity, measures directly the shear modulus, G.

From linear elasticity

$$E = 2(1 + \nu)\, G \quad \ldots\ldots\ldots\ldots\ldots\ldots\ldots \quad (27)$$

and hence to determine the Young's modulus, E, from the shear modulus, G, requires knowledge, or an assumption, regarding the Poisson's ratio, ν.

The appropriate Poisson's ratio during a test is unknown and is conventionally taken as 0.33. For a no volume change material,

(i.e. undrained saturated clay) the Poisson's ratio would approach 0.5. The Young's modulus is a function of Poisson's ratio and the changes in Poisson's ratio have been shown to significantly affect lateral load deflection behavior (29). In all the subsequent discussion the material is characterized by shear modulus, G, and Poisson ratio, ν.

The relationship between the soil modulus, E_s, and the modulus of subgrade reaction, k_s, given in Eq. 14 can be rearranged as follows

$$E_s = k_s D \quad \ldots\ldots\ldots\ldots\ldots\ldots\ldots\ldots \quad (28)$$

which assumes k_s to be constant over the projected diameter, or width, of the pile.

Elasticity

Consider the element of soil adjacent to an expanding pressuremeter and a moving pile of the same radius, R, in Fig. 8(a-d). The cavity is of infinite length and the soil is weightless, isotropic, elastic and homogeneous and movement is radial only in plane strain conditions. For the pressuremeter the radial and circumferential stresses are principle stresses by reason of symmetry and it follows

$$\sigma_r = -\sigma_\theta \quad \ldots\ldots\ldots\ldots\ldots\ldots\ldots\ldots \quad (29)$$

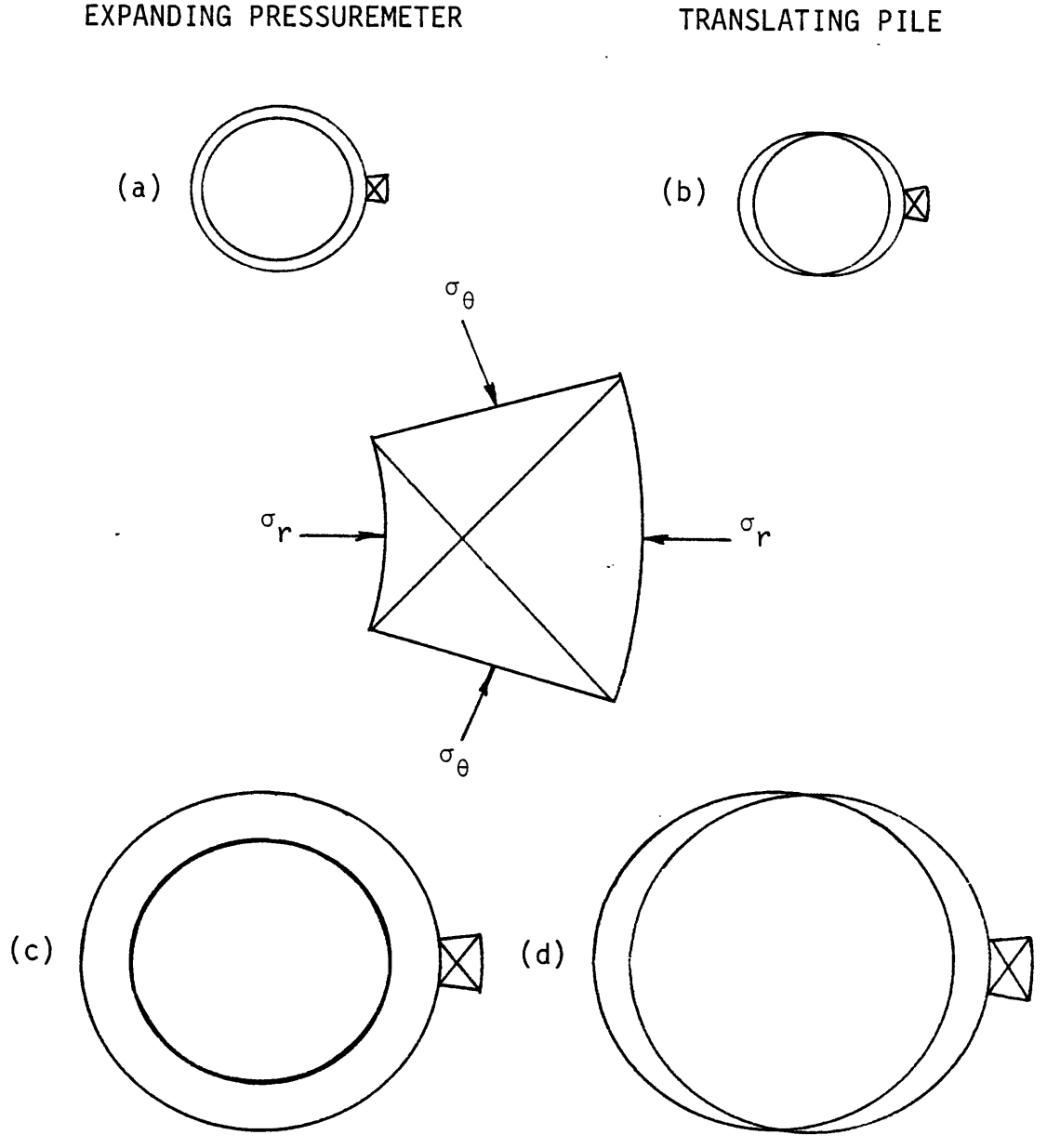

FIG. 8 - Comparison at the Element Level between Pile and Pressuremeter

The corresponding strains at the cavity wall are determined from the displacement field and are shown, (11), for small strain to be

$$\varepsilon_\theta = \frac{y_o}{R_o} \quad \ldots\ldots\ldots\ldots\ldots\ldots\ldots\ldots\ldots\ldots \quad (30)$$

$$\varepsilon_r = \frac{dy_o}{dR_o} \quad \ldots\ldots\ldots\ldots\ldots\ldots\ldots\ldots\ldots\ldots \quad (31)$$

where ε_θ = circumferential strain

ε_r = radial strain

R_o = initial radius

y_o = increase in radius.

Further, in plane strain, for the case of no volume change it follows

$$\varepsilon_\theta = -\varepsilon_r \quad \ldots\ldots\ldots\ldots\ldots\ldots\ldots\ldots\ldots\ldots \quad (32)$$

It can also be shown in linear elasticity that the relationship between the pressure on the cavity wall, p, and the strain is

$$p = p_o + 2G \frac{y_o}{R_o} \quad \ldots\ldots\ldots\ldots\ldots\ldots\ldots\ldots\ldots\ldots \quad (33)$$

where p_o is the initial pressure in the cavity at radius R_o. Hence a modulus of pressuremeter resistance, k_{pmt}, may be defined as

$$k_{pmt} = \frac{p}{y_o/R_o} = \frac{pR_o}{y_o} = 2G \quad \ldots\ldots\ldots\ldots\ldots\ldots\ldots \quad (34)$$

The maximum shear stress occurs at the borehole edge and is equal to the net pressure change.

If the simple assumption is made that the normal pressure mobilized across the projected width of a pile, Fig. 8d, is constant and equal to the pressure generated from the pressuremeter at the same circumferential strain then the following is obtained

$$E_s = \frac{p}{y_1} = \frac{2pR_1}{y_1} \quad \ldots\ldots\ldots\ldots\ldots\ldots\ldots \quad (35)$$

But $$\frac{y_o}{R_o} = \frac{y_1}{R_1} \quad \ldots\ldots\ldots\ldots\ldots\ldots\ldots\ldots \quad (36)$$

at equal pressures, p,

where R_1 = pile radius

y_1 = pile horizontal displacement

Then, rearranging Eq. 36 and substituting for $\frac{R_1}{y_1}$ in Eq. 35 gives

$$E_s = \frac{2pR_o}{y_o} = 2\ k_{pmt} \quad \ldots\ldots\ldots\ldots\ldots\ldots \quad (37)$$

which shows the pile spring soil modulus, E_s, to be twice the modulus of pressuremeter resistance, k_{pmt}, and independent of the pile width.

Combining Eqs. 34 and 37 gives

$$E_s = 4\ G \quad \ldots\ldots\ldots\ldots\ldots\ldots\ldots\ldots \quad (38)$$

The stress and displacement fields around a laterally moving infinitely long cylinder, in plane strain, have been presented by Baguelin et al. (8). The model used is a disc having a fixed outside radius of R, representing the soil, with a rigid section fixed at its center, radius r_o, representing the cross section of the pile, Fig. 9a. Perfect pile to soil adhesion is assumed and a load per unit depth, T, is applied to the pile causing uniform translation. In polar co-ordinates the stress distribution around the pile circumference is described by the following analytical expressions in the case where $R > 10r_o$.

$$\sigma_r = \frac{T}{2\pi r_o} \cos \theta \quad \ldots\ldots\ldots\ldots\ldots\ldots\ldots\ldots \quad (39)$$

$$\sigma_\theta = \frac{-T}{2\pi r_o} \cos \theta \quad \ldots\ldots\ldots\ldots\ldots\ldots\ldots\ldots \quad (40)$$

$$\tau_{r\theta} = \frac{-T}{2\pi r_o} \sin \theta \quad \ldots\ldots\ldots\ldots\ldots\ldots\ldots\ldots \quad (41)$$

to a first order approximation. The distributions of the components of the radial force, f_r, and the tangential force f_θ, are shown in Fig. 9b. The total horizontal reaction is uniformly distributed around the circumference. From Eq. 39 and Eq. 40 it can be seen that

$$\sigma_r = - \sigma_\theta \quad \ldots\ldots\ldots\ldots\ldots\ldots\ldots\ldots \quad (42)$$

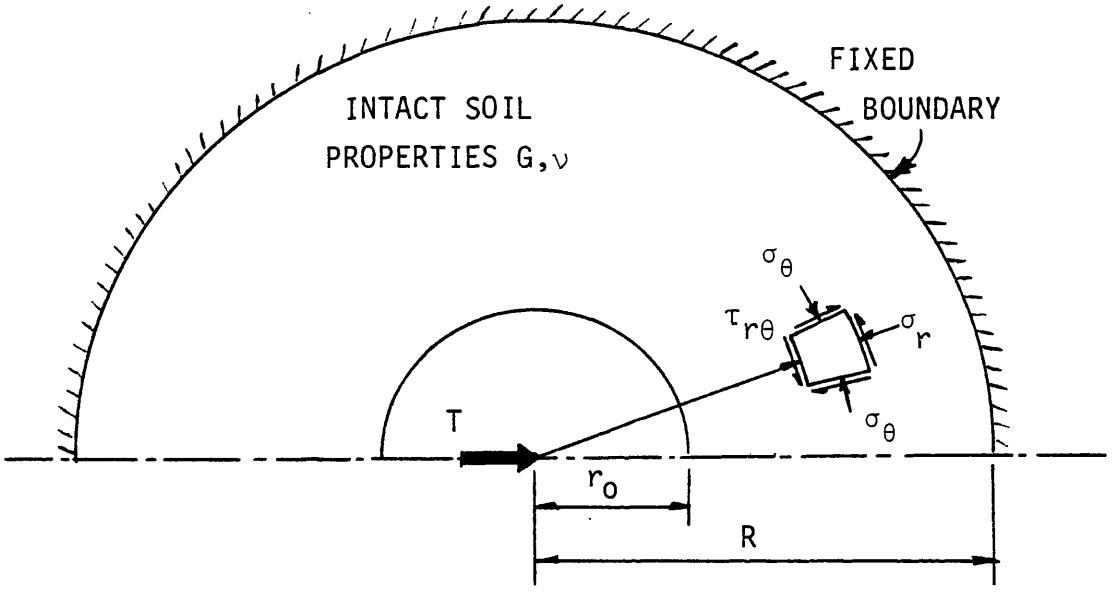

(a)

$$dQ = f_r = \sigma_r \, \text{Cos}\theta \; r_o d\theta$$

$$dF = f_\theta = \tau_{r\theta} \, \text{Sin}\theta \; r_o d\theta$$

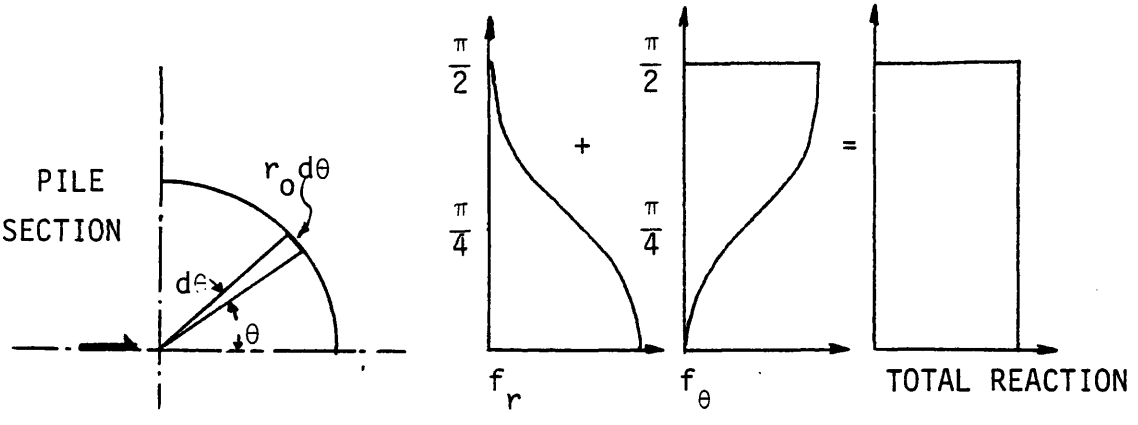

(b) [after Baguelin et al.(8)]

FIG. 9 - Mobilized Radial and Tangential Reactions Around a Translating Pile in Plane Strain

for all elements around the cirumference which corresponds to Eq. 29 for the pressuremeter. The corresponding displacement field depends upon the integration radius, R. The pile translation tends towards infinity as R tends towards infinity. If the case is taken where

$$\frac{R^2-r_o^2}{R^2+r_o^2} \simeq 1 \quad \ldots\ldots\ldots\ldots\ldots\ldots\ldots\ldots \quad (43)$$

then the pile displacement is given by

$$y = \frac{T}{16\pi G(1-\nu)} \left[(3-4\nu) \ln \left(\frac{R}{r_o}\right)^2 - \frac{2}{(3-4\nu)} \right] \ldots\ldots (44)$$

Considering any element around the circumference of the pile a modulus of pile element resistance may be defined as

$$k_{pile} = \frac{\sigma_r \, \mathrm{Cos}\theta + \tau_{r\theta} \mathrm{Sin}\, \theta}{y/r_o} \quad \ldots\ldots\ldots\ldots\ldots\ldots \quad (45)$$

where y = horizontal translation of the pile.

Then for the element where $\theta = 0$, Figs. 8(b), 8(d), we have:

$$k_{pile} = \frac{\sigma_r}{y/r_o} \quad \ldots\ldots\ldots\ldots\ldots\ldots\ldots\ldots \quad (46)$$

and substituting from Eq. 39 and Eq. 44 for σ_r and y, respectively give

$$k_{pile} = \frac{8G(1-\nu)}{\left[(3-4\nu) \ln \left(\frac{R}{r_o}\right)^2 - \frac{2}{(3-4\nu)} \right]} \quad \ldots\ldots\ldots\ldots \quad (47)$$

Also, a modulus of pile resistance, k_{pil}, is defined by

$$k_{pil} = \frac{p}{y/r_o} = \frac{pr_o}{y} \quad \ldots\ldots\ldots\ldots\ldots\ldots \quad (48)$$

and since $p = \frac{T}{2r_o}$

then $$k_{pil} = \frac{T}{2y} \quad \ldots\ldots\ldots\ldots\ldots\ldots \quad (49)$$

By rearranging Eq. 44 it is found

$$k_{pil} = \frac{8\pi G\,(1-\nu)}{\left[\,(3-4\nu)\,\ln\left(\frac{R}{r_o}\right) - \frac{2}{(3-4\nu)}\,\right]} \quad \ldots\ldots\ldots \quad (50)$$

This shows, for equal model to pile ratios, $\frac{R}{r_o}$, that the modulus of pile resistance is independent of changes in the pile radius R. The ratio of the respective moduli for the pile and pressuremeter is then found from Eq. 34, Eq. 47 and Eq. 50, and gives

$$\frac{k_{pil}}{kpmt} = \pi\,\frac{k_{pile}}{kpmt} = \frac{4\pi(1-\nu)}{\left[\,(3-4\nu)\,\ln\left(\frac{R}{r_o}\right)^2 - \frac{2}{(3-4\nu)}\,\right]} \quad \ldots \quad (51)$$

which is plotted in Fig. 10. The influence of increasing Poisson's ratio is to stiffen the pile's response as the material is forced to undergo less volume change.

Douglas and Davies (29) developed the theory to obtain displacements and rotations of a thin rigid vertical plate within a linear

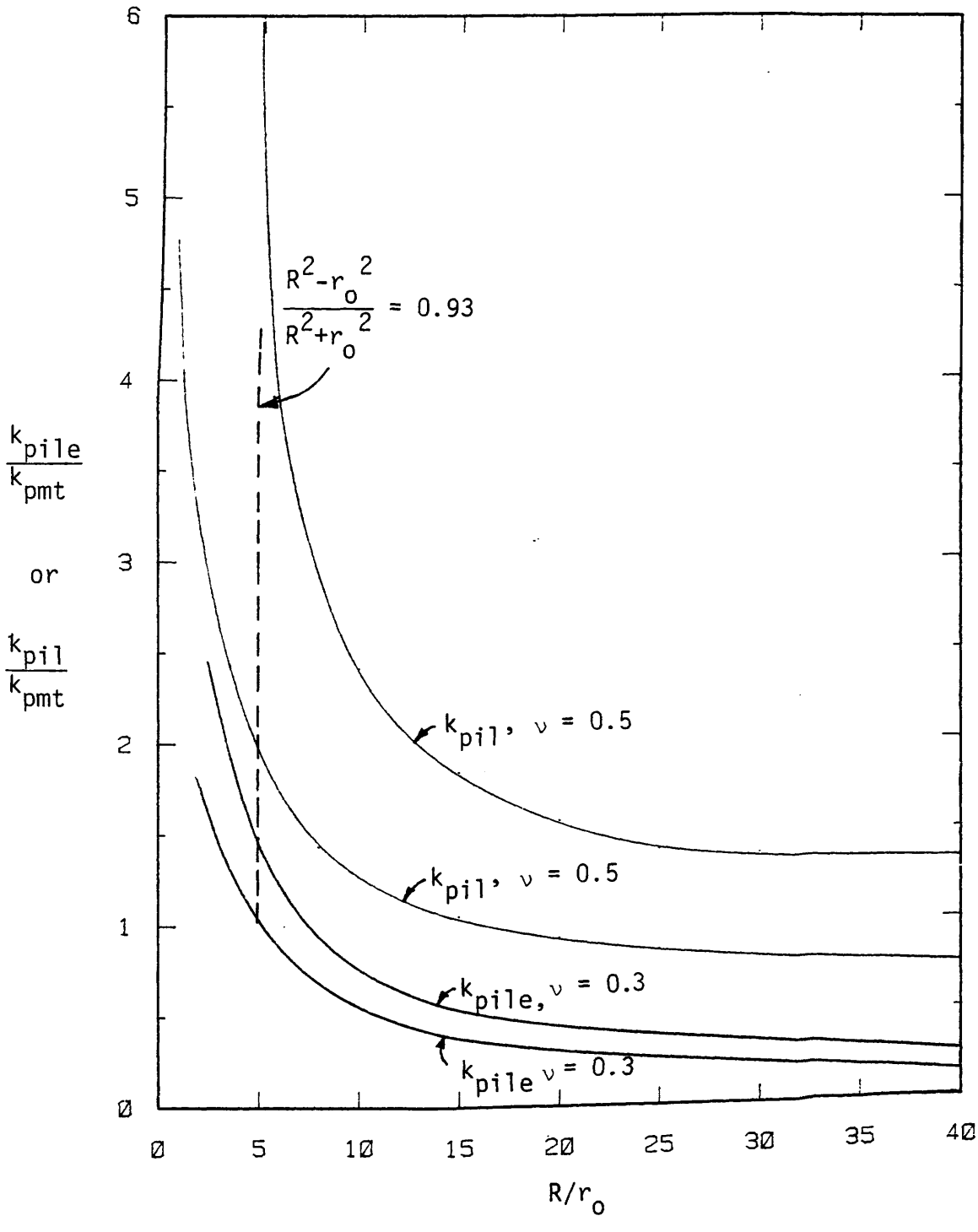

FIG. 10 - The Variation of the Ratio of k_{pile}/k_{pmt} and k_{pil}/k_{pmt} as a Function of R/r_o

elastic half space when subjected to horizontal and overturning loads. The solution was applied by Poulos (77), who considered the pile to be represented by a thin plate in order to study the factors influencing the displacements, rotations and moments of a laterally loaded pile. For a vertical rectangular plate subjected to horizontal pressure, p, the displacements along the top and bottom edges are

$$y_1 = \frac{pD}{32\pi G(1-\nu)} \left[(3-4\nu)F_1 + F_2 + 4(1-2\nu)(1-\nu)F_3\right] \quad . \ . \ . \ . \ (52)$$

$$y_2 = \frac{pD}{32\pi G(1-\nu)} \left[(3-4\nu)F_1 + F_4 + 4(1-2\nu)(1-\nu)F_5\right] \quad . \ . \ . \ . \ (53)$$

where y_1 = horizontal displacement of top edge

y_2 = horizontal displacement of bottom edge

D = plate width

F_{1-5} = dimensionless influence factors (functions of C_1/D and C_2/D)

and C_1 = vertical distance from free surface to plate top

C_2 = vertical distance from free surface to plate bottom.

For the closest approximation to plane strain conditions, $C_1 \to \infty$, $C_2 \to \infty$, $y_1 = y_2 = y$, and a modulus of plate resistance is defined by

$$k_{plate} = \frac{pD}{2y} \quad . \ . \ . \ . \

to be compatible with the previously defined moduli. For this condition the plate displacement, y, is given by

$$y = \frac{pD(3-4\nu)F_1}{32\pi G(1-\nu)} \quad \ldots\ldots\ldots\ldots\ldots\ldots\ldots \quad (55)$$

combining Eqs. 54 and 55 gives

$$k_{plate} = \frac{16\pi G(1-\nu)}{F_1(3-4\nu)} \quad \ldots\ldots\ldots\ldots\ldots\ldots\ldots \quad (56)$$

The ratio of the respective moduli for the plate and pressuremeter is then found from combining Eq. 34 and Eq. 56 which gives

$$\frac{k_{plate}}{k_{pmt}} = \frac{8\pi(1-\nu)}{F_1(3-4\nu)} \quad \ldots\ldots\ldots\ldots\ldots\ldots\ldots \quad (57)$$

The dimensionless influence factor, F_1, is a function of the ratio of plate depth to plate width, H/D, and Eq. 57 is plotted in Fig. 11.

Plasticity

Considering pressuremeter expansion the elements of material adjacent to the wall will yield initially and become plastic when the deviator stress reaches a certain limit. In purely cohesive material with no volume change, a Tresca yield criterion is appropriate

$$\sigma_r - \sigma_\theta = 2\, C_u \quad \ldots\ldots\ldots\ldots\ldots\ldots\ldots \quad (58)$$

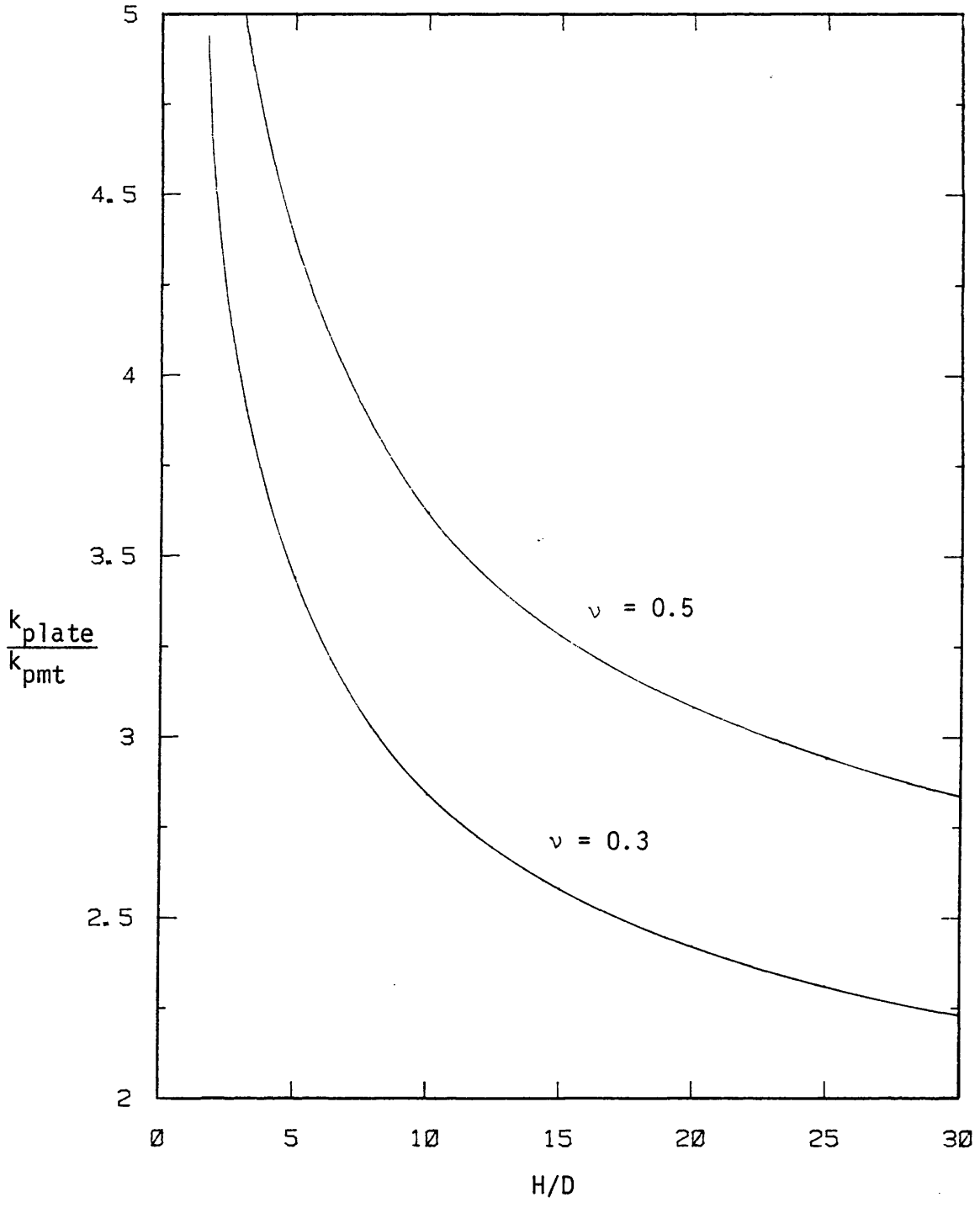

FIG. 11 - The Variation of the Ratio k_{plate}/k_{pmt} as a Function of H/D

At yield, the maximum shear stress is reached at the cavity wall. If the soil has both cohesion and frictional properties and obeys the Mohr-Coulomb yield criterion with no volume change, then the pressure in the cavity to initiate yield is given by

$$p_f = p_o (1+\sin\phi) + c \cos\phi \quad \ldots\ldots\ldots\ldots\ldots\ldots \quad (59)$$

where p_f = cavity pressure to cause plastic yield

p_o = initial cavity pressure

ϕ = angle of frictional resistance

c = cohesion.

For both the purely cohesive material and combined cohesion and friction material, the plastic zone propagates into the material as the pressure and cavity expand. The limiting cavity pressure, p_L, at which indefinite cavity expansion occurs is shown (11) to be

$$p_L = p_o + C_u \left[1+\ln \left(\frac{G}{C_u}\right)\right] \quad \ldots\ldots\ldots\ldots\ldots \quad (60)$$

in a cohesive material if zero volume change continues to occur in the plastic zone. For a soil with cohesion and friction the expression becomes

$$p_L = (p_o + c \cot\phi)(1+\sin\phi)\left(\frac{G}{C_u}\right)^{\frac{1-k_a}{2}} - c \cot\phi \quad \ldots\ldots \quad (61)$$

where $K_a = \tan^2(45 - \frac{\phi}{2})$ = coefficient of active earth pressure.

Clearly the limiting pressure in the cavity, for both cohesive materials and cohesion plus friction materials, is a function of the shear modulus to shear strength ratio. However, the difference between the final cavity pressure reached in the field pressuremeter test p_1 and the limiting cavity pressure, p_L, is not a function of this ratio in cohesive soils but is found to be,

$$p_L - p_1 = 0.69\, C_u \quad \ldots\ldots\ldots\ldots\ldots\ldots \quad (62)$$

Since small strains are considered then it can also be shown that

$$\frac{C_u}{G} = 2\varepsilon_f \quad \ldots\ldots\ldots\ldots\ldots\ldots\ldots\ldots \quad (63)$$

Theoretical pressuremeter curves with the associated relationship between p_L-p_f and failure strain ε_f, are given in Figs. 12 and 13 for the purely cohesive case and cohesion plus friction case respectively.

The special case of undrained cavity expansion, in which a saturated cohesive soil would undergo no volume change, has made possible the derivation of the shear stress-strain curve, Palmer (73), Ladanyi (55) and Baguelin et al. (10), directly from the pressuremeter expansion curve. The effects of drained behavior ($\Delta V \neq 0$) on the derived stress strain curve have also been theoretically explored by Baguelin et al. (11) and Wroth and Windle (105).

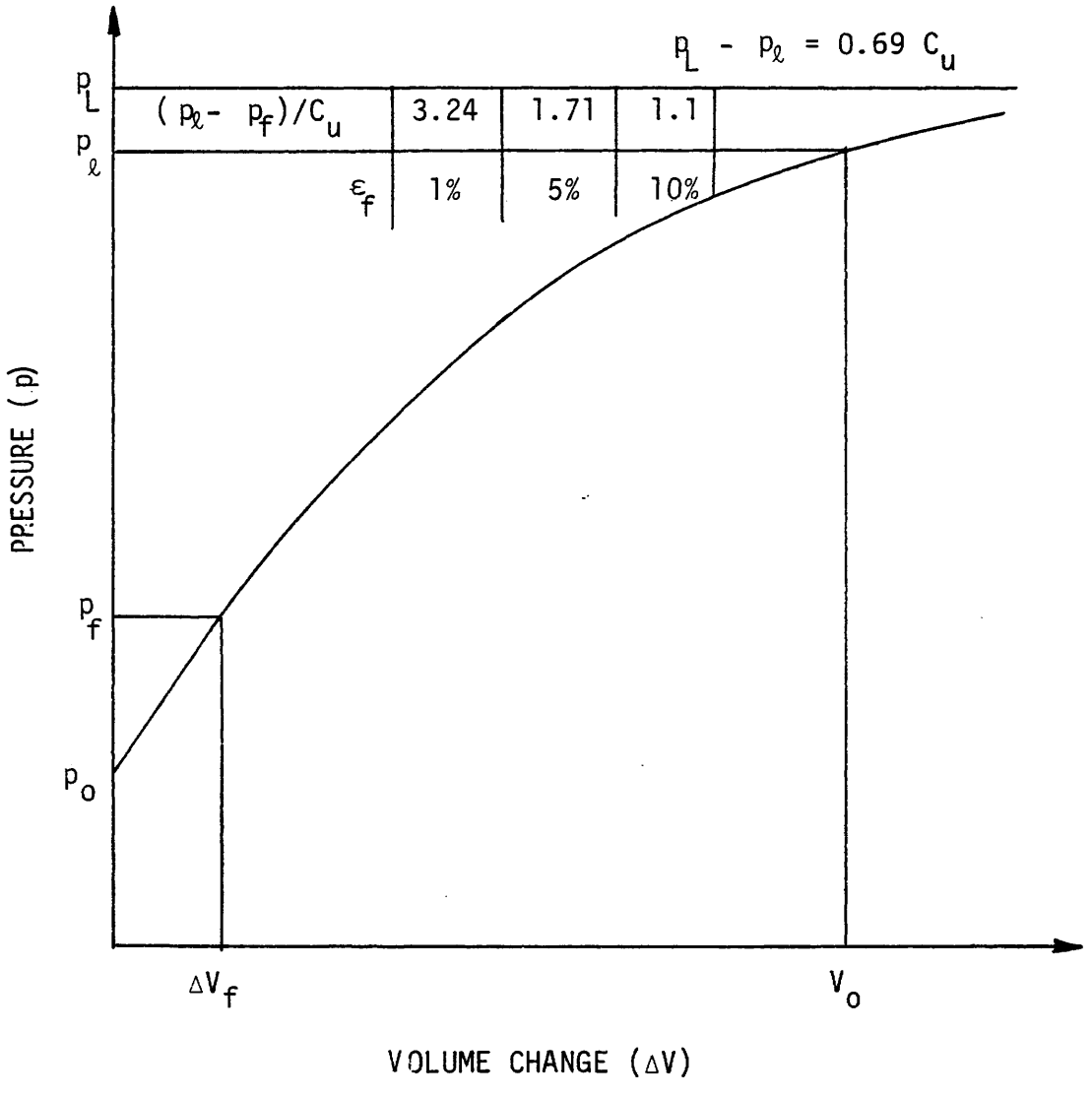

FIG. 12 - Theoretical Pressuremeter Expansion Curve in a Cohesive Material (ϕ =0)

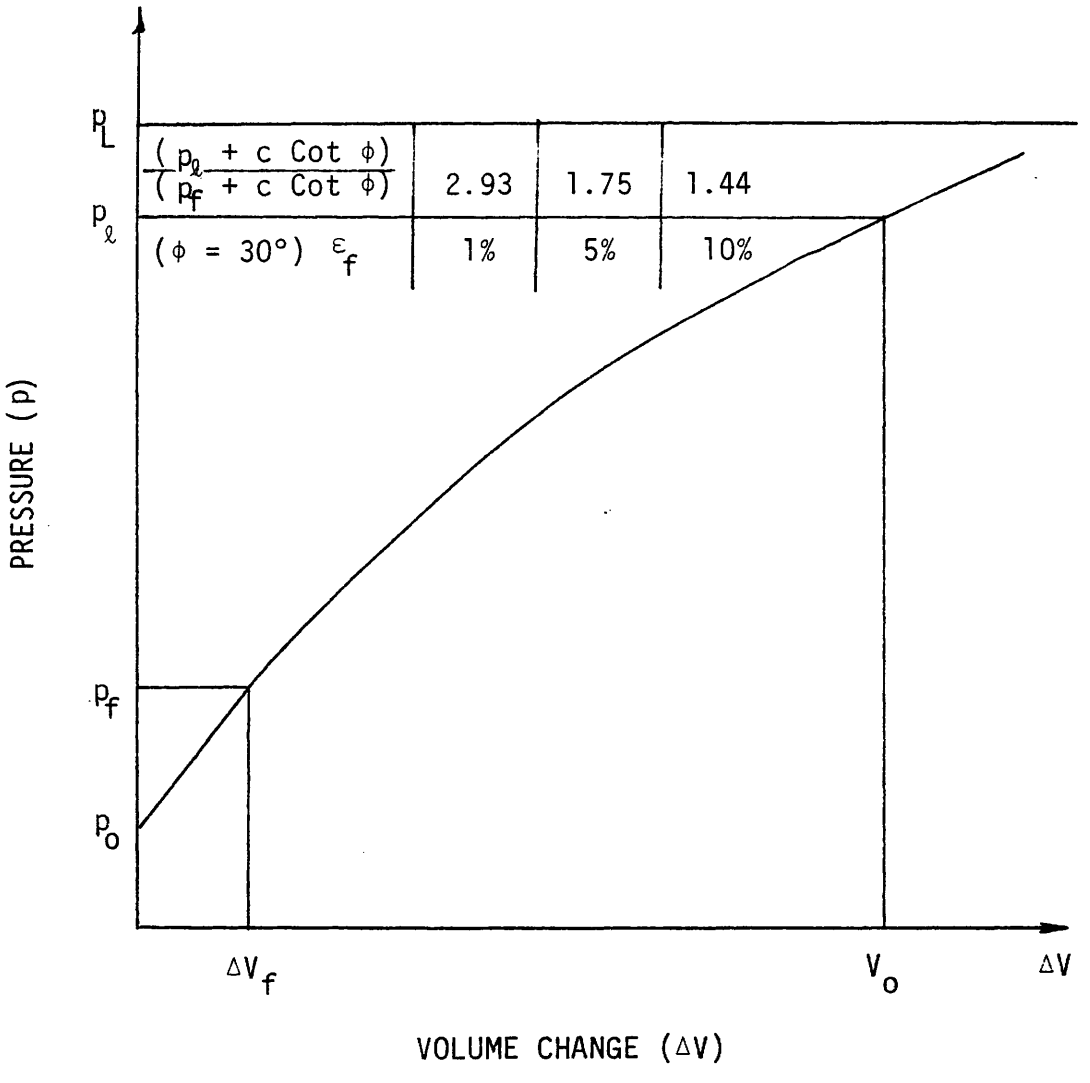

FIG. 13 - Theoretical Pressuremeter Expansion Curve in a Cohesion plus Friction Material

The onset of yield and propagation of the plastic zones around a laterally moving pile in plane strain have been examined by Baguelin et al. (8) using the finite element method. A cohesive soil was represented and the Tresca yield criterion expressed as

$$\sigma_1 - \sigma_2 \leq 2c \quad \ldots\ldots\ldots\ldots\ldots\ldots\ldots\ldots \quad (64)$$

was adopted for elastic plastic behavor. Both intact soil and the case of a disturbed zone around the pile as a result of pile placement were examined. Cohesion and Young's modulus in the zone were reduced by equal amounts. In general the first stage of plasticity is characterized by the yield of the material on the pile face parallel to the axis of loading for both the intact and disturbed material, Figs. 14(a) and 15(a) respectively. It is evident that shear reaction is quickly mobilized and reaches a maximum. Further the contribution of the front reaction increases which results in the total reaction curve remaining linear, Figs. 14(b) and 15(b). The second stage of plasticity is the final propagation of the plastic zones in the direction of loading during constant shear reaction. Figs. 14(b) 15(b) are normalized P-y curves for the finite element model. Baguelin et al. (8) concluded that disturbance has the same effect during the plastic phase as in the elastic phase and only significantly affects the shear reaction contribution.

To determine the value of the ultimate resistance available to the pile, plasticity theory is used. Poulos and Davies (78) present the

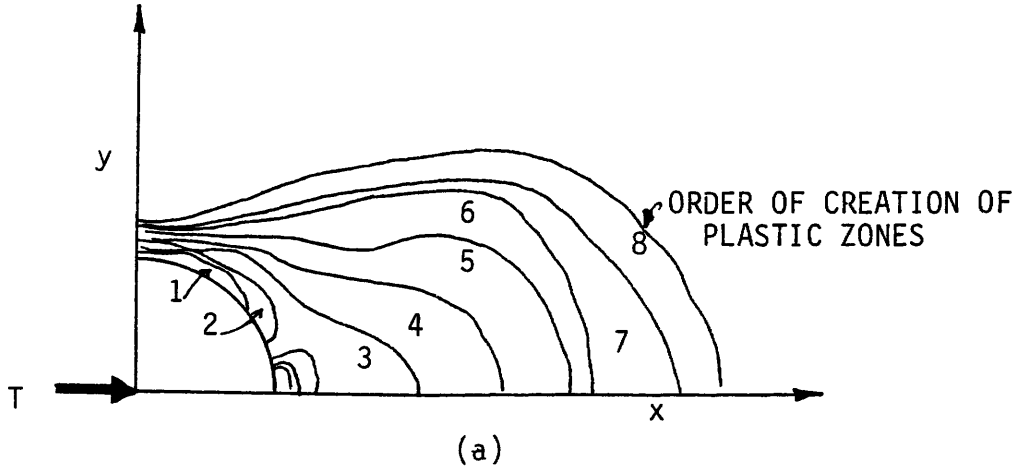

(a)

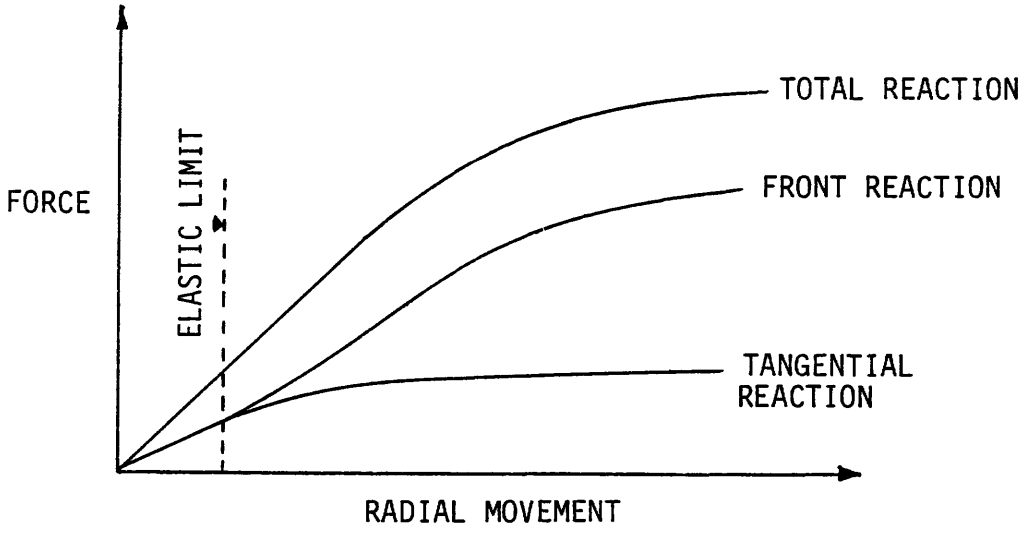

(b) [after Baguelin et al. (7)]

FIG. 14 - Expansion of Plastic Zones and Loading Curves for Intact Material

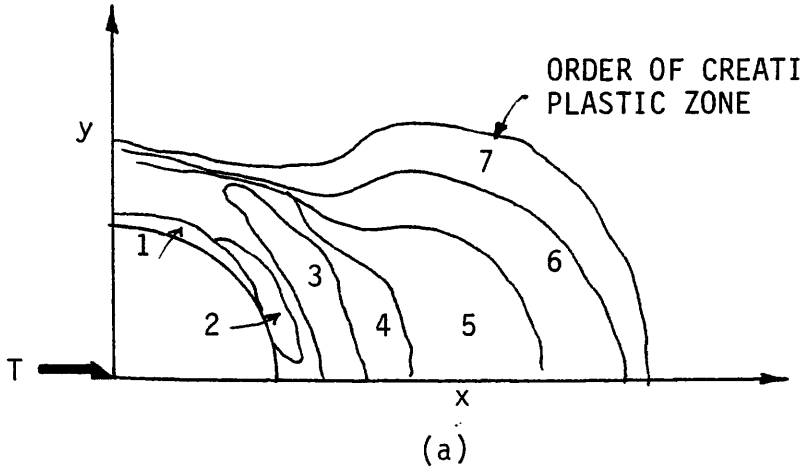

(a)

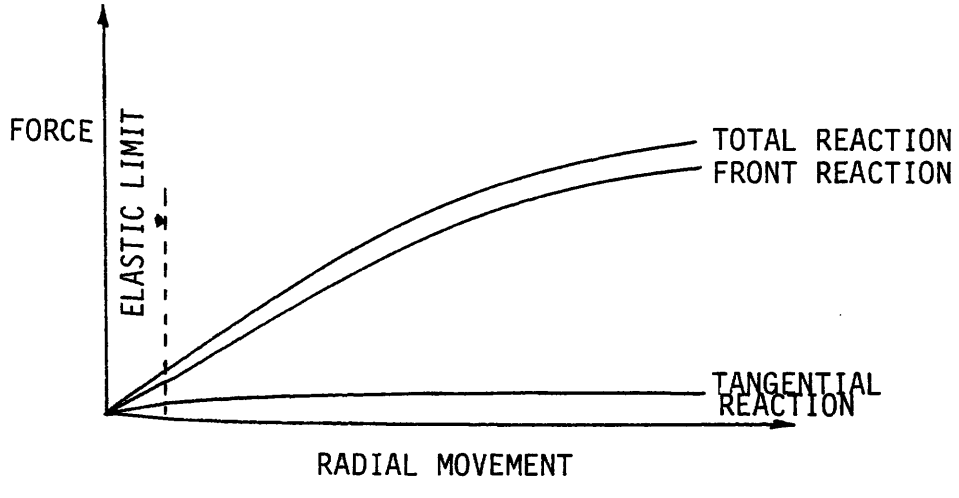

(b) [after Baguelin et al. (7)]

FIG. 15 - Expansion of Plastic Zones and Loading Curves for Disturbed Material

following solutions for a rhomb pile section of varying proportions in a cohesive soil. If

$$P_u = k_c\, c \quad \ldots\ldots\ldots\ldots\ldots\ldots\ldots\ldots\ldots\ldots \quad (65)$$

where P_u = ultimate lateral soil resistance

k_c = dimensionless factor

c = cohesion

then for a section of equal proportions and pile adhesion equal to the soil cohesion $k_c = 11$ and hence

$$P_u = 11\, c \quad \ldots\ldots\ldots\ldots\ldots\ldots\ldots\ldots\ldots\ldots \quad (66)$$

which compares with the value of 9c generally assumed.

Hansen (38) developed the solution from classical earth pressure theory for a soil having both friction and cohesion. The ultimate resistance at any depth, z, below the surface is expressed as

$$P_u = q\, k_q + c\, k_c \quad \ldots\ldots\ldots\ldots\ldots\ldots\ldots\ldots\ldots \quad (67)$$

where q = vertical overburden pressure

k_c, k_q = dimensionless factors which are functions of Φ and $\frac{z}{D}$

Combining Eq. 67 and Eq. 61 the ratio of limiting soil resistance for the pile to pressuremeter becomes

$$\frac{p_u}{p_L} = \frac{q\,k_q + c\,k_c}{(p_o + c\,\mathrm{Cot}\phi)(1+\mathrm{Sin}\phi)\left(\frac{G}{C_u}\right)^{(1-k_a/2)} - c\,\mathrm{Cot}\,\phi} \quad \ldots\ldots \quad (68)$$

which is plotted in Fig. 16. For the cohesive case reported by Poulos and Davies (78), expressed in Eq. 65, the corresponding k_c from Hansen (38) is 8.14.

Broms (22) simplified the assumptions of Hansen but, based on limited empirical evidence, suggested that in frictional materials

$$k_q = 3\,k_p \quad \ldots\ldots\ldots\ldots\ldots\ldots\ldots\ldots \quad (69)$$

where $k_p = (1 + \mathrm{Sin}\,\phi)/(1 - \mathrm{Sin}\,\phi)$

at all depths.

Reese (79,80) considered the problem by idealizing the pile with a square cross section and soil as displaced square blocks. By a compatability of 'stress blocks', the following expressions are obtained

$$p_u = 12\,C_u \quad \ldots\ldots\ldots\ldots\ldots\ldots\ldots \quad (70)$$

for a cohesive material, and

$$p_u = k_a\,D\,\gamma'H\,(\tan^8\beta - 1) + k_o\,D\,\gamma'H\tan\phi\,\tan^4\beta \quad \ldots \quad (71)$$

where $\beta = 45 + \phi/2$

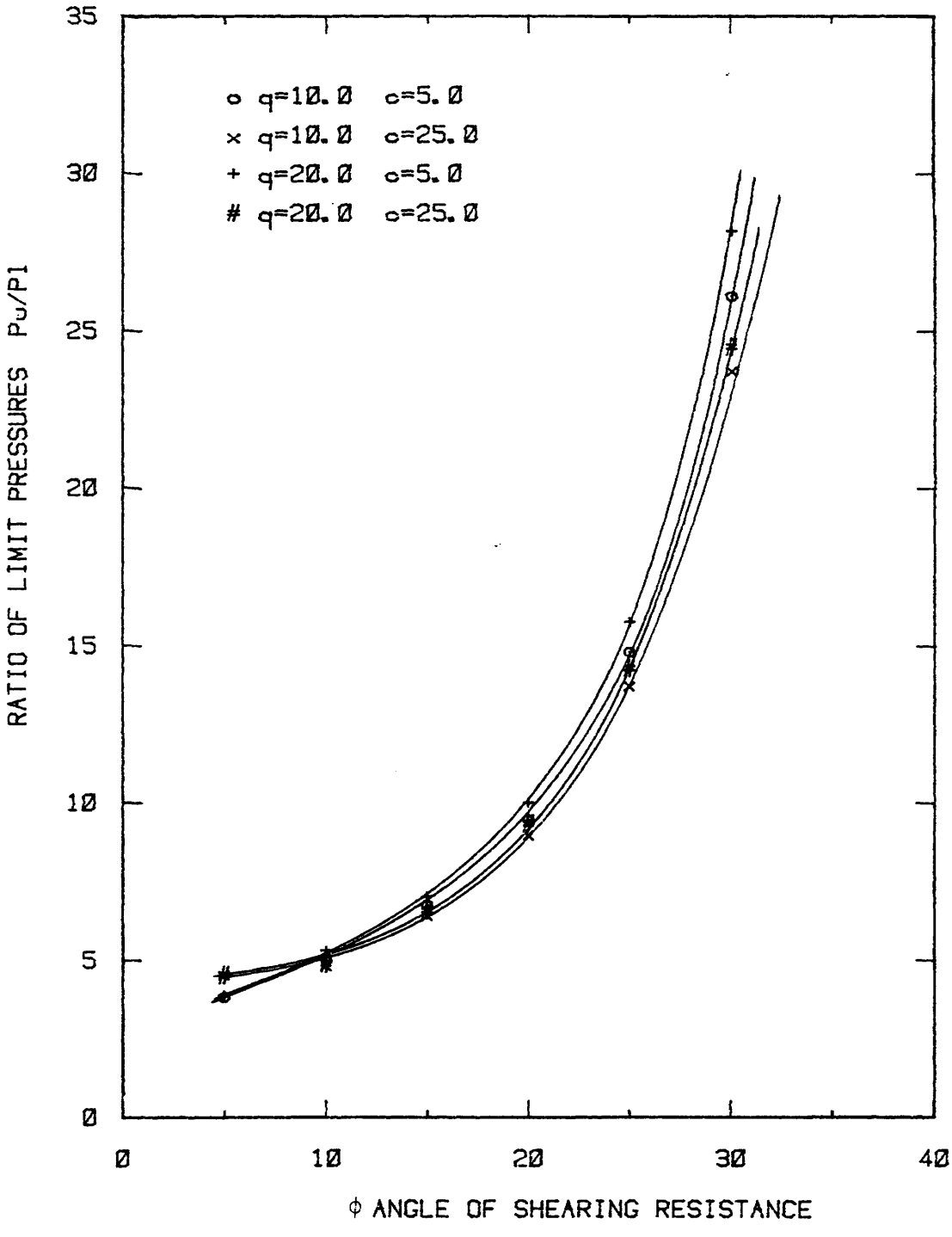

FIG. 16 - Ratio of Limiting Pressures for the Pile and Pressuremeter as a Function of ϕ

γ' = effective unit weight

H = depth below surface

k_o = coefficient of at rest earth pressure

for cohesionless materials.

The slip line analysis of Marti (63) gave:

$$p_u = 11.42\ C_u \quad \ldots\ldots\ldots\ldots\ldots\ldots\ldots\ldots \quad (72)$$

which was confirmed by laboratory experiments for a cohesive material.

Summary

The nonlinear subgrade reaction ('Winkler') soil model is expressed in the form of a load per unit length versus deflection or P-y curve. The reaction, P, is generated by the pile moving laterally through the soil and is the integrated mobilized pressure distribution. Using a measured modulus of subgrade reaction has the limitations of scale effects and inherent empiricism. By elastic continuum analysis the model can incorporate all interaction and shear effects but the real soil around the pile cannot transmit the large theoretical tensile stresses. Poulos and Davies (78) reported comparisons between elastic and subgrade reaction solutions for displacements of a stiff fixed head pile. They concluded that subgrade reaction theory tends to overestimate displacement and rotations, the difference increasing with lower embedment depth to diameter ratios.

The mechanisms of soil resistance and subsequent plastic failure in an elastic plastic material have been theoretically presented for the expanding pressuremeter cavity and a laterally moving pile. Only plane strain conditions were explored as a sound basis for comparison but many limitations are present from the assumptions made. In both elasticity and plasticity the pressuremeter expansion has been shown (11) to be sensitive to borehole disturbance. The disturbance effects on the pile from a finite element model are limited to the generation of the shear reaction.

In elasticity the relationship between the moduli of pile and pressuremeters Fig. 10 (p.38), is shown to be a function of the radius of integration since displacements are considered. Theoretically, and considering Fig. 8 (p. 31), the elements of material adjacent to the cavity wall and in the axis of pile loading should respond in a similar manner. In plasticity the limit pressure of infinite expansion for the pressuremeter is shown to be a function of the strain to failure, ε_f, in all materials. In the plasticity approach to a laterally moving pile section in cohesive materials the ratio of pile to pressuremeter resistance, P_u/P_L, is the order of 2-3.

In conclusion, based on the work of Baguelin et al. (8), it is apparent that pile installation disturbance can significantly affect the contribution of shear reaction to the P-y curve. This, together with the other theoretical considerations, suggests the production of the P-y curve from an assembly of front reaction and shear reaction curves which are constructed separately. The effects of pressuremeter borehole disturbance and pile disturbance, together with reaction

distributions, may then be quantified on each curve. From the work of Baguelin et al. (11) the effects of borehole disturbance on the pressuremeter have little effect on the limit pressure but can significantly affect the modulus.For a relatively insensitive material,e.g., stiff cohesive soils, the reduction in pressuremeter modulus is no greater than 15%. A more sensitive material will suffer a reduction in modulus of the order of 15% - 70% depending upon the extent of the remolded zone.

DETAILS OF THE SELECTED SITES

Details of the instrumented lateral pile load tests and site conditions at which pressuremeter test curves are available are given below. Details of the pressuremeter tests can be found in a later section.

Houston Site

Reported by Reese and Welch (86) to develop criteria for stiff clay above the water table, the Houston site was located at the intersection of State Highway 225 and Old South Loop East (see location plan Fig. 17). The load test was conducted in 1971.

The soil consisted of 28.0 ft (8.5 m) of stiff to very stiff red clay, known locally as Beaumont clay, underlain by 2.0 ft (0.6 m) of interspersed silt and clay layers and very stiff tan silty clay to a 2,000 lb/ft^2 depth of 42 ft (13 m). Undrained shear strength is reported at (100 kPa) and the water table was located at a depth of 18.0 ft (5.5 m).

The pile consisted of a drilled reinforced concrete shaft, 30 in. (760 mm) in diameter, 42 ft (13 m) deep, which extended 2.0 ft (0.6 m) above the ground surface. The shaft was instrumented to measure bending strains with gages spaced at 15 in. (380 mm) intervals for the top two-thirds of the shaft and at 30 in. (760 mm) intervals for the bottom one-third.

The loading test consisted of applying a lateral load at the

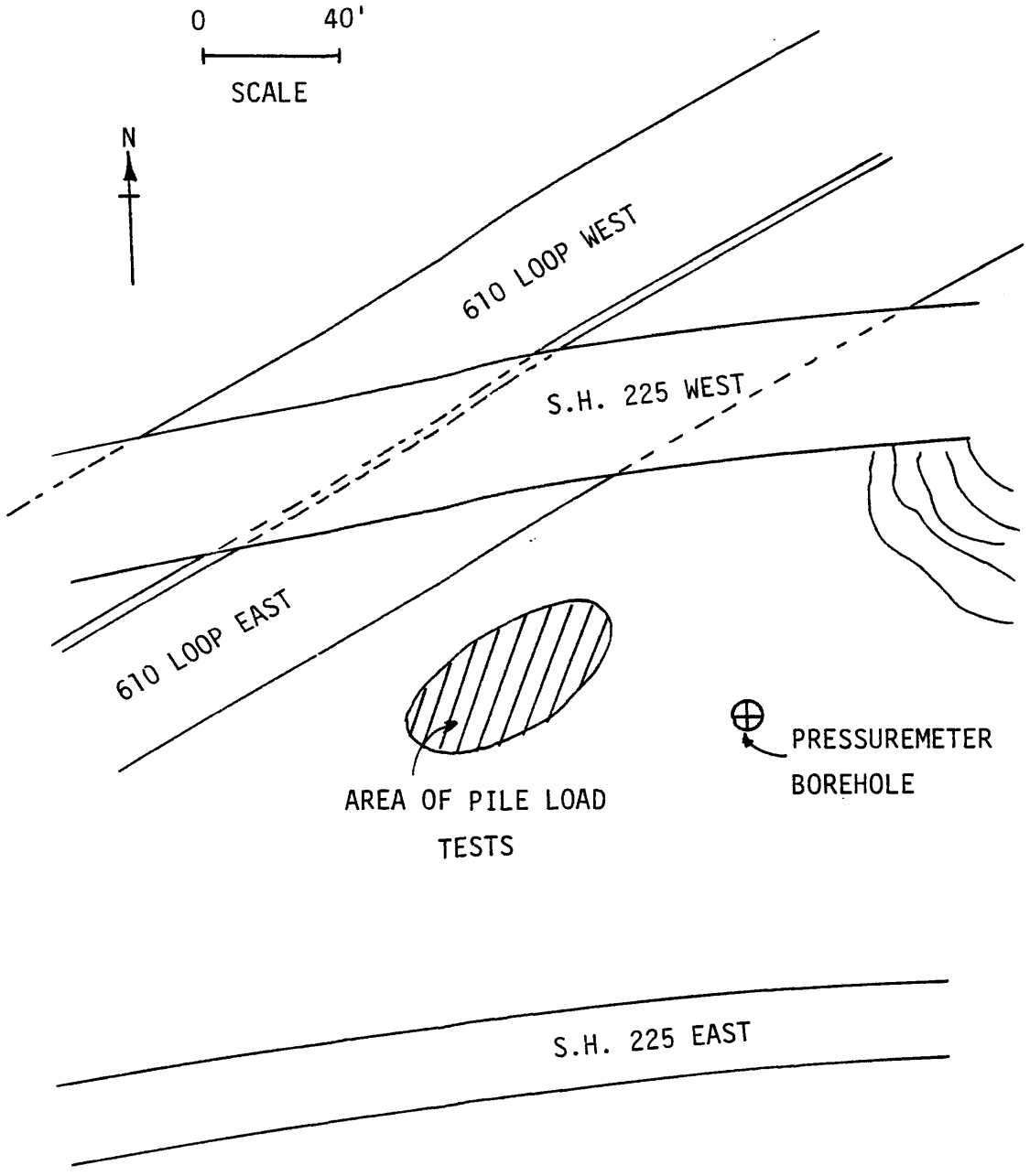

FIG. 17 - Location of the Houston Site

ground surface in a free head condition, and measuring the top slope, deflection and bending strains along the length of the shaft. Flexural stiffness of the shaft was determined by site loading to be approximately 2.8×10^{11} lb.in.^{2} (8.09×10^5 kN.M^2).

Pressuremeter tests were conducted in November 1981 and the variation of limit pressure with depth is given in Fig. 18.

Sabine Site

At a site near the mouth of the Sabine river (Fig. 19) in 1960 a series of lateral load tests in free and fixed head conditions were performed and reported by Matlock (64).

The soil consisted of slightly overconsolidated inorganic clay of high plasticity with a single sand layer between 16.0 ft (5.0 m) and 20.0 ft (6.1 m). Thin sand partings and a few sand seams varying in thickness from 1 in. to 4 in. (25 mm to 100 mm) were scattered throughout the clay. Unconfined compression test shear strengths ranged from 100 lb/ft^2 (5 kPa) near the mudline to 500 lb/ft^2 (24 kPa) at a depth of 30.0 ft (9.1 m). The water table was reported at, or near, the ground surface.

The tests were performed in a pit 4.0 ft (1.2 m) deep flooded to a depth of 6 in. (150 mm). The pile was 12.75 in. (310 mm) in diameter and instrumented with 35 pairs of electric resistance strain gages to determine bending moment. The pile was driven, open ended, to an embedded depth of 36.0 ft (10.9 m) with 6.0 ft (1.8 m) projecting above the test mudline.

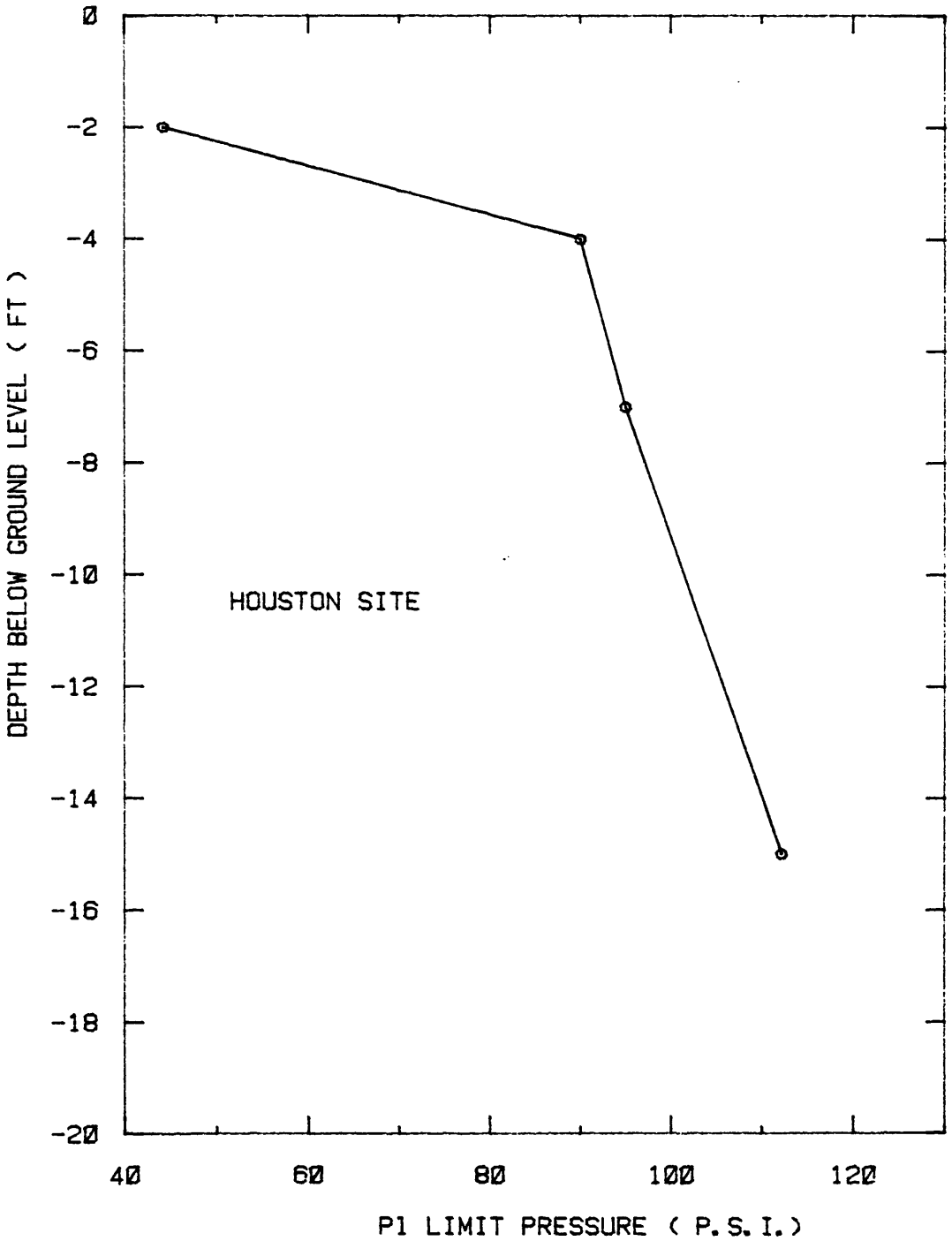

FIG. 18 - Variation of Limit Pressure with Depth for the Houston Site

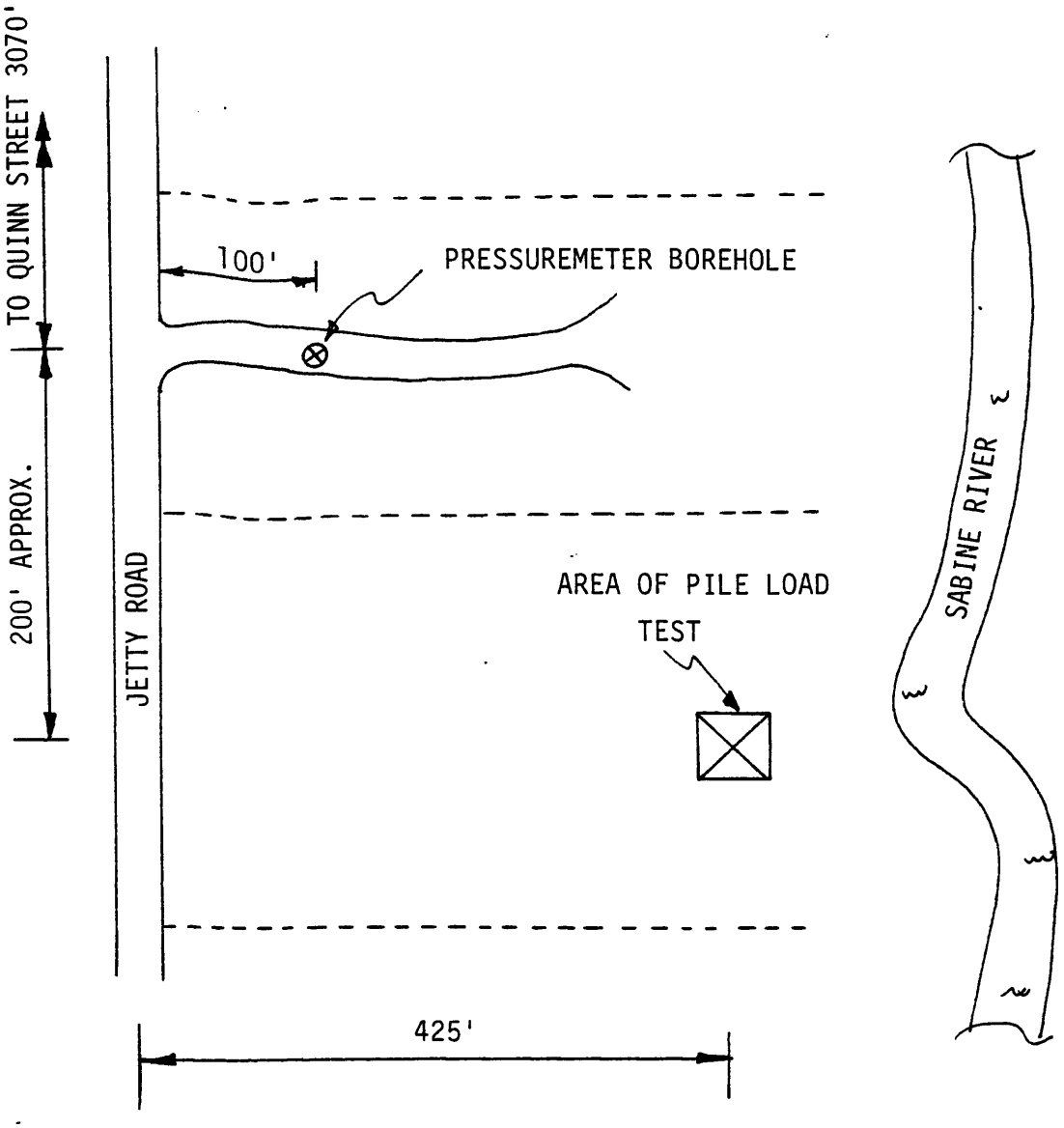

FIG. 19 - Location of the Sabine Site

The loading sequence comprised both cyclic and static lateral load tests with a free head and fixed head restraint conditions. At each load step surface deflection and slope were measured, together with continuous recording of bending strains. Flexural stiffness of the pipe pile was specified as 11.3 x 10^9 lb.in.^{2} (3.26 x 10^4 kN.M^2).

Pressuremeter tests were conducted during June 1982, and the variation of limit pressure with depth is given in Fig. 20.

Lake Austin Site

Free head lateral load tests conducted on the shore of Lake Austin, at the location given on Fig. 21, were reported by Matlock (64). The lateral load tests were performed in March 1956.

The soil conditions consisted of inorganic clays and silts of high plasticity deposited during this century behind Lake Austin dam. The upper deposits have been subjected to desiccation during periods of prolonged drawdown leaving joints and fissures. Vane shear strengths averaged 800 lb/ft^2 (38 kPa) with little variation with depth and unconfined shear strength tests gave 500lbs/ft^2 (24 kPa). The lateral load tests were performed in a 2 ft (610 mm) deep pit, which remained flooded.

The tubular steel test pile was 12.75 in. (324 mm) in diameter and instrumented with 35 pairs of electric strain gages to determine bending moment. The pile was driven, closed endedthrough an 18 ft (5.5 m) deep 8 in. (203 mm) diameter pilot hole to an embedment depth of 40.0

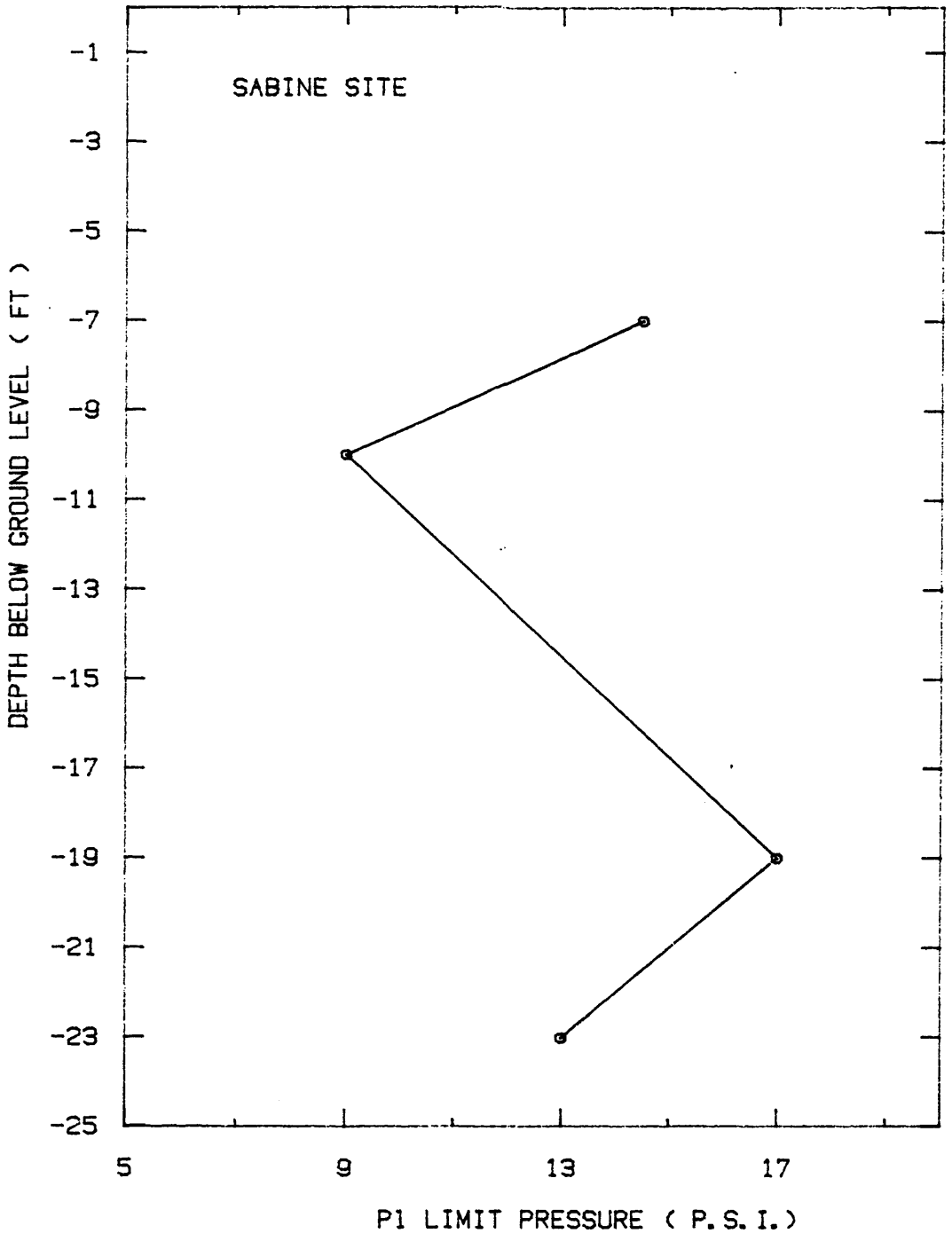

FIG. 20 - Variation of Limit Pressure with Depth for the Sabine Site

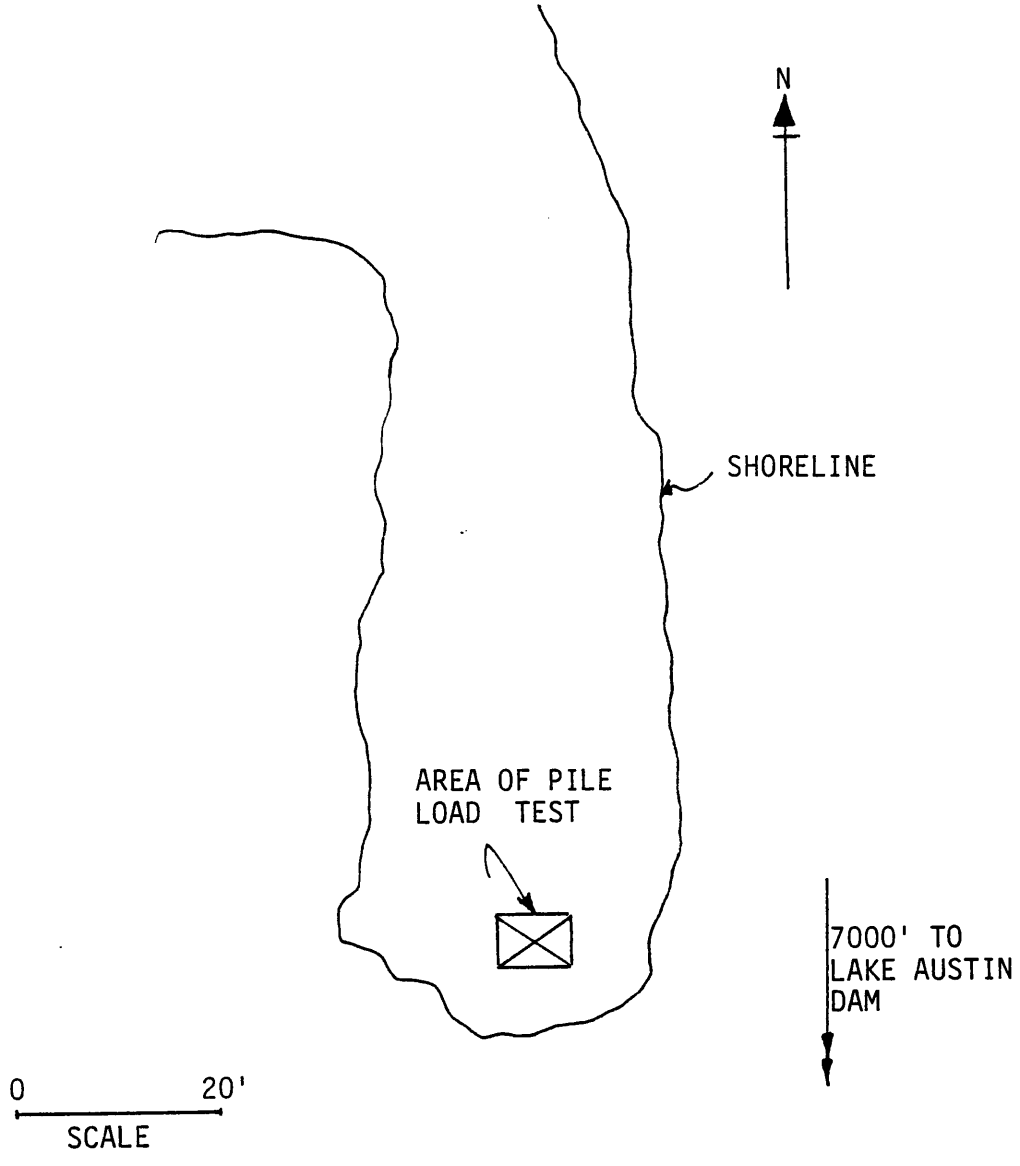

FIG. 21 - Location of the Lake Austin Site

ft (12.2 m) below the test mudline.

A series of free head static lateral load tests were reported and a single preliminary cyclic test. During each load step head deflection , inclination and bending strains were measured. Flexural stiffness of the pile was determined by experiment before installation, to be 10.9 x 10^9 lb $in.^2$ (3.5 x 10^4 $kN.M^2$).

Pressuremeter tests were conducted during November 1981 and the variation of limit pressure with depth is given in Fig. 22.

Mustang Island Site

Two test piles were loaded laterally in sand at a site on Mustang Island near Corpus Christi, Texas, (83) at the location shown in Fig. 23. The sand at the test site varied from clean fine sand to silty fine sand with high relative densities. The angle of shearing resistance, ϕ , was 39 degrees from SPT correlations and the submerged unit weight, γ', was found to be 66 lbs/ft^3 (10.5 kN/M^3).

The variation of standard penetration (SPT) resistance with depth is in a later Section. The lateral load tests were performed within a 5.5 ft (1.9 m) deep pit with the water table maintained at, or slightly above, the test pit bottom. The steel test piles were 24 in. (610 mm) in diameter and a wall thickness of 3/8 in. (10 mm), and instrumented with strain gages. The piles were driven to a total embedded depth of 69 ft (21 m) with 9 ft (2.7 m) projecting above the test mudline.

The loading sequence comprised both cyclic and static lateral load

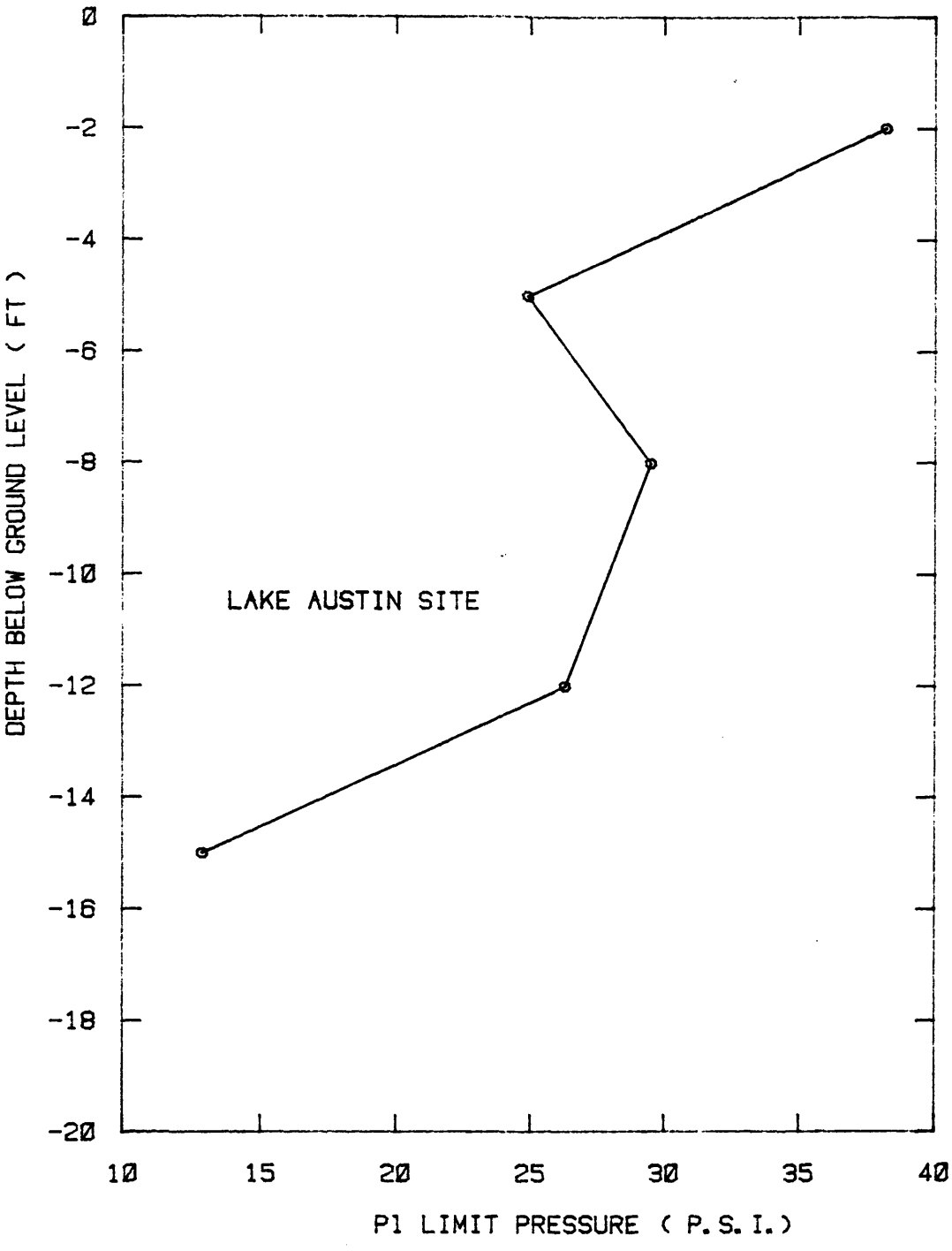

FIG. 22 - Variation of Limit Pressure with Depth for Lake Austin Site

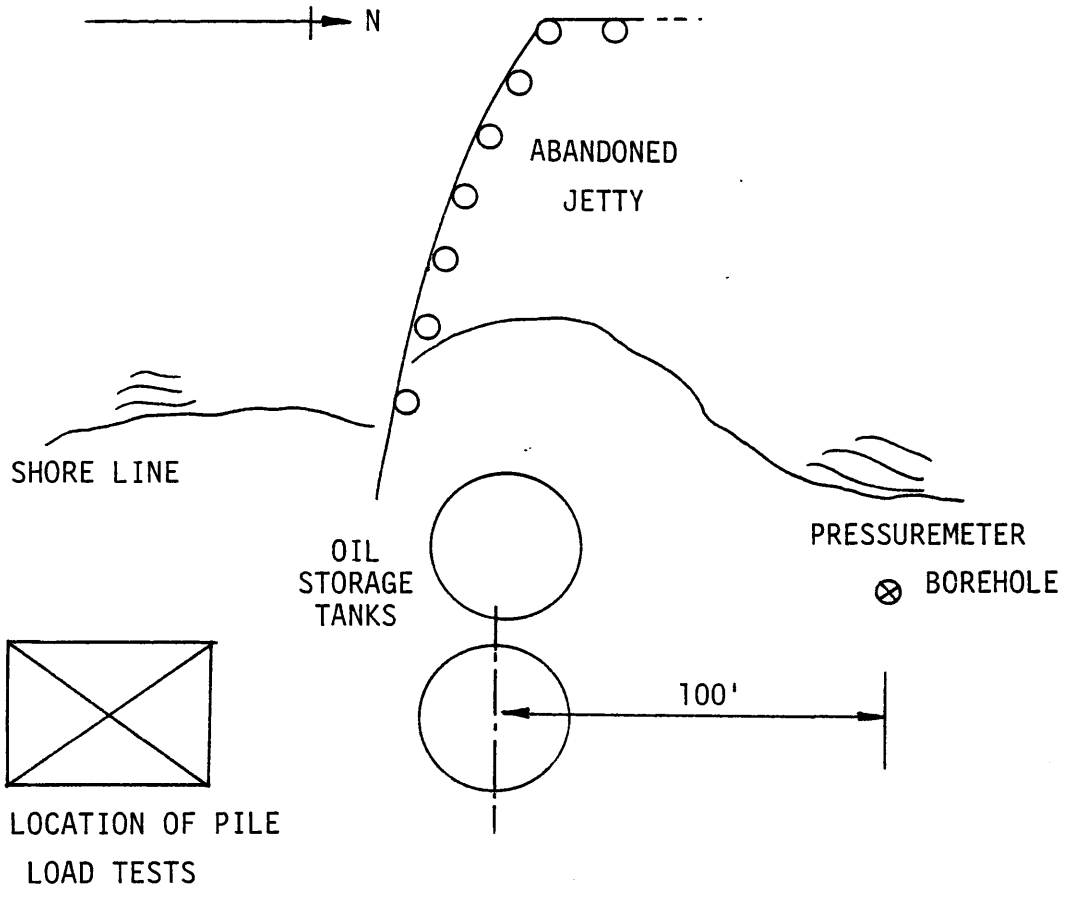

FIG. 23 - Location of the Mustang Island Site

tests in a free head condition. Deflection and inclination of the pile at the mudline was recorded, as well as bending strains. The flexural stiffness of the pile was determined to be 5.867×10^{10} lb.in.^{2} (1.69×10^5 kN.M^2). The pile load test was conducted in 1966.

The variation of pressuremeter limit pressures with depth from an investigation conducted in May 1982 is presented in Fig. 24.

Manor Site

Free head lateral load tests were conducted at a location five miles to the northeast of Austin, Texas, adjacent to US Highway 290 at a location shown on Fig. 25 in May 1967.

The soil consisted of stiff preconsolidated clays of marine origin with a slickensided secondary structure. Unconfined compressive strengths varied from approximately 4,000 lb/ft^2 (191 kPa) at the surface to 8,000 lb/ft^2 (383 kPa) at a depth of 15.0 ft (4.5 m).

Two tubular steel test piles of different sizes were selected to study scale effects. The first test pile was 25.25 in. (640mm) in diameter for the top 24.0 ft (7.3 m) and 24 in. (610 mm) in diameter for the remaining 25.0 ft (7.6 m). Total embedment depth was 49.0 ft (14.9 m) below the test mudline. The second test pile was 6.625 in. (168 mm) in diameter with a total embedment depth of 30.0 ft (9.1 m) below the test mudline. Both piles were instrumented with electric strain gages and driven, open ended, to the design penetration.

The loading sequence comprised both cyclic and static lateral load

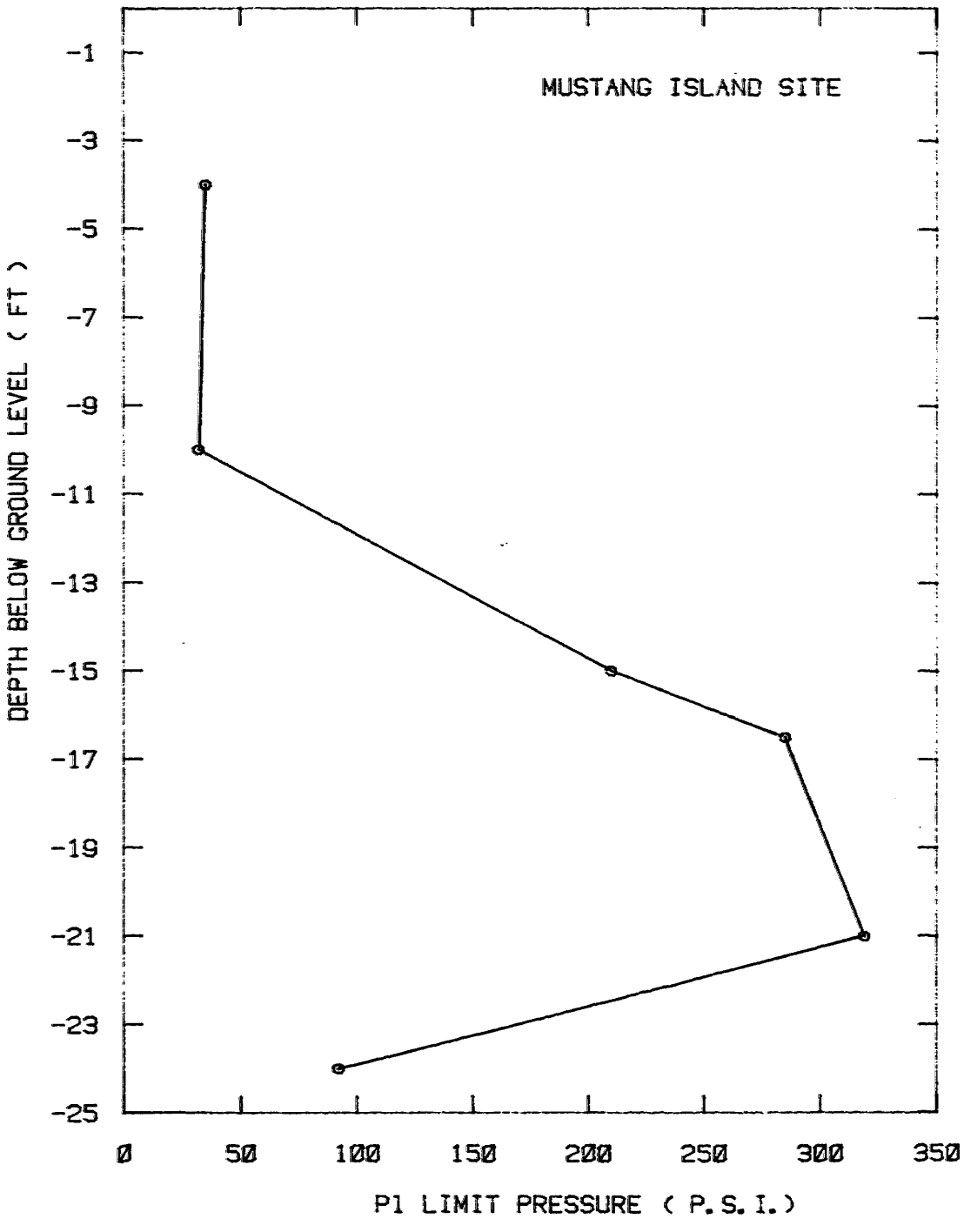

FIG. 24 - Variation of Limit Pressure with Depth for the Mustang Island Site

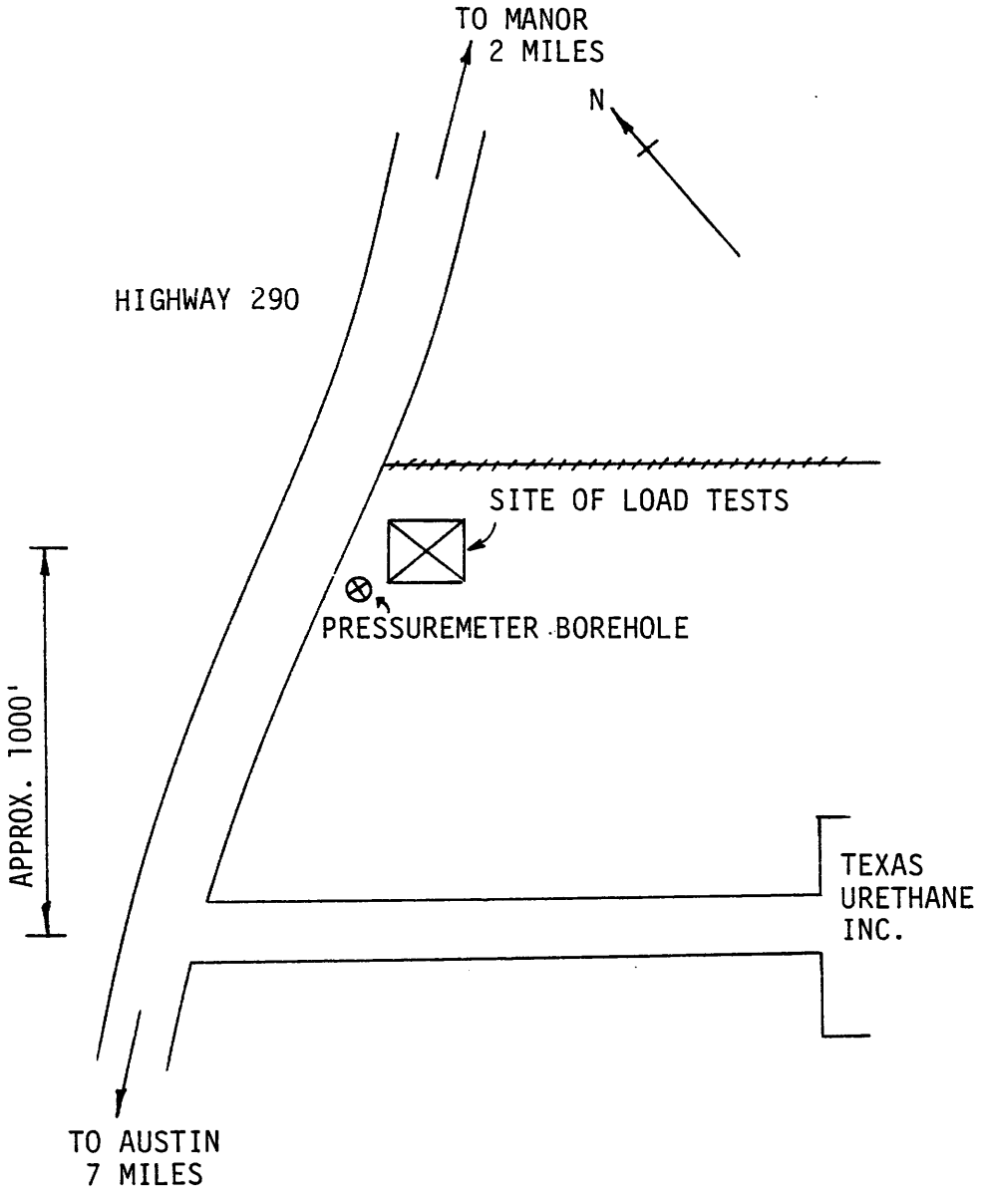

FIG. 25 - Location of the Manor Site

tests in a free head condition for the 25.25 in. (640 mm) pile, and free and fixed head condition for the 6.625 in. (168 mm) pile. Deflection and inclination of the surface were recorded at each load step and with measurement of bending strains. The flexural stiffness of the 25.25 in. (640 mm) pile was 1.7204×10^{11} lb.in. (4.97×10^5 kN.M^2) and 5.867×10^{10} lb.in.^{2} (1.69×10^5 kN.M^2) for the top and bottom sections respectively. The flexural stiffness of the 6.625 in. (168 mm) pile was 1.772×10^9 lb.in.^{2} (5.12×10^3 kN.M^2) and 1.084×10^9 lb.in.^{2} (3.13×10^3 kN.M^2) for the top and bottom sections respectively.

The variation of pressuremeter limit pressures with depth from an investigation conducted in November 1982 is presented in Fig. 26.

Texas A&M Site

Three lateral load tests were conducted on drilled shafts at a location near College Station, Texas, shown on Fig. 27.

The soil consisted of stiff slickensided clay preconsolidated by desiccation. To a depth of 5.0 ft (1.52 m) the soil remained fairly uniform, medium stiff to stiff sandy clays of medium plasticity. Underlaying this deposit was stiff to very stiff fissured red clay of high plasticity. Unconfined compression shear strengths were 2,000 lb/ft^2 (95 kPa). The ground water table was located at 15.0 ft 4.58 m) to 18.0 ft (5.49 m) below the ground level.

The three piles consisted of drilled reinforced concrete shafts of

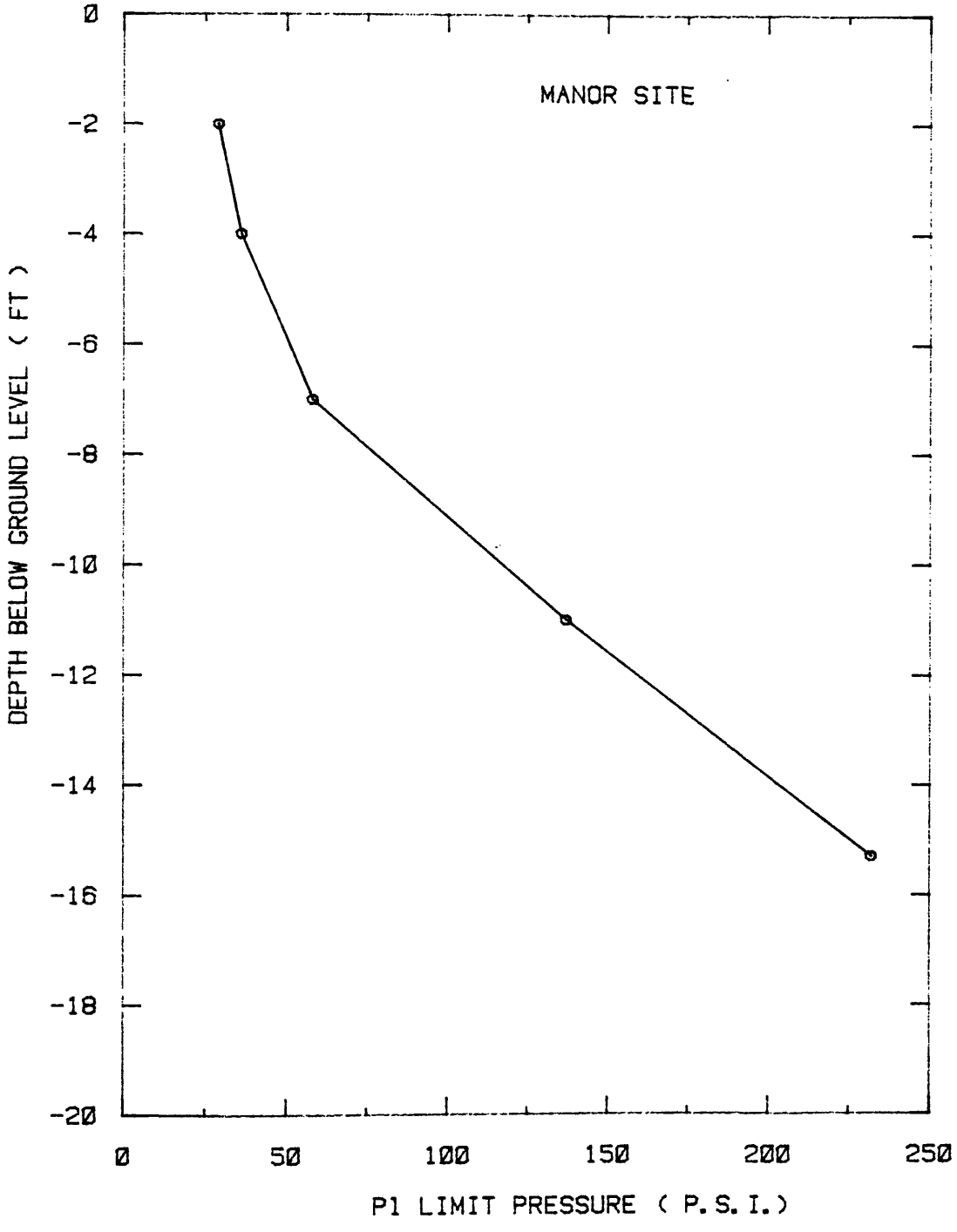

FIG. 26 - Variation of Limit Pressure with Depth for the Manor Site

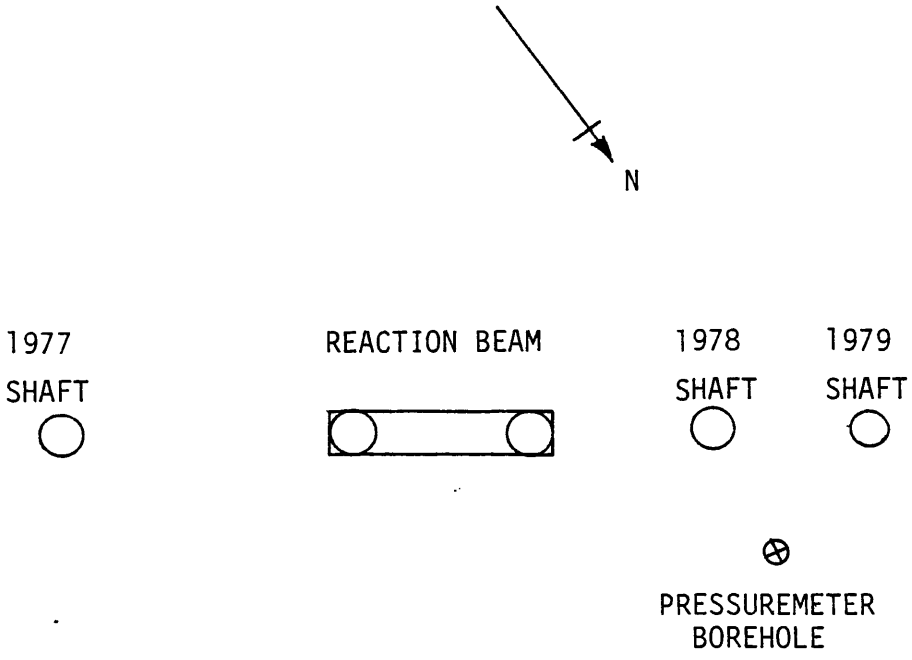

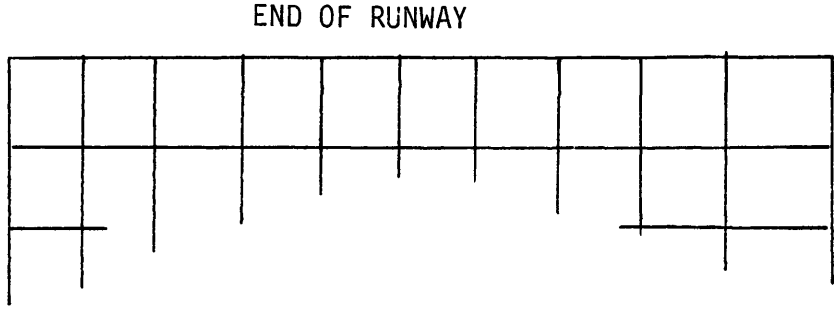

FIG. 27 - Location of the Texas A&M Site
at the Texas A&M Research Annex

diameters 3 ft, (915 mm) and 2.5 ft (762 mm) with embedment depths 20 ft (6.1 m), 15.0 ft (4.6 m) and 15.0 ft (4.6 m) respectively. The shafts were instrumented with earth pressure cells at 15 in. (381 mm) spacing to measure the soil pressure during lateral loading.

The loading sequence consisted of applying a lateral load, through a cable winch system, in a free head condition at a position 2.5 ft (762 mm) above the ground level. During each load step shaft rotation, groundline deflection and the pressure cell response were measured.

Pressuremeter tests were conducted during November 1981 and the variation of limit pressure with depth is given in Fig. 28.

Lock and Dam 26 Site

An extensive series of lateral load tests were conducted at the proposed site of Lock and Dam No. 26 on the Mississippi river. Two piles of the series, an'H' pile (HP 14 x 73), T3, and pipe pile (ref. PP 14 x 0.375), T4, were instrumented with strain gages. Flexural stiffnesses of the 'H' pile, T3 and pipe pile, T4, are 2.2 x 10^4 kN.M^2) and 1.16 x 10^{10} (33 x 10^4 kN.M^2) respectively.

The soil consisted of recent fine to coarse sand to a depth of 20.0 ft (6.1 m) overlaying 5.0 ft (1.5 m) of stiff sandy silt. Underlying the silt was coarse sands and gravels of glacial outwash origin. The variation of SPT resistance with depth is given on Fig. 29.

The steel test piles were driven to a total embedded depth of 50.0 ft (15.2 m), pipe pile T4 was driven open ended and the soil plug, 33.0

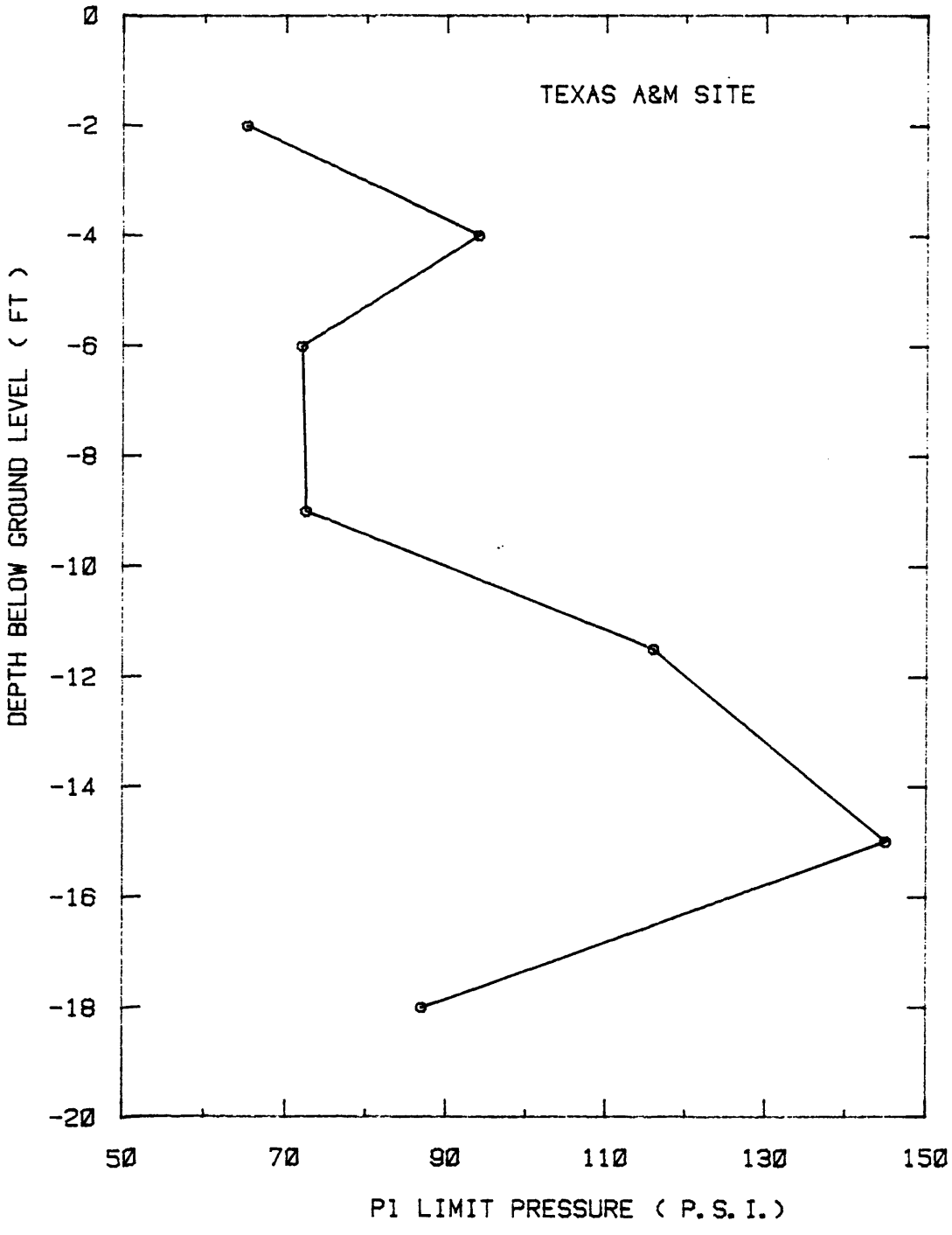

FIG. 28 - Variation of Limit Pressure with Depth at the Texas A&M Site

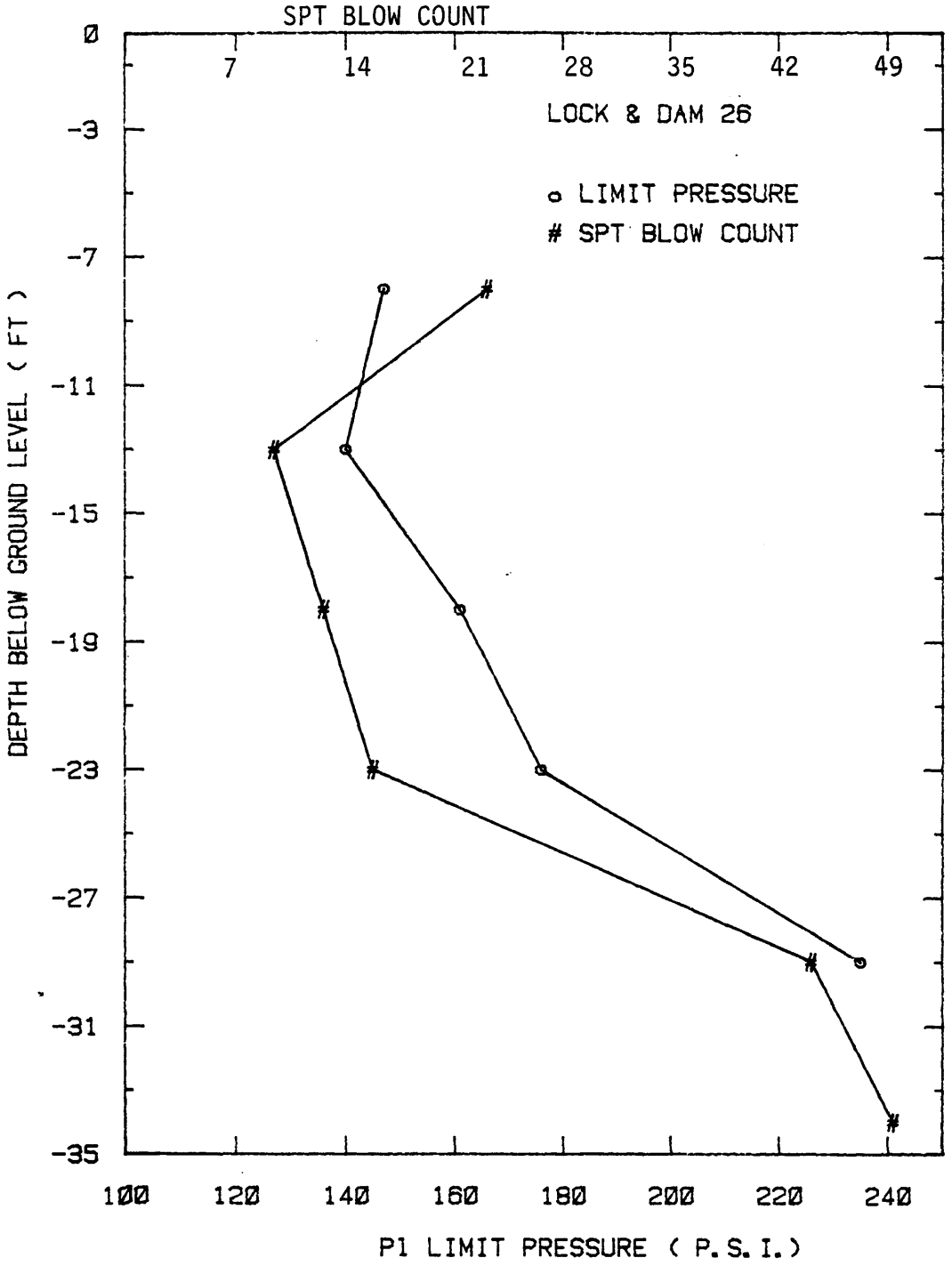

FIG. 29 - Variation of SPT Blow Count and Limit Pressure with Depth at Lock and Dam 26

ft (10.0 m) below ground level, was grouted after driving.

Lateral loads were applied between 9 in. to 18 in. (229 mm to 458 mm) above the ground level in 5.0 ton (43.8 kN) increments in a static series of tests. Deflection at the ground surface was recorded, as well as measurement of bending strains. Pressuremeter test results are available, and the variation of limit pressure with depth is given on Fig. 29.

Plancoet Site

Two instrumented piles are reported, together with pressuremeter results, which were tested at the Plancoet experiment station of the Laboratoire Central des Ponts et Chaussees, Paris, France (11,6).

The first pile was a caisson pile fabricated from four Larsen III 'S' sheet piles welded together to have a total width of 37.0 in. (0.95 mm) and embedded length 14.5 ft (4.4 m). The pile was jacked in place and disturbance is reported (8) to have reduced the undrained cohesion to a quarter of the undisturbed value in a zone of width 8 in. (20 mm).

The second pile was in reality a set of two 'H' type piles which are considered as square since the space between the flanges was covered. The frontal width of each H pile was 11 in. (280 mm) and the total embedded depth was 20.0 ft (6.1 m). Both piles were instrumented with Glotzl total earth pressure cells.

The soil consisted of sensitive loose silt to a depth of 11.5 ft

(3.5 m) with average vane shear strength of 620 lb/ft^2 (30 kPa) underlain by fine sand.

The loading sequence for the Larsen pile comprised application of increasing static lateral load, 6.0 ft 10 in. (2.1 m) above the ground surface in a free head condition. The H pile was subjected to both static and cyclic loading in a free head condition.

A summary of pressuremeter limit pressures with depth is given on Fig. 30.

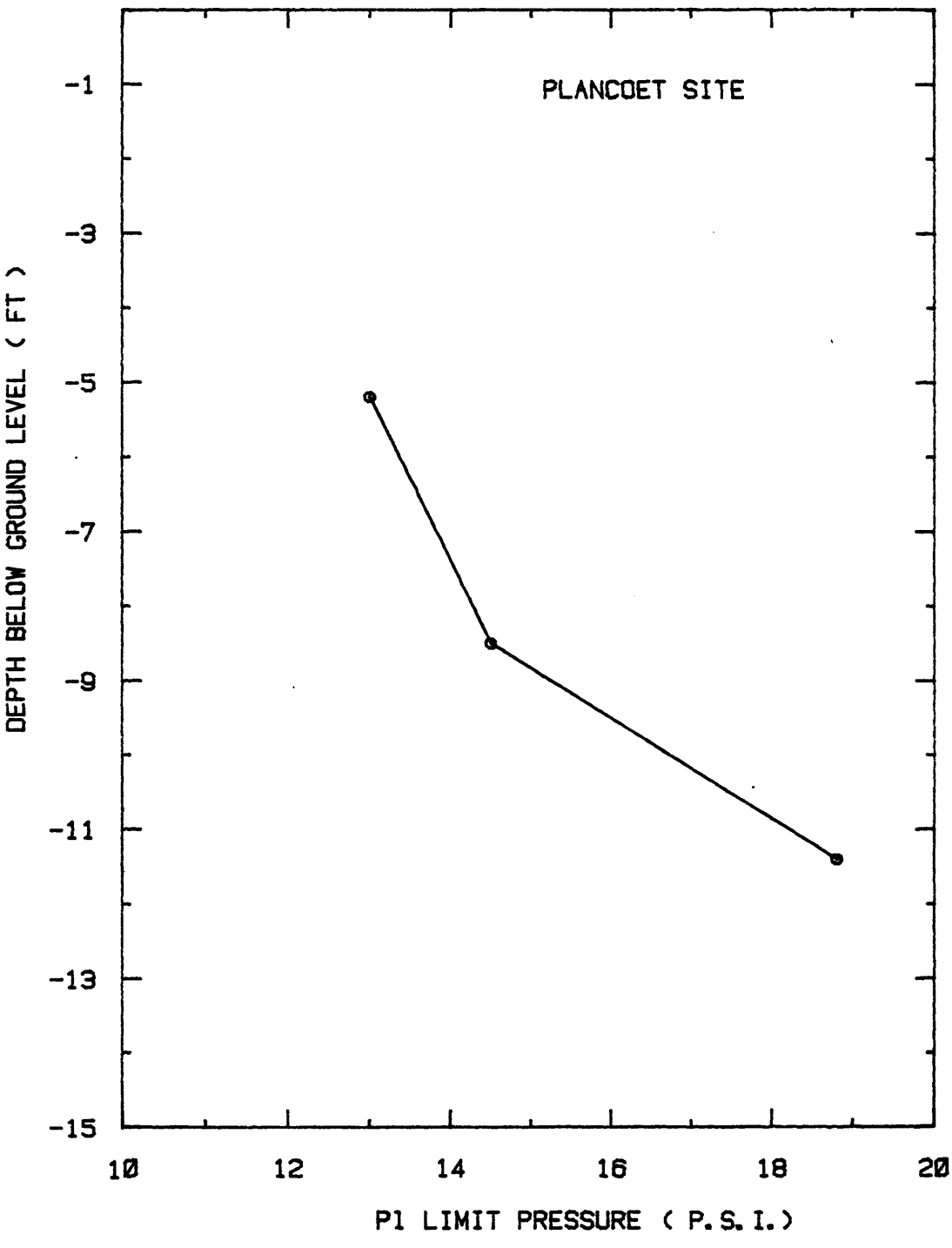

FIG. 30 - Variation of Limit Pressure with Depth at the Plancoet Site

P-y CURVES FROM THE PREBORING PRESSUREMETER TEST

The Concept of Front Resistance (Q-y) and Friction Resistance (F-y) Curves

Previously the theoretical distributions of the radial stress and tangential stress around a laterally moving pile were given by Eqs. 39 and 41 respectively. The distribution of the radial force, f_r, and tangential force, f_θ, is then given by the following

$$f_r = dQ = \sigma_r \cos\theta \; r \, d\theta \quad \ldots\ldots\ldots\ldots\ldots\ldots \quad (72)$$

$$f_\theta = dF = -\tau_{r\theta} \sin\theta \; r \; d\theta \quad \ldots\ldots\ldots\ldots\ldots\ldots \quad (73)$$

where r = pile radius

respectively, and is shown in Fig. 9(b) (p. 35). By integration of Eq. 72 the average pressure against the projected face (i.e.,diameter) of a circular pile is $\frac{\pi}{4}$ times the pressure at the center of the face. It has also been shown (9) that the average pressure against the face of a square pile is 1.13 times the pressure at the center of the face. This mobilized front pressure reaction, Q, is a function of the pile displacement, y, and the response can be measured in the field as a Q-y curve.

Contact pressures behind the pile will quickly reduce to the active state, or lose contact entirely. It would be more appropriate to consider the mobilization of shear stresses on the front

half of the pile only.

By integration of Eq. 73 the average shear stress mobilized on each of the projected sides of the front half of the circular pile is 0.79 times the maximum shear stress. For the square pile the average shear stress on the pile side is 0.88 times the maximum. This mobilized shear reaction, F, must also be a function of pile movement, y.

Further, if the mobilized pressure at the center of the pile front face, σ_r, and mobilized shear at the pile side, $\tau_{r\theta}$, are known, then the theoretical distributions allow the calculation of the full reaction. The total load per unit depth of the pile, i.e. P of the required P-y curve, is then given by the sum of the two components shear reaction, F, and pressure reaction, Q, illustrated on Fig. 31. Thus at any deflection,y ,

$$P = Q + F \quad \ldots\ldots\ldots\ldots\ldots\ldots\ldots\ldots \quad (74)$$

$$= D\,[(\sigma_r \times SQ) + (\tau_{r\theta} \times SF)] \quad \ldots\ldots\ldots\ldots \quad (75)$$

where D = pile diameter or width

σ_r = mobilized front pressure at y

$\tau_{r\theta}$ = mobilized shear stress at y

SQ = shape factor for pressure reaction

= $\pi/4$ for circular piles

= 1.13 for square piles

SF = shape factor for shear reaction

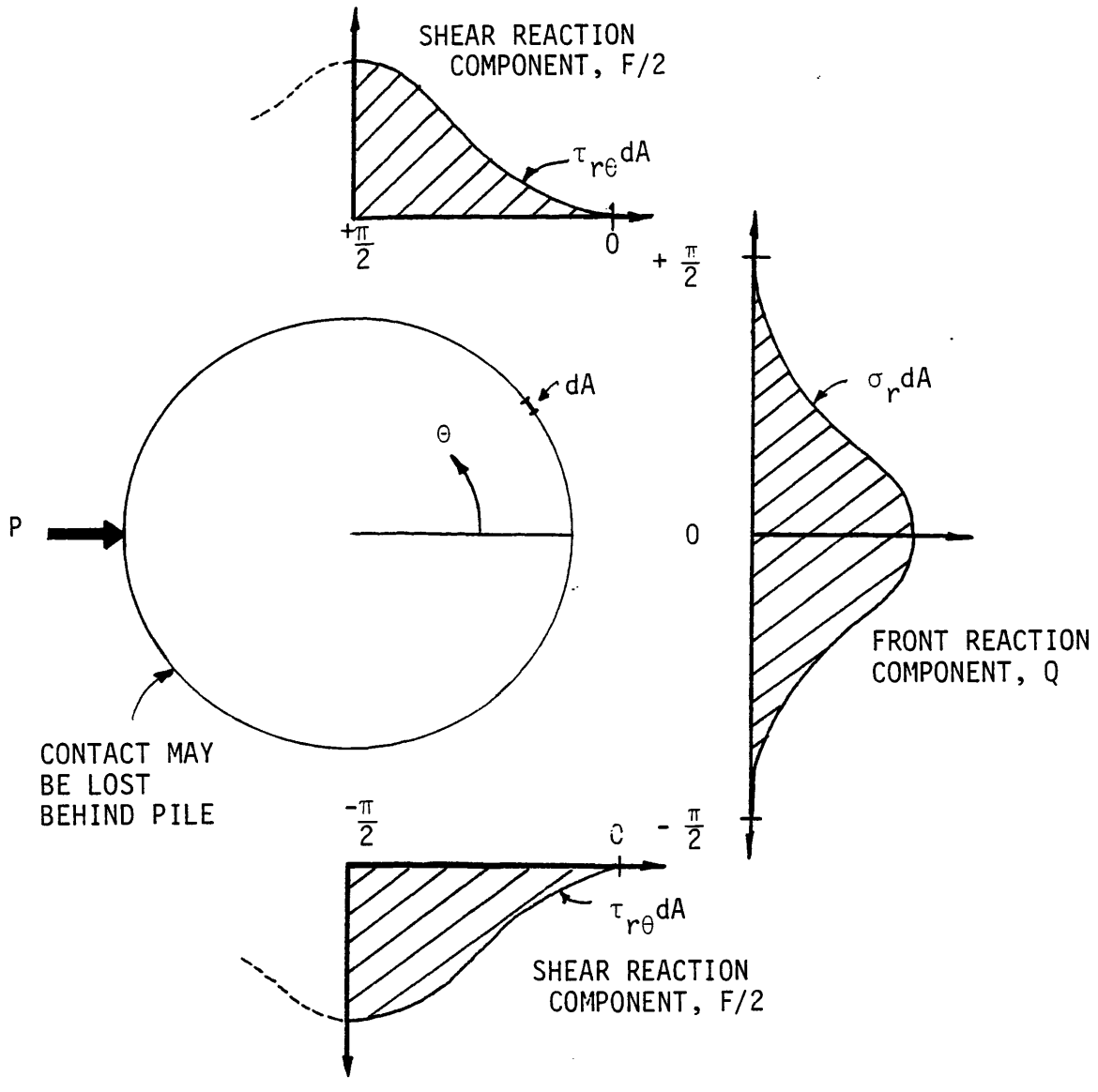

FIG. 31 - The Two Components Q and F Comprising the Lateral Force P

= 0.79 for circular piles

= 2(0.88) = 1.76 for square piles

By separation of the force P into the two components, Q and F, a theoretically rigorous construction of the P-y curve can be made. The separate effects of the pile installation technique and the relationship to the pressuremeter can also be assessed from field measurements on each curve separately.

Measurement of Q-y Curves

It is shown in Fig. 10 that in linear elasticity the radial pressure mobilized at the element immediately ahead of the pile is approximately one third of the radial pressure mobilized around the expanding pressuremeter at the same radial strain. For the plasticity approach it was shown previously that the ratio of the ultimate pressure mobilized across the projected width, or diameter, of the pile, p_u, to the limiting cavity pressure available from the pressuremeter, p_L, is of the order 2-3. Since p_u is considered an equivalent pressure uniformly distributed across the pile width, or diameter, the actual ultimate pressure measured at the front face will be less. The measured ratio $\frac{p_u}{p_L}$ may therefore be somewhat less than 2-3 and closer to unity. However, the effects of both stress relief and soil disturbance have been shown (11) to affect both the prebored pressuremeter and the pile over the full range of behavior. The actual relationship can be examined from the reported case histories of piles loaded laterally, instrumented with earth pressure cells, and where pressuremeter results are available.

For the site at Texas A&M University (13), for which details were given previously, the response of the pressure cells below the depth that the surface has any influence and the accompanying pressuremeter expansion curves are given in Fig. 32(a). At the depth of 4.5 ft (1.37m) on shaft No. II, pressure cells were also located at two additional positions around the circumference, at position A and position C. The theoretical distribution, based on the cell response at position B, and the measured response is shown on Fig. 32(b) Excellent agreement is found for the psuedo-linear range between the measured response of the pile and pressuremeter. A similar trend is reported by Bigot et al. (15) for a 36 in. (900 mm) pile vibrofloated through soft silt at Provins, France. The prebored pressuremeter gave very good agreement for the full range of pile movement, i.e. up to 20% radial movement.

The finite element studies reported by Baguelin et al. (7) suggested that disturbance effects on the mobilized front pressure reaction were small. It may be concluded that the effects of stress relief and disturbance have reduced the pressuremeter resistance by an order of 3 at the Texas A&M and Provins sites. Further, it is well recognized (11,62) that the linear modulus measured by the prebored pressuremeter is too low by this order of magnitude. For reasons of disturbance, different stress paths and large strains, the Centre d'Etudes Menard (1975) propose a range of values by which the calculated modulus should be divided to evaluate the Young's modulus of the undisturbed material.

The selfboring type of pressuremeter is generally considered to

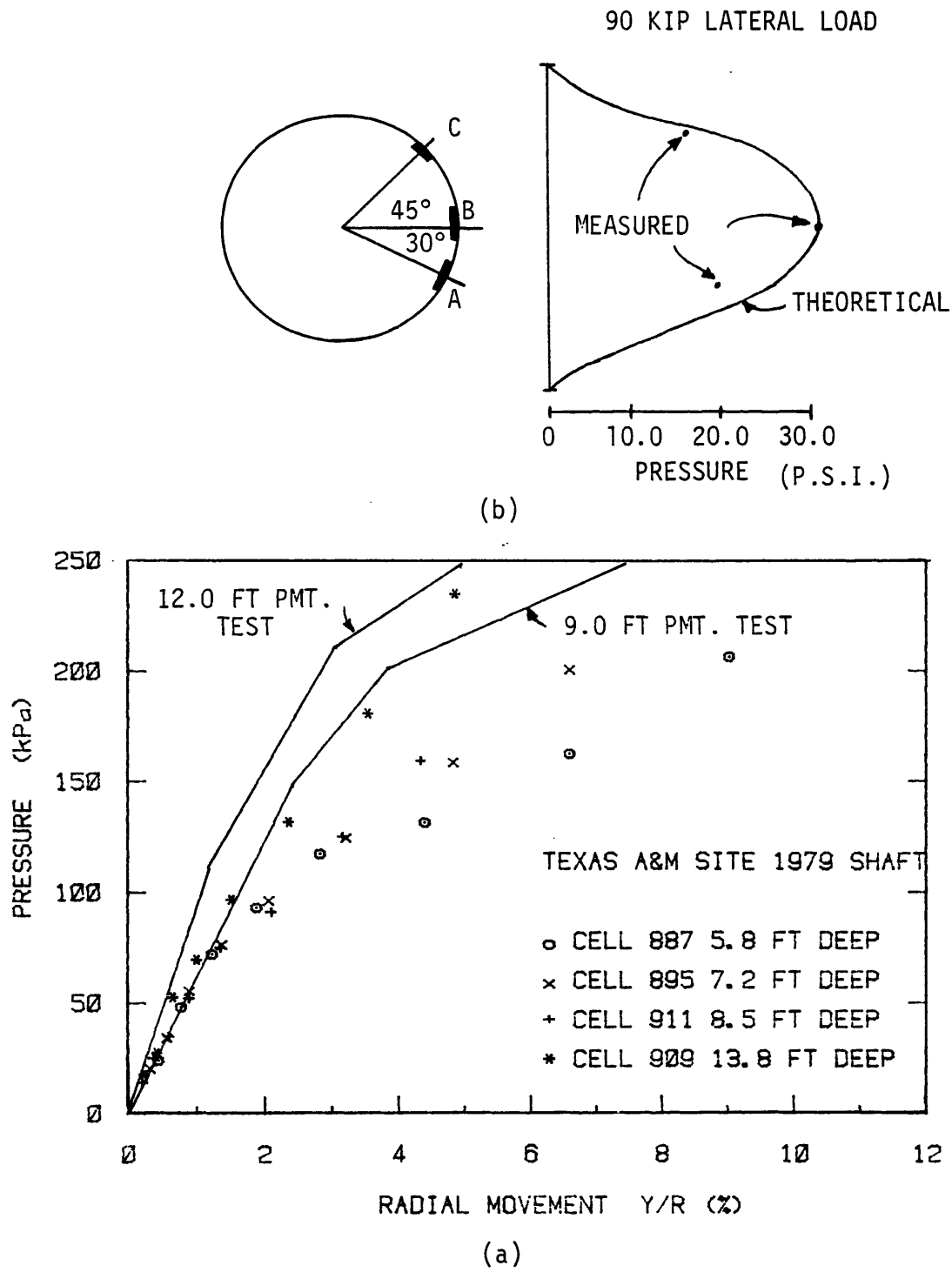

FIG. 32 - Measurement of the Front Reaction, Q, Curve at the Texas A&M Site

measure a secant modulus, at 2% circumferential strain, which is a better estimate of intact soil modulus. The piles tested at the Plancoet site had pressure cells and the site investigation included selfboring pressuremeter results. It is reported that the installation of the Larsen pile caused the properties of the soil to be reduced by 75% in a zone of thickness equal to 45% of the pile radius. The comparison of experimental and selfboring pressuremeter data are shown in Fig. 33. The trend of the pressuremeter curves gives a higher modulus and a greater degree of nonlinearity, resulting in a lower ultimate pressure, when compared to the pile. This relationship better approximates the theoretical relationship presented previously. The second series of tests reported at Plancoet, (6), confirmed this relationship. The piles were closed-in 'H' section piles instrumented with strain gages and pressure cells. The response of the cell at a depth of 5.3 ft (1.6m) for three tests and the corresponding selfboring pressuremeter curve are shown in Fig. 34. The higher pressuremeter modulus and slightly lower ultimate pressure predicted theoretically is again evident. Baguelin et al. (11) also report that the limit pressures reached by both the selfboring and prebored pressuremeter were in excellent agreement with the ultimate pressure reached by the pressure cells on the pile. In the case of this square pile the early onset of plastic yield near the front face edge would slightly decrease the slope of the pressure cell response.

In summary, from the experimental evidence, it is found:

(1) The pressure mobilized at the front face of the pile is well approximated in the pseudo linear range to the

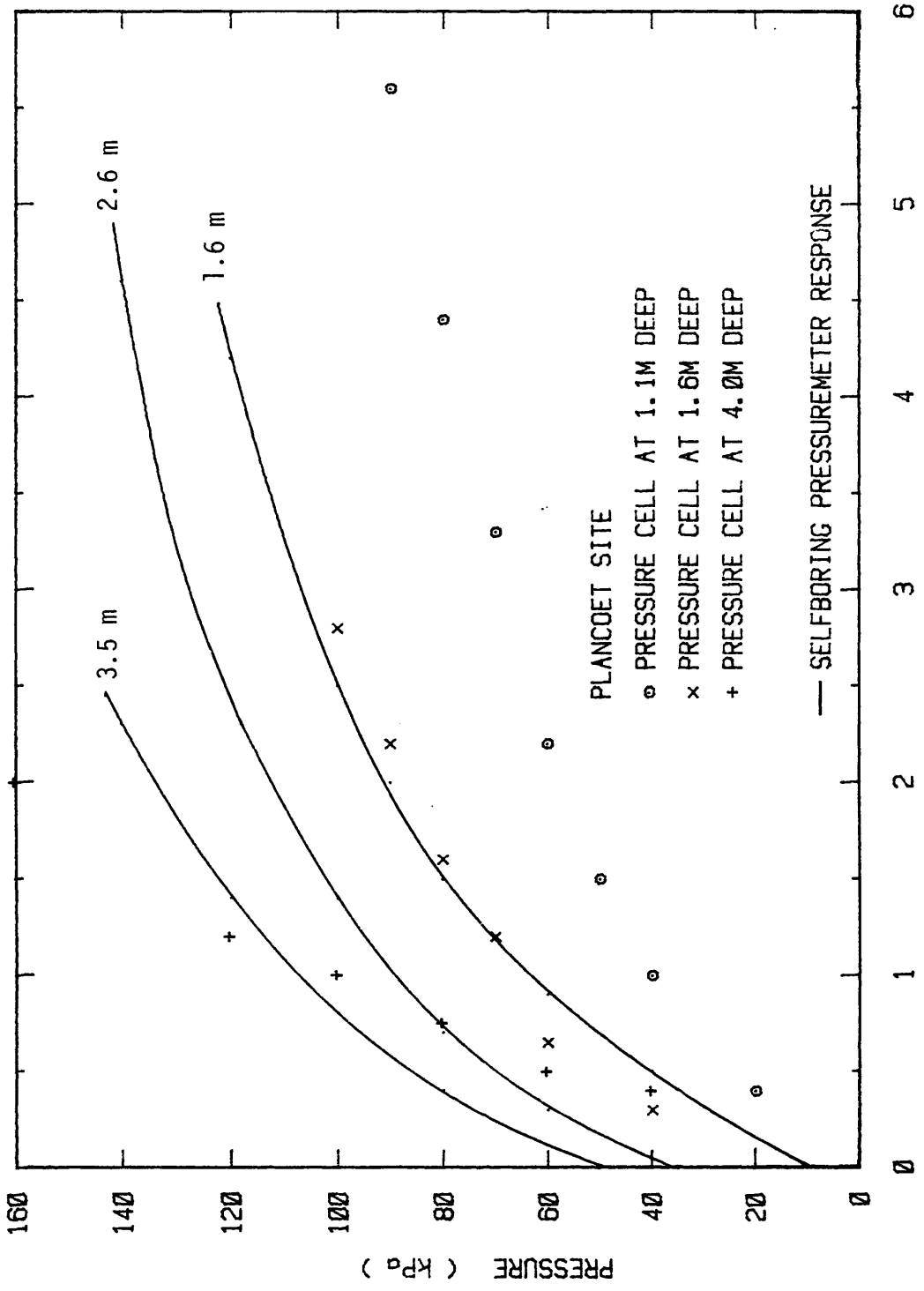

FIG. 33 - Measurement of the Front Reaction, Q, Curve at the Plancoet Site

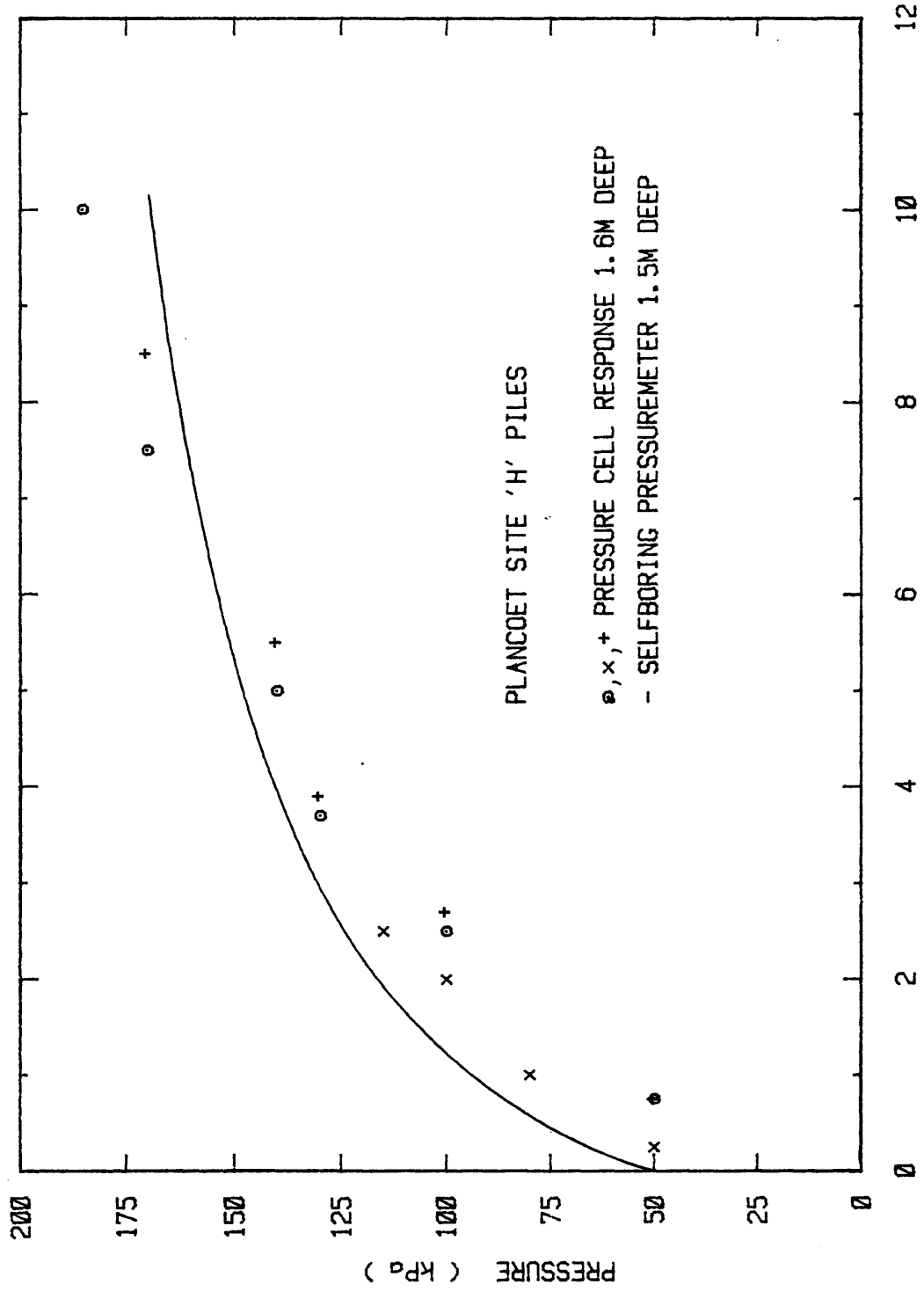

FIG. 34 - Measurement of the Front Reaction, Q, Curve at a Depth of 1.6 m Deep At Plancoet

pressure generated by an expanding preboring pressuremeter at equal radial movements, i.e. at equal y/R.

(2) This relationship is confirmed theoretically if the known 'softer' response characteristic of the preboring pressuremeter is considered.

(3) The selfboring pressuremeter closely approximates the theoretical relationship by minimizing stress relief and disturbance effects.

(4) The effects of soil disturbance and surface fissuring on the front pressure reaction by different pile insertion techniques is small.

(5) The effect of the lack of perfect pile to soil adhesion is considered small based on close theoretical to measured pressure responses.

(6) The evidence suggests that the ultimate pressure reached by the pile will exceed the net limit pressure from the prebored pressuremeter. However, experimental evidence is inconclusive; therefore the pressuremeter mobilized pressure is considered valid for all radial movements of the pile.

In conclusion it is proposed that the front pressure reaction curve, Q-y, be taken as

$$Q = (p - p_{OH}) \times SQ \times D \quad \ldots\ldots\ldots\ldots\ldots\ldots \quad (76)$$

where p = mobilized pressure from the prebored pressuremeter expansion curve

p_{OH} = initial state of horizontal stress in the ground

SQ = shape factor for pressure reaction

and y_1 = increase in radius of the probe from R_o

R_o = radius of the soil cavity at pressure p_{OH}

at a pile translation, y, from equal radial movements; therefore

$$y = y_1 \times \frac{R}{R_o} \quad \ldots\ldots\ldots\ldots\ldots\ldots\ldots\ldots \quad (77)$$

where R = pile radius.

Hence from Eq. 76 and Eq. 77 the coordinates of the net Q-y curve can be found. This curve is considered valid at the depth of the pressuremeter test if this depth is below the depth of reduced resistance close to the ground surface.

It is well recognized that the driving of a pile closed end, or of a plugged hollow pile, leads to soil disturbance and generally to higher horizontal ground stress around the pile. By lateral movement of the pile under load, the stress on the back of the pile is likely to be reduced down to the at rest pressure, or even reach the active state. In Eq. 76, p_{OH} is subtracted from p. This is equivalent to making the conservative assumption that the pressure in the back of the pile remains at p_{OH}. The value of p_{OH} should be assessed, prior to calculation of the front pressure reaction, from all information available from a site investigation including the pressuremeter results.

Measurement of F-y Curves

The construction of the F-y curve requires knowledge regarding the generation of lateral friction against the pile side. The technical literature contains case histories which studied the vertical mobilization of shear to resist axial loads but at the present time, none which report the measured generation of lateral friction.

The theoretical studies of Baguelin et al. (7) based on finite element model of Fig. 9(a) (p.35) are discussed previously. The studies show that with a Tresca yield criterion, the peak shear reaction was mobilized at approximately 1% circumferential strain in an undisturbed material. The amount of strain to mobilize the shear reaction in a disturbed material is reduced, together with the magnitude of the shear available. This is illustrated in Figs. 14(b) and 15(b) (p. 47and 48). From the field measurement of axially loaded piles (88) the amount of movement which mobilizes the peak shear resistance is not considered to be a function of diameter and is generally taken to be of the order of 0.1 in. (2.5 mm). The field experience with the 'Wave Equation' technique and the work of Smith (89) substantiates this.

The contribution of the front pressure to the total reaction can be evaluated from the field measurements of earth pressure against laterally loaded piles by using the technique described in the previous section. If the total reaction is known then the magnitude of the missing shear contribution can be found, but not its distribution. Briaud et al. (20) examined the Texas A&M and Plancoet sites, with a site at Grenoble [Dunand (30)] by this technique. From the Texas A&M

site, shaft III, at the applied lateral load of one half the ultimate (at which structual failure occurred) it was found that friction contributed 62% of the total horizontal resistance. At Plancoet the disturbance effects on the sensitive silt reduced the shear contribution drastically and only 18% of the applied moment was resisted by side shear. At Grenoble, large overturning moments were applied to a square augered rigid concrete shaft in soft plastic grey clay. It was found shear forces contributed 60% of the moment resistance at a factor of safety of 1.5 on the applied load. In all cases at the load level examined the full undrained shear strength was assumed to have been mobilized and equilibrium was close to being satisfied.

The simultaneous work of Baguelin et al. (10), Landanyi (54) and Palmer (73) produced a theoretical derivation of the full shear stress-shear strain relationship from the pressuremeter test. The only restrictions were homogeneity, incompressibility and axisymmetric deformation. Baguelin et al. (10) produced the relationship

$$\tau = x(1+x)\frac{dp}{dx} \quad \ldots\ldots\ldots\ldots\ldots\ldots\ldots\ldots\ldots\ldots \quad (78)$$

where $x = \frac{\Delta V}{V_o}$

ΔV = change in cavity volume from the initial volume V_o.

Further, x is numerically equal to twice the circumferential strain, ε_θ, at the edge of the borehole but of opposite sign. The conditions

of material incompressibility and plane strain imply that

$$\varepsilon_r + \varepsilon_\theta \simeq 0 \quad \ldots\ldots\ldots\ldots\ldots\ldots\ldots\ldots\ldots\ldots (79)$$

where ε_r = radial strain

and the maximum shear strain at the edge of borehole is given by

$$\gamma = \varepsilon_r - \varepsilon_\theta \simeq 2\varepsilon_\theta \quad \ldots\ldots\ldots\ldots\ldots\ldots\ldots\ldots (80)$$

where $\varepsilon_\theta = \dfrac{\text{Increase in cavity radius from initial cavity radius}}{\text{Initial cavity radius}}$

The derivation of Palmer gives

$$\tau = \frac{1}{2}\ \varepsilon_\theta(1 + \varepsilon_\theta)\ (2 + \varepsilon_\theta)\ \frac{dp}{d\varepsilon_\theta} \quad \ldots\ldots\ldots\ldots\ldots (81)$$

where ε_θ is considered positive and if

$$\frac{2 + \varepsilon_\theta}{2} \simeq 1 \quad \ldots\ldots\ldots\ldots\ldots\ldots\ldots\ldots\ldots\ldots (82)$$

then Eq. 81 and Eq. 78 are approximately equal. Further, in small strain, $1 + \varepsilon_\theta \simeq 1$ and both equations reduce to the following simple geometric construction.

$$\tau \simeq \varepsilon_\theta \frac{dp}{d\varepsilon_\theta} \quad \ldots\ldots\ldots\ldots\ldots\ldots\ldots\ldots\ldots (83)$$

Typically the peak shear stress is mobilized at a shear strain of less than 10% in the pressuremeter test.

The effects of drainage in the material during the expansion of the pressuremeter were theoretically explored by Wroth and Windle (105). In soft fully saturated clays the assumption of undrained behavior is close to being satisfied for the strain controlled test lasting approximately 10 minutes. However, sands, silts and fissured overconsolidated materials may undergo partial or full drainage during the test. Wroth and Windle showed that if full drainage occurred in a contracting material then the error in finding the mobilized shear stress, τ, by using the undrained analysis given by Eq. 81 is an underestimation of the peak strength of approximately 15%. The point is made that the actual soil strength mobilized in a partly drained test is greater than the undrained strength. In consequence the above differences may cancel and the undrained analysis may yield a shear strength close to the undrained value. For a dilatant dense sand the derived shear stress, if calculated on the incorrect basis of an undrained analysis, would be overestimated by 25%-30%. At present the measurement of volumetric strain during a pressuremeter test is impractical. It can also be shown that using the small strain approximation of Eq. 83 gives a 9% underestimation of the actual mobilized shear strength at a circumferential strain of 6%.

The known 'softer' response of the prebored pressuremeter is a characteristic discussed in the previous section. This factor further distorts the stress strain curve derived from a prebored test and it is recognized the relationship is of the trend shown in Fig. 35. Evidence

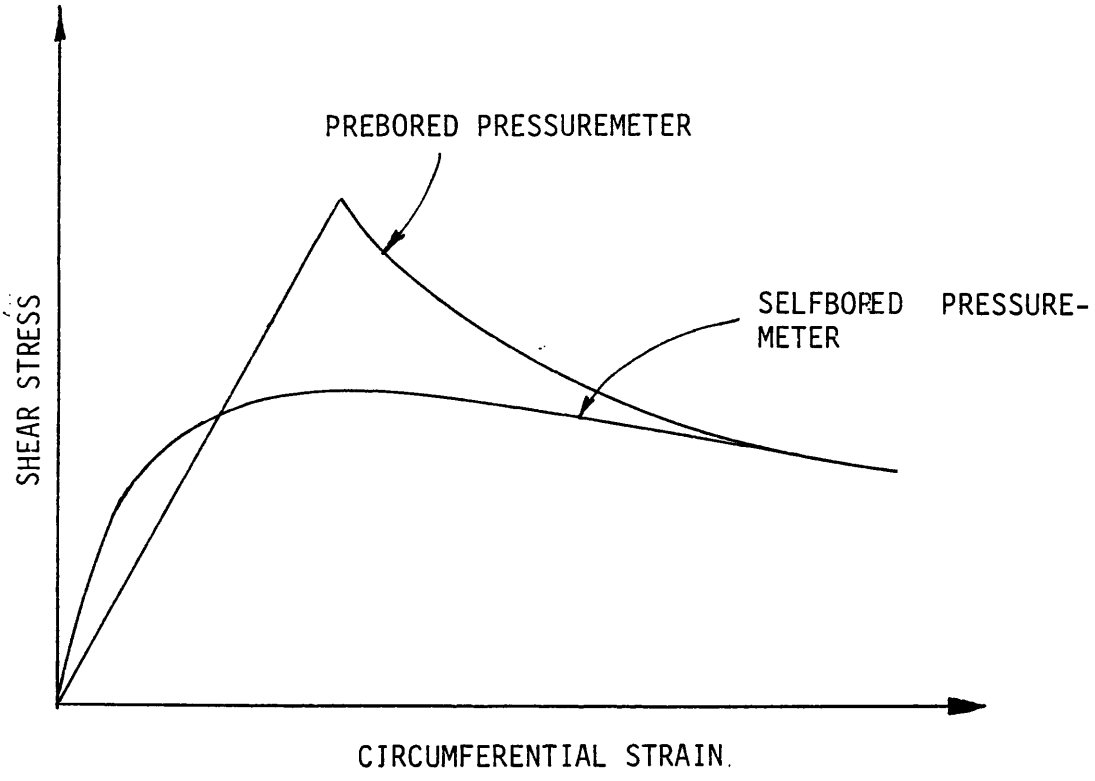

FIG. 35 - Comparison of the Derivation of Shear Stress from Prebored and Selfbored Pressuremeters

from the technical literature, Baguelin et al. (11), Marsland and Randolph (62), Windle and Wroth (100), suggests that a reload modulus from an unload-reload cycle is comparable to the results from the initial curve from a selfboring unit. Further, the mobilization of shear stress against the pile side to generate the F-y curve is clearly dependent upon the contact stresses which exist against the pile. In consequence the effects of pile installation technique, and any resulting soil disturbance, would seriously affect the mobilized shear stresses in the highly local zone against the pile face. Therefore, derivation of the F-y curve, for some piles from the reload pressuremeter behavior may be more appropriate.

It is proposed to construct the friction reaction contribution curve, F-y, from the mobilization of shear stress in a prebored pressuremeter test from Eq. 78 [after Baguelin et al. (11)] i.e.

$$\tau = x(1+x)\frac{\Delta p}{\Delta x} \quad \ldots\ldots\ldots\ldots\ldots\ldots\ldots\ldots \quad (84)$$

and

$$F = \tau \times Dx \times SF \quad \ldots\ldots\ldots\ldots\ldots\ldots\ldots\ldots \quad (85)$$

This shear reaction is mobilized at equal radial movements for both the pressuremeter and pile.

Therefore

$$\frac{y_{pile}}{R_{pile}} = \frac{y_{pmt}}{R_{pmt}} \quad \ldots\ldots\ldots\ldots\ldots\ldots\ldots\ldots \quad (86)$$

which gives

$$y_{pile} = y_{pmt} \frac{R_{pile}}{R_{pmt}} \quad \ldots\ldots\ldots\ldots\ldots\ldots\ldots\ldots \quad (87)$$

and corresponds to Eq. 77.

Assembling the P-y Curves

In the previous two sections, proposals were made to construct the front reaction contribution, Q, and the shear reaction contribution, F from the prebored pressuremeter test. These two reactions, which are functions of the pile shape in cross section and projected diameter, are separate components of the required P from the P-y curve and thus

$$P = Q + F \quad \ldots\ldots\ldots\ldots\ldots\ldots\ldots\ldots \quad (88)$$

at equal radial movements. A P-y curve constructed from the initial probe expansion curve is called the initial criteria, and from a single unload-reload cycle is called the reload criteria. The unloading cycle should commence after the completion of the linear range on the initial loading cycle at point A on Fig. 36. By consideration of an elastic plastic model, this point corresponds to the onset of plastic yield in the soil at the elements around the soil cavity. Unloading should be continued until the pressure reaches the earth pressure at rest condition and then the reloading takes place up to the limit pressure.

The sequence of calulations is

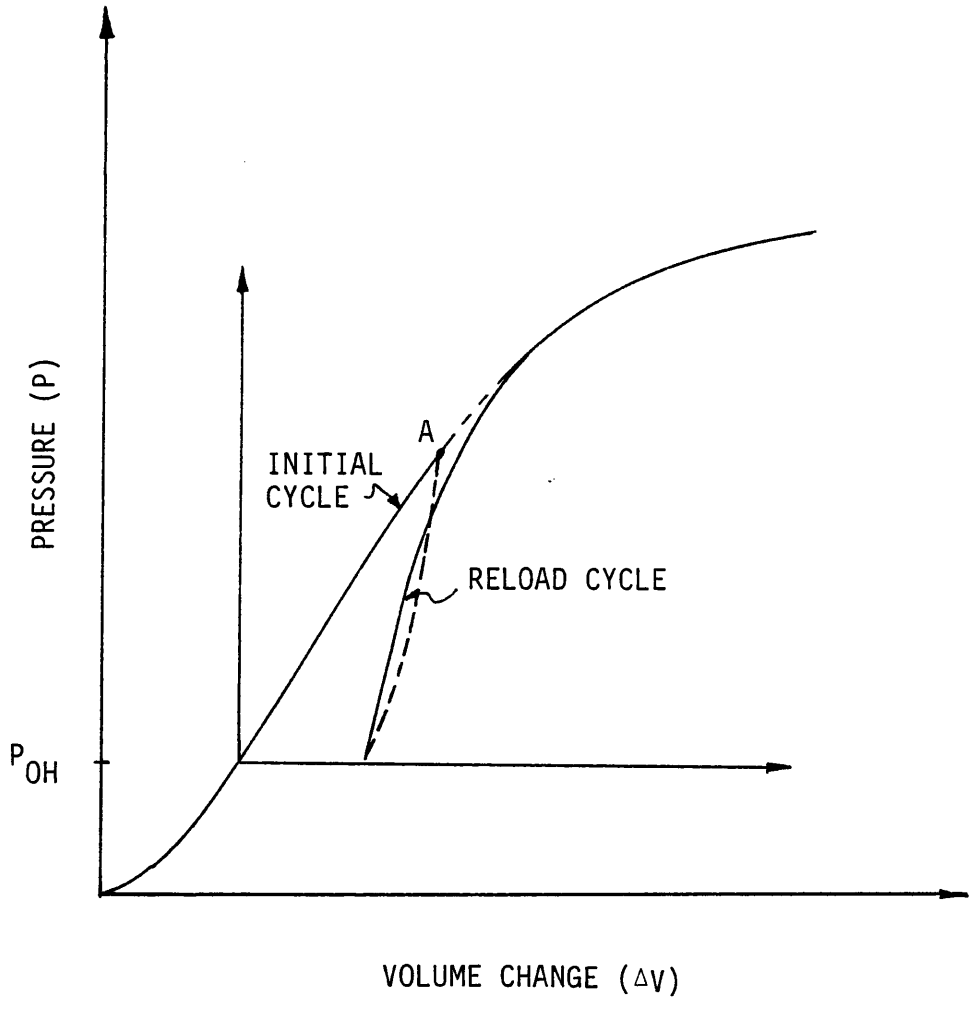

FIG. 36 - Typical Pressuremeter Curve
with Initial and Reload Cycles

$$p^* = p - p_{OH} \quad \ldots\ldots\ldots\ldots\ldots\ldots\ldots\ldots \quad (89)$$

then $$Q = p^* \times SQ \times D \quad \ldots\ldots\ldots\ldots\ldots\ldots\ldots \quad (90)$$

where p = pressure in the soil cavity

p_{OH} = horizontal earth pressure at rest

SQ = pile shape factor for Q (p.79) approximatedby

= 0.75 for circular piles

= 1.0 for square piles

D = pile projected diameter or width

and $$\tau = x(1+x)\ \frac{dp^*}{dx} \quad \ldots\ldots\ldots\ldots\ldots\ldots\ldots \quad (91)$$

Then $$F = \tau x\ SF \times D \quad \ldots\ldots\ldots\ldots\ldots\ldots\ldots \quad (92)$$

where $$x = \frac{\Delta V}{V_o}$$

ΔV = change in cavity volume from earth pressure at rest condition.

V_o = initial cavity volume corresponding to earth pressure at rest

$\frac{dp^*}{dx} \simeq \frac{\Delta p^*}{\Delta x}$ = tangent modulus at p^*

τ = mobilized shear stress against the pile

The shape factor SF is increased from those values cited earlier, due to the additional contribution from shear behind the pile.

SF = pile shape factor for F

= 1.0 for circular piles

= 2.0 for square piles.

A short computer program titled PYGEN, has been written in Fortran IV to complete this series of calculations and is detailed in Appendix III.

The final form of the P-y curve is shown to be highly sensitive to the derivation and mobilization of the shear reaction curve, F. Previously the disturbance effects on the prebored pressuremter test and pile were discussed. The existing theoretical and experimental evidence suggests that the pressuremeter modulus is sensitive to borehole remoulding. Both Baguelin et al. (11) and Lukas and de Bussy (60) have suggested that the reload cycle modulus of the prebored test can be used to obtain an intact, 'undisturbed' modulus. Since, during the probe expansion, the radial stress increases while the circumferential stress decreases, the resulting modulus is probably an average of both an unloading and a loading modulus.

For the pile, the theoretical studies have shown only the shear reaction to be sensitive to soil disturbance upon installation. The mobilized peak shear and the radial movement necessary to reach that peak are both drastically reduced by the presence of only a moderate zone of remoulded soil. In the case of a strain softening, overconsolidated stiff fissured clay, the P-y curve can also be expected to show

a peak at, or around, the peak shear stress (usually less than ε_θ= 5%).

Driving a full displacement pile into a cohesionless material is likely to increase the horizontal stress and improve the mobilized shear stress. This increased horizontal stress is perhaps a better origin for the shear reaction mobilization but is contained in a highly local zone against the pile wall. This suggests the use of the reload cycle for friction curve but the larger zone influenced by the front reaction warrants use of the initial loading curve.

Further evidence for consideration of the reload cycle is found in Menard's work (66). Excessive deflection of the pile at the ground surface only mobilize small movements of the pile at depth. Consequently both small 'micro-deformation' and 'large-deformation' moduli are required. Menard recognized that the pressuremeter is measuring a 'large-deformation' modulus. It is suggested that the reload cycle gives a closer secant modulus at small strain for 'micro deformation'.

Clearly predicting stress states around the pile, disturbance effects, and the resulting net effect on the final P-y curve is a complex task. From the evidence available and by consideration of the previous discussion two criteria are available. A) use the initial loading curve for obtaining the P-y curve, and B) use the reload cycle. One limitation of the reload cycle criteria is that less volumetric strain is available upon reinflation of the probe since permanent deformation occurs on the initial cycle. However, the ultimate value of P from both criteria will usually coincide.

THE CRITICAL DEPTH

The Phenomenon

There are many geotechnical problems in which the presence of the unrestrained ground surface radically alters the stress and deformation fields which are generated. As the vertical distance to the ground level increases the deformation pattern changes until a depth is reached where no further changes with depth take place, and hence no direct influence is present from the surface. Natural soils frequently exhibit an increase in modulus with confining pressure, or depth, and therefore load deformation relationships for the field problems may still exhibit a stiffer response with depth. A critical depth, D_c, is defined as the depth, above which, deformation fields are influenced by the presence of the ground surface.

All reported research has focused on calculating the critical depth at ultimate load only, taking no account of the critical depth phenomenon at small deformations. Akinmusru (1), by experimental observation, reported that the critical depth of a long ground anchor in sand, $\phi = 35^{o}$, was 6.5 times the anchor vertical height. Audibert and Nyman (4) defined three failure mechanisms; shallow, intermediate and deep for circular buried pipelines moving horizontally in sand. The depth of transition between shallow and intermediate was 3 pipe diameters and between intermediate to deep was between 12-24 pipe diameters. For axially loaded piles in clay the point bearing is

maximum at 4 pile diameters, and between 10 and 30 diameters for loose and dense sand respectively.

A critical depth also exists for the laterally loaded pile and, all researchers agree, the zone is of paramount importance due to the major contribution to the total resistance offered by these surface layers. Within these layers the deformation is not in plane strain around the pile but has significant vertical components. Further, the deflections reached may also be sufficient to lose contact entirely with the soil at the ground level behind the pile, a phenomenon observed in the field.

In the analysis of the pressuremeter test, plane strain axisymmetric deformation conditions are assumed to be valid. However, Baguelin (6), Jezequel (46) and Briaud and Shields (19), all recognize a critical depth of reduced resistance exists and influences the pressuremeter limit pressure p_1. But much uncertainty exists as to whether the pressuremeter modulus is subject to a depth of reduced resistance but the assumption of plane strain is also invalid during the modulus range (11).

If the pressure mobilized by the expanding probe is reduced within the pressuremeter's critical depth then this should be taken into account before deriving the corresponding P-y curve for the pile.

In the final development of the technique to predict lateral load P-y curves from pressuremeter results, two separate critical depth phenomenon must be superimposed. The first is the pressuremeter critical depth phenomenon and the second is the pile critical depth

phenomenon.

Existing Approaches

The Pile

The work of McClelland and Focht (71), and the subsequent reported discussion, was the earliest clear evidence that the critical depth of reduced resistance, D_c, for a laterally loaded pile warranted investigation.

By replacing the circular cross section with a square pile section two separate modes of failure for shallow and deep failure were defined by Reese (79). At a depth below D_c a stress 'block' approach, Fig. 37(a), was used in plane strain; the stress behind the pile was taken as zero for a cohesive material. It was then found that the ultimate force per unit depth, P_u, is given by

$$P_u = 12\ C_u\ D \quad \ldots\ldots\ldots\ldots\ldots\ldots\ldots \quad (93)$$

The shallow failure was idealized as a passive wedge of material moving up in front of the displaced pile, Fig. 37(b). By equilibrium and assuming the wedge angle, θ, is 45^o, the value of the force P_u can be obtained. At the ground surface the formulation yields

$$P_u = 2\ C_u\ D \quad \ldots\ldots\ldots\ldots\ldots\ldots\ldots \quad (94)$$

The critical depth of reduced resistance is then found by equating the

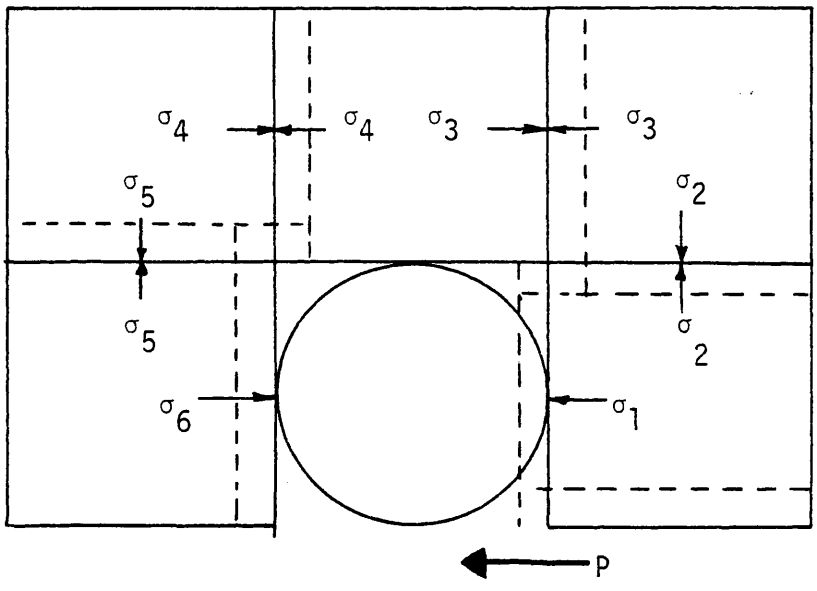

(a)

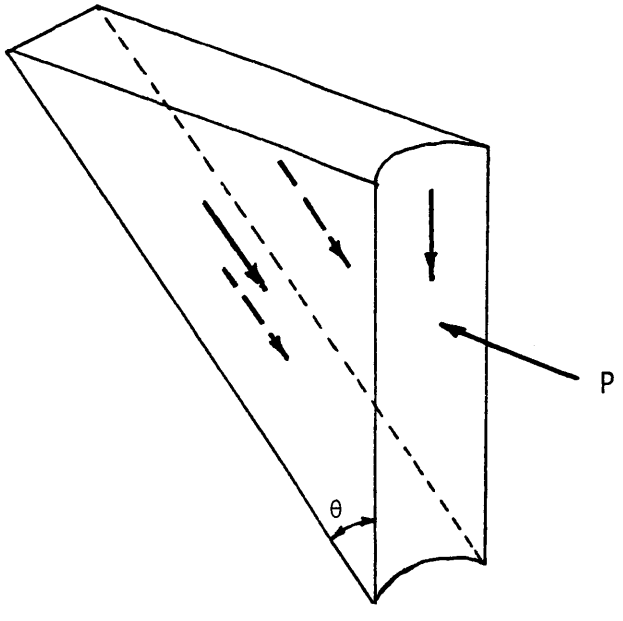

(b)

[after Reese (78)]

FIG. 37 - Deep and Shallow Failure Mechanisms in Clay

derived expression for the wedge failure with plane strain stress block failure and was reported as approximately 3 pile diameters below the ground surface.

A similar wedge, Fig. 38, and stress block failure mode was proposed and analysed by Frazier and Reese (33) for cohesionless materials. The critical depth is found by equating the derived equations and by assuming no vertical shear stresses develop between the pile and soil, straight line failure surfaces, and mobilization of active pressures on the pile back.

Broms (21) accepts the values presented by Reese for the cohesive case at the ground surface and proposes ignoring any generated soil resistance in the top zone, 1.5 pile diameters deep. Thereafter a maximum value of mobilized pressure of 9 C_u is recommended constant with depth. For cohesionless materials the recommended maximum earth pressure within 1 pile diameter is the maximum passive pressure and below this depth, due to soil arching, the maximum attainable is 3 times the passive pressure. Hansen (38) generalized the equations for the c-ϕ soil ; for the cohesive case, given by Eq. 66, D_c is approximately 3 pile diameters. For the cohesionless soil, a critical depth does not exist since the ultimate force, P_u, which can be developed, is a linear function of the overburden pressure.

Based on evaluation of the soil response by the pressuremeter Baguelin et al. (11) suggest the stiffness at the ground surface is 1/2 the value at depth and D_c is of the order 2 pile diameters for cohesive materials and 4 pile diameters in cohesionless soils.

The accepted state of the art expression to evaluate the increase

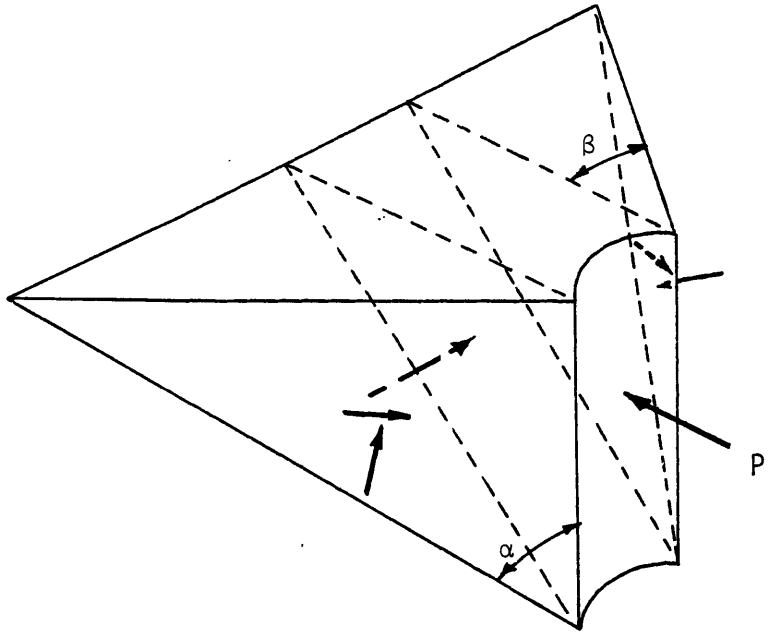

[after Frazier and
Reese (32)]

FIG. 38 - Shallow Failure Wedge in Sand

in soil spring force is that derived from the shallow wedge failure and at depth plane strain flow. In general terms the ultimate resistance may be expressed for clays as:

$$P_u = (L + \frac{\sigma'_z}{C_u} + J \frac{z}{D}) C_u \quad \ldots\ldots\ldots\ldots\ldots\ldots\ldots \quad (95)$$

where C_u = average undrained shear strength within depth z for stiff clays, or undrained shear strength at depth z in soft clays

σ'_z = effective overburden pressure at depth z

z = depth considered

L = surface resistance factor

J = empirical adjustment constant

Eq. 95 comprises three separate contributions; the first term is the surface resistance, the second is the increase in resistance available from the overburden pressures and the third term is a geometric contribution. The apparent inconsistency of deriving a total stress unit from effective stress units is from the semi-empirical nature of the equation. The parameter J was introduced to correct the theoretical predictions to agree with the field 'measured' ultimate forces from instrumented pile load tests. The measured range of the parameter J is reported as 0.5 for the Sabine site (cited earlier) to 2.83 at the Manor site (cited earlier). No apparent relationship exists between J and undrained shear strength.

Recent investigators have studied the results of field lateral

load tests and suggested modifications to the empirical parameters, without theoretical basis. Stevens and Audibert (93) proposed that the ultimate lateral soil resistance was reached at a distance 4 times the pile diameter and gave a recommended distribution with depth based on observed values. The resistance available at the surface was found to be

$$P_u = 5\ C_u\ D \quad \ldots\ldots\ldots\ldots\ldots\ldots\ldots\ldots\ldots\ldots \quad (96)$$

and below D_c was given by

$$P_u = 12\ C_u\ D \quad \ldots\ldots\ldots\ldots\ldots\ldots\ldots\ldots\ldots\ldots \quad (97)$$

Bushan, Haley and Fong (24) reported the results of 12 drilled piers in stiff overconsolidated clays and gave recommendations based on a parametric study of the empirical factors. From these studies, the variations of the factors, within their recommended ranges, gave changes in predicted groundline deflection of over 100%.

For clays the increase in the ultimate soil reaction within the critical depth may be expressed as follows

$$P_u = N_p\ C_u\ D \quad \ldots\ldots\ldots\ldots\ldots\ldots\ldots\ldots\ldots\ldots \quad (98)$$

where N_p = lateral capacity factor.

With this notation a summary of the existing approaches is given on Fig. 39.

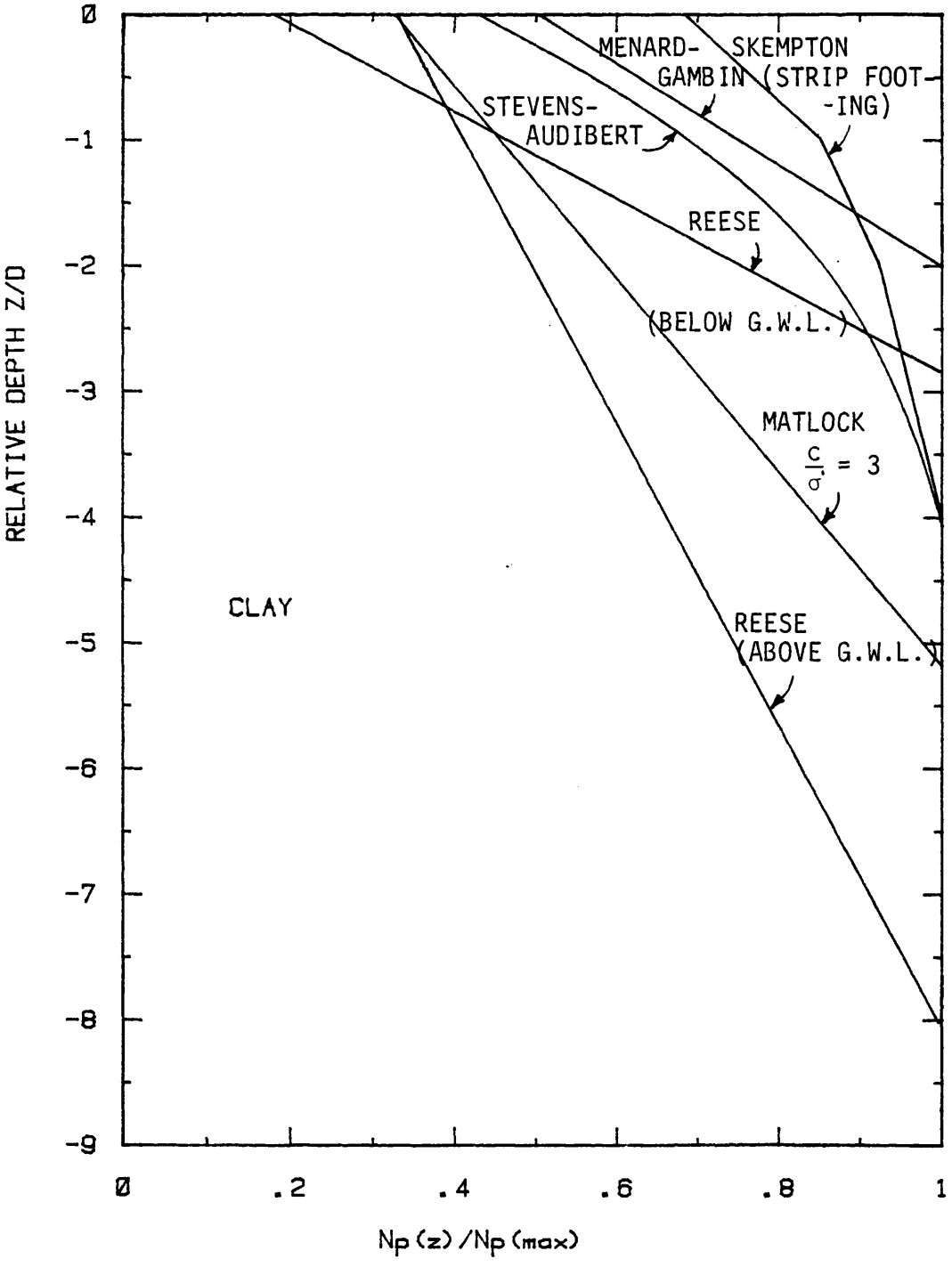

FIG. 39 - Summary of the Existing Approaches to Critical Depth in Clay

In sands the wedge and stress block failure also form the theoretical basis for predicting D_c, and the reduction in ultimate soil reaction available to the surface. The comparison between the theoretical and 'measured' ultimate soil reactions at Mustang Island were found to be very poor and the following equation is proposed by Reese, Cox and Koop (83).

$$P_u = A\,P_c \quad \ldots\ldots\ldots\ldots\ldots\ldots\ldots\ldots \quad (99)$$

where A = empirical adjustment factor

P_c = ultimate reaction from theory.

Further, A is a function of depth varying from 2.9 at the surface to 1.0 at 4 pile diameters below the ground level for static loading. In general, the calculated value of D_c is in excess of 10 pile diameters.

Meyerhof, Mather and Volsandkar (69) correlated Menard pressuremeter results and the critical depth ratio, D_c/D, for sand. For loose sand, $\phi = 30^o$, the ratio is approximately 10 and in dense sand, $\phi = 45^o$, increased to approximately 30. The technique used to record D_c from field load tests is not reported and no recommendations are given for the reduction in resistance within the critical depth. Below D_c it is suggested the ultimate soil resistance can be measured directly by the pressuremeter.

For sands by defining a reduction factor, RF, as

$$RF = \frac{\text{soil reaction mobilized at } Z}{\text{soil reaction mobilized at } D_c} \quad \ldots\ldots\ldots \quad (100)$$

the existing approaches to the critical depth problem can be summarized and are shown on Fig. 40.

It is increasingly clear that there is a lack of agreement, and even conflict, in the current approaches to the critical depth problem for a laterally loaded pile. The prediction of soil stiffness at these shallow depths is of paramount importance if the governing soil P-y curve is to be accurately measured. All existing theories ignore the pile geometry (normally idealizing a square section), and are valid for ultimate conditions only. Pile flexural stiffness is ignored as a controlling variable and the calculated soil reactions are far from substantiated by field measurements. Further, the practical modifications suggested to improve the existing criteria are directed toward improving the critical depth predictions. These modifications have all been empirical in nature.

The recent advances in application to geomechanics of the finite element method, FEM, have permitted a more detailed study of the problem, but solution of the general 3-dimensional pile problem with material and geometric nonlinearity is still beyond reach. Thompson (96) by the use of the FEM, reports a range of N_p values at a depth of 12 pile diameters of 5.7 to 10.93. Angelides and Roesset (3) employed the FEM to incorporate nonlinear soil behavior, slippage and plasticity. By a study of increasing pile stiffnesses and length, in a uniform material

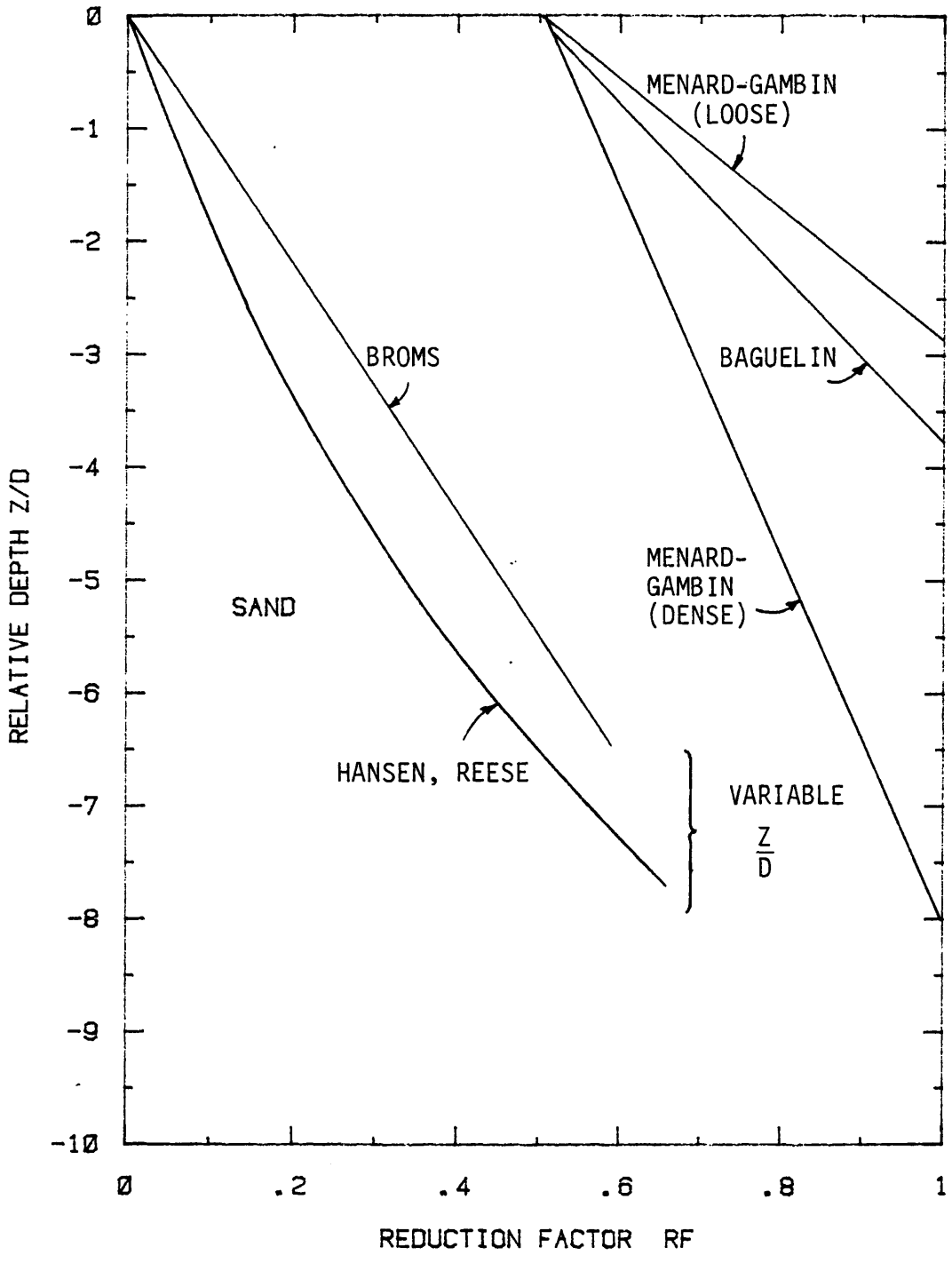

FIG. 40 - Summary of the Existing Approaches to Critical Depth in Sand

of constant shear modulus and Poisson's ratio, they illustrated that the critical depth of reduced resistance is not constant. For the soil springs under increasing lateral load, D_C increased by almost 100% and may therefore be idealized as a wave front. This suggests that D_C is not only a function of pile diameter and soil properties, but of displaced soil volume. Pise (76) illustrated that the depth of the surface layer controlling the pile behavior is a function of the relative pile to soil flexibility. The stiffer the soil modulus the smaller the depth of the controlling layer.

In summary, the current procedures available to reduce the mobilized soil spring response within the critical depth of reduced resistance appear inadequate. By consideration of earth pressure theories the mobilized front reaction, Q , contribution to the soil spring force P is clearly reduced by the critical depth phenomenon. The same cannot be stated for the shear contribution, F. The critical depth phenomenon for the nonlinear soil spring would appear to be not only a function of pile diameter but a complex interaction phenomenon influenced by plasticity, pile rigidity and the volume of displaced soil.

The Pressuremeter

Very little experimental work is available with respect to the critical depth phenomenon for the cavity expansion of a pressuremeter. Further, all theoretical approaches developed to analyze pressuremeter results must include plane strain and axisymmetric deformation to proceed. During the expansion of the probe, radial stresses, σ_r, and

circumferential stresses, σ_θ, are considered principal stresses.

For pressuremeters designed with a single cell, the experimental work with radiograph and lead shot techniques, reported by Wroth and Hughes (104) and Suyama, Ohya and Imai (94), confirm the close approximation to plane strain deformation. Over the total length of the monocell probe used by Suyama, Ohya and Imai, with a length to diameter ratio of 10:1, differences in probe expansion compared to a three cell unit were less than 5%. However, if the test is conducted within close proximity of the ground surface,a component of vertical strain is introduced and the radial stress is no longer a principal stress due to the mobilization of vertical shear stress.

For the shallow test, the deformation pattern around the probe is altered and a plane of symmetry is no longer created through the probe center line. If failure is governed by the Mohr-Coulomb criterion then failure is initiated when a critical ratio between major and minor principal stresses is reached. Wood and Wroth (102) point out that if the vertical stress began, and remained, the major principal stress, as is the case for some shallow tests, then plane strain assumptions are invalid due to the failure occuring on the non-vertical z:θ plane, Fig. 41. For failure to be initiated between the radial stress, as the major principal stress, and the circumferential stress a rotation of principal stresses has occured.

Briaud and Shields (18) report a series of tests conducted in the laboratory and in the field specifically to explore the critical depth phenomenon. Surface deformation was recorded during expansion of the

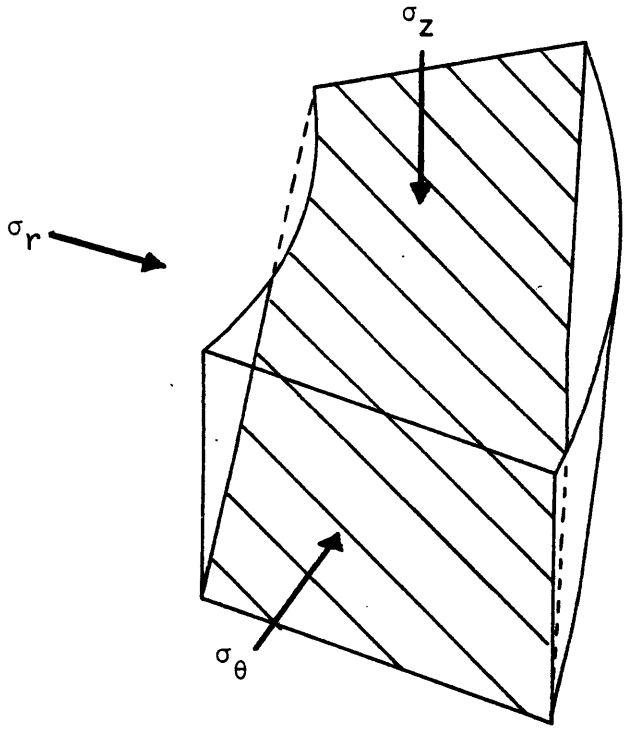

FIG. 41 - Failure on the Z:θ Plane for the Pressuremeter

pressuremeter and it was concluded that the surface was not involved in the deformation process beyond a depth of 20 probe diameters at full inflation. No critical depth could be clearly identified for the pseudo-elastic expansion phase of the pressuremeter test. These conclusions substantiated the comments of Menard (67) and Jezequel et al. (46) in confirming the existence of a critical depth, at least for limit pressure. Baguelin et al. (11) state the Menard pressuremeter critical depth is approximately 3 ft (1 m) in clay and 6 ft (2 m) in sand. This corresponds to around 20 and 40 probe diameters respectively.

Measured Pile Critical Depths from Reported Case Studies

Definition

Previously the technique of using strain gage instrumented piles to develop the mobilized 'measured' soil P-y curves was described. This technique was successfully used on some of the piles described previously. These sites include Houston and Manor in stiff clay, Sabine and Lake Austin in soft clay and Mustang Island in a uniform sand. These load tests represent the most complete series of case histories at which soil reaction distributions, with depth, are available. A characteristic of these sites was their uniformity of soil conditions and properties with depth. This highlights the critical depth effects. In addition, an offshore Louisiana lateral load pile test was conducted on an instrumented 2 ft (0.6 m) tubular steel pile, driven to

a penetration of 75 ft (23 m), reported by Parrack (74). By the double differentiation and integration process described previously the variations of soil reaction and deflection with depth were calculated, and presented by Parrack. The P-y curves were assembled and reported by McClelland and Focht(70). Finally, a total of three lateral load tests were reported by Bierschwale and Coyle (13) during which the distribution of mobilized soil pressures was measured directly, with depth, under increasing loads.

Examination of the variation with depth of mobilized soil reaction, P, or soil pressure, p, and deflection, y, for all case histories, gives the characteristic distribution near the surface shown in Fig. 42. For a material with uniform properties and if no D_c exists, the soil spring modulus, E_s, is constant with depth. Rearranging Eq. 6 gives

$$P = E_s y \quad \ldots\ldots\ldots\ldots\ldots\ldots\ldots\ldots\ldots\ldots \quad (101)$$

and hence increases in deflection cause an increase in soil reaction. If this hypothesis were true then the distribution of soil reaction is equivalent to the distribution of pile horizontal deflection, line A on Fig. 42. If the soil model becomes an elastic-plastic model, constant with depth, then at a certain deflection the soil reaction remains constant. This is represented by line B on Fig. 42. It is well accepted that in sands the modulus of deformation is a function of confining pressure, or depth. A closer assumption would be an increase

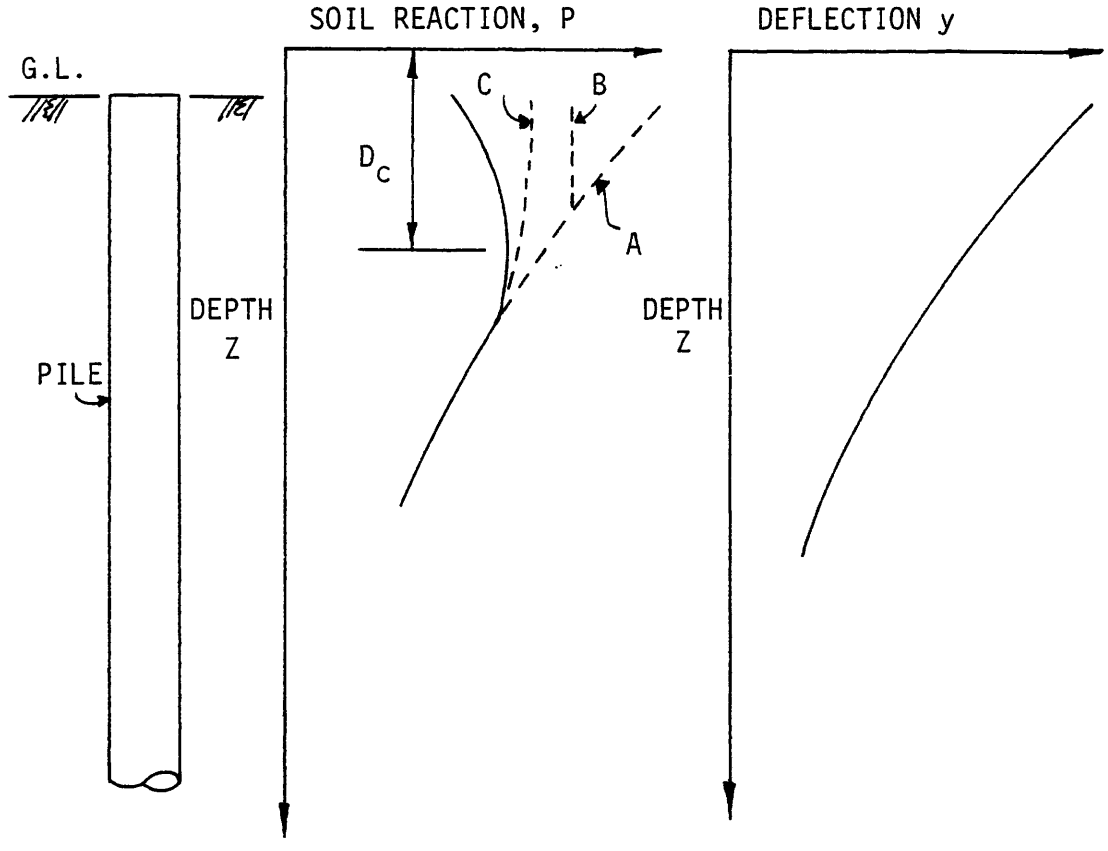

FIG. 42 - Characteristic Distribution of Soil Reaction with Depth

in the spring soil modulus of the form

$$E_s = k\, z^n \quad \ldots\ldots\ldots\ldots\ldots\ldots\ldots\ldots\ldots\ldots \quad (102)$$

where k = modulus constant

z = depth below the ground surface

n = exponent.

Typically, the exponent is less than unity and from a non-dimensional solution (65) it can be shown that the variation of soil reaction is given by line C.

It is apparent that the reduction in soil reaction from the peak which is observed on field load tests is a measure of the surface effects. A conservative assumption is to consider the peak soil reaction as representing the maximum attainable reaction without a depth effect. It is proposed to consider the depth to the peak reaction as the critical depth.

Measured Behavior of Critical Depth

Using the previously presented technique of identifying the effects from the surface on the soil spring reaction, each field load test can be examined. It is found that in all cases the critical depth increases as the load increases to reach an ultimate value at large deflections, Fig. 43, and thereafter remains stationary under

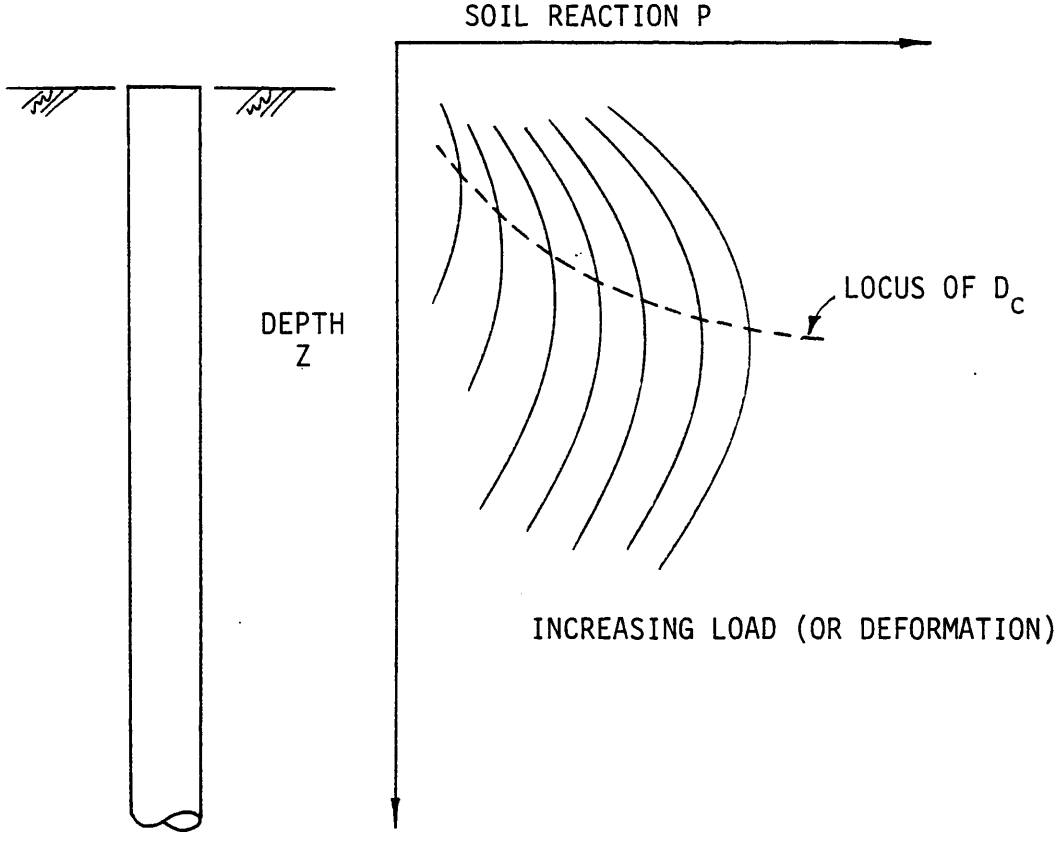

FIG. 43 - Observed Behavior of
Critical Depth

increasing load (or increasing deformation). The following definitions are made to describe the phenomenon

Z_c = instantaneous critical depth

D_c = ultimate critical depth

$\frac{Z_c}{D_c}$ = critical depth ratio

$\frac{Y}{R}$ = radial movement of the pile at the ground surface.

This observed behavior may be idealized as a wave front moving down the pile and supports the comments made by Angelides and Roesset (3), based on the FEM, that Z_c is a function of displaced material volume. Fig. 44 shows the observed evaluation of the critical depth for all the sites considered, expressed in dimensionless form as the critical depth ratio, Z_c/D_c, versus radial pile movement at the surface, Y/R . Table 1 gives the ultimate value of the critical depth as a function of pile radius, R, for each site investigated, together with the average pressuremeter limit pressure within the depth D_c.

A number of comments can be made from the observed trend in Fig. 44 and in Table 1.

1) The critical depth begins at approximately 0.4 times the ultimate value.

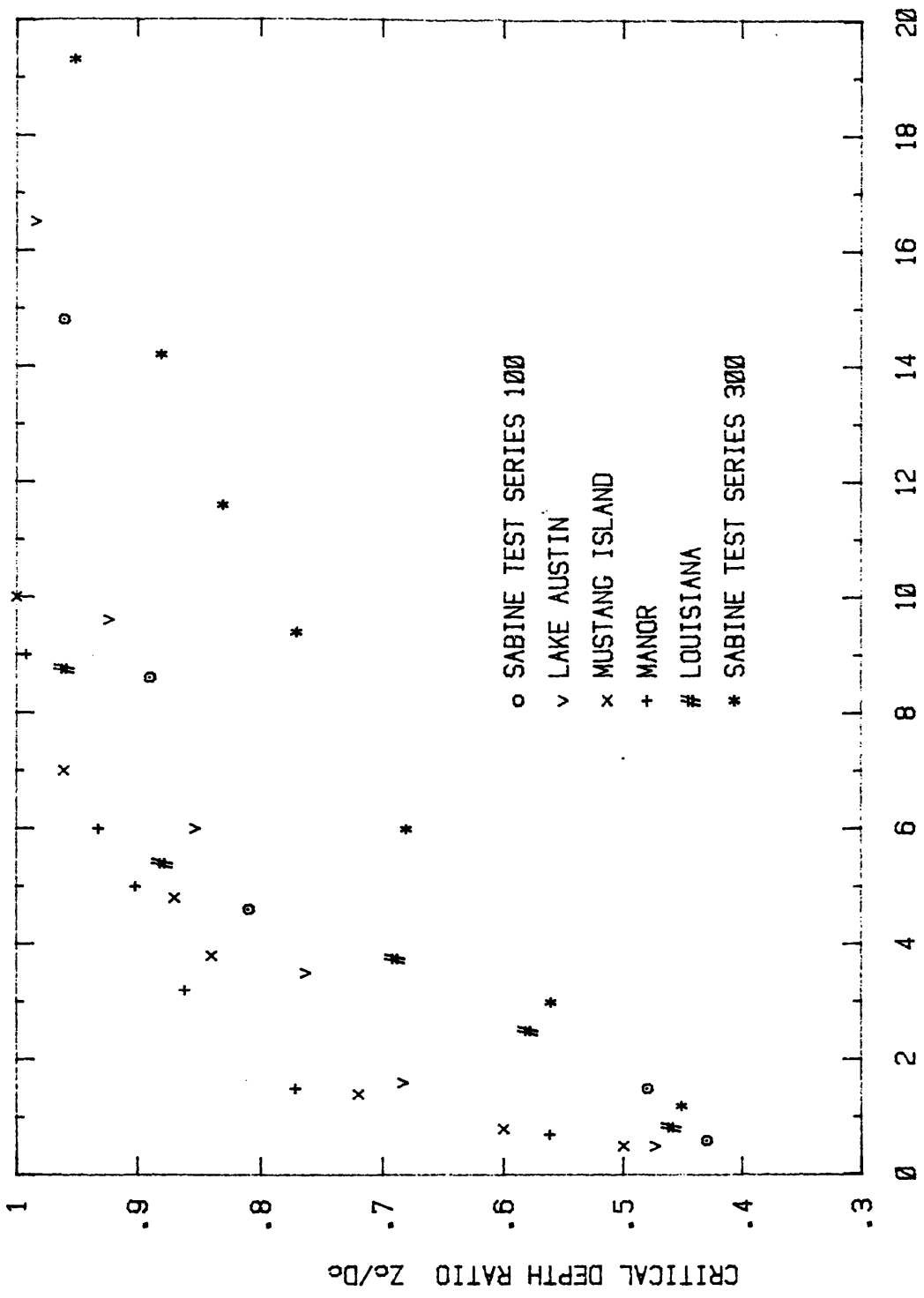

FIG. 44 - Observed Critical Depth Displacement as a Function of Radial Movement

Table 1 - Observed Ultimate Critical Depth Ratios

SITE	ULTIMATE CRITICAL DEPTH RATIO (D_c/R)
Houston	3.0
Manor	7.0
Sabine	19.0
Lake Austin	13.0
Mustang Island	8.3
Louisiana	13.0
Texas A&M	4.5

2) The ultimate value, D_c, is attained at different values of pile radial movement.

3) The stiffer the material, characterized by the pressuremeter limit pressure, the shallower D_c/R becomes.

To represent the observed behavior of the dependent variable Z_c as a function of the independent variables, radial movement and ultimate critical depth ratio, the following model is proposed

$$\frac{Z_c}{D_c} = 1 - e^{-(A + B \frac{Y}{R})} \quad \ldots\ldots\ldots\ldots\ldots\ldots \quad (103)$$

where A, B = constants of nonlinear regression.

A, B were found from a linear regression model with $\frac{D_c}{R}$ as the independent variable as

$$A = .713 - 0.0126 \frac{D_c}{R} \quad \ldots\ldots\ldots\ldots\ldots\ldots \quad (104)$$

$$B = 0.57 - 0.0243 \frac{D_c}{R} \quad \ldots\ldots\ldots\ldots\ldots\ldots \quad (105)$$

and are shown on Fig. 45. Based on the model predictions of Eqs. 103, 104 and 105, a family of curves to describe the movement of Z_c is shown on Fig. 46.

The range of field conditions covered by the scope of the lateral load test data is broad. The sample includes both rigid and flexible piles in sand, stiff clays, soft clays and silts. The observed

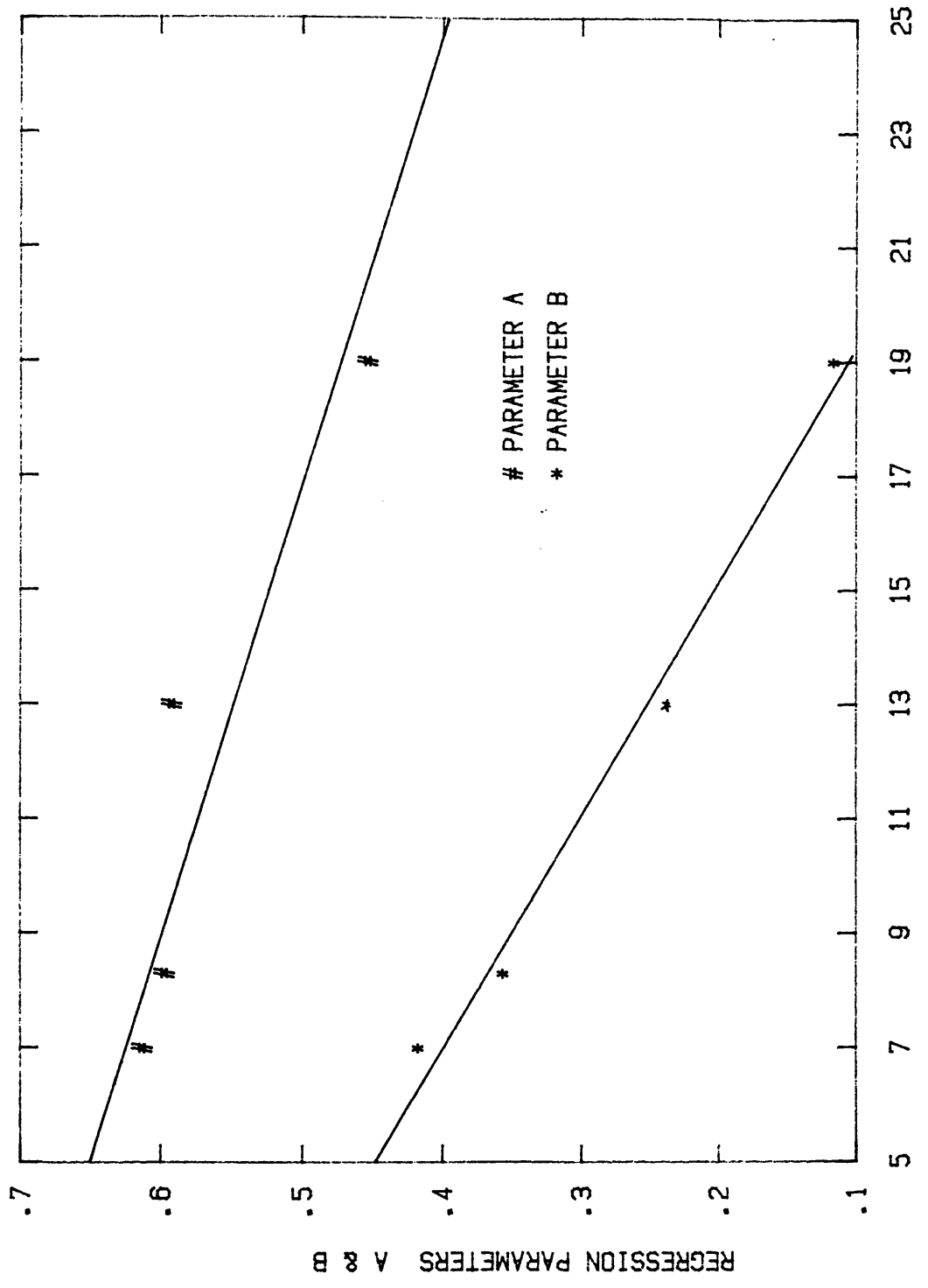

FIG. 45 - Nonlinear Regression Parameter A, B as a Function of the Ultimate Critical Depth Ratio

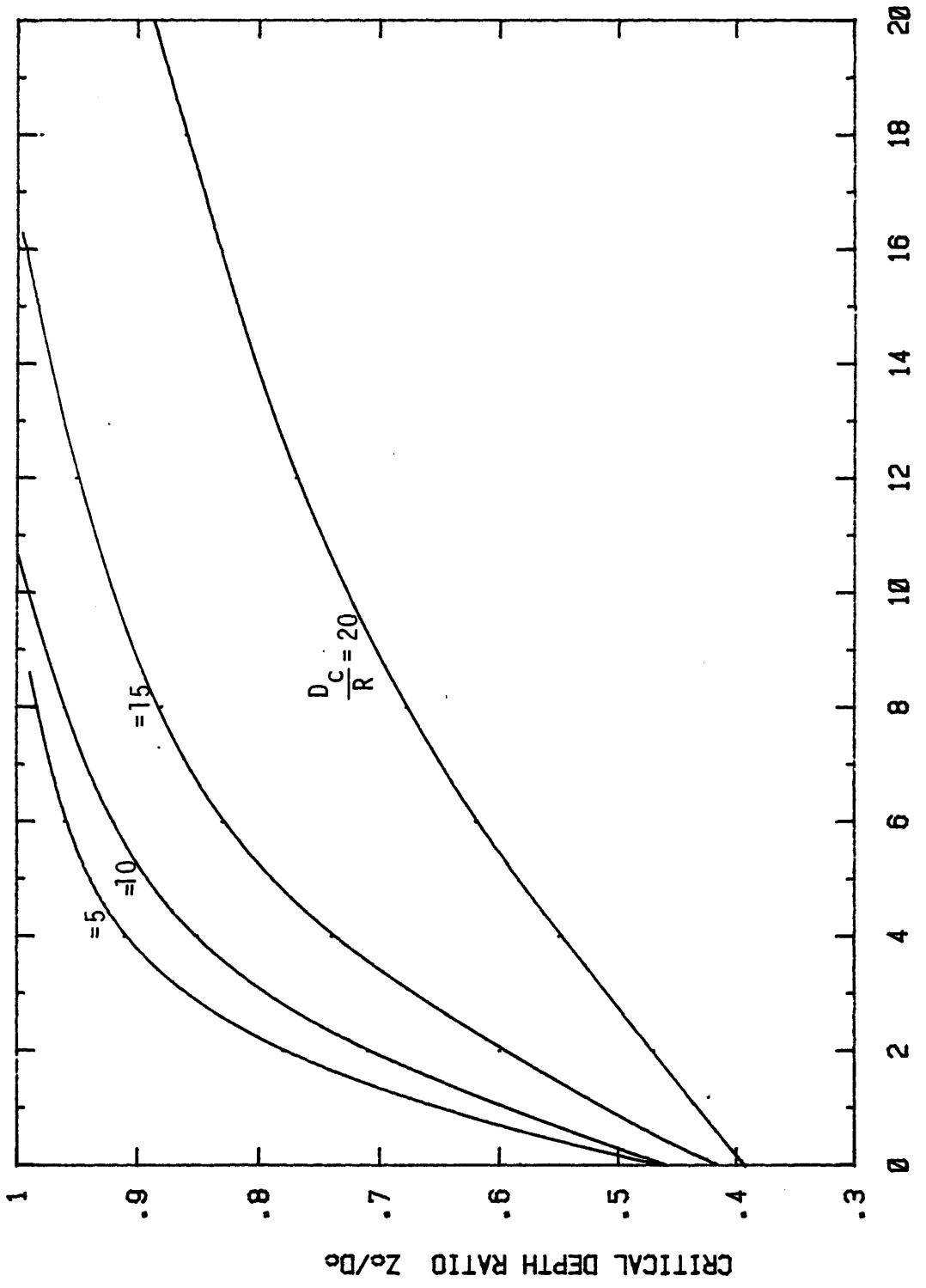

FIG. 46 - Predicted Behavior of Critical Depth from Nonlinear Model

behavior incorporates all the variables which are believed to control the behavior of Z_c and substantiates certain conclusions reached in limited analytical studies. However, the consequences for designing P-y curves should be considered. Since the mobilized soil reaction is now a function of surface movement as well as a function of soil properties, a unique soil P-y cannot be determined within the critical depth. This point is confirmed at sites where both fixed and free head restraint conditions were used. Since the pile deformation patterns are altered by head restraint, 'measured' soil P-y curves are also found to change.

For the purposes of proposing a tentative design procedure the critical depth is considered stationary at the average value. This permits correction of a derived P-y curve from the pressuremeter by a reduction factor. The magnitude of this reduction can be taken from the decay in pressure shown in Fig. 42 (p 117). Making the assumption that the shape of the distribution is unchanged at increasing load levels, all the sites can be plotted on Fig. 47 with dimensionless depth Z/D_c against dimensionless soil reaction P/P_u. A mean curve is proposed for the clay and for the sand.

Table 1 and Fig. 44 (p 121) show that the behavior of Z_c is controlled by the material stiffness or pressuremeter limit pressure. To represent all the known variables, the pile flexural stiffness should also be incorporated. Both experimental and analytical studies indicate that the critical depth is a pile-soil interaction phenomenon and a variety of pile stiffnesses would be subject to different D_c in the

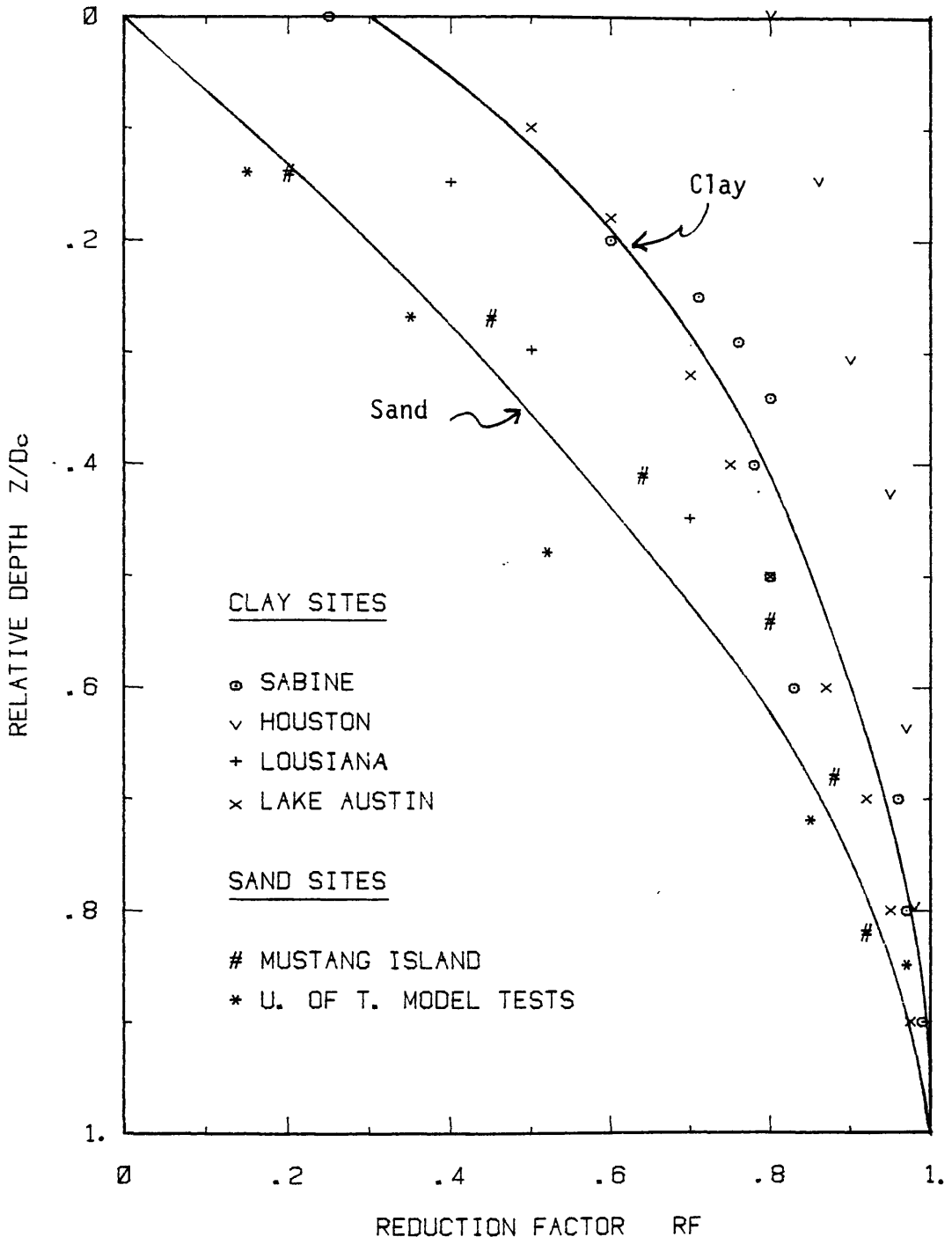

FIG. 47 - Measured Relative Depth as a Function of the Reduction Factor

same material. A constant from the closed form solution, (65), to a laterally loaded pile is termed the flexibility factor, T, and is given by

$$T = \frac{1}{D}\sqrt[4]{\frac{4EI}{E_s}} \quad \ldots\ldots\ldots\ldots\ldots\ldots\ldots\ldots \quad (106)$$

The pressuremeter modulus, E_m, could be used to describe E_s but better precision is available on the limit pressure, p_l^*. A large number of case histories exist which report p_l^* and it is proposed to quantify E_s by p_l^*. Therefore a Relative Rigidity, RR, is defined

$$RR = \frac{1}{D}\sqrt[4]{\frac{EI}{p_l^*}} \quad \ldots\ldots\ldots\ldots\ldots\ldots\ldots\ldots \quad (107)$$

and the average value of Z_c attained in all the pile load tests $Z_{c(av)}$ can be summarized on Fig. 48. A linear model is proposed and a least squares regression, within the limits $7.0 < RR < 13.0$, gives

$$\frac{Z_{c(av)}}{D} = 0.778\ RR - 3.66 \quad \ldots\ldots\ldots\ldots\ldots\ldots\ldots\ldots \quad (108)$$

which can be well approximated by the expression

$$\frac{Z_{c(av)}}{D} = \frac{\pi}{4}(RR-5) \quad \ldots\ldots\ldots\ldots\ldots\ldots\ldots\ldots \quad (109)$$

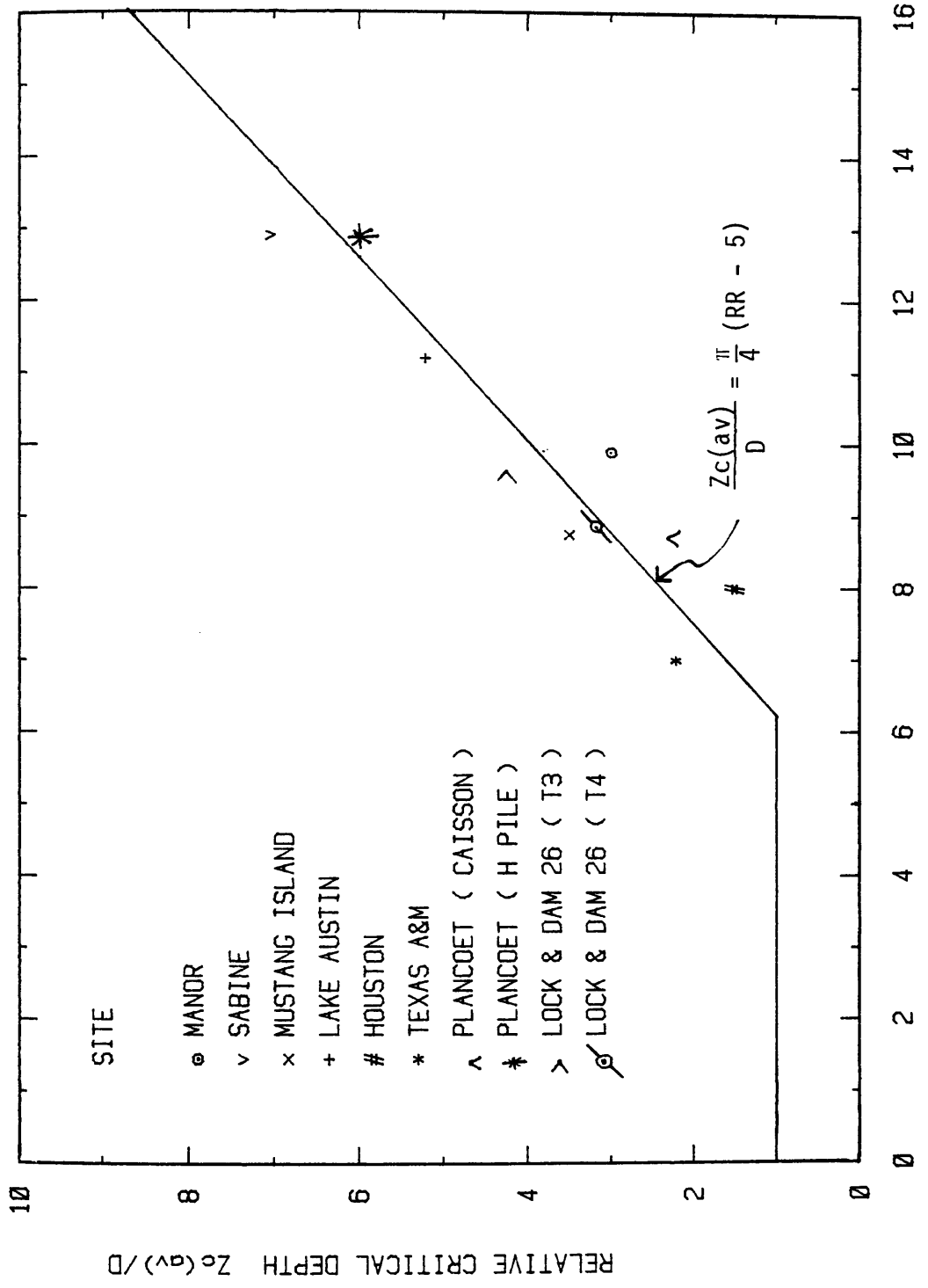

FIG. 48 - Pile Relative Critical Depth as a Function of the Relative Rigidity Factor

For all values of RR less than approximately 6, a relative critical depth of 1 is proposed. The average value of critical depth can be calculated from the piles flexural stiffness and the soils limit pressure, within Z_C.

Pressuremeter Critical Depth: FEM Study

Introduction

Solutions in linear elasticity, using a common definition of D_C, from Mindlins equations (70) indicate that changes in Poisson's ratio have a significant effect on the depth of surface influence. As Poisson's ratio increases the material is forced to undergo less volume change, and D_C increases. This is accompanied by a decrease in the absolute value of deflection. This equates to real soils where loose sands and normally to lightly overconsolidated clays tested under drained conditions show an increase in Poisson's ratio from the order of 0.3 to 0.5. For sands it is also well recognized the stress-strain relationship is strongly dependent upon confining pressure, σ_3, and thus increases with depth. Further, all soils are generally highly nonlinear in behavior throughout the range of strains the soil is subjected to, by the expanding pressuremeter. To gain an increased understanding of some of these effects upon the critical depth phenomenon for the pressuremeter, the FEM method was selected with nonlinear material behavior. Both a medium sand and clay were modeled.

It is recognized (11,46) that surface effects may influence

the limit pressure but little information either experimental or analytical, is available with respect to the pressuremeter modulus, especially with small strain. Hartman (39) noted in studying the separate effects of increased depth and lateral confinement for sand that both effects upon the pressuremeter modulus are identical. This suggests that an observation of deformation patterns and the deviation from assumed plane strain conditions gives a clearer critical depth indication.

FEM Code 'AXISYM'

The 'AXISYM' code, reported by Holloway, Clough and Vesic (41), makes use of the nonlinear hyperbolic stress dependent soil modulus model to describe the constitutive behavior of the soil in each element. An incremental displacement formulation is used in an axisymmetric finite element discretization described in radial, r, vertical, z, and circumferential, θ, directions for boundary pressure loading exclusively. A five node quadrilateral element is employed allowing linear strain variation within the element while constant strains are prescribed at the element boundaries. Full axial symmetry is assumed with respect to problem geometry, material properties and loading conditions. Hence any θ plane containing the Z axis is a principal plane. The program incorporates a mesh generator and permits rectangular zones of material types to be defined by "boundary" rows and columns. In each prescribed loading step additional iteration can be specified to improve convergence although no convergence criterion

is available. Each iteration updates the value of the tangent modulus, E_t, for each element to update stiffness matrices and re-solves for nodal displacements, strains and stresses.

The material constitutive behavior is modeled by the hyperbolic stress level approach in initial loading, and a subsequent unload-re-load cycle, proposed by Duncan and Chang (31). The tangent soil modulus is related to changes in strain, Poisson's ratio, confining pressure (σ_3), and the theoretical ultimate principal stress difference, $(\sigma_1-\sigma_3)_u$, based on the observed soil response under triaxial loading. The hyperbolic stress-strain relationship and parameters are defined by

$$(\sigma_1-\sigma_3)= \frac{\varepsilon}{\frac{1}{E_i} + \frac{\varepsilon}{(\sigma_1-\sigma_3)_u}} \qquad \text{(110)}$$

and is illustrated in Fig. 49. A summary of the parameters employed in AXISYM to define the nonlinear soil behavior is given in Table 2. In AXISYM the Poisson's ratio is held constant until "failure", defined by the actual principal stress difference $(\sigma_1-\sigma_3)$ reaching the theoretical maximum within an element, is reached and a revised failure Poisson's ratio is substituted.

Any structural material may be modeled as linear elastic with constant Young's modulus and Poisson's ratio. A number of limitations with respect to the FEM code and the material model should be stated:

1) The step increase of Poisson's ratio at failure is a crude representation of real behavior. Further, shear dilatant

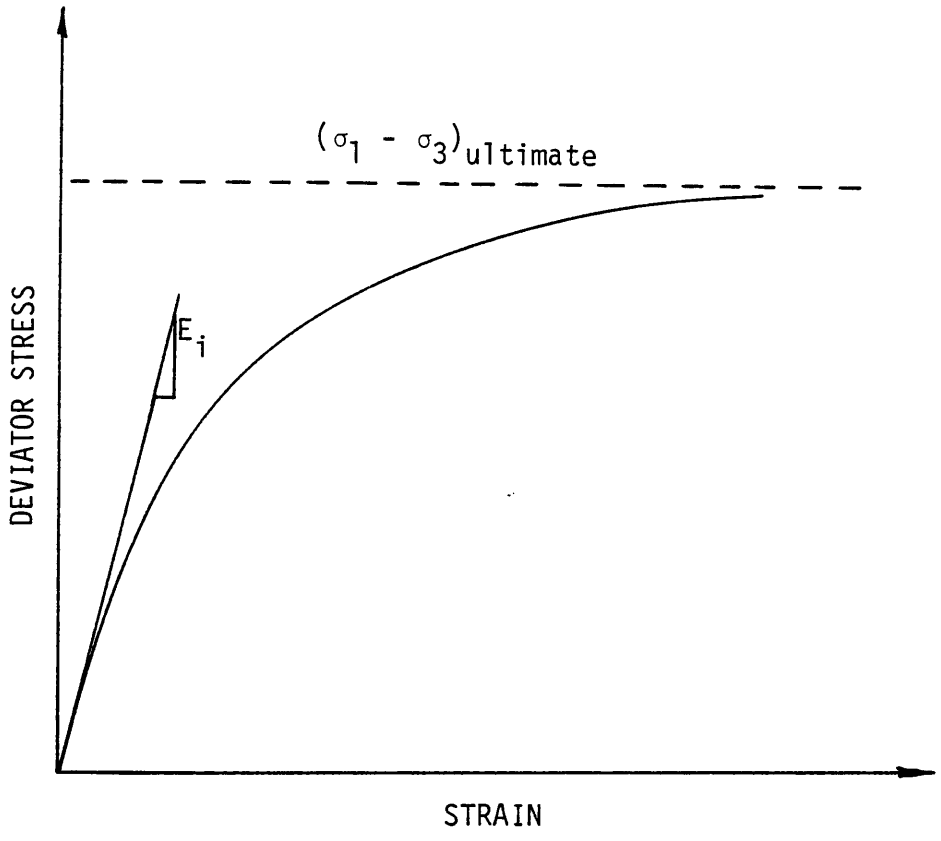

[after Duncan and Chang (31)]

FIG. 49 - The Hyperbolic Stress-Strain Model

Table 2 - Nonlinear Soil Parameters in AXISYM

PARAMETER	SYMBOL
Poissons Ratio Before Failure	ν
Poissons Ratio at Failure	ν_f
Unit Weight	γ
Correlation Factor: Ratio of Ultimate hyperbolic to measured strength	R
Coefficient of Earth Pressure at Rest	K_o
Friction Angle	ϕ
Exponent	n
Coefficient in equation expressing value of initial tangent modulus as a function of confining Pressure	K_I
Cohesion	c
Young's Modulus	E

material, e.g., dense sands, with $\upsilon > 0.5$ cannot be modeled.

2) The stress-strain relationship relies on the generalized Hooke's law and is most suitable for predicting stresses and deformation prior to failure.

3) Small strain is considered and thus significant error can be introduced if the full range of pressuremeter volumetric strains is attempted.

4) An open borehole cavity is represented in the mesh to simulate the pressuremeter cavity and its expansion; however, by this approximation the probe length cannot be of fixed length. The field pressuremeter is of fixed length.

In view of the errors in large strain, and the onset of failure in the elements around the probe, the investigation is limited to small strain, $\varepsilon_\theta < 10\%$, in both sand and clay. This is the range of behavior for which least is known with respect to the pressuremeter expansion.

FEM Meshes and Material Models

To record the response of a pressuremeter expansion, radial movements need to be ascertained from a known boundary pressure loading Radial deformation is therefore expressed as

$$\varepsilon_\theta = \frac{y}{R} \quad \ldots\ldots\ldots\ldots\ldots\ldots\ldots\ldots\ldots\ldots \quad (111)$$

where y = radial deflection

R = pressuremeter cavity radius

and ε_θ = circumferential strain.

The pressuremeter is modeled as a borehole cavity loaded over a length L based on the work of Hartman (39)

$$\frac{L}{R} = 6.0 \quad \ldots\ldots\ldots\ldots\ldots\ldots\ldots\ldots\ldots\ldots \quad (112)$$

and with borehole cavity expansion taken as the average deflection over the center half of the length to minimize end effect.

In linear elasticity the stresses and strains vary away from the cavity as the inverse of the square of the distance. Based on this and the work of Hartman (39), a representative FEM of width 20 R was selected. A total depth of 60 R was taken to minimize boundary restraint effect and permit examination of the pressuremeter response to a depth of 40 R. The general form of the chosen grid is shown in Fig. 50 for the pressuremeter at the surface, Z/R = 3. For a grid of proportion 5.0 ft (1.5 m) radius by 15.0 ft (4.5 m) deep a cavity of radius 3 in. (75 mm) is represented with the center line of the pressuremeter at a depth of 9 in. (225 mm). The grid has a total of 204 elements and 234 nodes with 6 elements contained within the probe length. A total of eight pressuremeter tests were simulated at depth to cavity radius ratios of 3,5,7,10,15,20,30 and 40, by varying the mesh in the vicinity of the probe. To confirm the accuracy of the mesh, a depth of Z/R = 10 was chosen to compare to the closed form elastic solution of Livneh et al. (59). The displacement of the cavity wall, u_r, in linear elasticity under a pressure p is given by

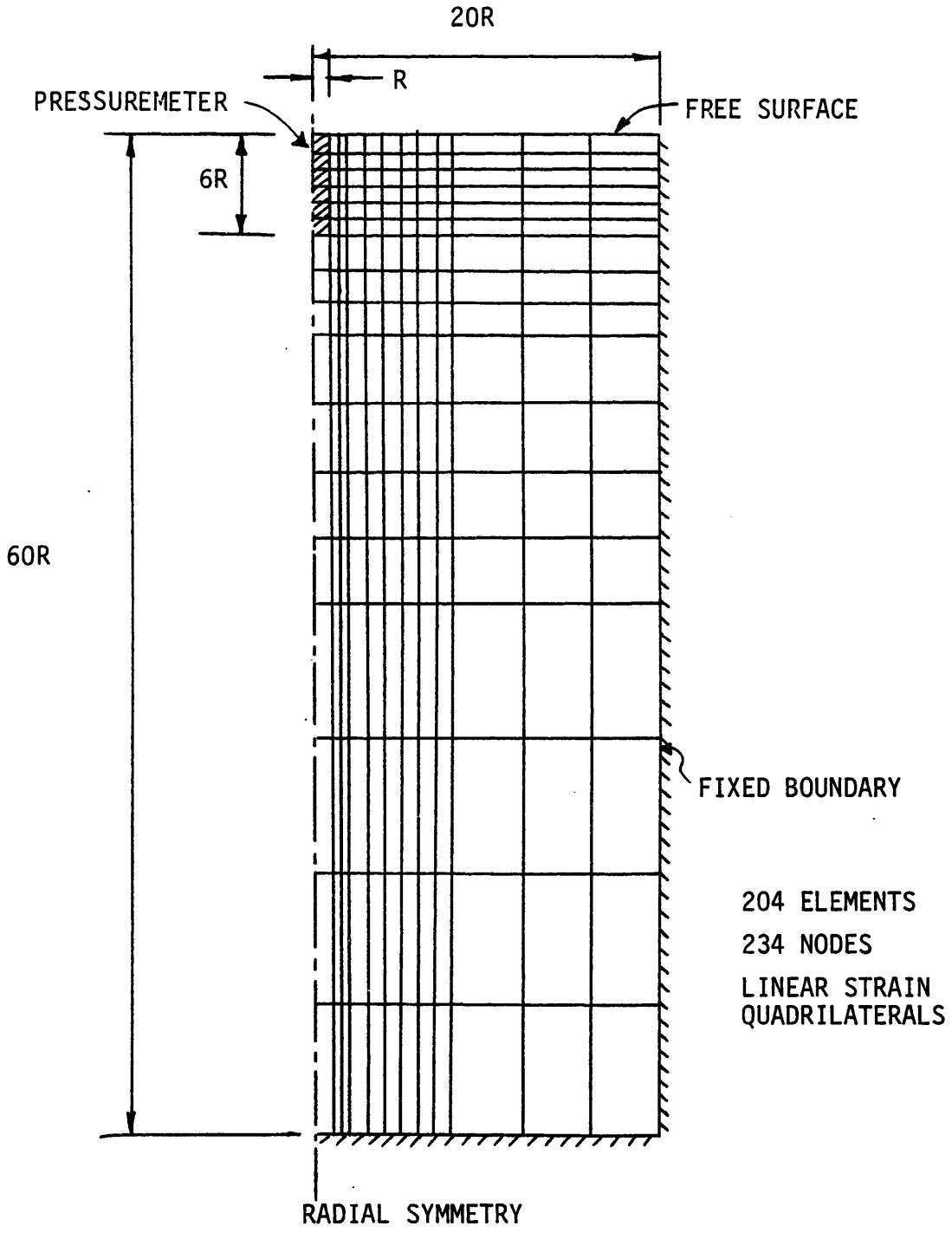

FIG. 50 - The General Form of the FEM Grid (shown for Relative Depth of 3)

$$u_r = \frac{p(1+\nu)R}{E} \quad \ldots\ldots\ldots\ldots\ldots\ldots\ldots\ldots \quad (113)$$

and the difference the FEM solution was found to be 8% lower at a circumferential strain of 0.35%.

The effect of the surface on both deformation patterns and the pressuremeter response is evaluated in a purely cohesive material, $C > 0$, $\phi = 0$, and a frictional material, $C = 0$ and $\phi > 0$. The parameters given in Table 3 were selected based on the extensive laboratory tests performed by Wong and Duncan (101). The sand parameters represent those closest to the reported soil properties of Mustang Island and the clay represents a typical medium stiff clay.

The material contained within and above the probe to the free surface was idealized as a structural material of constant (low) modulus and simulates drilling fluid in the field. These parameters are also shown in Table 3.

Results

A level of approximately 5% circumferential strain was chosen to compare the cavity expansion results at different elevations. Typically, three loading steps were employed in each, and based on numerical experiment and the work of Katona, Vittes, Lee and Ho (50), 3 iterations were used within each load step. By expressing the modulus of the cavity expansion as

$$k_{cav} = \frac{\sigma_r}{y/R} \quad \ldots\ldots\ldots\ldots\ldots\ldots\ldots\ldots \quad (114)$$

Table 3 - Nonlinear Material Parameters Selected

PARAMETER	SAND	CLAY	DRILLING FLUID
ν	0.3	0.42	0.2
ν_f	0.45	0.42	0.2
γ	120 lb/cu ft	120 lb/cu ft	150 lb/cu ft
R	0.72	0.57	1.0
K_o	0.4	0.4	1.0
ϕ	39.0	0.0	0.0
n	0.64	0.15	0.0
K_I	340.0	36.0	1.0
c	0.0	7000 lb/ sq.ft	0.0
E	0.0	0.0	10.0 lb/ sq.ft

where σ_r = increase in radial stress applied to the cavity wall,

the results for sand and clay can be summarized by Fig. 51 and Fig. 52 respectively. At each selected depth the amount of vertical movement at the probe center line is given expressed as a percentage of the horizontal movement.

Examination of Fig. 51 for the sand shows a distinct nonlinear relationship with depth. This results from the chosen sand stress-strain model being a hyperbolic power function of confining pressure. What is not clear, however, is the degree to which the surface may have further reduced the modulus. It is proposed that less than 10% vertical deformation at the probe center line be taken as a good approximation to plane strain deformation. With this criterion, violation of plane strain expansion has occurred to a depth of approximately 11-12 times the cavity radius. The free surface deflection pattern for relative depths 3,5 and 7 in sand is shown in Fig. 53. By taking the approximate hyperbolic law of Janbu (43), the deformation modulus, E_T, of granular soils can be expressed by

$$E_T = K (\sigma_3)^n \quad \ldots\ldots\ldots\ldots\ldots\ldots\ldots\ldots\ldots\ldots \quad (115)$$

and, if the minor principal stress is a function of depth, then Eq. 113 can be written for the pressuremeter cavity as

$$k_{cav} = K \left(\frac{Z}{R}\right)^n \quad \ldots\ldots\ldots\ldots\ldots\ldots\ldots\ldots\ldots\ldots \quad (116)$$

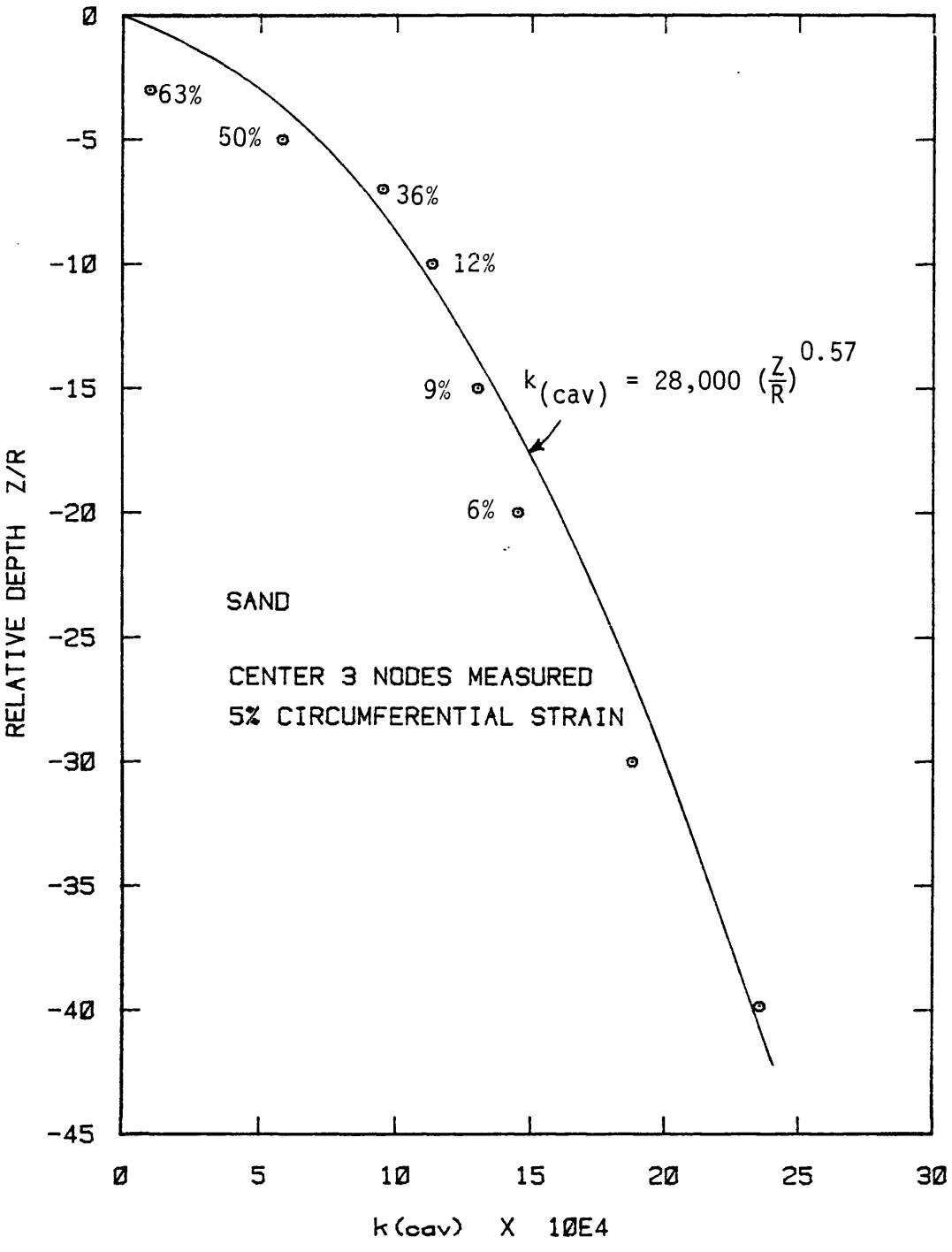

FIG. 51 - The FEM Prediction of Cavity Modulus as a Function of Relative Depth for Sand

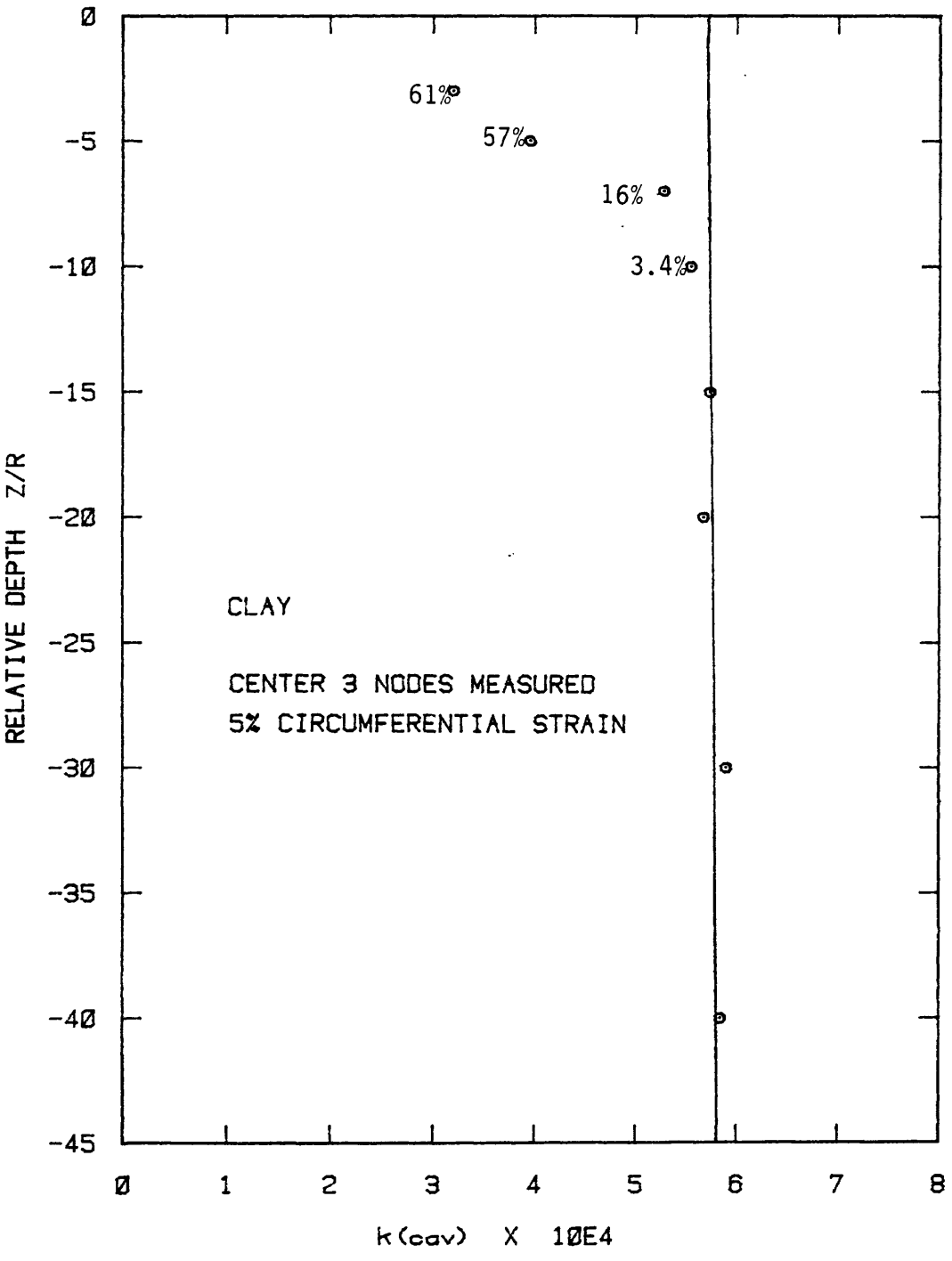

FIG. 52 - The FEM Prediction of Cavity Modulus as a Function of Relative Depth for Clay

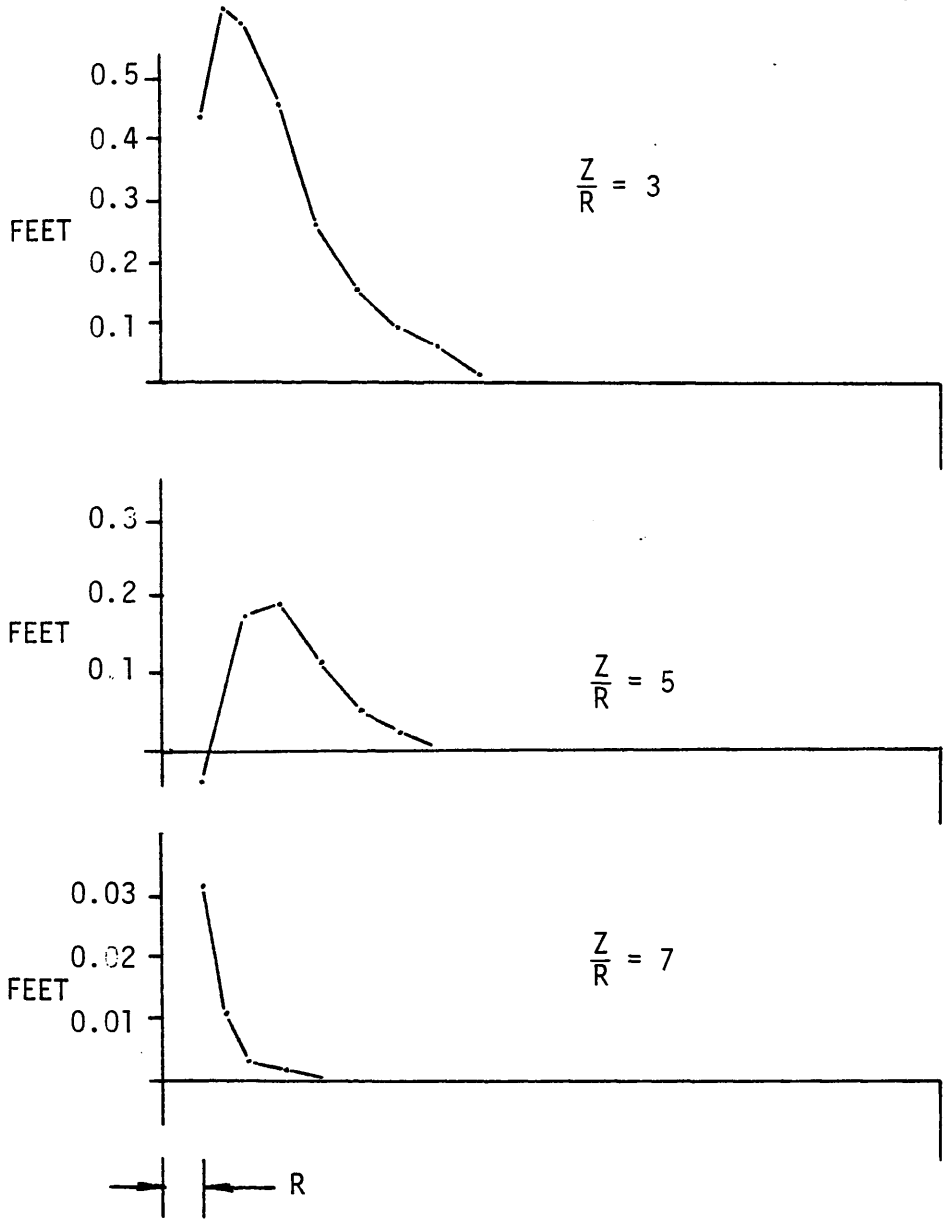

FIG. 53 - The Free Surface Deflection Pattern in Sand

By omitting the test results at relative depths of 3, 5 and 7, in which plane strain is violated, a nonlinear regression gives

$$k_{cav} = 28{,}000 \left(\frac{Z}{R}\right)^{0.57} \quad \ldots\ldots\ldots\ldots\ldots\ldots \quad (117)$$

which is shown on Fig. 51 (p. 141).The hyperbola is extremely sensitive to the nonlinear parameters K and n at low values of the relative depth.

Examination of Fig. 52(p. 142) for the clay gives an indication of the surface effects. The expansion of the cavity in clay is shown to be independent of surface effects below a depth of 8 R. Further, the reduction of the modulus toward the surface can be adequately represented by a linear variation.

In summary, both sand and clay are shown to possess a critical depth of reduced resistance, at small strain, for the expansion of a cavity. The reduction in resistance can be quantified by a comparison of the predicted resistance, without depth effects, and the mobilized resistance. In view of the lack of further evidence from the technical literature and the small scope of this study, a linear variation with depth is proposed. The reduction in resistance versus relative depth is given in Fig. 54 and Fig. 55 for sand and clay respectively, based on Fig. 51 (p. 141) and Fig. 52 (p. 142).

Summary

For both pile and pressuremeter lateral movements, the mobilized

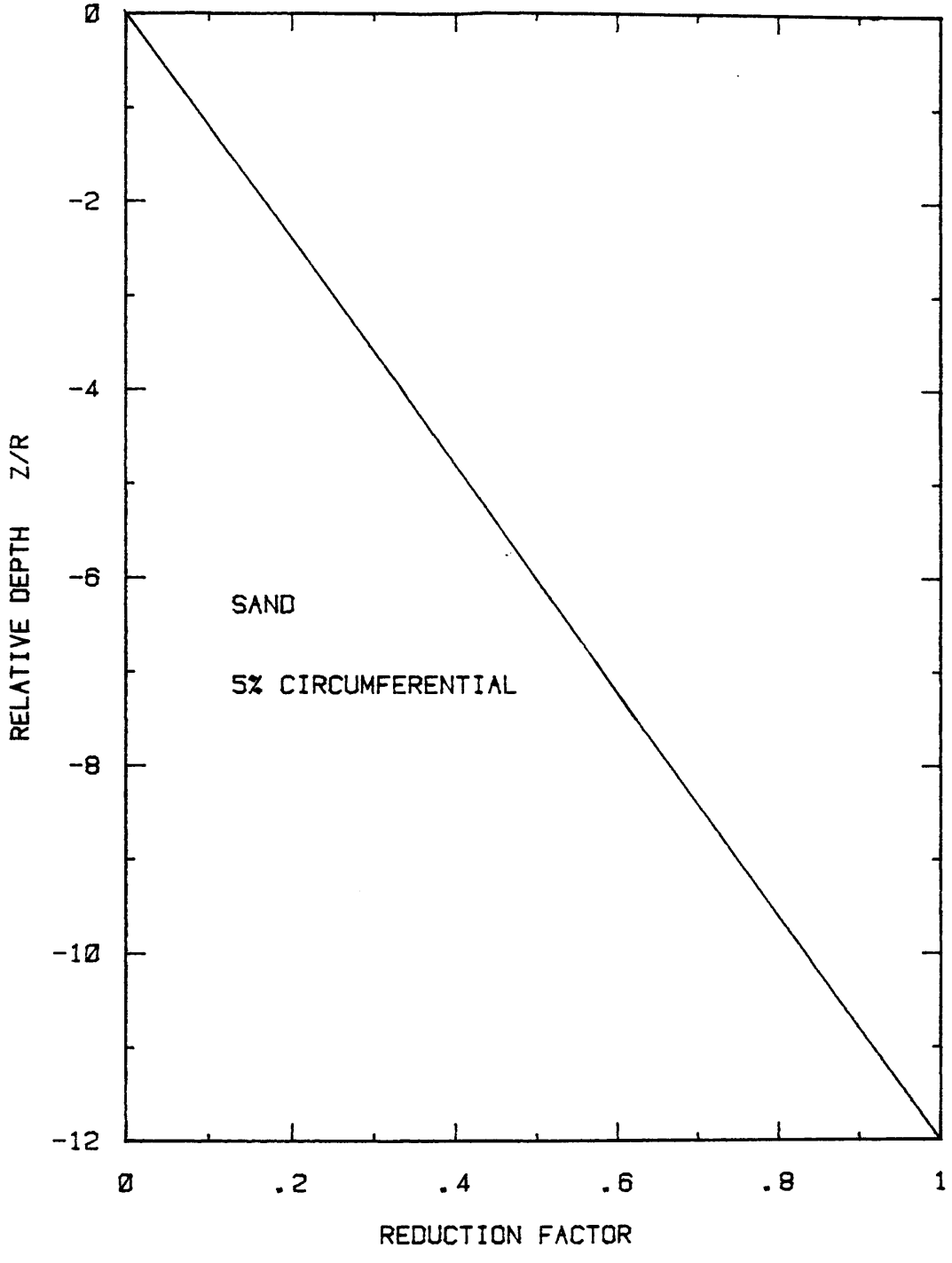

FIG. 54 - Reduction Factor for the Pressuremeter in Sand

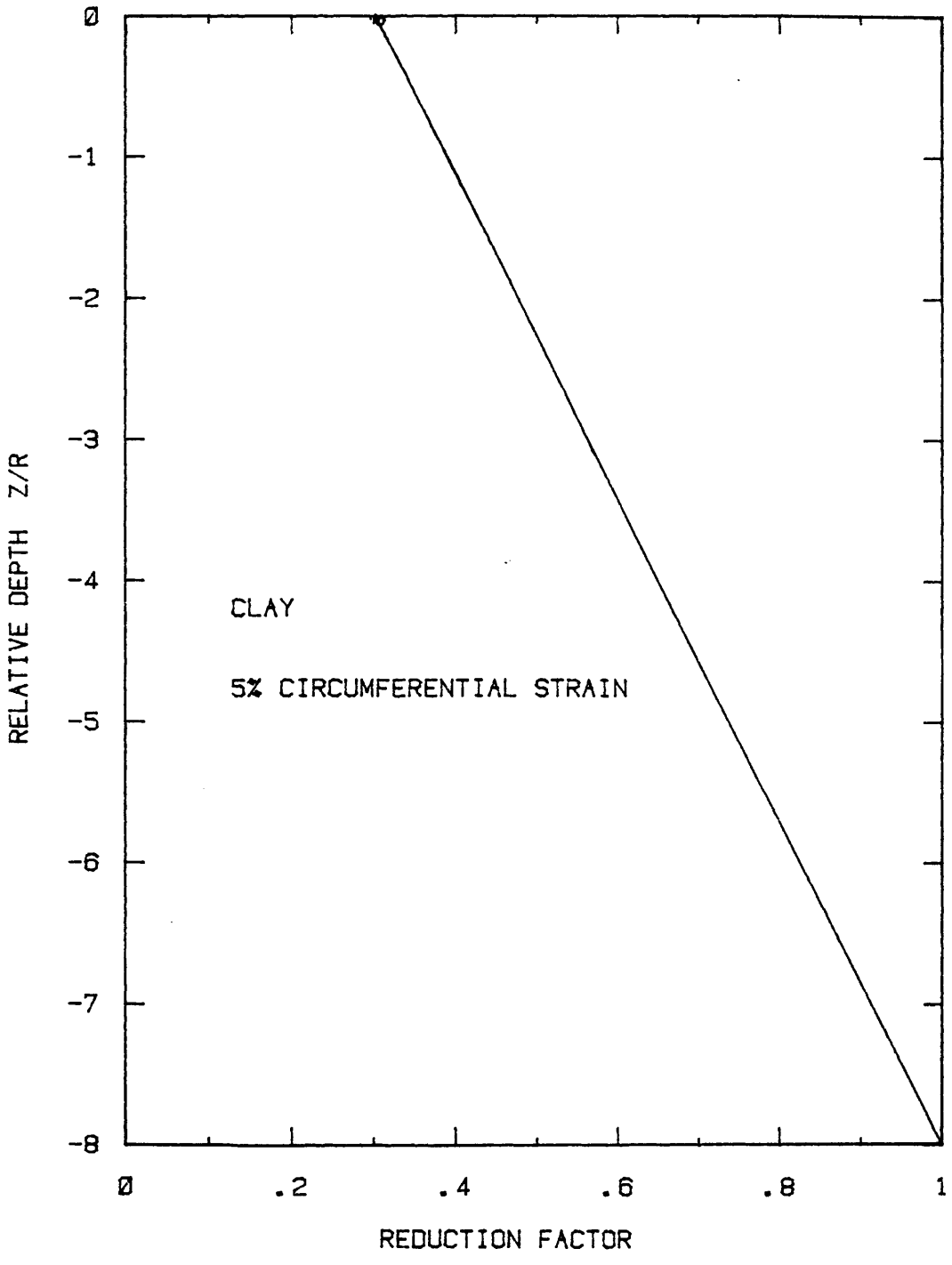

FIG. 55 - Reduction Factor for the Pressuremeter in Clay

soil resistance is shown to be reduced in a zone close to the unrestrained ground surface.

At small strains the zone of influence for the pressuremeter is very close to the surface. In sands, violation of plane strain assumptions around the probe center line takes place in a zone approximately 12 times the pressure probe radius. For conventional commercially available pressuremeters the maximum initial radius of the probe is approximately 1.5 in. (38 mm), this zone is therefore 18 in. (460 mm). This is to be compared with the depth of reduced resistance on the limit pressure cited earlier, of 6.0 ft (1.8 m) in sands.

In clay, by the same argument, the zone of influence for small strains is found to be 12 in. (300 mm) deep compared to a reported value of 3 ft (910 mm) deep on the limit pressure. This suggests that the critical depth for the expanding pressuremeter is a function of the displaced volume of soil. The decay in mobilized resistance toward the surface is taken as linear within D_c, as given on Fig. 54 for sand and Fig. 55 for clay. It is proposed to use a depth of 3 ft (.9 m) in clay and 6 ft (1.8 m) in sand for field studies and reduce the full pressuremeter expansion curve.

For the pile it has been observed that the depth of reduced resistance is a function of pile-soil relative stiffness and displaced volume. Hence, the mobilized front reaction curve, Q, component of the P-y curve is subject to a depth effect factor given by Fig. 47 (p.127).

By evaluating the soil spring response from the pressuremeter, the critical depth effects of both pile and pressuremeter should be superimposed. As an illustration, Fig. 56 shows the reduction factor

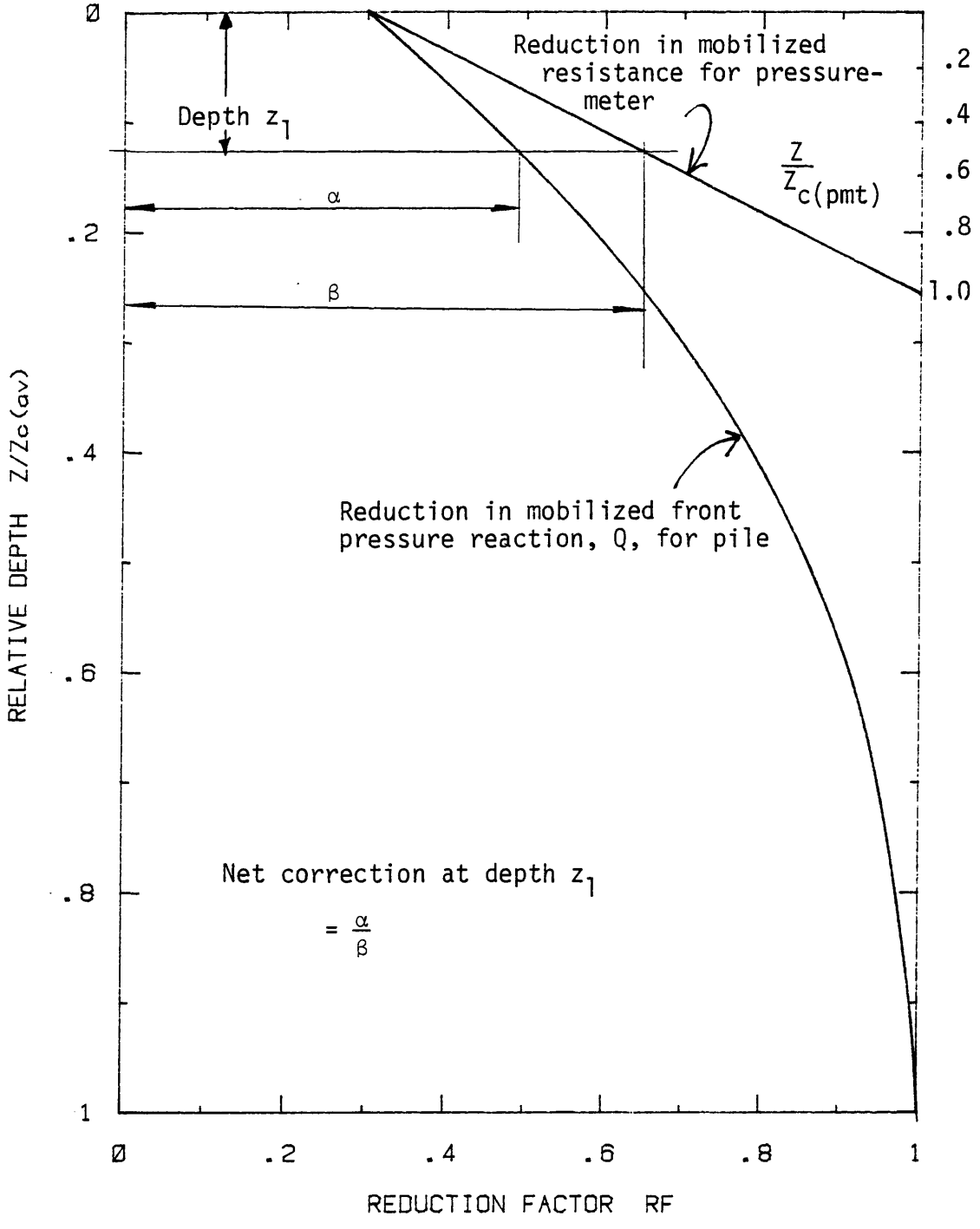

FIG. 56 - Superimposed Pile Critical Depth and Pressuremeter Critical Depth.

against relative depth for both the pile and pressuremeter in clay. Due to the scale differences between pressuremeter and pile, the physical depth of reduced resistance is much less for the pressuremeter compared to the pile. Considering Z_1 in Fig. 56 (p.148) the actual mobilized front pressure for the pile is reduced by a factor 'α' from the 'at depth' pressure. However, at depth Z_1 the measured pressuremeter test is within the critical depth and the response has been decreased to a factor 'β'. Clearly the reduction factor applied to the pile should take into account the pressuremeter critical depth. To make this correction the relative scale between a commercial pressuremeter radius and a typical pile critical depth should be chosen. A maximum pressuremeter radius of 1-1/2 in. (38 mm) and a field pile radius of 12 in. (305 mm) with D_c/R of 6 giving a critical depth of 12 ft (3.6 m), is considered. For field piles of greater critical depth the generated pressure contribution, Q, is slightly unconservative and for a smaller critical depth slightly conservative.

The final pile reduction curves, within the critical depth, corrected for pressuremeter critical depths are given in Fig. 57 and 58 for sand and clay respectively.

Recommended Procedure

To determine the average value of critical depth, and the reduction factor to be applied within that depth for a laterally loaded pile the following steps detail the recommended procedure.

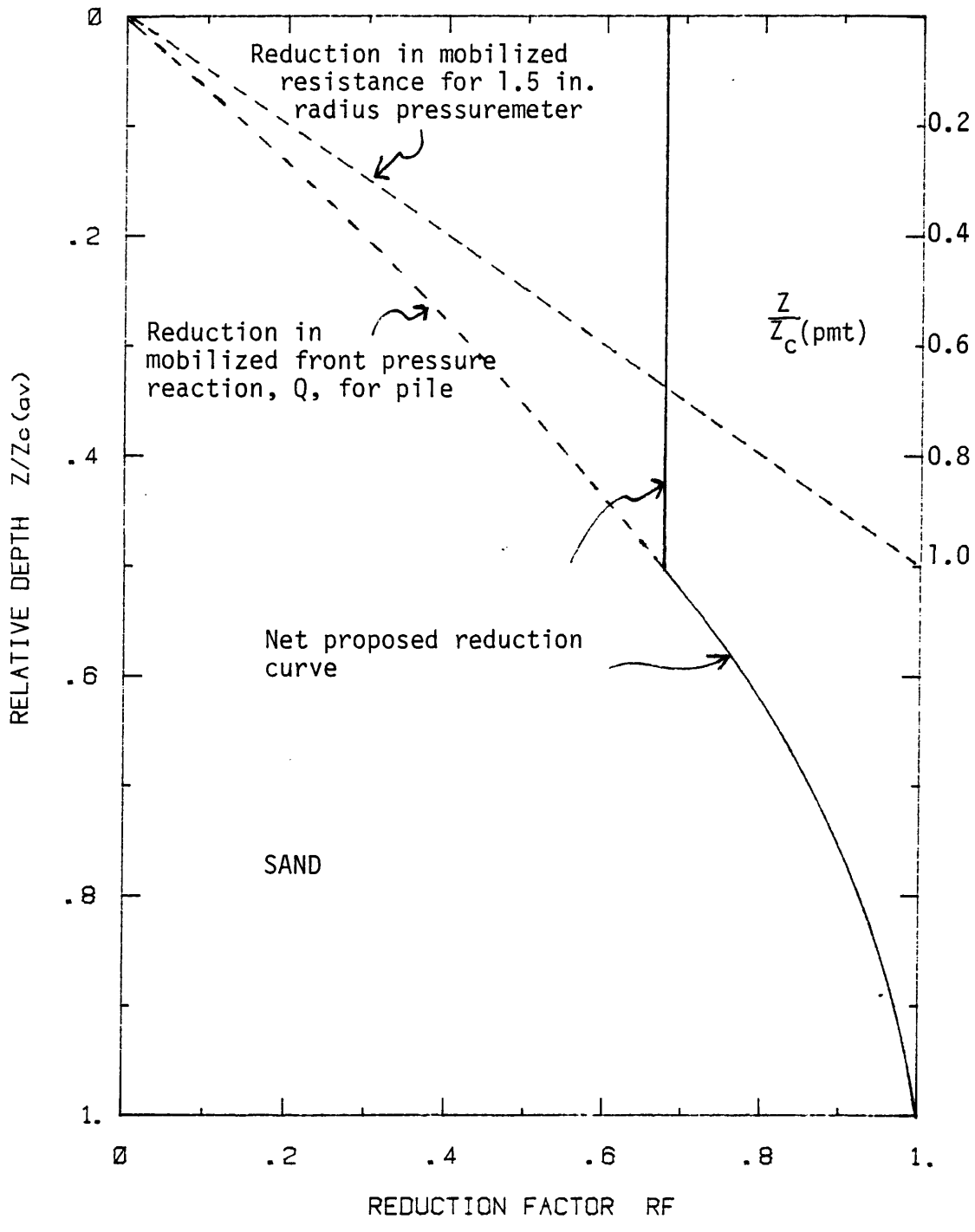

FIG. 57 - Reduction Factors Applied to Pile and Pressuremeter Within Their Critical Depth in Sand.

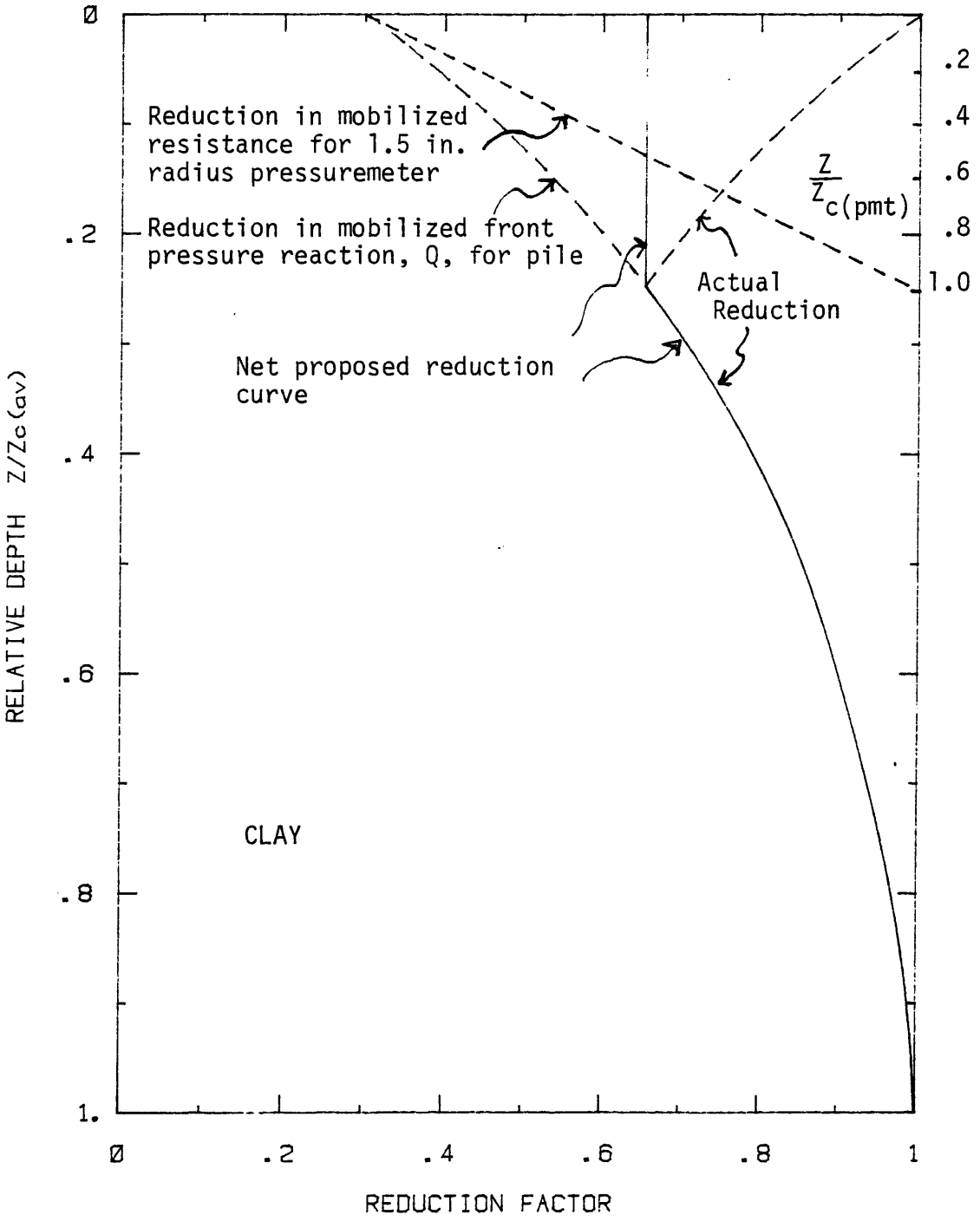

FIG. 58 - Reduction Factors Applied to Pile and Pressuremeter Within Their Critical Depths in Clay.

1) Obtain the average value of the net pressuremeter limit pressure p_1^* within the approximate estimated critical depth.

2) From the piles flexural stiffness, EI, and projected front width, D, calculate the relative rigidity factor from Eq. 107.

$$RR = \frac{1}{D} \sqrt[4]{\frac{EI}{p_1^*}} \quad \ldots\ldots\ldots\ldots\ldots\ldots \quad (107)$$

3) Calculate the critical depth ratio, $Z_{c(av)}/D$ by Eq. 108.

$$\frac{Z_{c(av)}}{D} = \frac{\pi}{4} (RR - 5) \quad \ldots\ldots\ldots\ldots\ldots\ldots \quad (108)$$

based on Fig. 48 (p. 129).

4) Calculate the critical depth, $Z_{c(av)}$ and compare to the assumed value in step 1). Repeat steps 2) and 3) if necessary.

5) Reduce the mobilized front pressure contribution, Q, to the P-y curve by the reduction factor, RF, from Fig. 57 in sand and Fig. 58 in clay for all pressuremeter tests within the depth $Z_{c(av)}$.

This tentative procedure is recommended for the field studies contained in a later Section only.

LABORATORY STUDIES

A full index of all laboratory tests referenced in this chapter can be found in Appendix III.

Laboratory Apparatus

Design and Construction

The testing rig was designed to apply a lateral load to a model instrumented pile, driven or augered in position, in either a free or fixed head restraint condition at a constant rate of lateral deflection. Plane strain soil conditions were assumed to be valid by confining the material to prevent vertical movement of the soil. Subsequent to a pile test, and after replacing the soil in its undisturbed state, a pressuremeter test, using a pressuremeter of equal size to discount scale effects, was inserted by the same technique and its response evaluated. A soil container of dimensions 2.5 ft x 2.5 ft x 2 ft deep (0.75 m x 0.75 m x 0.6 m) was chosen. This container is of similar size to previous laboratory investigations of laterally loaded model piles, Allen and Reese (2), and the ratio of pressuremeter (or pile) to soil volume exceeds those of previous investigations, Jewell et al. (45) and Briaud and Shields (19). Further, this volume of material presented no problems in handling, placing or in uniformity determination. Testing took place in clay, loose sand and dense sand.

The schematic layout of the apparatus, developed and built by the research facilities of Texas A&M University, is shown in Fig. 59 and

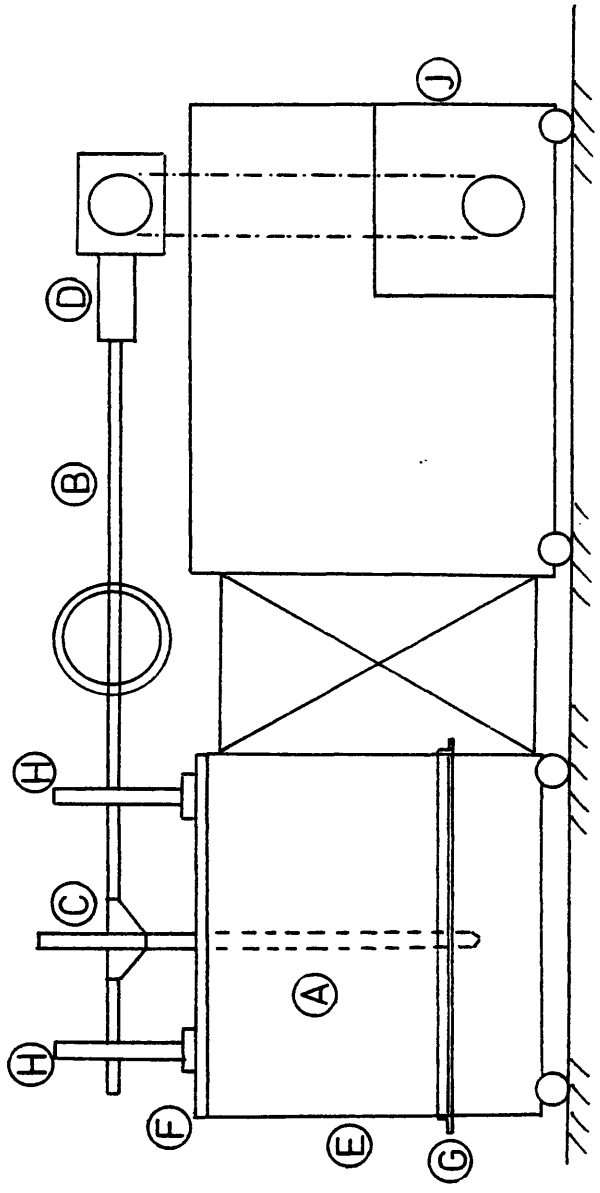

FIG. 59 - Schematic Layout of the Laboratory Test Rig

Fig. 60. The 1.356 in. (34.5 mm) diameter hollow instrumented model pile (A) is connected to a main delivery shaft (8) by a rigid head jig (C) for fixed head tests. A flexible wire rope is substituted for the head jig to perform free head tests. The total travel allowed by the piston (D) is 1.0 in. (25 mm) in either a push or pull mode of operation giving a total travel of 2.0 in (51 mm). The pile, embedded in the test material filling the soil container (E), can then undergo deflections equivalent to $\pm$ 145% radial movement, well in excess of the deflections considered the limit of pile serviceability. The soil container and lid (F) are fabricated from 1 in. (22 mm) plywood braced with 1-1/2 in. (37 mm) steel angle iron (G) to prevent lateral deflection of the container.

The 2 in. (51 mm) diameter delivery shaft passes through two sets of high lateral capacity, low friction, roller pin bearing units (H) and is connected to a 500 lbs (225 kg) load transducer. The piston actuating the shaft, is chain driven by an electrically powered motor through a gear box (J). The gearing allows a range of displacement rates from 0.001 in./min to 0.20 in./min (.025 mm/min to 5.1 m/min) which corresponds to radial movements of 0.148%/min to 29%/min. Pile displacement and rotation is continuously monitored during a test by a linear voltage displacement transducer (L.V.D.T) (K) at a position 1 in. (25 mm) above the soil surface, and a dial gauge 12 in. (304 mm) above the soil surface.

Load transducer and L. V.D.T. signals are amplified, then recorded onto an Honeywell visicorder unit, Fig. 61.

FIG. 60 - Laboratory Testing Unit

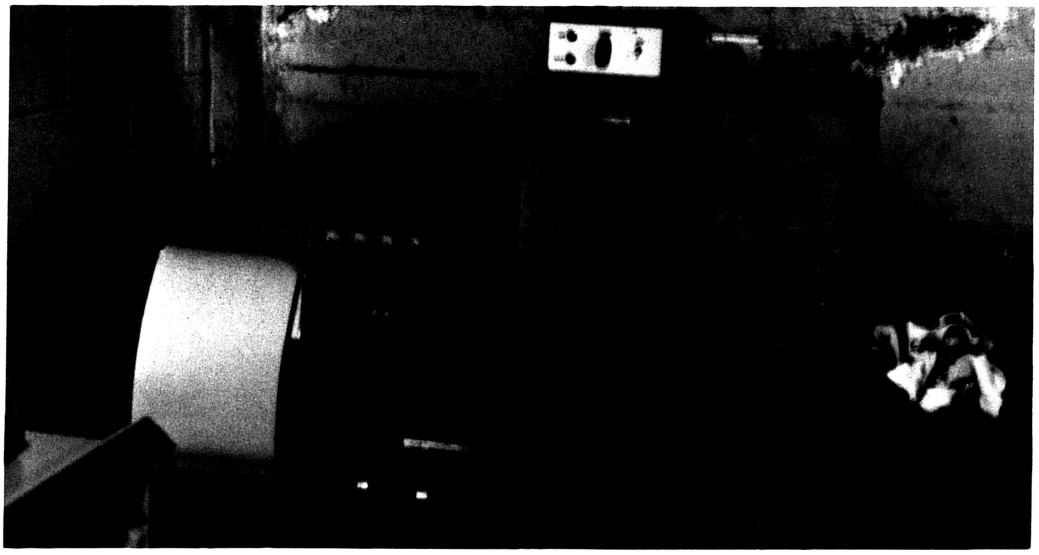

FIG. 61 - Visicorder Unit and Amplifier

After completion of each pile test the pile is removed, and the material is replaced by the same placement procedure each time. On reassembly of the test rig the laboratory pressuremeter is installed by the same technique as the pile. The initial state of stress, as a result of the installation disturbance, around the pile and pressuremeter will then be of the same nature. The response of the pressuremeter is then evaluated by inflating the probe.

From the pressuremeter test the P-y curve can be calculated by the procedure detailed previously. These P-y curves are then used in the finite difference solution to compare the measured lateral load versus head deflection response of the model pile to that predicted by the finite difference solution.

After completion of all tests in clay and loose sand, the test rig underwent modification to increase its capacity prior to commencing tests in dense sand. These modification consisted of:

a) replacing the instrumented hollow model pile with a solid shaft pile of equal size, and
b) replacing the 500 lb (225 kg) load transducer with a 1,000 lb (450 kg) proving ring.

Model Pile and Laboratory Pressuremeter

The model pile for the first test series was fabricated from 1.36 in. (34.5 mm) diameter 1018 carbon steel tubing with a wall thickness of 3/8 in. (9.5 mm) and is shown in Fig. 62. The pile length was 40 in. (1.0 m) including a 2 in. (51 mm) 60^{o} point unit. Seven

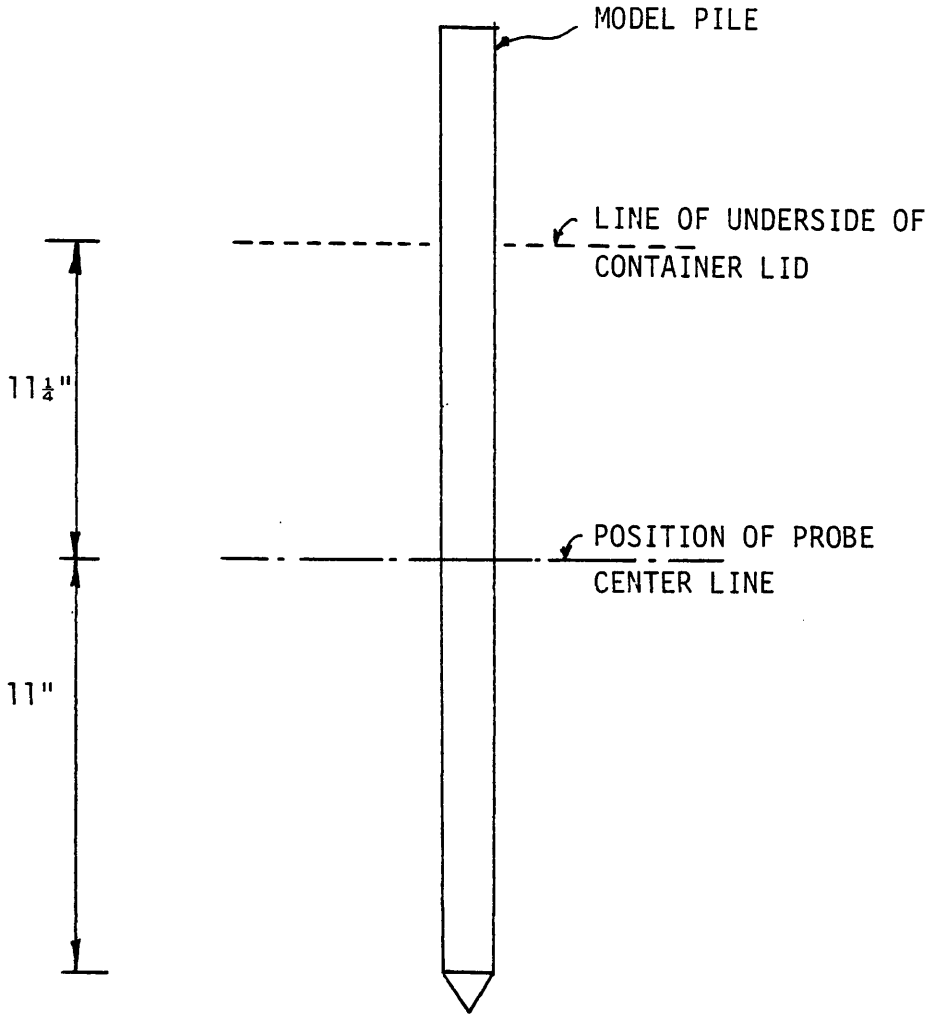

FIG. 62 - Laboratory Pile

electric metal foil type strain gages were bonded at a spacing of 3 in. (76 mm) along the outside of the piles embedded length of 22 in. (559 mm), commencing at the soil surface. Gage manufacturer was William T. Bean, Inc. of Michigan, gage designation number is BAE-XX-125AA-350 with a nominal length of 0.125 in. (3 mm). The manufacturers reported specification gives 5% accuracy of measured strains up to 3% elongation. Electrical connections were made to the gage and the leads taken through a small hole into the hollow pile to finally exit from the pile top. Flexural stiffness of the pile is 4.8×10^6 lb in.^{2} (13.8 kN m^2) by calculation.

The model pile for the second test series in dense sand was fabricated from a 1.36 in. (34.5 mm) diameter solid mild steel shaft with a 60^o point, and was uninstrumented. Flexural stiffness of the pile is 4.98×10^6 lb in.^{2} (14.3 kN m^2) by calculation.

The laboratory pressuremeter was developed by Briaud and Shields (18) for evaluation of pavement subgrades. This is the commercially available PAV, manufactured by ROCTEST, Inc., New York, and is a monocell unit. The single modification to the pressuremeter was installation of an electric pressure transducer to improve the reading accuracy of pressures. Test 245 details the calibration of the transducers used. The deflated probe diameter is 1.378 in. (35 mm) with a measuring cell length of 9.0 in. (230 mm) giving an initial volume of 13.5 in.^{3} (220 cc). The control unit allows an injected volume of 15.5 in.^{3} (100 cc) to be made which achieves approximately 45% volumetric strain, or 22.5% radial movement. Full inflation of the probe is reached in approximately 10 min, to give consistant rate

effects at a volumetric strain rate of 4.5% per minute. Reduction of the raw data is made by a short computer program written in BASIC language on a HP 85 desk top computer. Both membrane stiffness calibration and volume loss calibration are achieved by the use of statistical regression and are found to be of the order shown on Fig. 63.

The probe unit was fitted with a driving head and shoe to allow the pressuremeter to be driven in place. With the pressuremeter in place in the soil the control unit was located at an elevation to give zero hydrostatic correction at the gage level.

Calibration and Performance Tests

A series of tests were conducted to ensure the satisfactory performance of the test rig. With the soil container removed and the pile locked in position, the base of the pile was connected to a calibrated proving ring. By operating the test rig a series of calibration tests could be performed.

Tests 4 and 5 evaluated the contribution to the measured lateral load from bearing friction arising from the high rotational restraint they provided. Up to the load cell capacity of 500 lbs (225 kg) bearing friction contributed less than 4% under a bending moment of 13.8 kip-in. (1.5 kN-m) applied at the pile head.

Tests 107-112 were designed to check gage accuracy, creep under constant load and visicorder channel stability. From these tests, which are summarized in Apendix III, the following comments can be made:

1) Strain gages output gave strains 12% to 13.5% lower

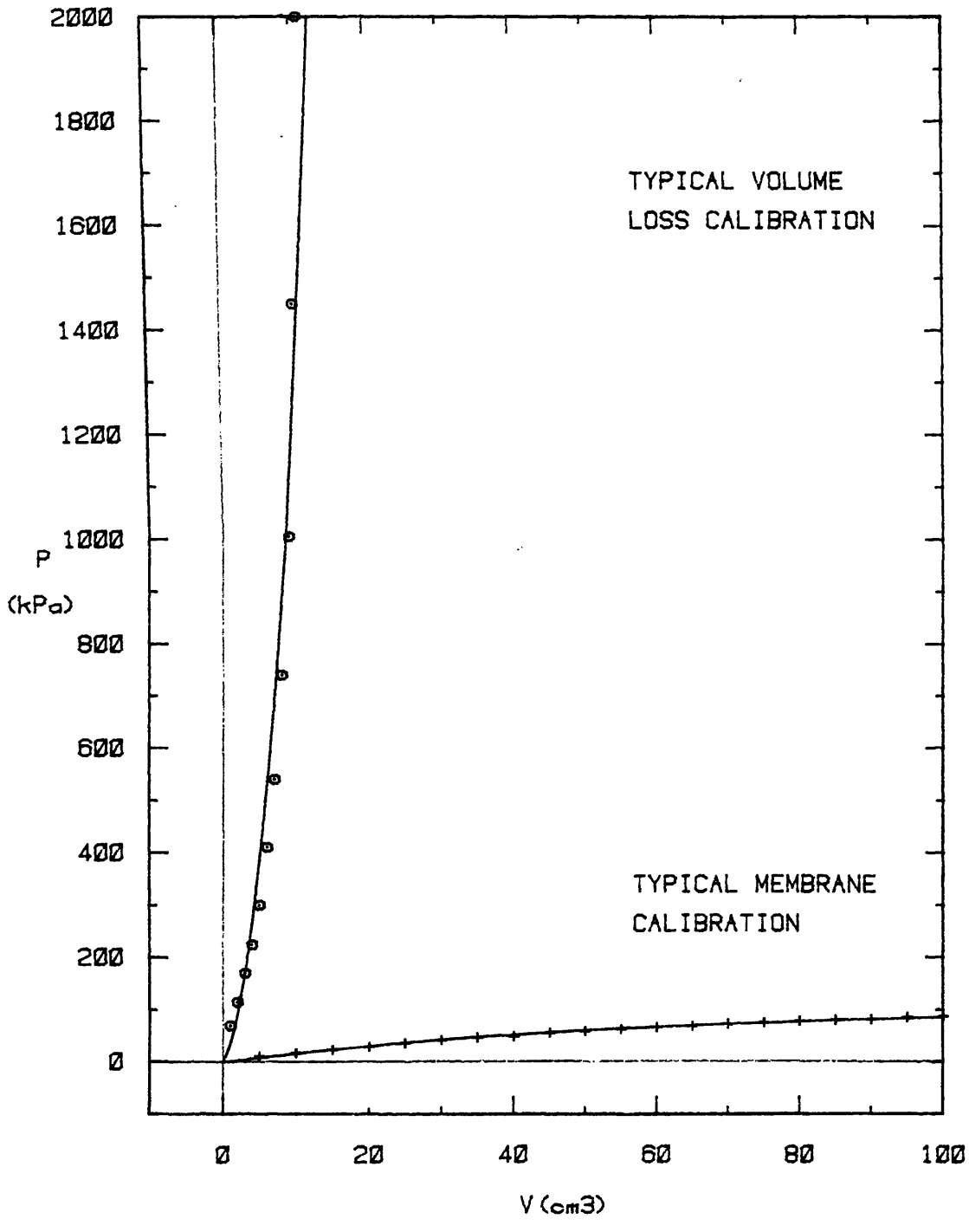

FIG. 63 - Typical Volume Loss and Membrane Resistance for Laboratory Pressuremeter

than those calculated.

2) All gage locations gave approximately the same percent error at all load levels with different amounts from gage to gage.

3) The gage error decreased with higher lever arms suggesting an error in the measured lever arm.

4) All gages were proved to be linear and repeatable. Variations within 10% were obtained from output interpretation.

Test 111 was held under constant load for 5 hrs to check recorder channel and gage stability, which proved satisfactory. Test 117 comprised cyclic 'exercising' of all gages and instrumentation prior to the dense sand tests, to a maximum load of 996 lbs. (451 kg).

In conclusion, the performance of the test rig was satisfactory and the accuracy limited by physical interpretation of the output.

To confirm the effectiveness of the lid to produce a confining pressure, a series of tests, 27-30, were performed in dense sand. From tests 27-29 it can be seen that without confinement the material is uniform with a limit pressure at approximately 40 psi (276 kPa) and the effect of confinement is an increase of limit pressure to approximately 56 psi (386 kPa).

The Selected Soils and Placement Procedures

Sand

The sand used in the study was a fine angular particle concrete sand. The results of sieve analysis tests, 18-21, are given in Fig. 64. From the grading curves, under the unified system of soil classification, U.S.S.C., the sand is classified as SP. The sand was placed

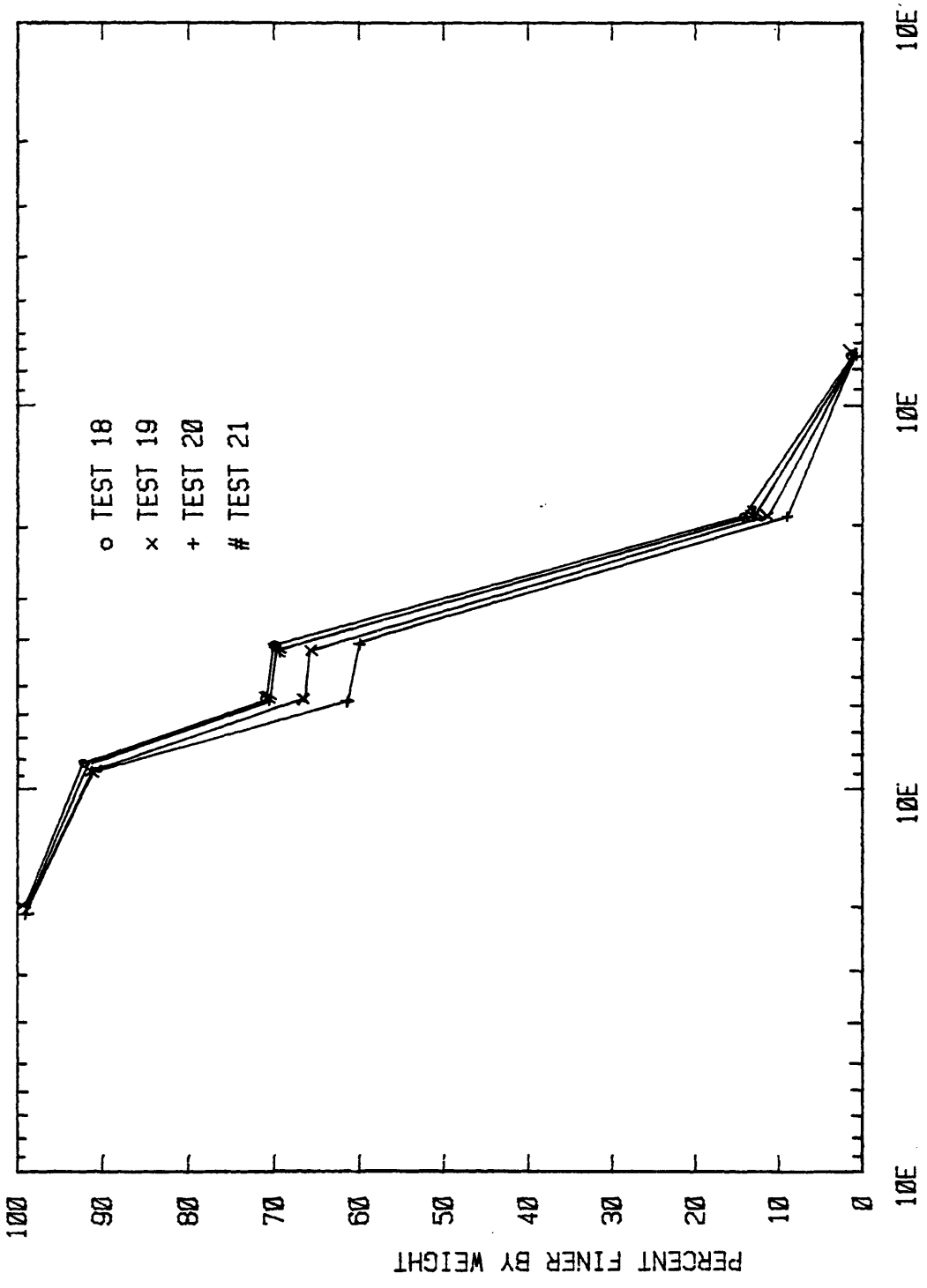

FIG. 64 - Sieve Analysis of Laboratory Sand

dry at all times to ensure the study of a purely frictional material. Relative density tests, 10-17, performed in a mould of 58.3 in.^{3} (955 cc) gave a minimum and maximum dry density of 94 lb/ft^3 (1507 kg/m^3) and 108 lb/ft^3 (1730 kg/m^3) respectively.

The deviator stress versus axial strain from a series of triaxial tests, 22-26, is plotted in Fig. 65(a). Shear stress, τ, versus normal stress, σ_n, as shown in Fig.65(b)gives the angle of shearing resistance of 40°-45°.

The results from Direct Shear Box tests, 143-146, gave angles of shearing resistance in the range 37°-44°.

It is widely recognized, (25,98) that the formation of sand beds with uniform porosity is a substantial problem. The investigation concentrated on pile and pressuremeter behavior in dense sand at a maximum attainable relative density. Dense sand samples are easier to reproduce consistently, a factor of prime importance when comparing a pile and pressuremeter test in material that is repeatedly replaced.To achieve this maximum density, with little anisotropy, a 2 in. (50 mm) vibrating concrete poker was selected and a standard pattern of insertions used. The total density achieved was continually monitored and is reported for each test in Appendix IV.

A series of penetrometer tests were made, 131, 133-135, 243-244, to study the sample uniformity and local vibrator withdrawal effects, see Fig. 66. The penetrometer comprised a 0.5 in. (12 mm) steel rod with a 0.75 in. (19 mm) cone tip. The number of blows were recorded for 12 in. (305 mm), 18 in. (460 mm) and 24 in.

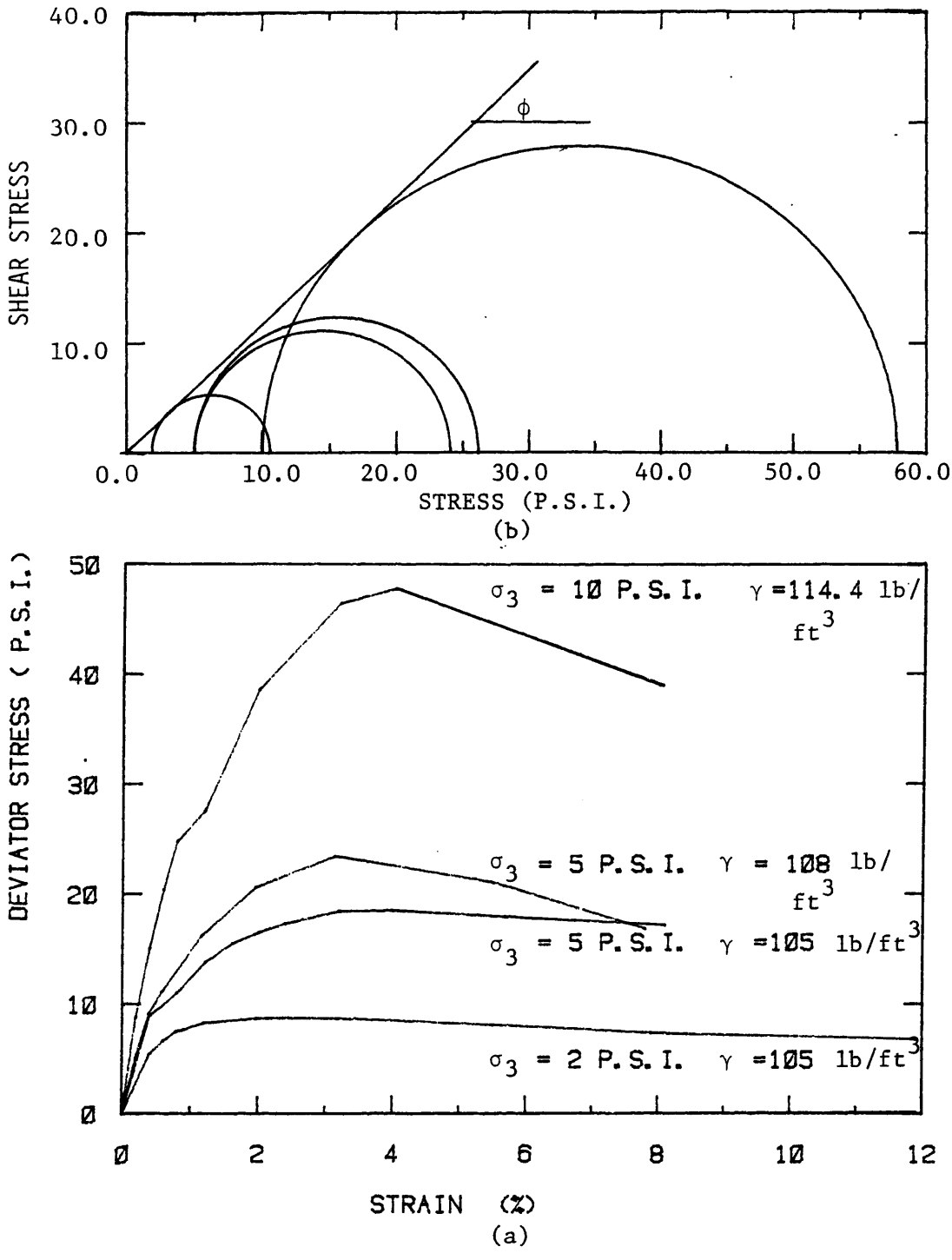

FIG. 65 - Triaxial Test Results on Laboratory Sand

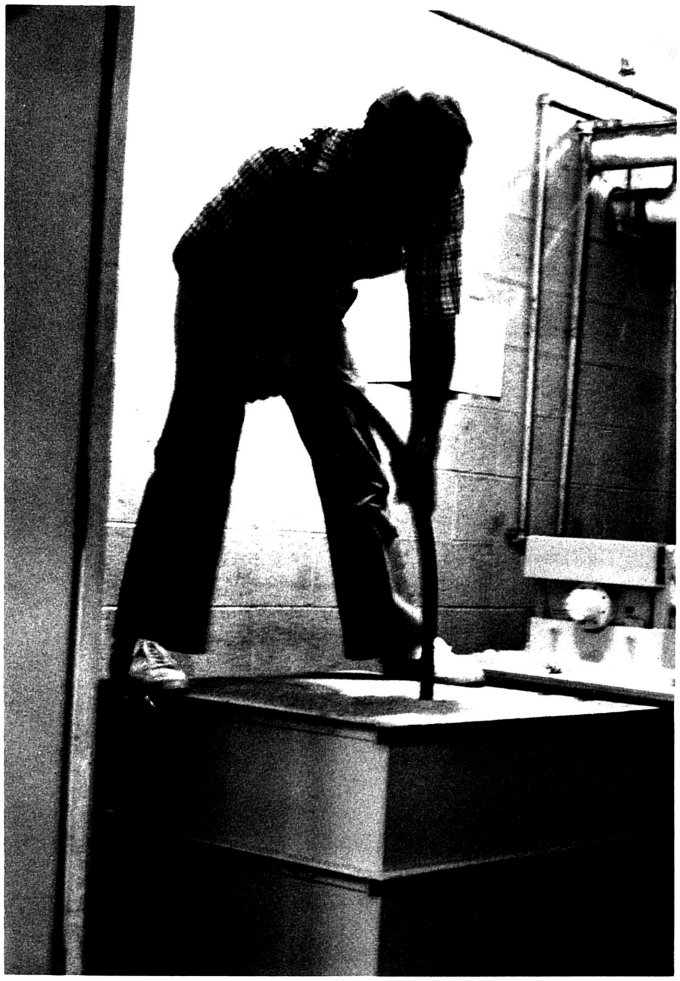

FIG. 66 - Compaction of Dense Sand by a Vibrator

(610 mm) penetration under a 10 lb (4.5 kg) weight falling 8 in. (200 mm). The results show the penetrometer to be highly sensitive to locate density variations. Test 51 investigated the phenomenon that withdrawal of the vibrating poker leaves a highly local zone of low density material. This phenomenon is illustrated in Fig. 68. After inserting the vibrating poker on a 9 x 9 pattern of insertions, in the order shown on Fig. 67, two penetrometer profiles were made, on axis A-A and B-B. The poker was last withdrawn at the center. The profiles clearly show a reduction of 75% at 12 in. (305 mm), 60% at 18 in. (457 mm) and 40% at 24 in. (610 mm) from the maximum blow counts.

Using the penetrometer, a final vibrator insertion pattern of (3 x 4) + 1, i.e. 13 total, at the locations shown in Fig. 69, was found to be acceptable to attain a uniform deposit at a maximum density of 115 lbs/ft^3 (1840 kg/m^3). Upon final removal of the sand density checks were made on a series of 4 in. (100 mm) layers. Density variation between layers showed a slight increase with depth, 9% from the top layer to the bottom layer.

Prior to the series of tests on dense sand, a short series of pile and pressuremeter tests were performed, tests 55, 70, 73 and 74 on loose sand. Following the recommendations of Kolbuszewski and Jones (52), the sand rain method was adopted. They concluded that the rain of sand which issues from a stationary sieve produces a uniform deposit when the sieve is above a critical height of fall. A large U.S. standard No. 10 concrete sieve was chosen and suspended above the box at a height which gave equal densities throughout the layer,

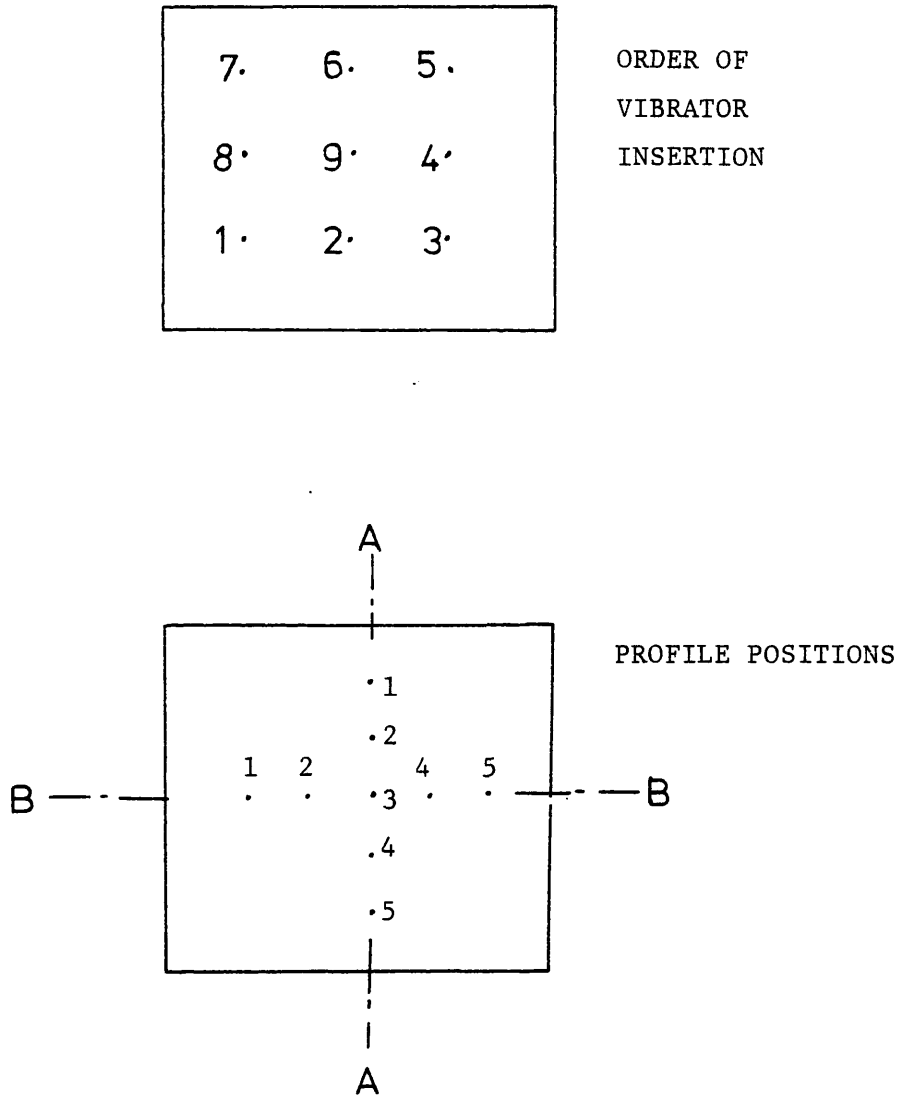

FIG. 67 - Soil Container Profile Positions and Vibrator Insertion Order

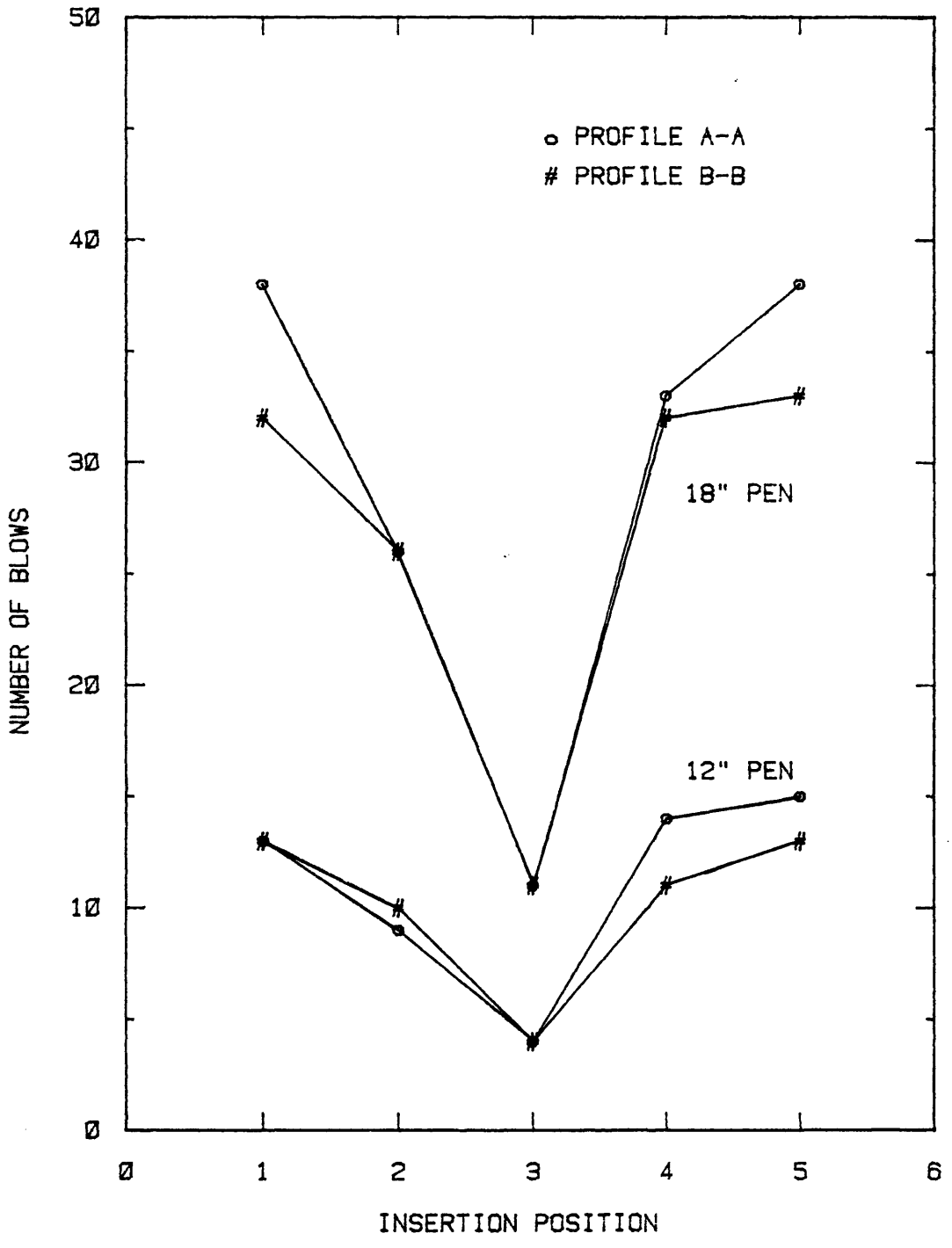

FIG. 68 - Penetration Results on Profiles A-A and B-B

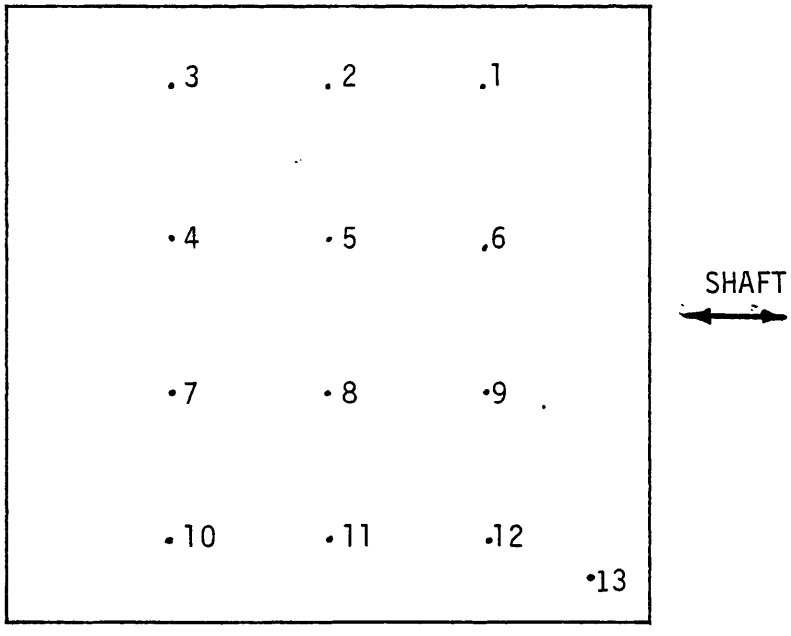

FIG. 69 - Vibrator Insertion Pattern
for Dense Sand

recorded by 30 ml Pyrex density pots. The density achieved was found to be 102 lb/ft^3 (1635 kg/m^3) by this technique.

Clay

A low plasticity remolded ceramic clay was selected with plastic limit, w_p, of 20%, liquid limit, w_L, of 43% and plasticity index of 23%. The classification according to the U.S.S.C. is CL. The ceramic application and Atterberg limits suggest the predominant clay mineral is koalin. The clay was supplied, pre-mixed, in thirty 50 lb (23 kg) packages at a mean water content of 28.7% and a standard deviation of 0.84%. Random hand vane shear strength determinations throughout the samples gave a range of 500 lbs/ft^2 (24 kPa) to 560 lbs/ft^2 (27 kPa). Unconfined triaxial compression tests gave shear strengths of 480 lb/ft^2 (23 kPa) and 462 lb/ft^2 (22 kPa).

Compaction was achieved in 30 layers by 0.8 in. (20 mm) lifts with approximately 1000-1100 blows per layer from a tamping plate. The tamping plate, shown in Fig. 70, comprised a 3 in. (78 mm) rod of total weight 3.1 lbs (1.4 kg). After the completion of each layer, 6.1 in^3 (100 cc) of distilled water was sprayed over the surface to avoid surface evaporation. The filling procedure is illustrated in Fig. 71. The level was flush to the container walls and slightly domed to the center. Upon bolting of the lid, effective vertical confinement was then ensured. The total unit weight was 122 lb/ft^3 (1950 kg/m^3).

After the completion of each test the pile, or pressuremeter, was removed and excavation of the sample center was made, 8 in. (200 mm)

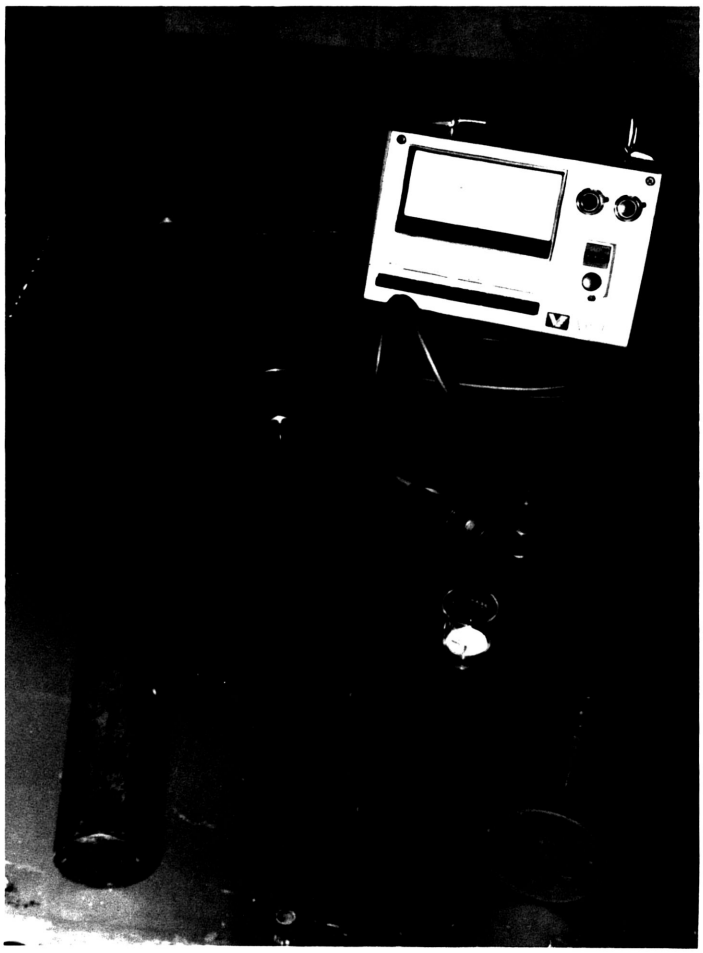

FIG. 70 - From the Left: Pile Hammer, Density Penetrometer, Pressure Transducer, Density Pot and Clay Tamping Plate

FIG. 71 - Clay Compaction Technique

in diameter, to the full depth. Replacement and recompaction of this center was made from the excavated material prior to commencement of the subsequent tests. The actual densities achieved for each test is shown in Appendix IV.

A pattern of hand vane shear strength determinations was made midway through the test series, 97 and 98, to ascertain any changes from the initial compaction state. Test depths of 0 in., 7 in. (177 mm) and 14 in. (355 mm) were selected and shear strengths remained in the range 500 lb/ft^2 (24 kPa) to 560 lb/ft^2 (27 kPa) which confirmed little or no changes had taken place. At all times, after initial filling of the box, the clay sample surface was maintained moist and covered, with the exception of the test location, with polyethylene.

To further confirm the uniformity of the material, a series of pressuremeter tests were conducted, 80-83, in 1.375 in. (35 mm) augered boreholes. These results show uniformity of limit pressures to within 7%. Average water contents on the pile center line during the test series, 116, and upon removal of the clay, 125, showed no change from the initial water content.

Pile Testing Procedure and Results

The soil container is fully detachable, moving on castors from the main rig to allow closely controlled soil placement procedures. After the soil is placed, the container and test rig are brought together and finally bolted around the lid in twelve positions and at

the top and bottom of the main rig frame. The pile is then inserted by driving, using the head jig as a driving guide. Installation of the pile is facilitated by a slot opening, 8.3 in. (210 mm) long by 3.8 in. (97 mm) wide in the container lid. The head restraint is then applied, by the head jig for a fixed head mode test,or a wire rope for a free head mode test. After placing the dial gages to record head rotation, the test commences at a constant displacement rate. The rate of displacement is set to approximate the rate of radial movement achieved by the pressuremeter test to minimize rate effects.

Typically,after assembling the head jig, premature bending strains were mobilized in the pile. These strains form the origin of all readings. After completion of the test the pile is withddrawn and the soil replaced by the procedure detailed in the previous section.

Table 4 details the number of free and fixed head tests in all soils. To investigate the effect of residual stresses from driving into the dense sand, tests 214 and 215 were conducted after relieving these stresses. This was accomplished by re-insertion of the vibrator in a zone away from the pile back, and carefully withdrawing it. To study the effects of variable embedment, tests 224, 225 and 226 where conducted at embedments of 10 in. (250 mm), 12 in. (304 mm) and 14 in. (356 mm) respectively.

A summary of the results from the five groups of tests indicated in Table 4 is given in Figs. 72, 73, 74, 75 and 76 by plotting applied lateral load versus deflection at the container lid line. The

Table 4 - Laboratory Model Pile Tests

HEAD RESTRAINT MODE	SOIL	TESTS NUMBER	TOTAL NUMBER OF TESTS	COMMENTS
Free	Clay	119,120	2	
Fixed	Clay	114,115,117 118	4	
Fixed	Loose Sand	129	1	
Fixed	Dense Sand	238,239,240, 241,132,210, 214,215,242	9	214,215,Relaxed stresses 240-242 Variable embedment
Free	Dense Sand	212,213,216, 217	4	216,217 Relaxed stresses
		TOTAL	20	

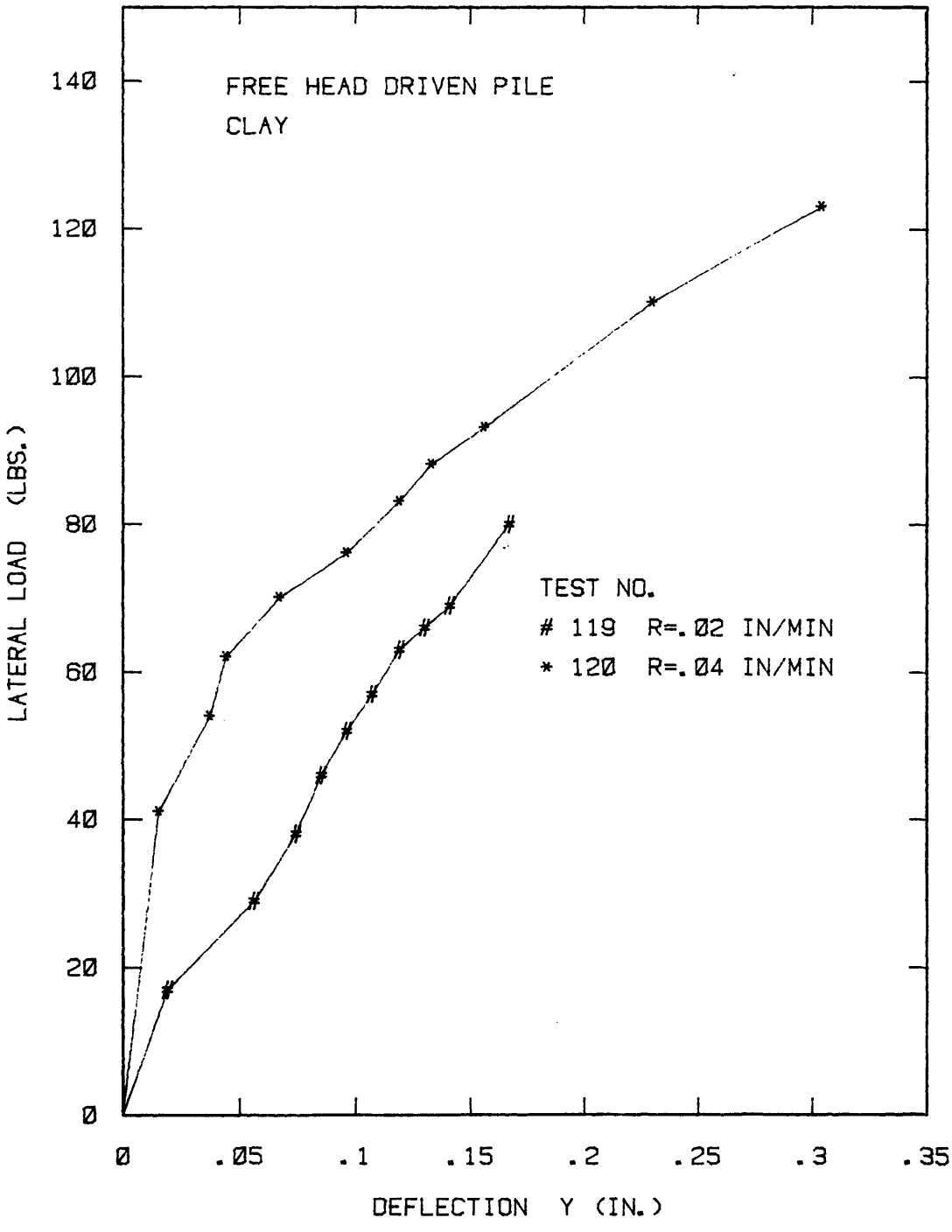

FIG. 72 - Model Pile Results for Free Head Restraint in Clay

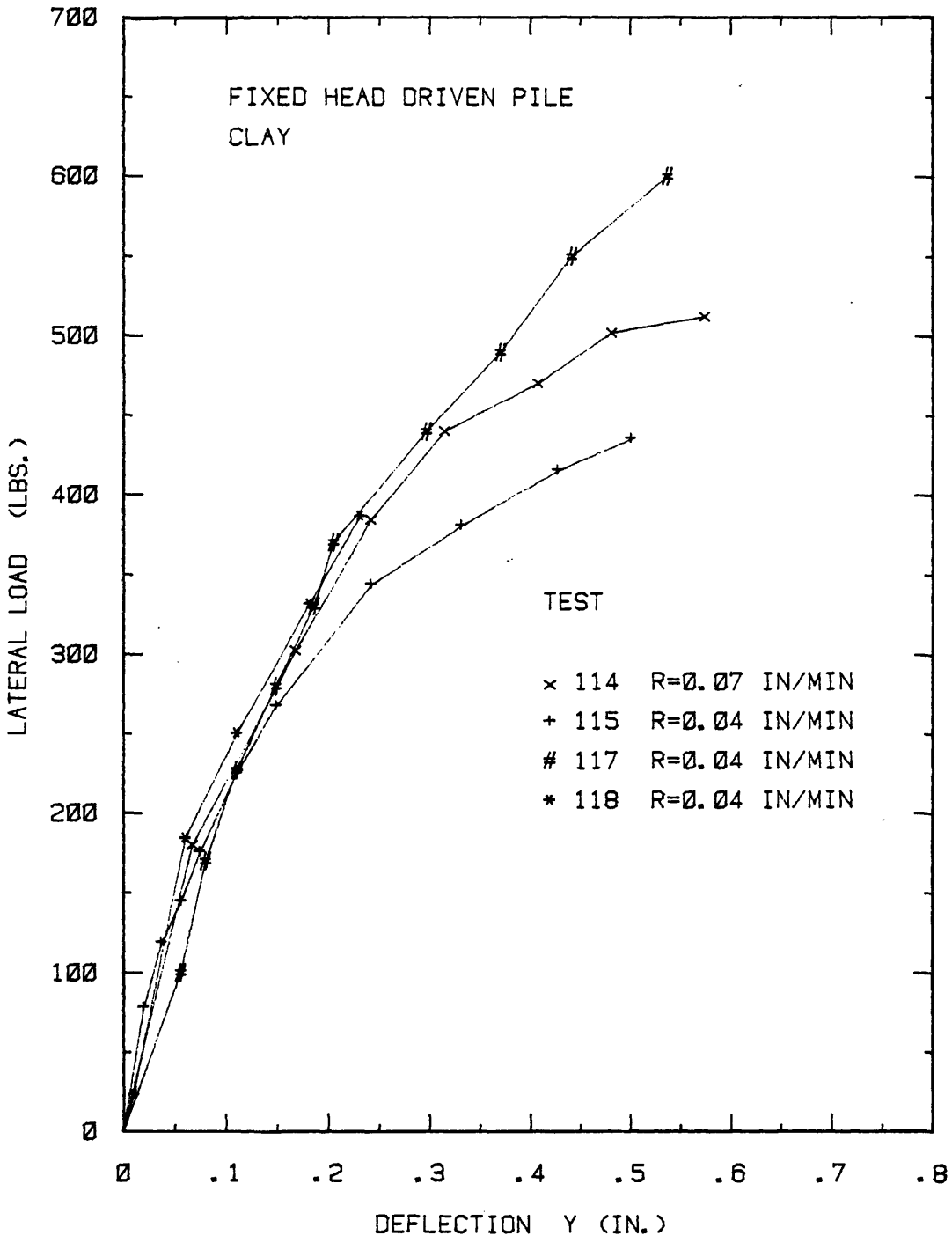

FIG. 73 - Model Pile Results for
Fixed Head Restraint in Clay

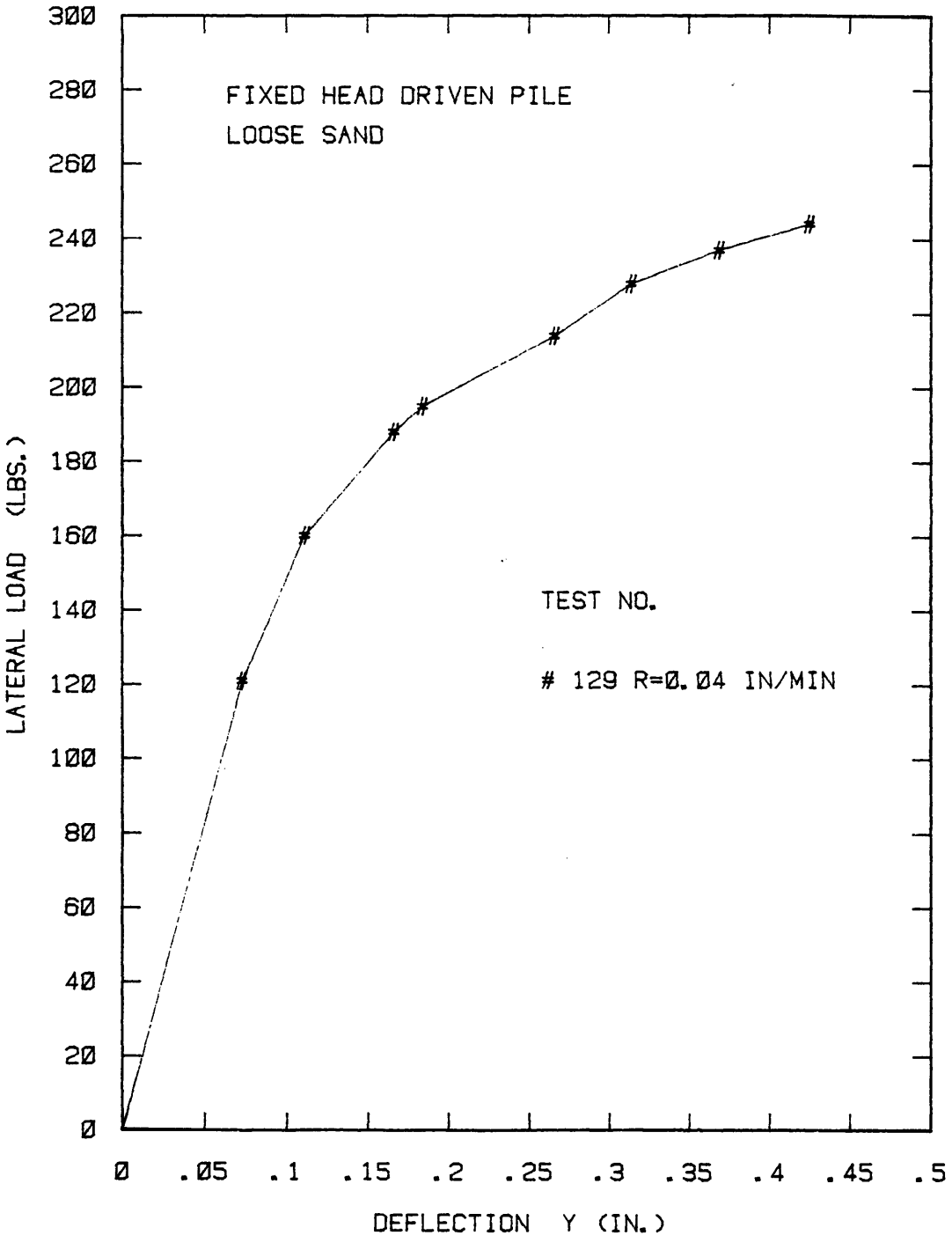

FIG. 74 - Model Pile Results for Fixed Head Restraint in Loose Sand

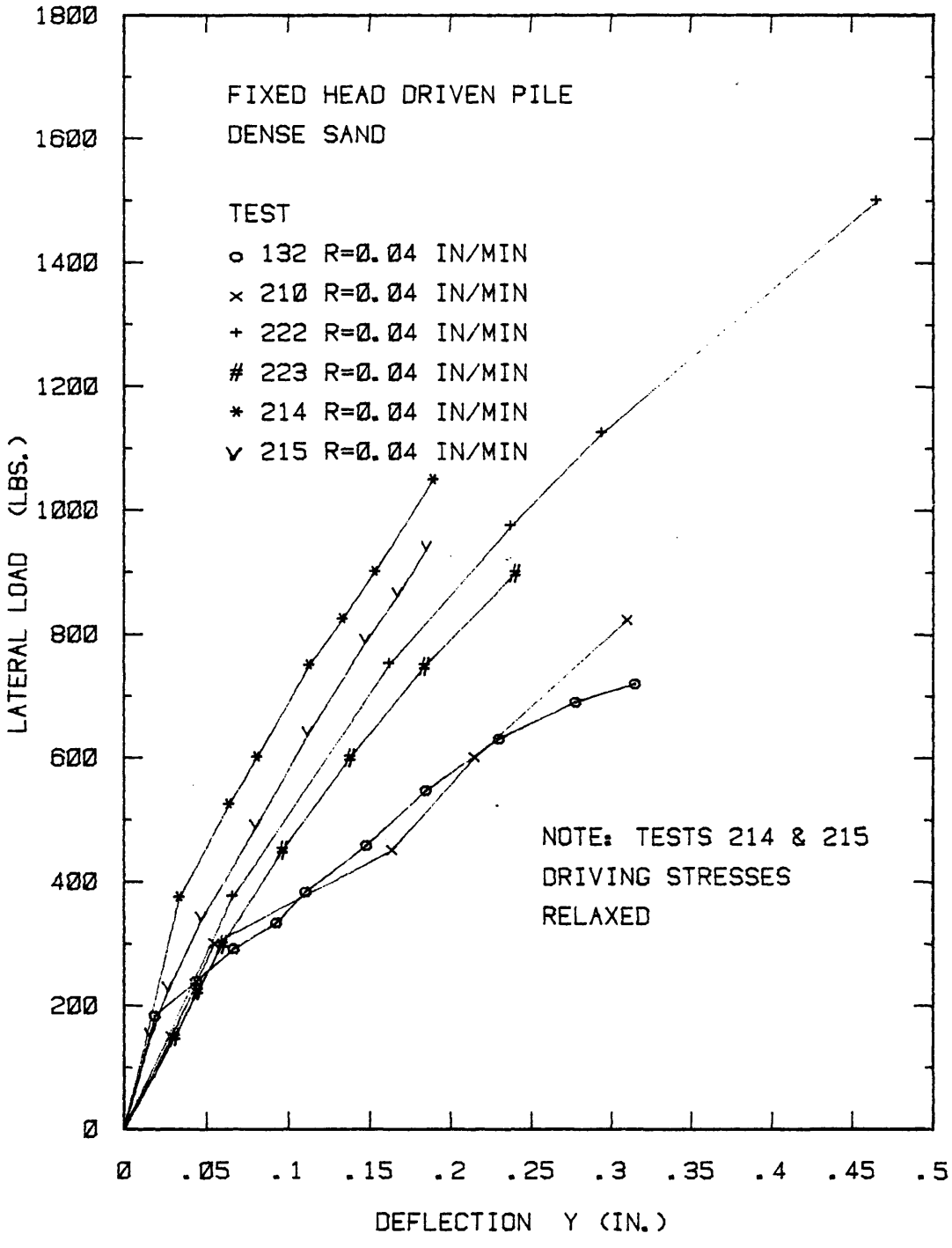

FIG. 75 - Model Pile Results for Fixed Head Restraint in Dense Sand

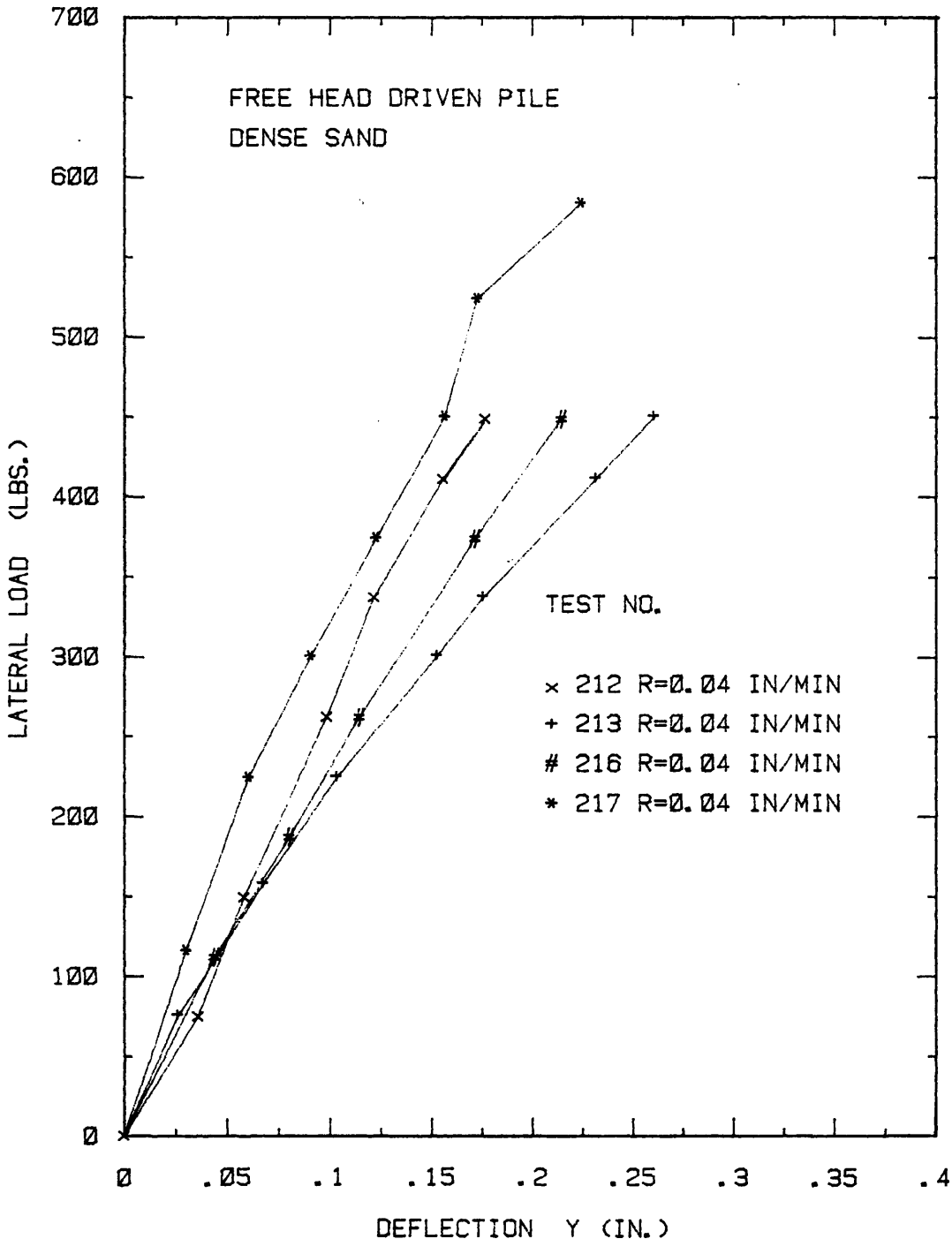

FIG. 76 - Model Pile Results for Free Head Restraint in Dense Sand

variable embedment tests 224, 225 and 226 are shown in Fig. 77.

Pressuremeter Testing Procedure and Results

A series of pressuremeter tests were conducted in both sand and clay after reproducing the same soil placement and pile installation techniques used for the model pile tests. The number of blows required to insert the pressuremeter for the driven tests is detailed in Appendix III. After installation, since no head restraint is required, the pressuremeter test was conducted and the response evaluated. At the commencement of each testing session, within the same day, membrane calibration and volume loss correction tests were performed.

Table 5 presents a summary of the pressuremeter tests undertaken. A single representative pressuremeter test from each of the four groups presented in Table 5 is given in Figs. 78, 79, 80 and 81. In all cases pressuremeter tests commenced within 20 minutes of installation.

Analysis of Results

Introduction

The technique developed in the previous Section to construct P-y curves is applied to the measured pressuremeter results. Allowance is made for a local critical depth effect due to the aperture in the container lid, by arbitrarily reducing the P-y curve within the top 1-1/2 diameters by 50%. The finite difference computer program, COM622, described previously is used with the pressuremeter P-y

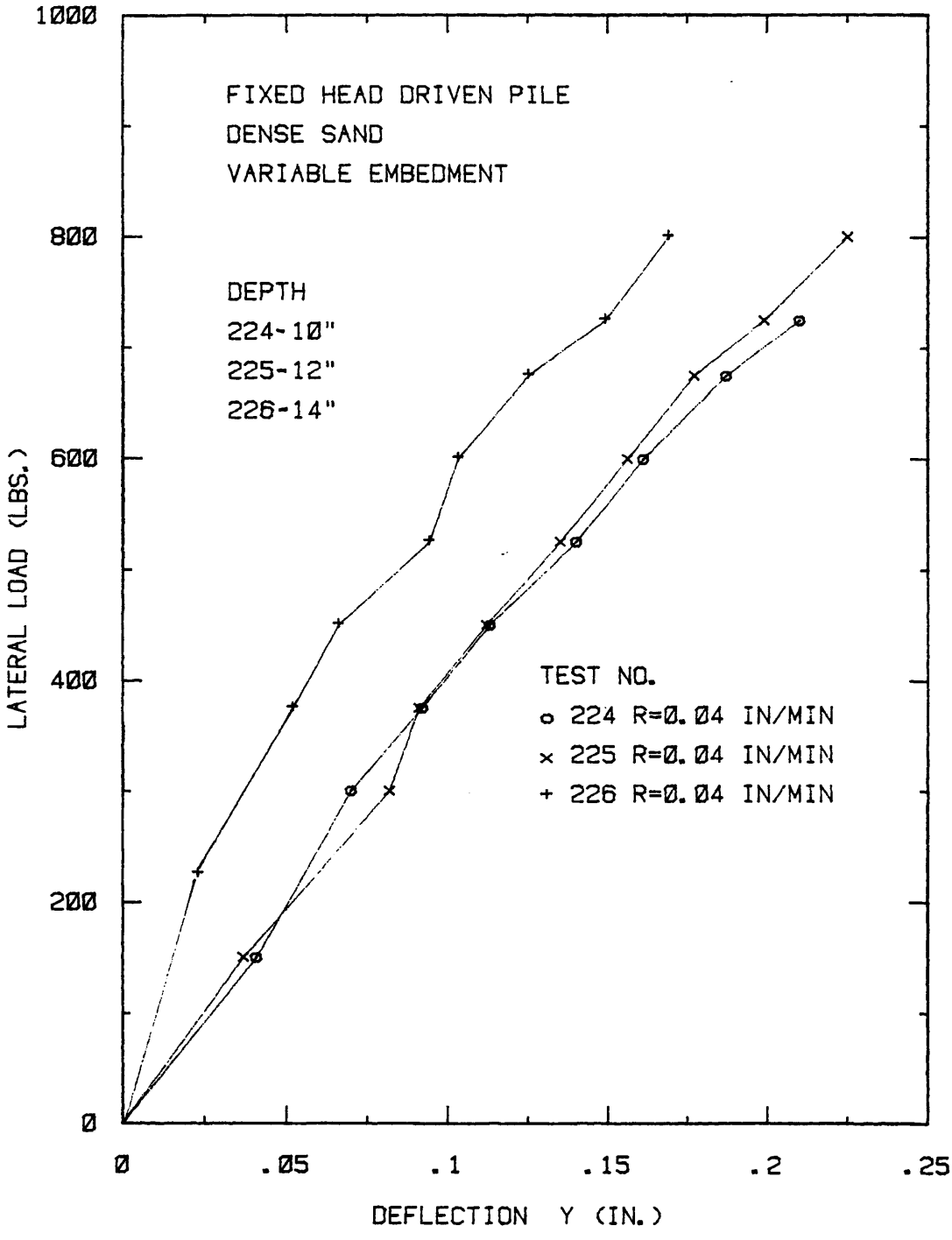

FIG. 77 - Model Pile Results for Variable Embedment with Fixed Head Restraint in Dense Sand

Table 5 - Laboratory Pressuremeter Tests

SOIL	INSTALLATION TECHNIQUE	TESTS NUMBER	TOTAL NUMBER OF TESTS	REMARKS
Clay	Driven	86,87,91,96 122	5	96,122 Cyclic
Clay	Augered	85,92,95,105	4	95 Cyclic
Dense Sand	Driven	48,49,57,36, 41,42,43,44 46,2234,235, 236,237	13	48,49 Relaxed Stresses
Loose Sand	Pushed	55,70,73,74	4	
		TOTAL	26	

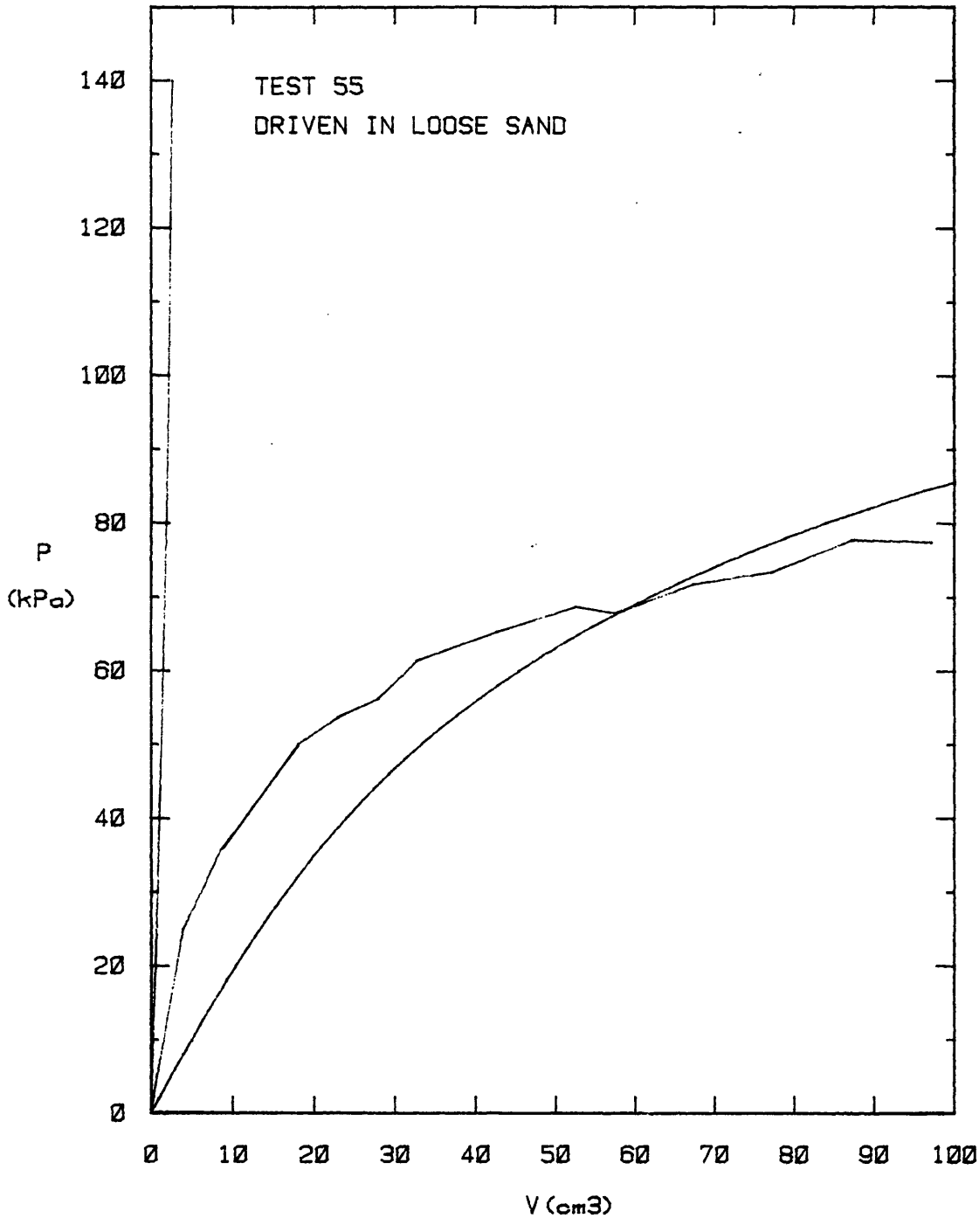

FIG. 78 - Selected Laboratory Pressuremeter Result in Loose Sand

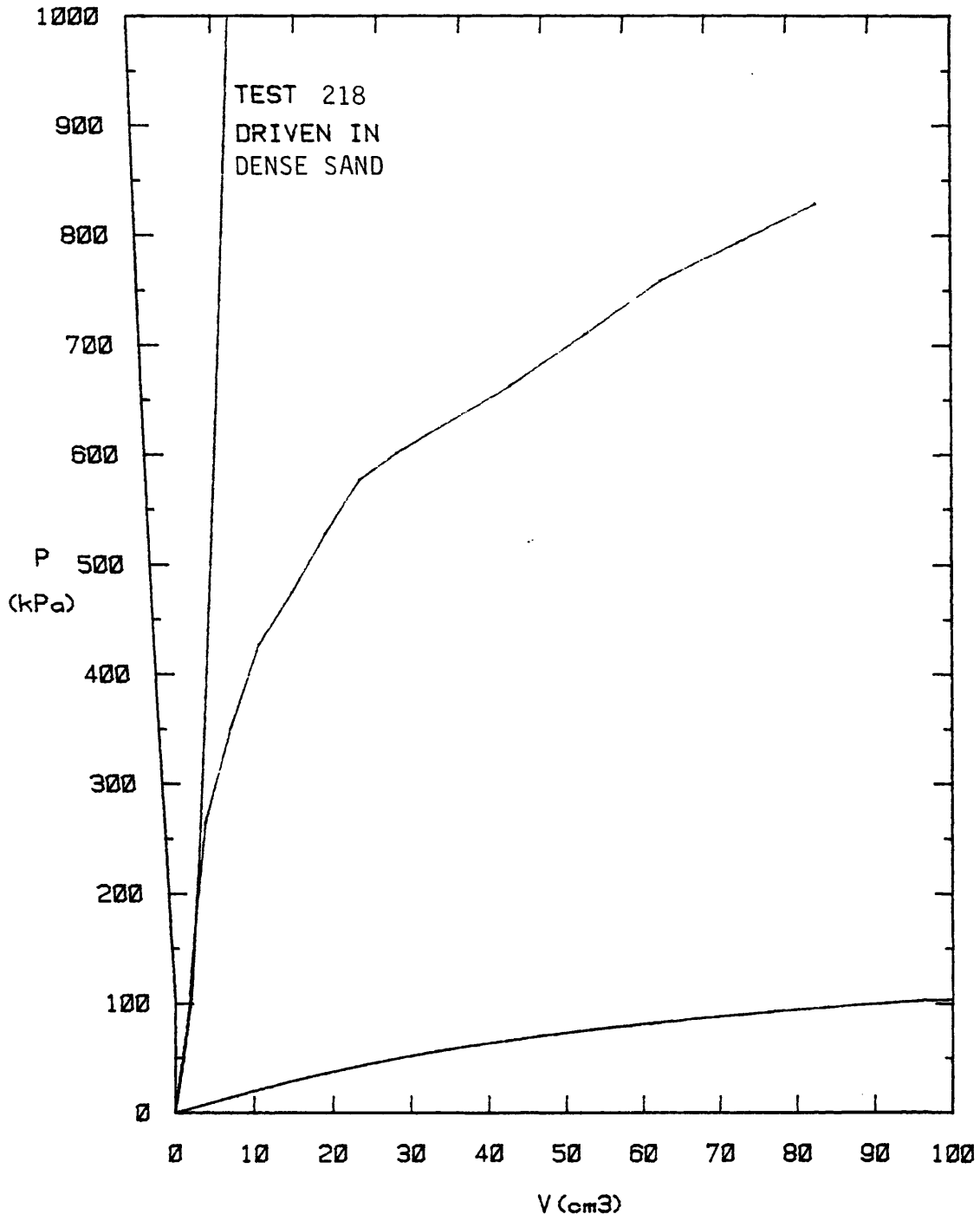

FIG. 79 - Selected Laboratory Pressuremeter Result in Dense Sand

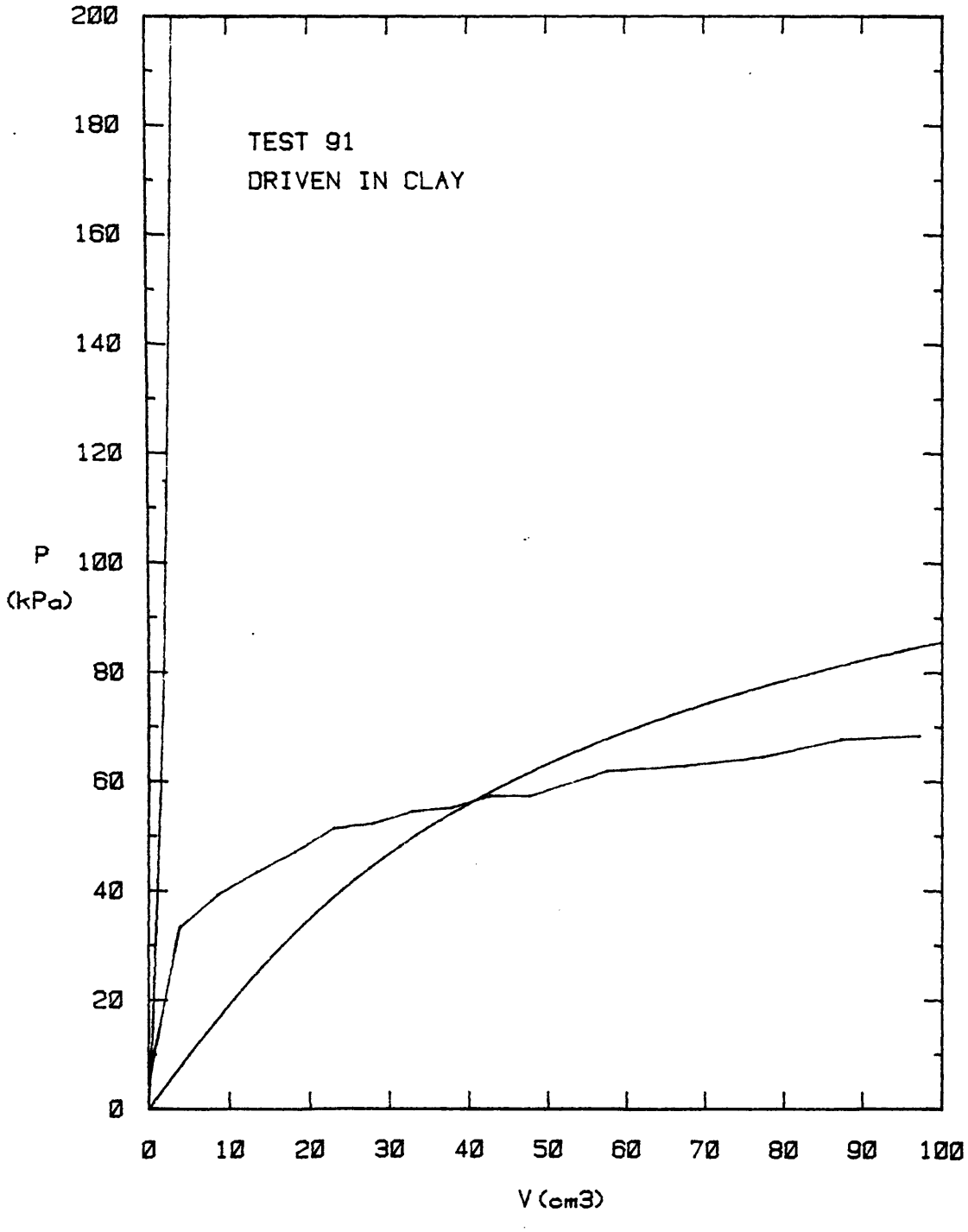

FIG. 80 - Selected Laboratory Pressuremeter Result Driven into Clay

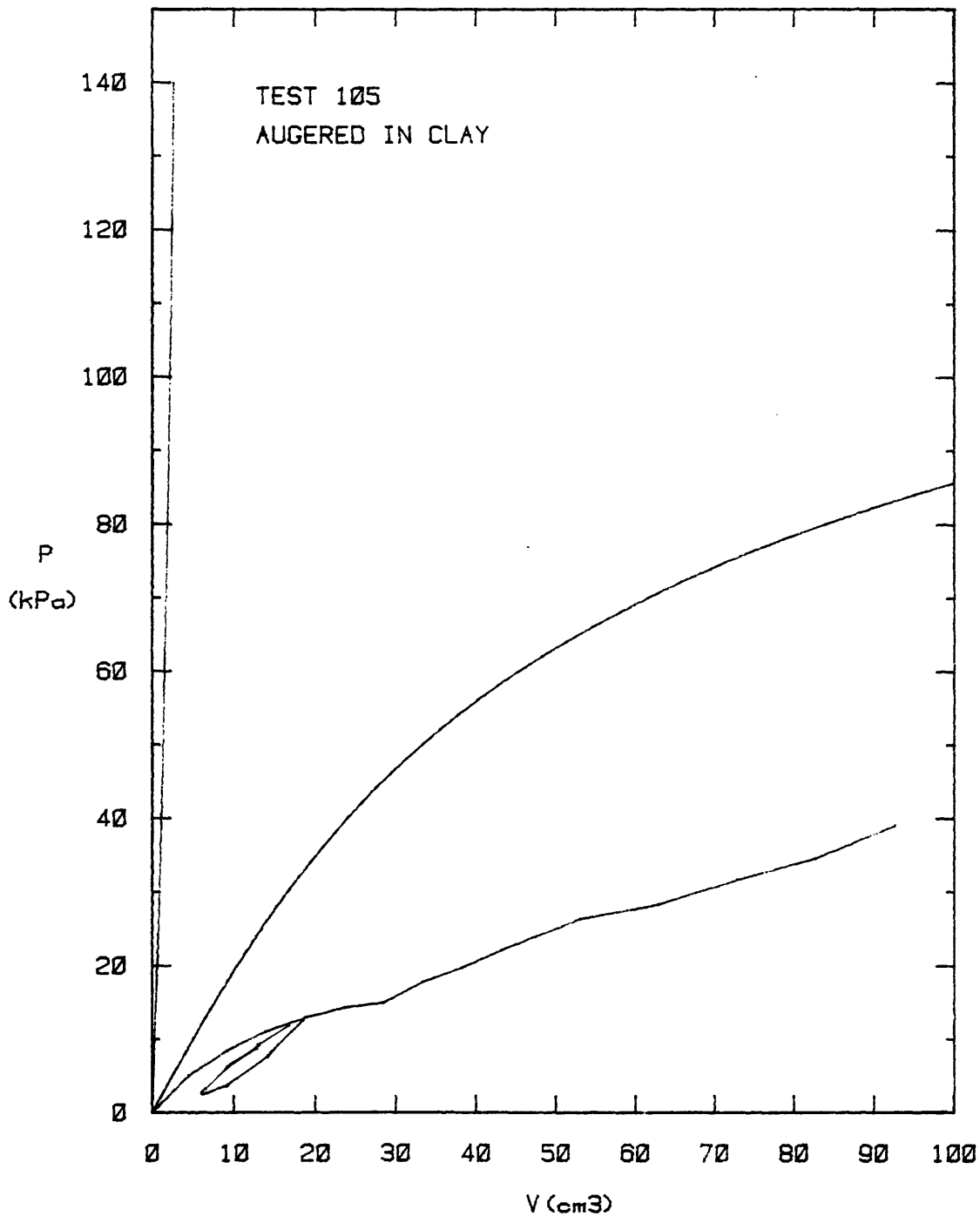

FIG. 81 - Selected Laboratory Pressuremeter Result Augered into Clay

required input. The lateral load versus surface deflection curves for the model pile tests are then predicted and compared with the measured results.

The radial movement available from the pressuremeter at a full volumetric strain of 45% is approximately 22%. This radial movement represents an increase in radius of 0.132 in. (3.35 mm); therefore, the maximum prediction within the range of the pressuremeter expansion is a pile displacement of 0.13 in. (3.3 mm). Prediction beyond this range of pile deflection involves extrapolation of pressuremeter P-y curves. For this reason comparison of the load deflection relationship is limited to the maximum deflection of approximately 0.2 in. (5.0 mm).

For the fixed head pile test predictions, COM622 is programmed with angular head restraint of 1.0×10^6 lb/in./θ (115 kN-m/θ), where θ is the angle of rotation, expressed as a tangent, to represent fixed head conditions. This is based on the calibration tests.

Loose Sand

Fig. 82 shows the prediction of a fixed head pile in loose sand based on the P-y curve derived from pressuremeter test 55. Excellent agreement is found in both the working range load-deflection modulus and the ultimate range. However, severe disturbance, accompanied by a rapid collapse of the sand structure, was observed on both pile test 129 and all pressuremeter tests. Contact was lost with the container lid and some depth effect is present. The pressuremeter probe is located at a centerline depth of approximately 15 radii. Based on the

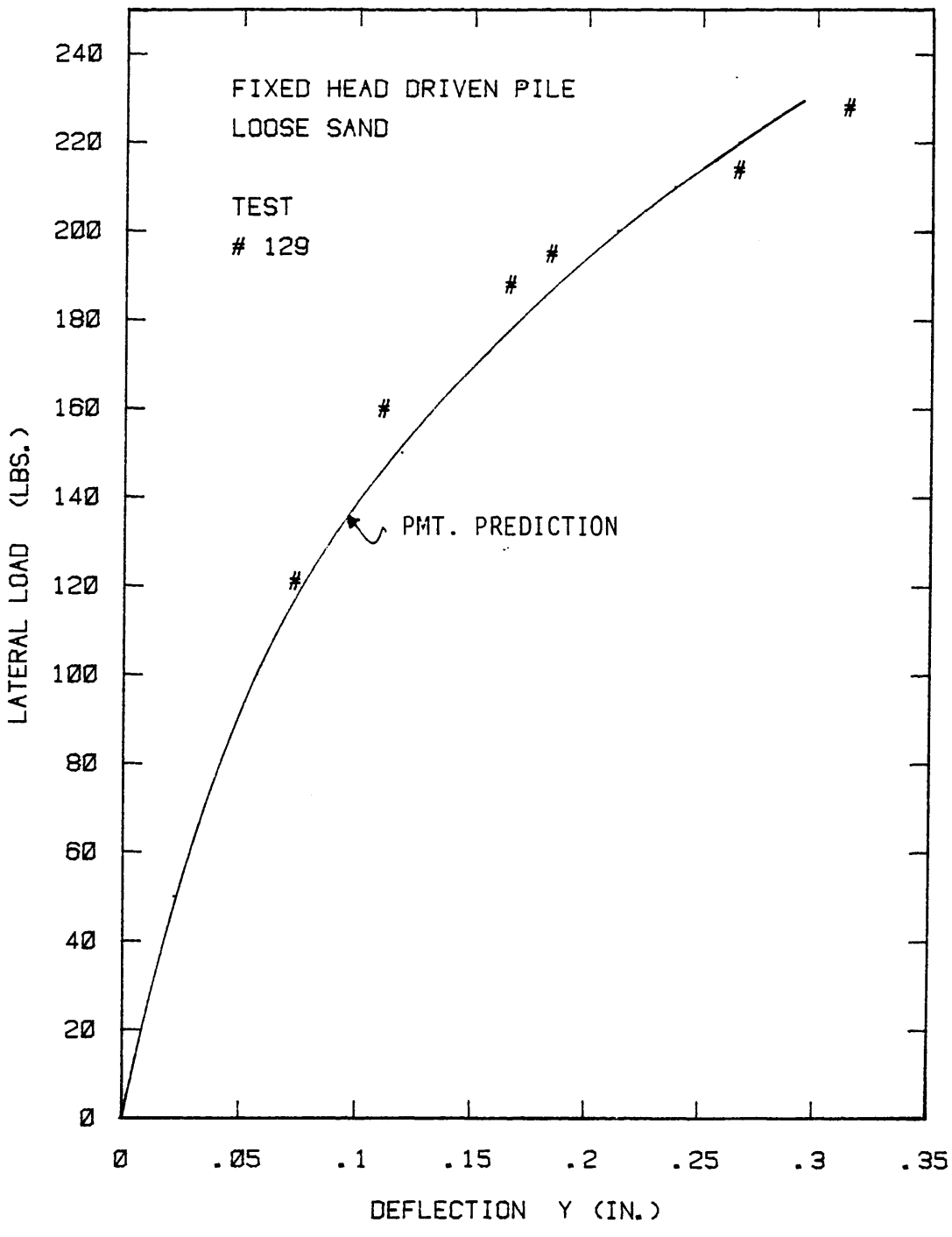

FIG. 82 - Prediction of Model Pile Response in Loose Sand

finite element study previously the pressuremeter is also subjected to a limited depth effect. Further, the sand density during the pile load test showed a 5% increase from pressuremeter test 55 reflecting the problem in accurately reproducing loose sand deposits.

In conclusion it can be inferred that the generated P-y curve in loose sand is slightly conservative, but the results of the installation disturbance are difficult to quantify.

Dense Sand

The predictions for fixed and free head pile tests in dense sand, based on P-y predictions from pressuremeter test 218, are shown in Figs. 83 and 84 respectively.

Pile load tests 214 and 215 in fixed head mode, and 216 and 217 in free head mode were conducted after removal of all driving stresses by re-insertion of the vibrator behind the pile. The lateral load versus deflection response is clearly stiffer than those without removal of driving stresses and suggests that pile driving dilates the dense sand and weakens the modulus. By re-inserting the vibrator, the original density is at least partially restored and the load deflection response stiffens. The increase in the tangent load deflection modulus, from the average load deflection response for piles with driving stresses relieved, is approximately 40% for the fixed head case and 20% for the free head case.

Figs. 83 and 84 both show that predictions based on pressuremeter test 218 P-y curves are unconservative. For the fixed head tests the

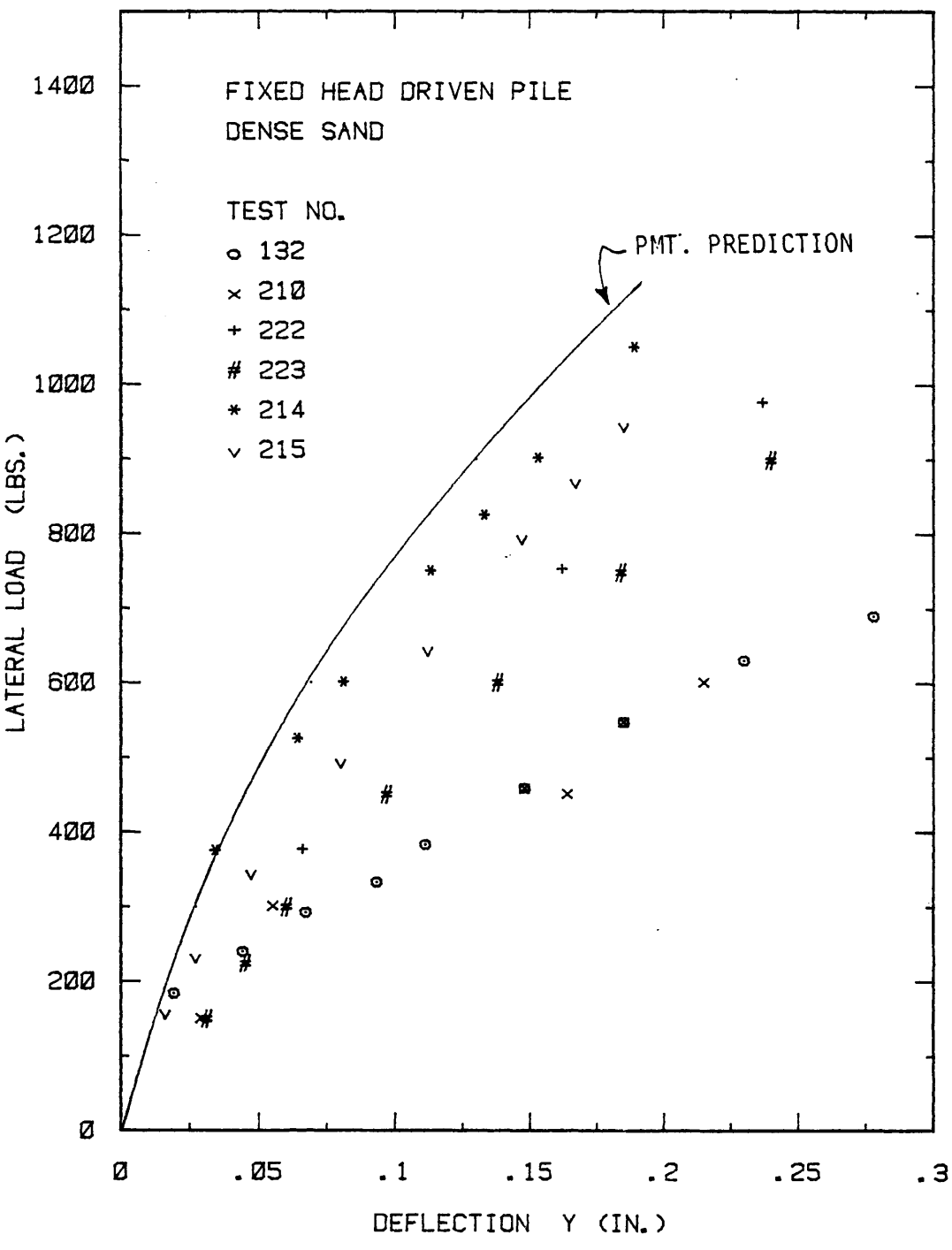

FIG. 83 - Prediction of Model Pile Response in Dense Sand with Fixed Head

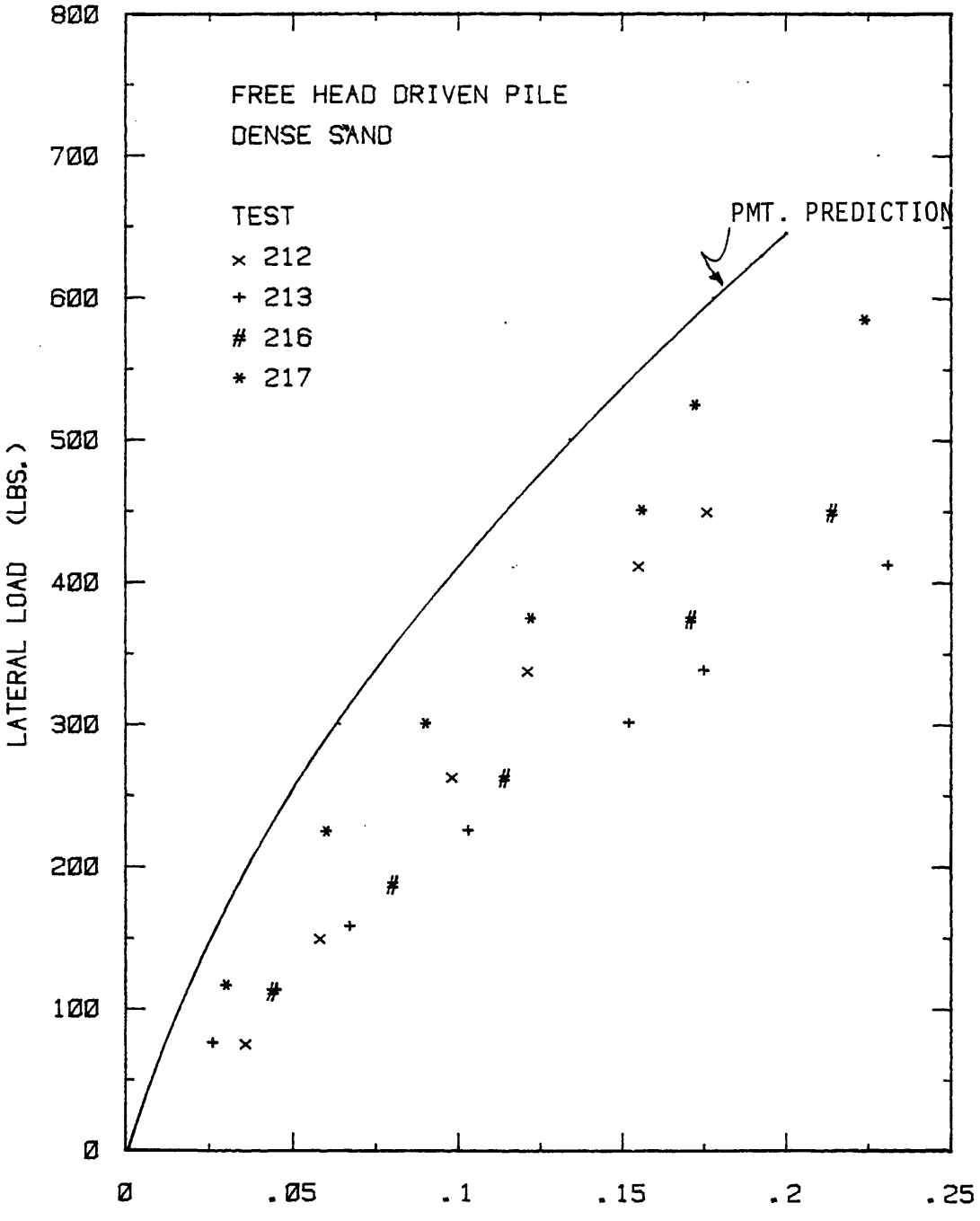

FIG. 84 - Prediction of Model Pile Response in Dense Sand with Free Head

predictions are approximately 50% unconservative and mark an upper bound for the relieved driving stress tests 214 and 215. Free head test predictions are of the order of 50% unconservative which suggests the pressuremeter P-y curves are consistently too high. The number of blows required to insert either the pile or the pressuremeter, together with the frequent density checks, reported in Appendix IV indicate some variability of the vibrated material. However, the pressuremeter tests confirm the repeatability of the tests with a general trend of slightly increasing density after each test. Misalignment of the model pile after driving and the subsequent generation of stresses into pile and sand from head clamping to the jig may cause some of the spread shown on Fig. 83 and Fig. 84.

No pressuremeter tests in sand were performed with a reload cycle and thus all derived pressuremeter P-y curves are generated from the initial cycle of driven tests.

The model pile tests 240, 241, and 242 were conducted at embedment depths of 10 in. (250 mm), 12 in. (300 mm) and 14 in. (300 mm) respectively. The lateral load versus deflection predictions based on pressuremeter test 218 are given in Fig. 85. This shows a trend similar to that reported on the full embedment tests. The predicted lateral load behavior is unconservative, by approximately 20% for 10 in. (250 mm) and 12 in. (300 mm) embedment and approximately 10% for the 14 in. (360 mm) embedment.

Clay

Results of the predicted lateral load versus deflection behavior

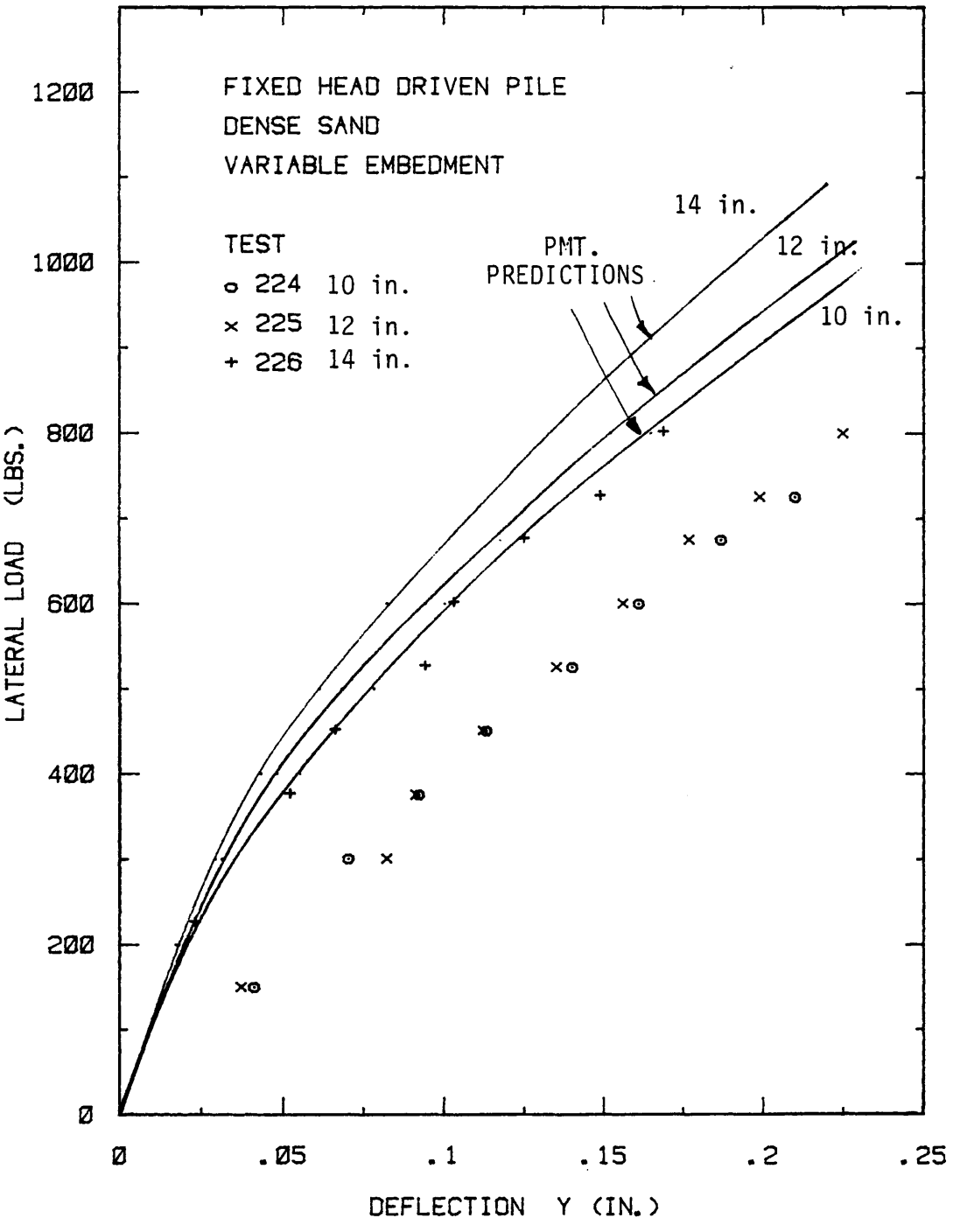

FIG. 85 - Prediction of Model Pile Response in Dense Sand: Variable Embedment

for the fixed head and free head piles in clay are given in Fig. 86 and Fig. 87 respectively. The predictions based on the driven pressuremeter test 91 P-y curves are in very good agreement to the mean driven model pile load test result, particularly in the earlier working range of pile behavior. A high degree of nonlinearity is evident which results from the nonlinearity present in the governing P-y curve for test 91. Within the limit of the pressuremeter expansion both free and fixed head predictions suggest the ultimate range of pile behavior is conservative. This reproduces well the expected relationship between pile and pressuremeter discussed previously.

A comparison between the suitability of using the initial loading curve from a driven pressuremeter test, 91, with the initial or reload cycle curve from the prebored test, 105, can be made. Fig. 86 includes the prediction using test 105 for the fixed head pile and Fig. 87 includes the reload cycle prediction from 105 on the free head pile test. Both gave conservative lower bound solutions for free and fixed head behavior. Fig. 38 shows the comparison of the calculated P-y curves between the initial and reload cycles of prebored test 105 and the initial cycle of driven test 91. The total generated force, P, and the contribution of the friction, F, are given (the difference between the curves being the front pressure contribution, Q) for all tests. The difference between initial and reload cycles of test 105 are seen to be small compared to driven test 91. Both tests give the same magnitude of shear contribution, but are mobilized differently. It is clearly the mobilization of front pressure

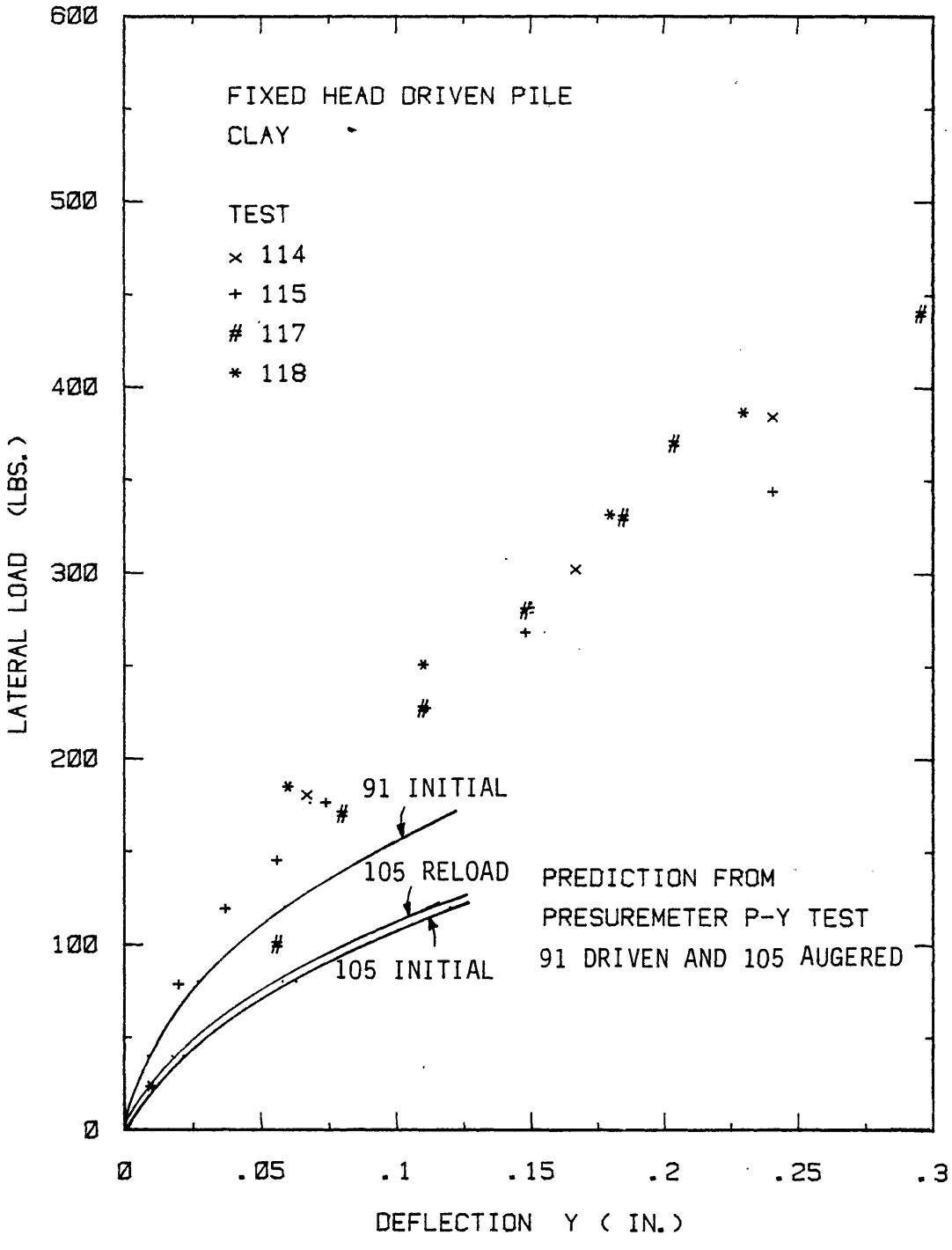

FIG. 86 - Prediction of Model Pile Response in Clay with Fixed Head

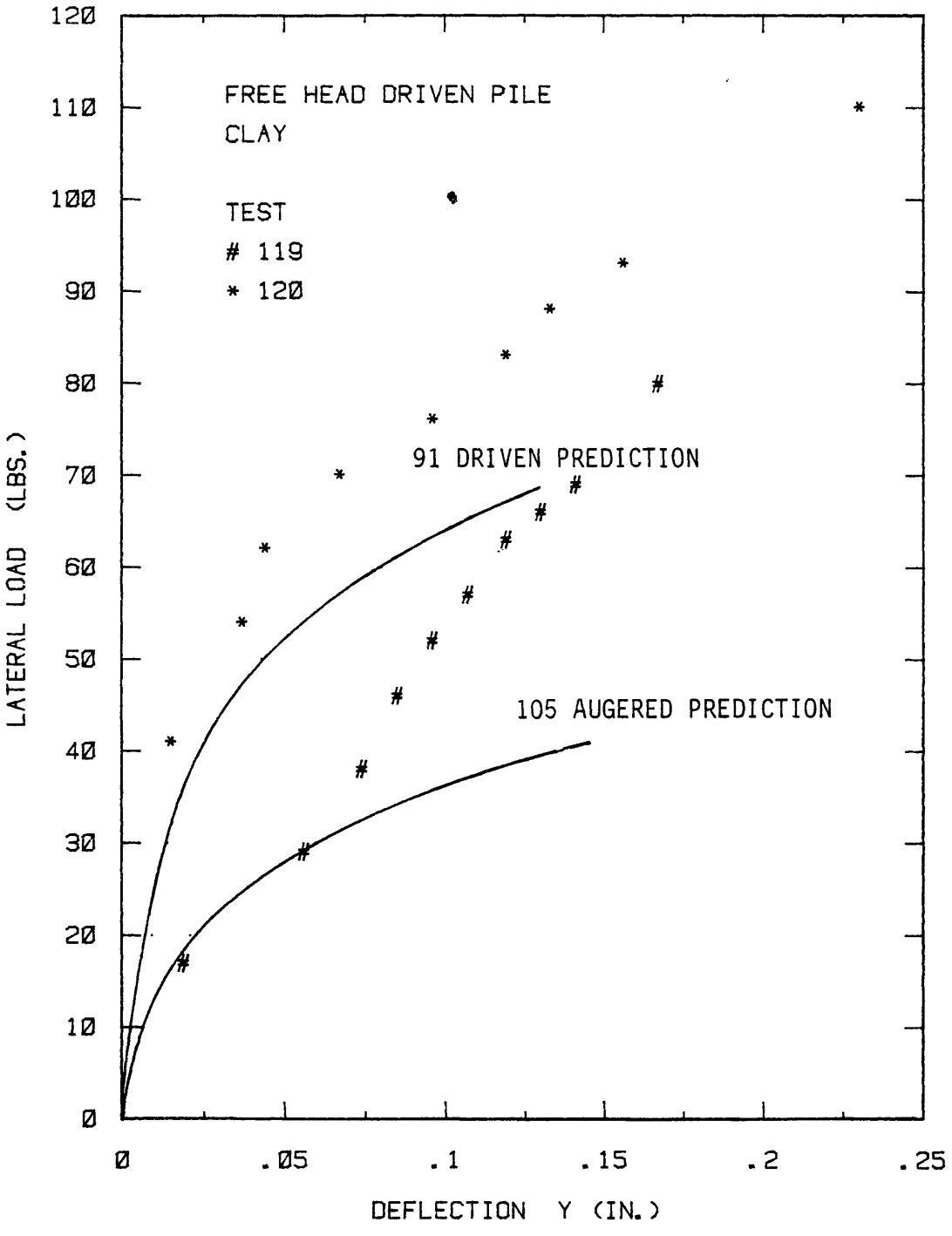

FIG. 87 - Prediction of Model Pile Response in Clay with Free Head

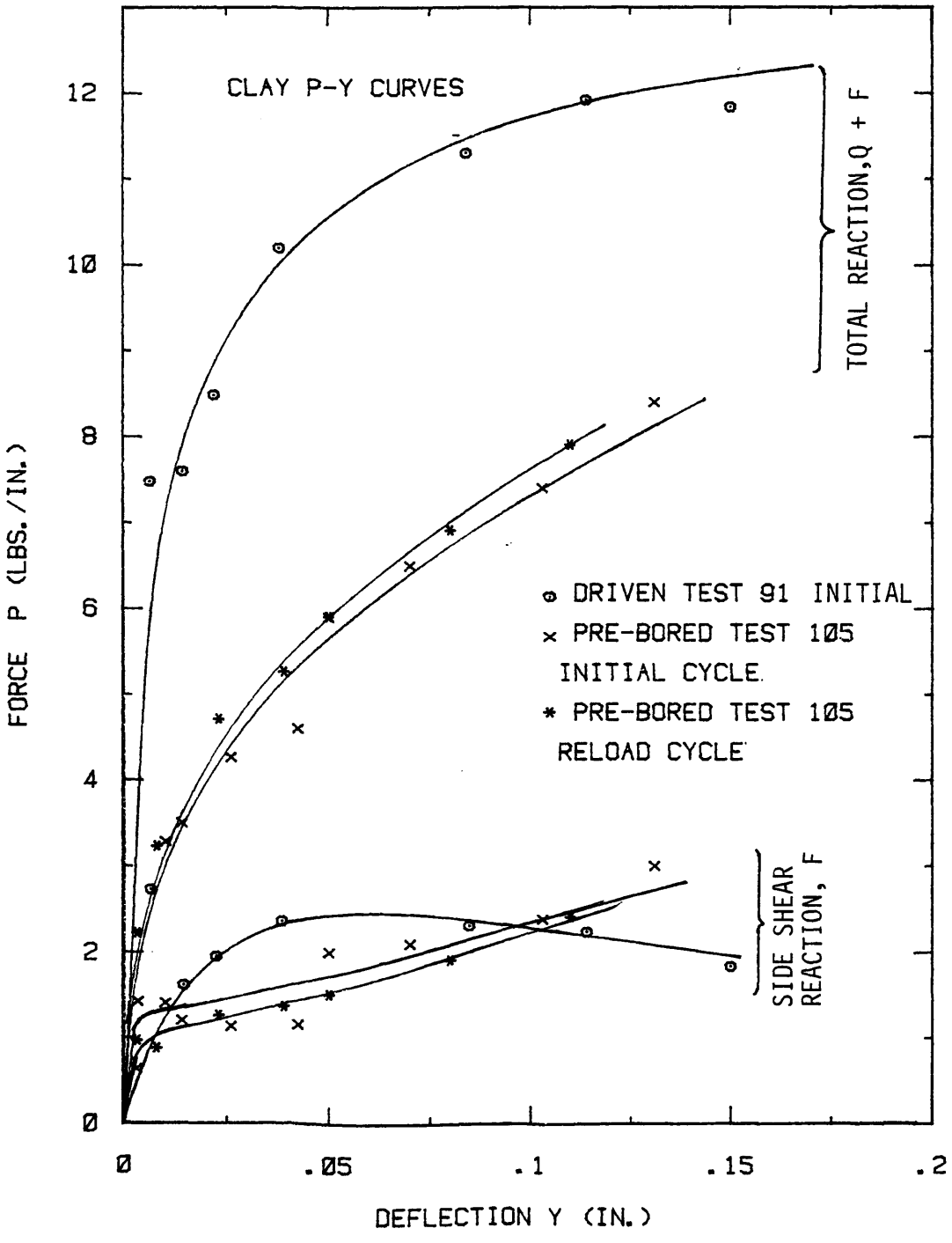

FIG. 88 - Derived P-y Curves in Clay

reaction which accounts for the difference. In both tests the mobilized shear stress derived from Eq. 78 reached approximately 76% of the undrained shear strength determined by unconfined compression testing. This agreement between driven and augered pressuremeter tests is reassuring since further remolding of a fully remolded clay should not influence the undrained shear strength. Fig. 88 also demonstrates the erratic behavior of the calculated mobilized shear stress based on an approximate differential technique.

The difference between a driven and prebored pressuremeter test consistently showed the driven test gave approximately a 50% increase in the small strain ($\varepsilon < 10\%$) response and approximately a 30% increase in the large strain response. Both were tested within 20 minutes of insertion.

In general the repeatability of the pile load tests indicate a uniform material and adequate placing precedures. The water content samples showed a slight decrease as a result of repeated compaction.

Summary

Based on this limited laboratory study of predicting lateral load versus deflection behavior for driven model piles, the following conclusions can be made.

1) The technique developed previously to construct lateral load P-y curves from a prebored pressuremeter test is acceptable.

2) In loose sand the derived P-y curves are conservative but the degree of disturbance to the material upon pile or pressuremeter installation is severe and difficult to quantify.

3) In dense sand the derived P-y curves are unconservative based on the initial cycle of a driven pressuremeter test.
In clay the derived P-y curves from the initial cycle of a driven test are in excellent agreement up to pile radial movement of approximately 10%. Beyond this amount of movement the P-y curves are conservative.

5) The pressuremeter driving disturbance and resulting stress changes in a remolded ceramic clay increase the front pressure reaction contribution, Q, to the P-y curves. No change is found in the shear contribution, F, between a prebored pressuremeter test and a driven pressuremeter test.

6) A slight increase is found in the derived P-y curve by using a reload cycle from the prebored pressuremeter test. However, from the limited evidence the reload cycle is a conservative estimate of a driven pressuremeter P-y curve.

The laboratory study confirms the suitability of deriving lateral load P-y curves from the pressuremeter test and their practical application. However, evidence is strictly limited and inconclusive with respect to the trend of P-y curves for different materials and installation procedures. No clear modifications to the recommendations can be made from the laboratory study in applying the technique to full size field piles for the following reasons:

1) For practical reasons, the full range of field pile and pressuremeter installation procedures were not available in the laboratory study. Therefore the effect of these procedures cannot be quantified on the P-y curves.
2) The field reference pressuremeter test is a prebored test, typically drilled with the circulation of a drilling fluid. In the laboratory, a prebored test was performed only in the clay, with no drilling fluid, and full borehole stress relief was present.
3) For the field piles in clay, the effects of radial consolidation and load test rates may seriously affect their results. All pressuremeter and model pile tests were conducted at similar rates. Testing commenced after a similar delay from installation had occured.
4) In the laboratory clay the low shear strength gave limit pressures between 50% to 80% of the membrane stiffness. Some problems occur in maintaining sensitivity of the readings, in particular on unload-reload cycles.

In conclusion the technique developed previously is recommended without modification for all field studies. Due to the erratic differentiation procedures in deriving the mobilized shear stress around the expanding pressuremeter, the shear stress, from PYGEN, should be checked against the known shear strength of the material and a P-y curve 'best fit' made. Both initial and reload predictions (if a reload cycle is available) should be made to gain increased experience and understanding.

FIELD STUDIES

Introduction

The sites introduced previously , and further discussed later on represent the most complete reported case histories of instrumented lateral pile load tests. A number of these sites have been visited, and pressuremeter tests conducted to evaluate the P-y curves by the procedure recommended in previously. A comparison at the P-y level has then been made, together with a prediction of the lateral load versus head deflection response, for those sites at which 'measured' P-y curve are available. The sites at which piles were tested laterally, without strain gage instrumentation, have no measured P-y curves and a comparison of the lateral load versus head deflection response only is made. During the course of this study all sites reported in this section were visited.

The exact location of the original pile load test is either not reported, or is no longer accessible for a number of the sites. Details of the pressuremeter test borehole locations can be found previously

At some sites the original pile load test ground line is below the present ground level, due to the recent deposition of fill. In all cases the best estimate of the ground line has been made based on local knowledge, engineering judgement and the original borehole logs.

For the sites at which load test and present ground datums are different, the critical depth effects for the pressuremeter and the

pile, are evaluated separately from Fig. 47 and 48 (p.127 and p.129) In all P-y curves the test mudline (M/L) is used as the reference datum.

For each site, pressuremeter net limit pressures, initial and reload moduli are presented together with the undrained shear strengths reported at the time of the load test. The following notation is used:

P_1^* = net limit pressure,

E_I = pressuremeter modulus from initial cycle,

E_R = pressuremeter modulus from reload cycle, and

C_u = undrained shear strength at the time of the load test.

In calculating both initial and reload modulus Poisson's ratio is assumed to be 0.33.

The more critical, shallow, pressuremeter test results are given using the notation of Fig. 89 and also a comparison to the shallow P-y curves is made, where applicable.

For the analysis of flexible piles the surface layers represent the most critical area. Rigid piers, however, are subject to rotation and little variation of slope down the pier. For rigid piers it is equally important to evaluate the P-y response to depth, particularly around the base of the pier.

Where possible, unrestrained (free) head pile tests are selected from each site. This avoids further assumptions with respect to the degree of head restraint provided on a fixed head test.

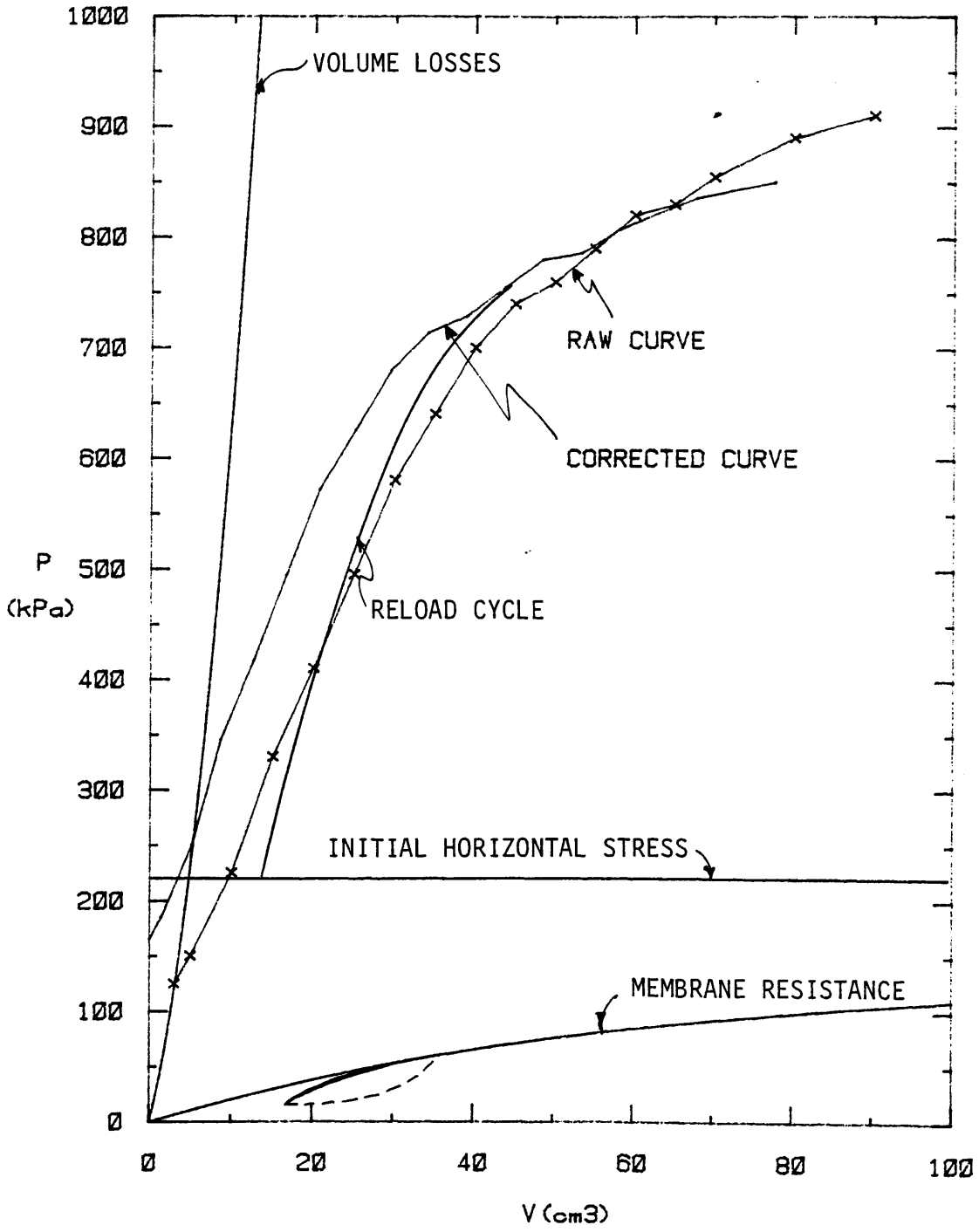

FIG. 89 - Notation for Field Pressuremeter Curves

The Field Pressuremeters

Two pressuremeters were used in the field studies, both monocell, strain controlled units. The first was the pressuremeter described in Section 7 for laboratory use without the pressure transducer attachment and is referenced as the PAV unit. The second field pressuremeter, Fig. 90, was designed and built during the course of the research and forms the prototype of the commercially available TEXAM unit, manufactured by ROCTEST, Inc., New York. The prototype, used in the field studies, had a probe of diameter approximately 2.36 in. (60 mm) with a measuring cell length of 15.75 in. (400 mm), giving a deflated initial volume of approximately 70 $in.^3$ (1030 cc). The center of the probe is hollow with an internal diameter of 1.37 in. (35 mm) to allow the free passage of drilling mud and reduce disturbance ahead of the probe. Water is used as the inflating medium and the surface control unit records pressures and injected volume. The displacement of a 4 in. (102 mm) diameter piston generates the injected volume which is calculated directly from the piston displacement measured by a vertical dial gage. A total pressure range of 0 to 100 atmospheres (1.47 ksi) is available, read from three, in-line, gages. Membrane resistance is of the order 7.3 lb/sq in. (55.0 kPa) and volume losses of the order 2.74 $in.^3$ (45.0 cc) at 15 atmospheres, with plain water a high degree of saturation and a 100 ft (30 m) long tubing.

In all tests employing the PAV unit, injected volumes are given up to a maximum of 6.0 $in.^3$ (100.0 cc). The tests were conducted without the use of drilling fluid. The holes were hand augered dry, unless

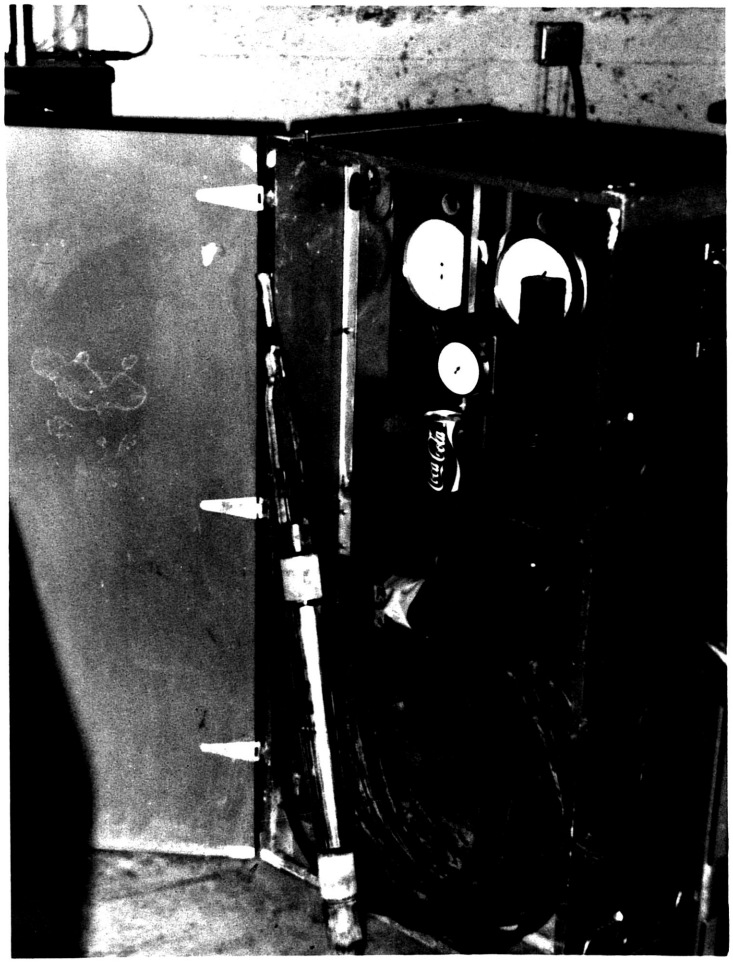

FIG. 90 - TEXAM Prototype Pressuremeter

below the water table, with a 1.375 in. (35 mm) auger bit.

Tests using the TEXAM unit give an injected volume of 61 in.^{3} (1000 cc) and were conducted in boreholes drilled by rotary drilling with a minimum of mud circulation. Drill bit type and size, and drilling procedures were frequently varied to maintain the highest quality hole. A general view of the field drilling operation is shown in Fig. 91 which illustrates the TEXAM unit being lowered to the test depth. To minimize disturbance, drilling to advance the hole was conducted after each successive pressuremeter test to the next required depth. In all tests the rate of probe expansion is set to double the cavity size in approximately 10 minutes.

Sites Chosen: 'Measured' P-y Available

Houston: Stiff Clay Above the Water Table

To estimate the initial at rest horizontal pressure in the Beaumont clay, the value of overconsolidation ratio (OCR), is taken from those reported by Mahar and O'Neill (61) at a local site. The summary of net limit pressures, initial modulus and reload modulus, together with the reported undrained shear strengths at the time of the load test, are given in Fig. 92. The rapid increase in soil stiffness at 4 ft (1.2 m) deep is well illustrated in the pressuremeter test results. The PAV probe was used in a hand augered dry hole. The water table reported by Reese and Welch (86) was at a depth of 18 ft (5.5 m).

The pressuremeter test results are given in Appendix IV for depths between 2 ft (610 mm) and 15 ft (4.6 m). Ground datum for

FIG. 91 - Field Operations

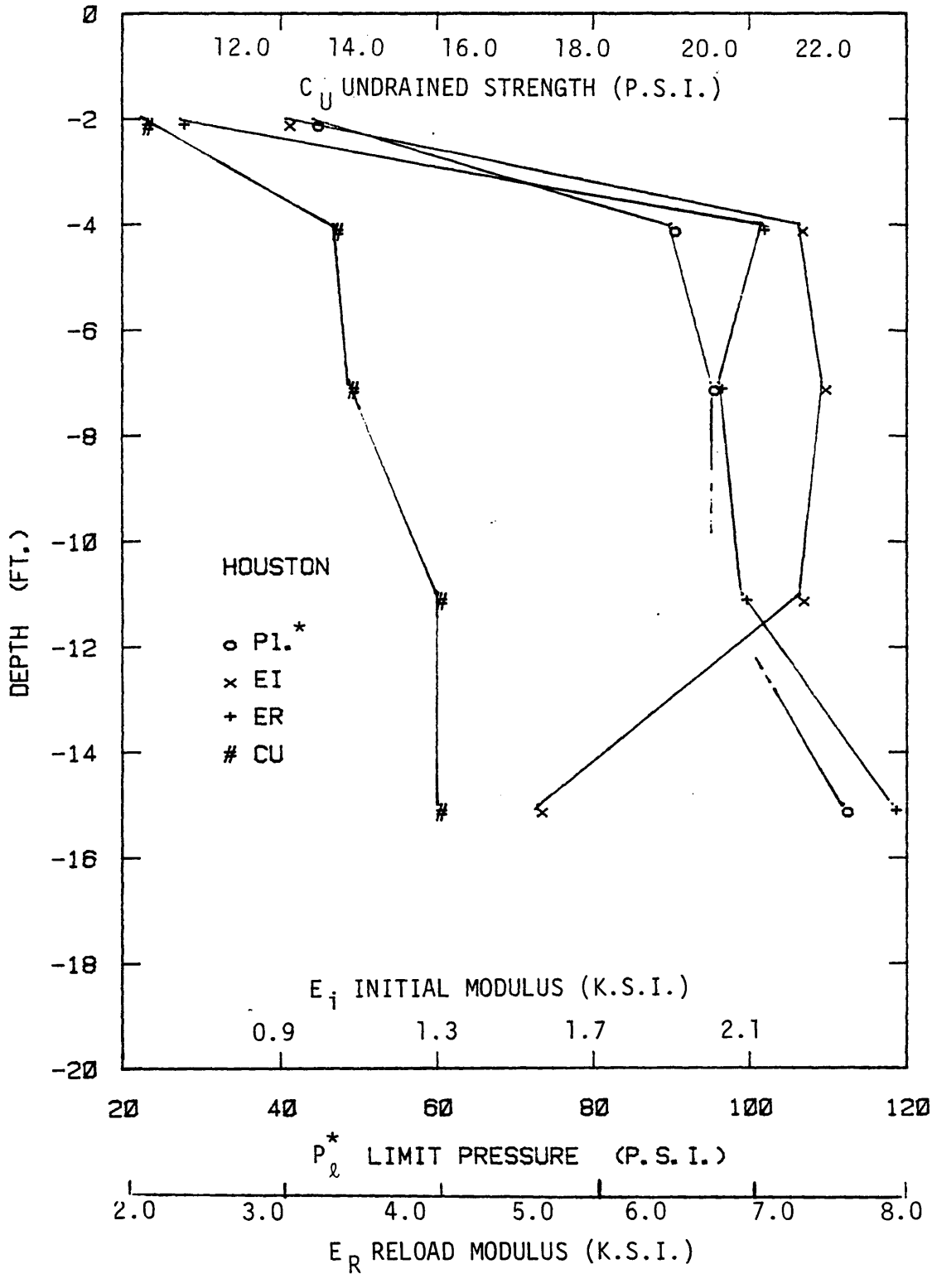

FIG. 92 - Pressuremeter Test Results and Undrained Shear Strength for the Houston Site

the load test and pressuremeter tests are considered equal.

A comparison between the reported 'measured' P-y curve at 3 ft (914 mm) depth and that derived from pressuremeter tests at 2 ft (610 mm) and 4 ft (1.2 m) is shown in Fig.93 . Very good agreement is found, in particular the small strain prediction of the reload criteria. Peak shear strengths from the reload cycle calculated by Eq. 78 are in agreement with those derived by Mahar and O'Neill from self-boring pressuremeter results, and are mobilized at approximately 2% circumferential strain. The initial pressuremeter cycle is shown to overestimate peak shear strengths by between 50% and 100%.

Examination of the reinforced concrete shaft, after the completion of the load test, down to depth of 20 ft (1.1 m) showed no serious distress in the shaft. However, the 25 ft (7.6 m) location, at which excessive spalling of the cover to the spiral reinforcement occurred, corresponds to the depth where flexural stiffness of shaft is 50% of the surface value. The ultimate bending moment of the intact section is calculated to be of the order 1.0×10^7 lb $in.^2$ (28.6 $kN.m^2$) and from COM622 is expected at a depth between 8 ft (2.4 m) and 12 ft (3.6 m).

The above comments suggest partial structural breakdown of the shaft. Despite the close agreement in the P-y curve (of which only one is reported by Welch and Reese) the predicted lateral load behavior, shown on Fig. 94 is unconservative at higher working loads, and at the ultimate load range. The rapid increase in groundline deflection for the field load test at 60 kips (267 kN) supports the hypotheses that structural breakdown of the shaft occurred. This breakdown, or change

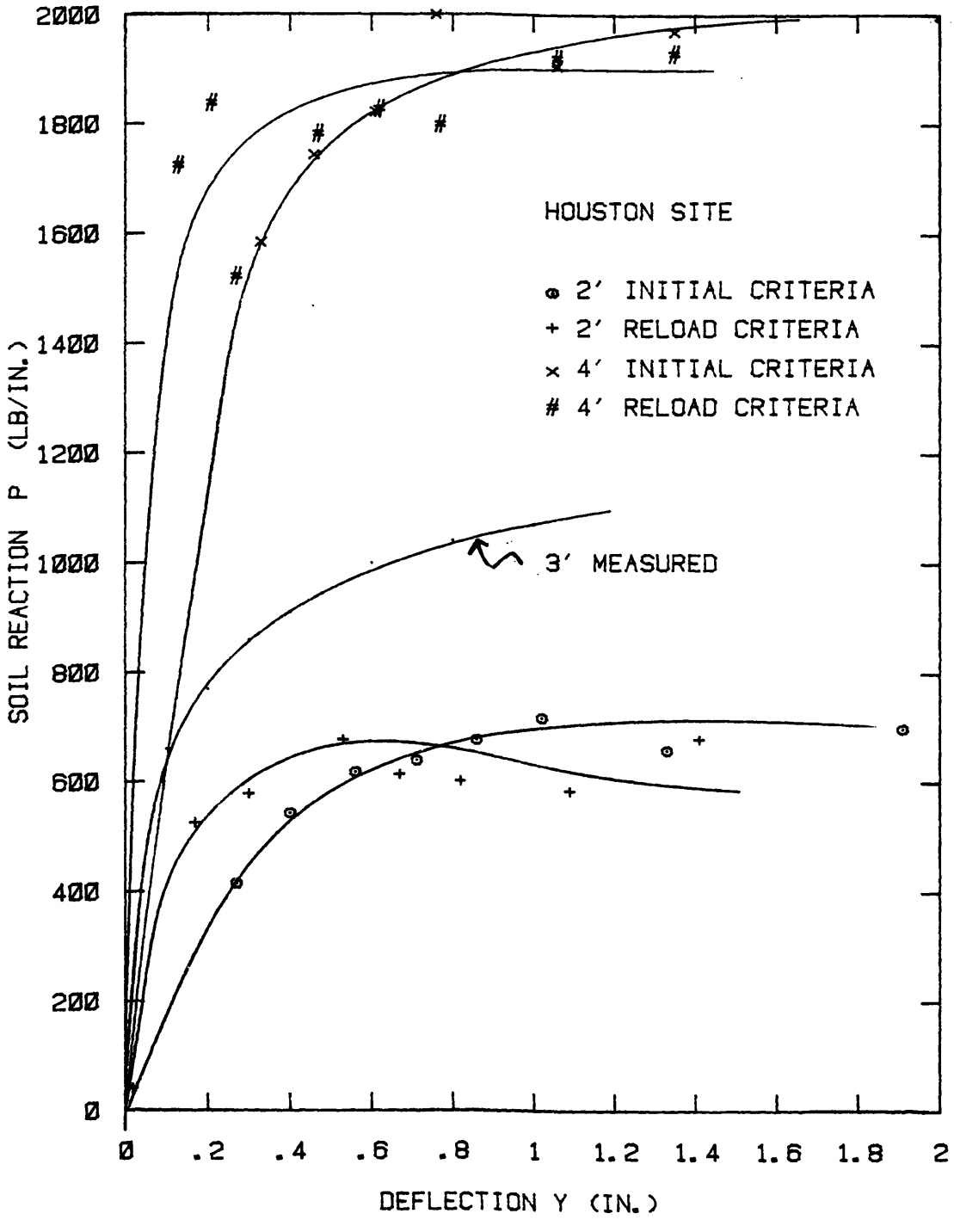

FIG. 93 - Houston Site: P-y Curve Comparison

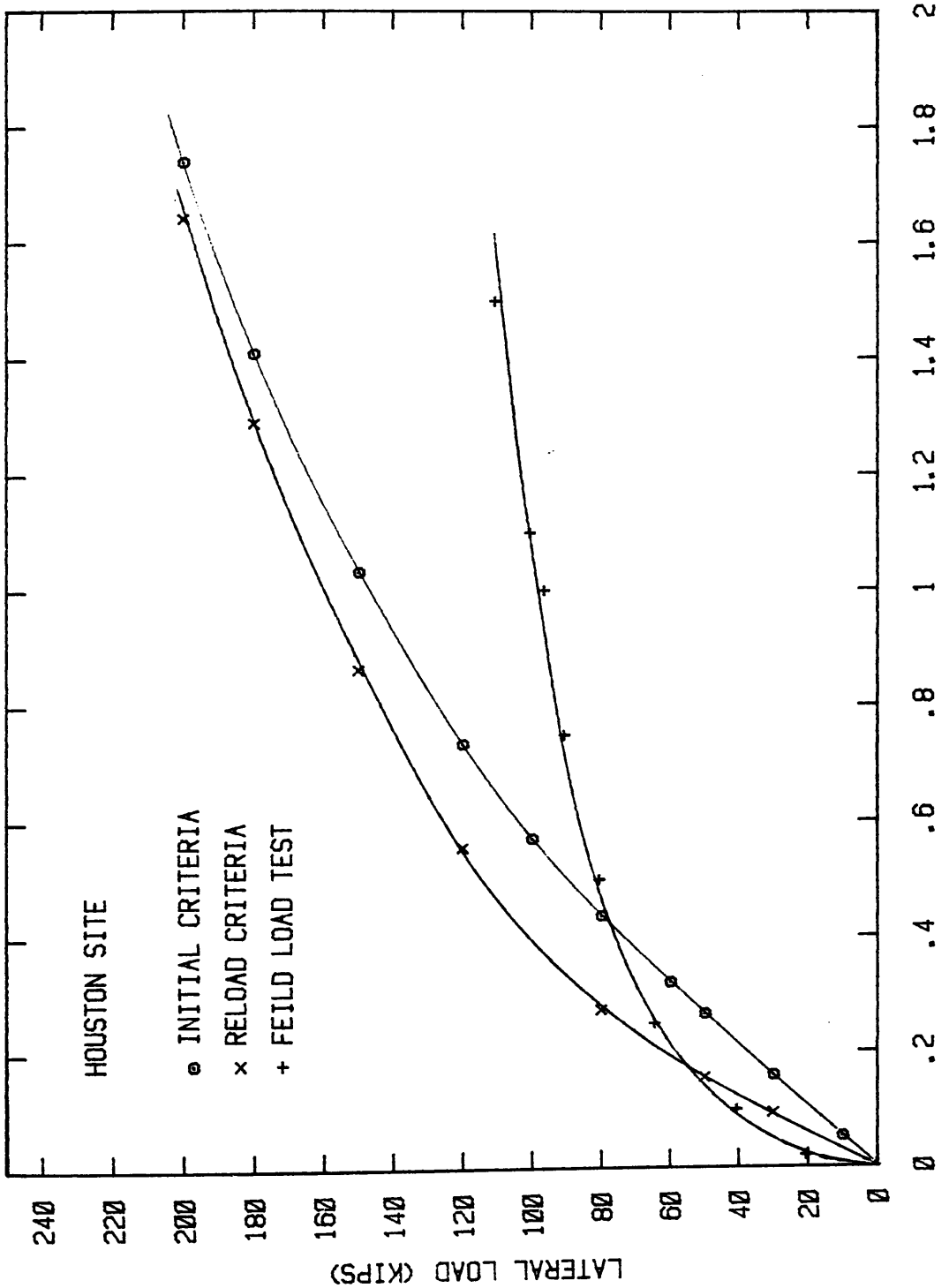

FIG. 94 - Houston Site: Comparison of Groundline Deflection

in flexural stiffness, is not modeled in COM622 and the flexural stiffness remains constant.

In summary the P-y curve at 3 ft (914 mm) depth is very well represented by the reload criteria in the stiff over consolidated material, and is shown to be a brittle response. The closely spaced, discontinuous, fissures which exist in the Beaumont formation make the drainage conditions, for pressuremeter and pile, difficult to quantify.

Sabine: Soft Clay Below the Water Table

The variations with depth of pressuremeter limit pressure, initial modulus and reload modulus, together with undrained shear strength are given on Fig. 95 for Sabine site. Clearly the pressuremeter test at 7 ft (2.13 m) shows a stiff layer which was not indicated by the site investigation at the time of the load test. This depth is 3 ft (914 mm) below the test mudline and therefore the P-y curve is in the critical shallow zone. The test at 7 ft (2.13 m) is therefore disregarded. Below this depth the variation of soil stiffness is well represented and all pressuremeter tests are considered valid.

Fig. 96 shows the results of three Atterberg limit determinations, at depths of 8 ft (2.4 m), 14.5 ft (4.4 m) and 19.5 ft (5.9 m), together with the limits reported at the time of the load test. Calculation of specific gravity is also in excellent agreement with the reported value. In all respects, with the exception of the shallow pressuremeter test, the site conditions, test results and location are considered to fully represent the soil conditions at the time of the load test.

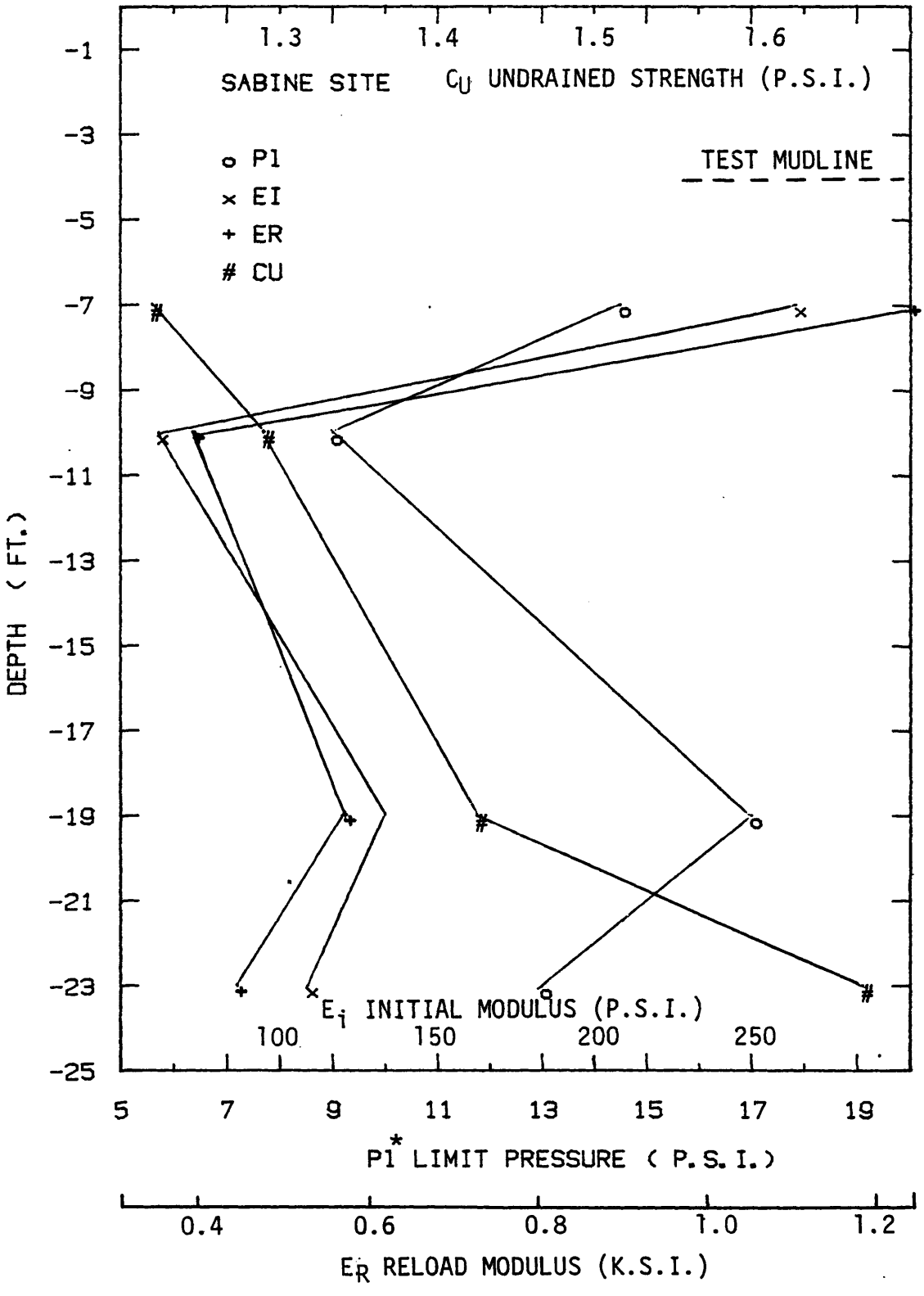

FIG. 95 - Pressuremeter Test Results and Undrained Shear Strength for the Sabine Site

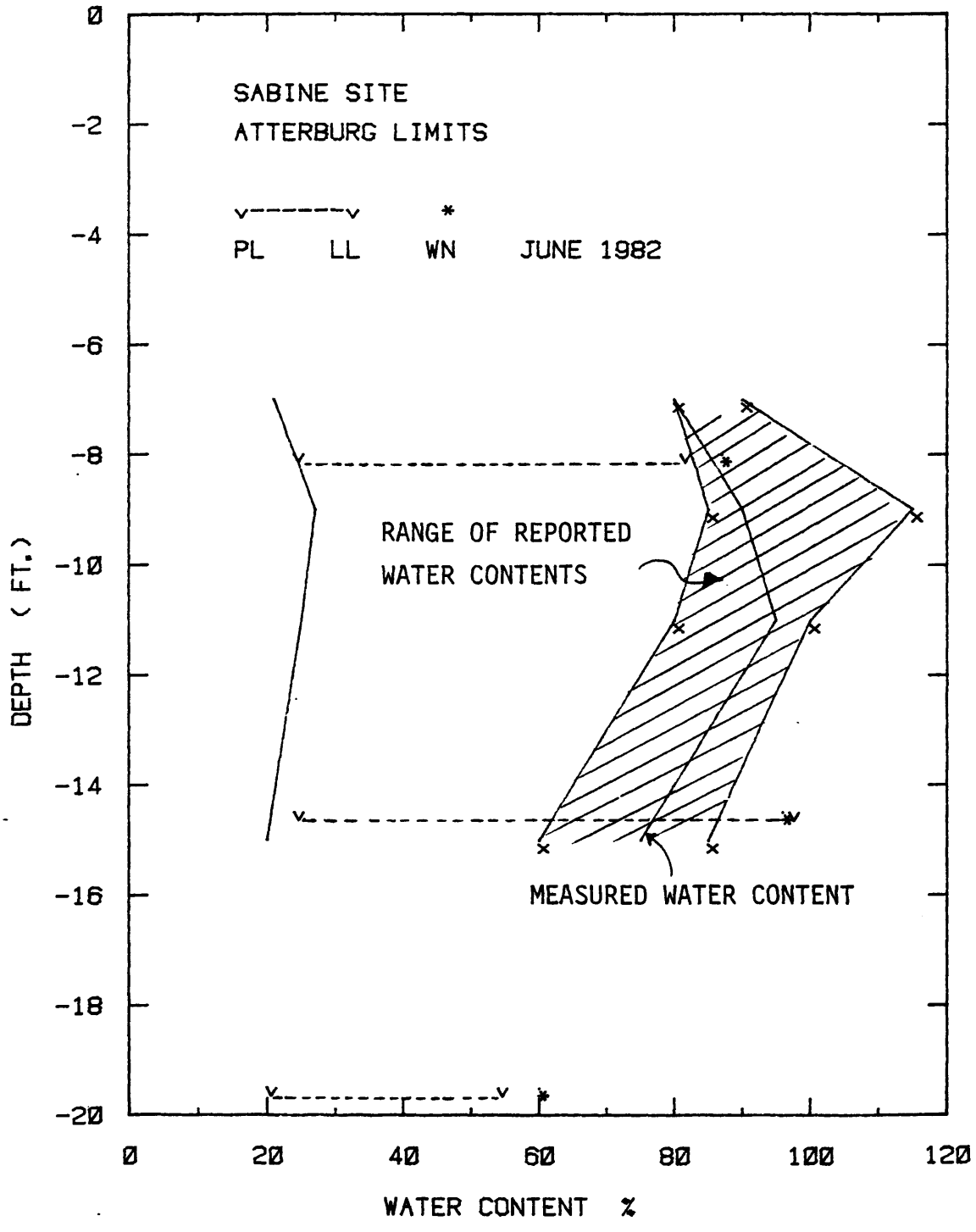

FIG. 96 - Comparison of Atterberg Limits for Sabine from the time of the Load Test to Present Day

Horizontal earth pressure at rest, taken from tests using a self-boring pressuremeter (91) indicate a coefficient of earth pressure at rest, K_o, of 0.5, which is consistent with a normally consolidated (N.C.) material.

The pressuremeter test results are given in Appendix IV for depths between 7 ft (2.3 m) and 23 ft (7.0 m), together with horizontal earth pressures. Mudline datum for the load test and ground datum are 4 ft (1.2 m) apart. The TEXAM unit was employed, with mud circulation at low pressure, and a 2.25 in. (57mm) diameter drill bit. Below 14 ft (4.26 m) the hole was advanced by open drillstring only with full mud circulation.

Comparison of the calculated P-y curves and those 'measured', at shallow depth are given in Figs. 97 through 99. Excellent agreement is found in the working range for the reload cycle and the pressuremeter P-y curves are conservative at ultimate range. Derived shear strengths from the initial criteria peak at 300% of the reported in situ strengths measured by the vane. Shear strengths derived from the reload criteria peak at 1.25% circumferential strain and are 50% higher than the vane strengths. The 'measured' P-y curves are those reported from Sabine test series 300, the static free head tests. The pile load test was completed within a 12 hour period.

The predicted lateral load and maximum bending moment versus mudline deflection is given in Fig. 100 and Fig. 101 respectively, for test series 300. The reload criteria is shown to be in excellent agreement and the initial criteria is up to 100% conservative on predicting deflections. Maximum bending moments are insensitive to the

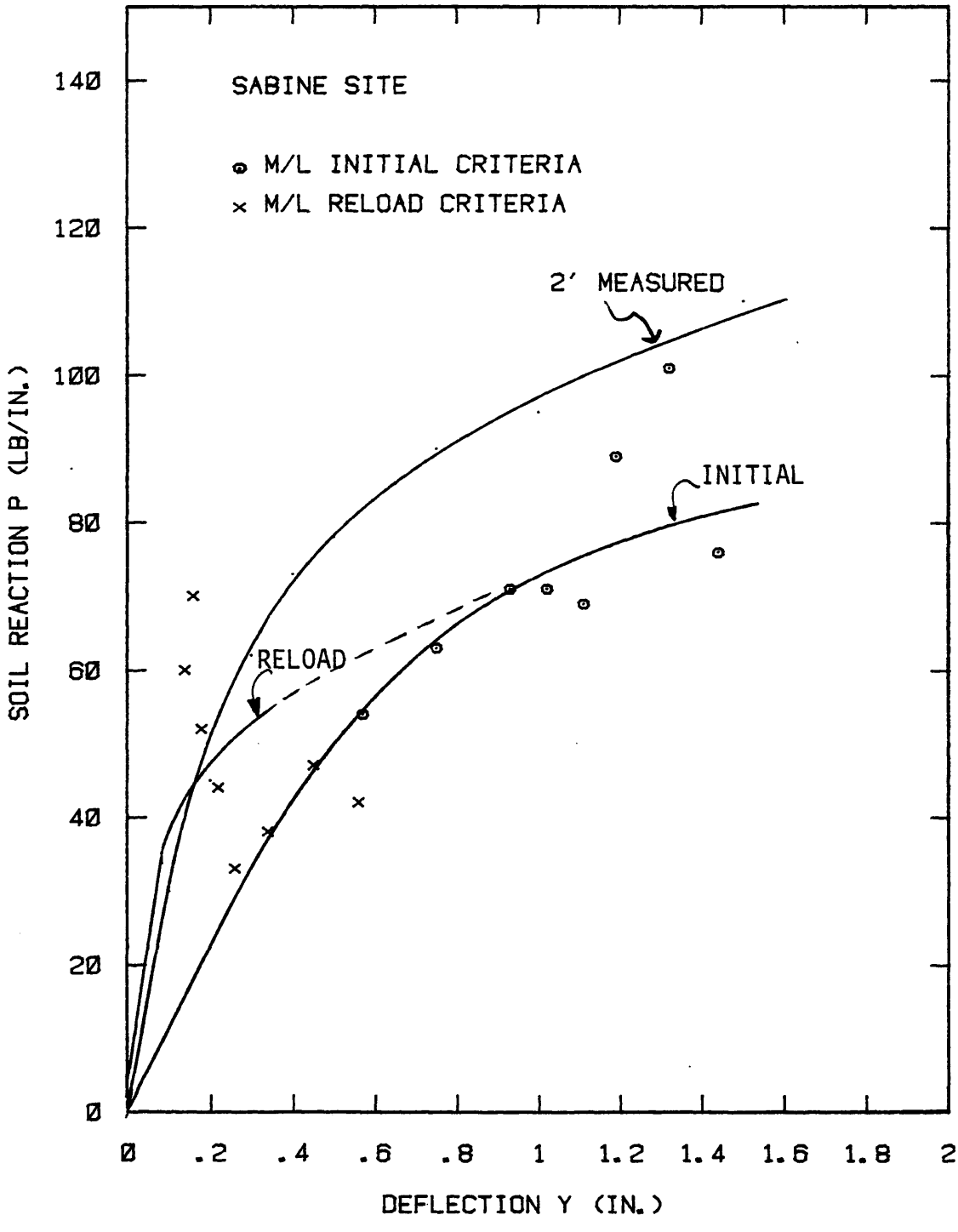

FIG. 97 - Sabine Site: P-y Curve Comparison for the Mudline

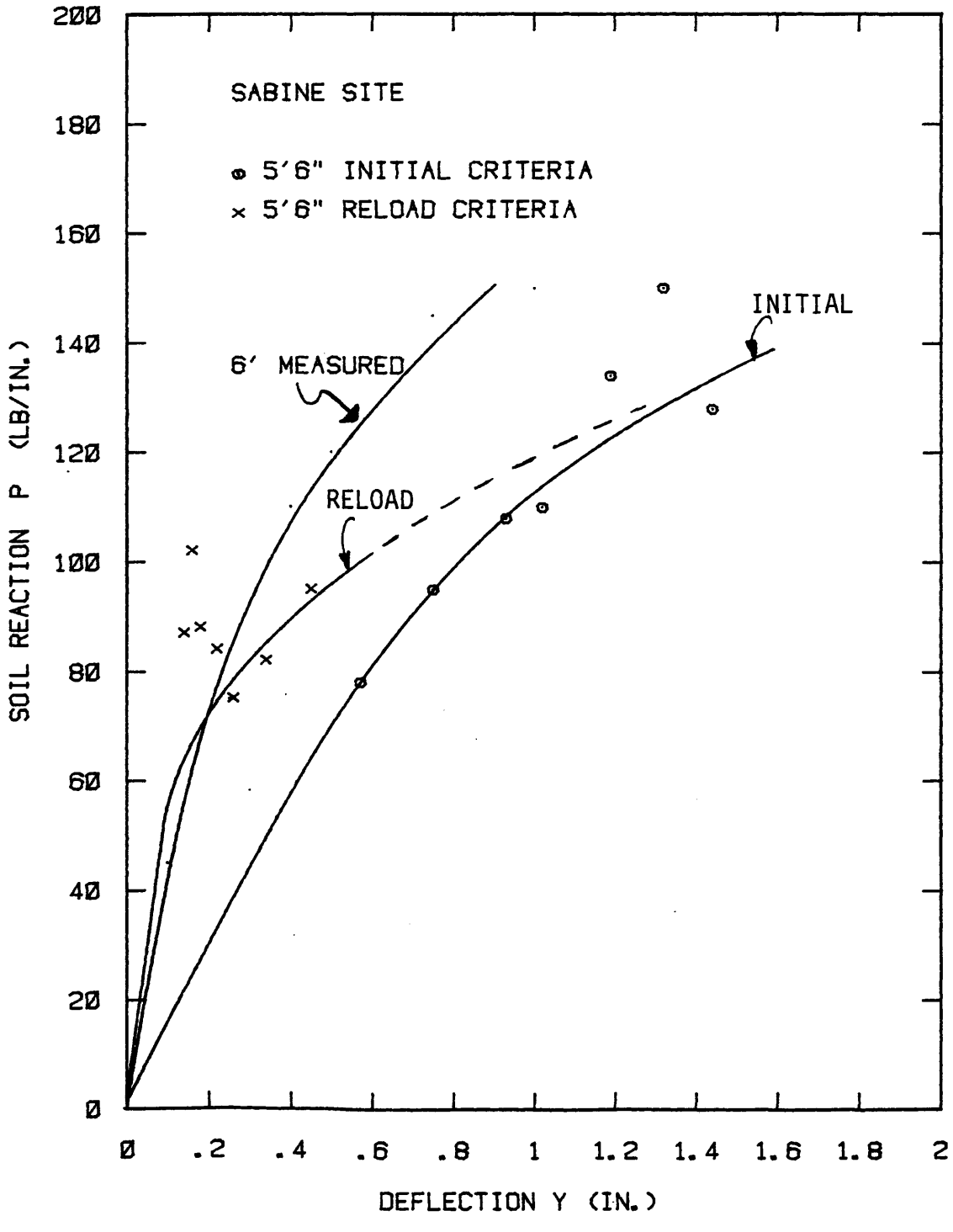

FIG. 98 - Sabine Site: P-y Curve Comparison for 6 ft. Deep

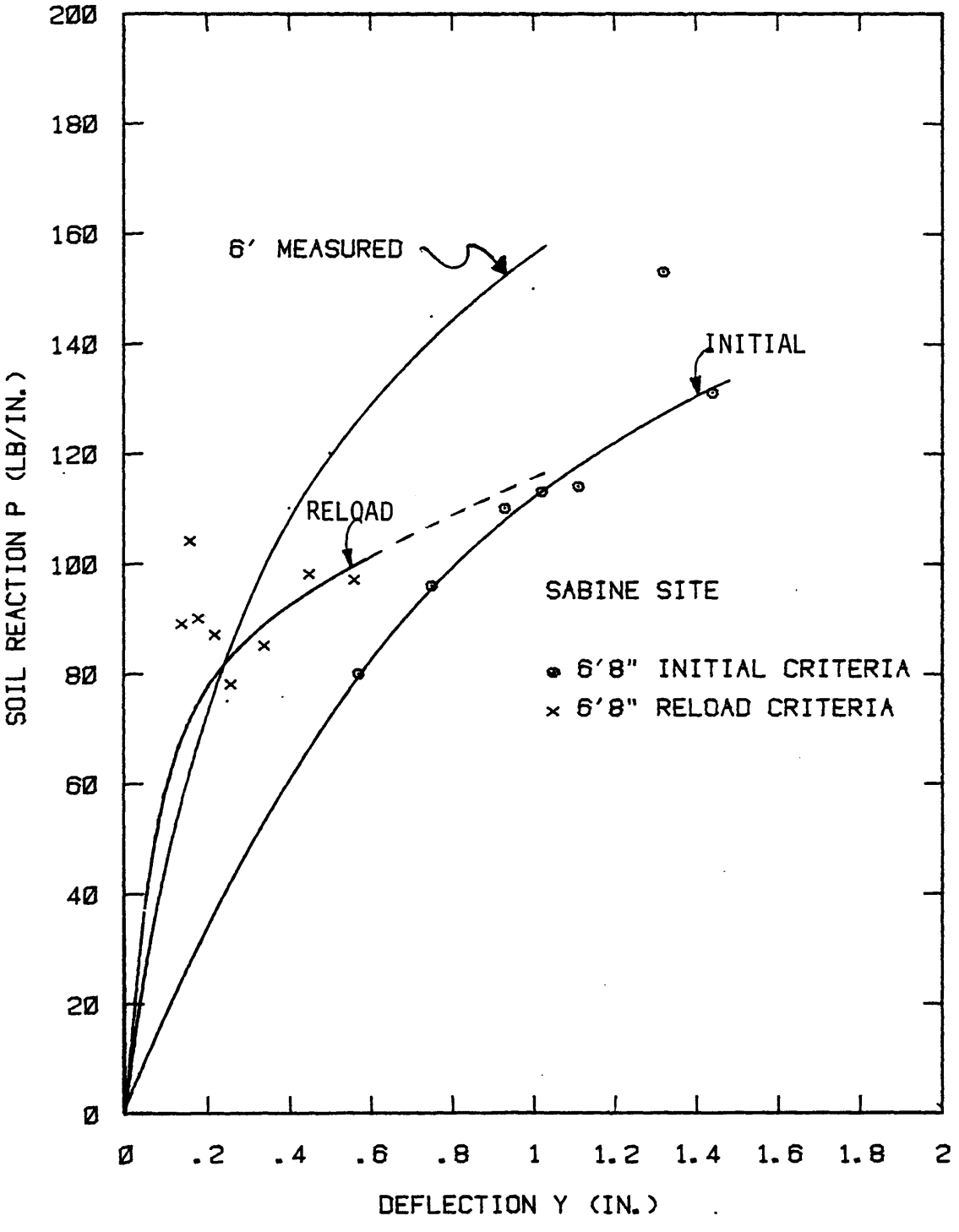

FIG. 99 - Sabine Site: P-y Curve Comparison for 6.66 ft Deep

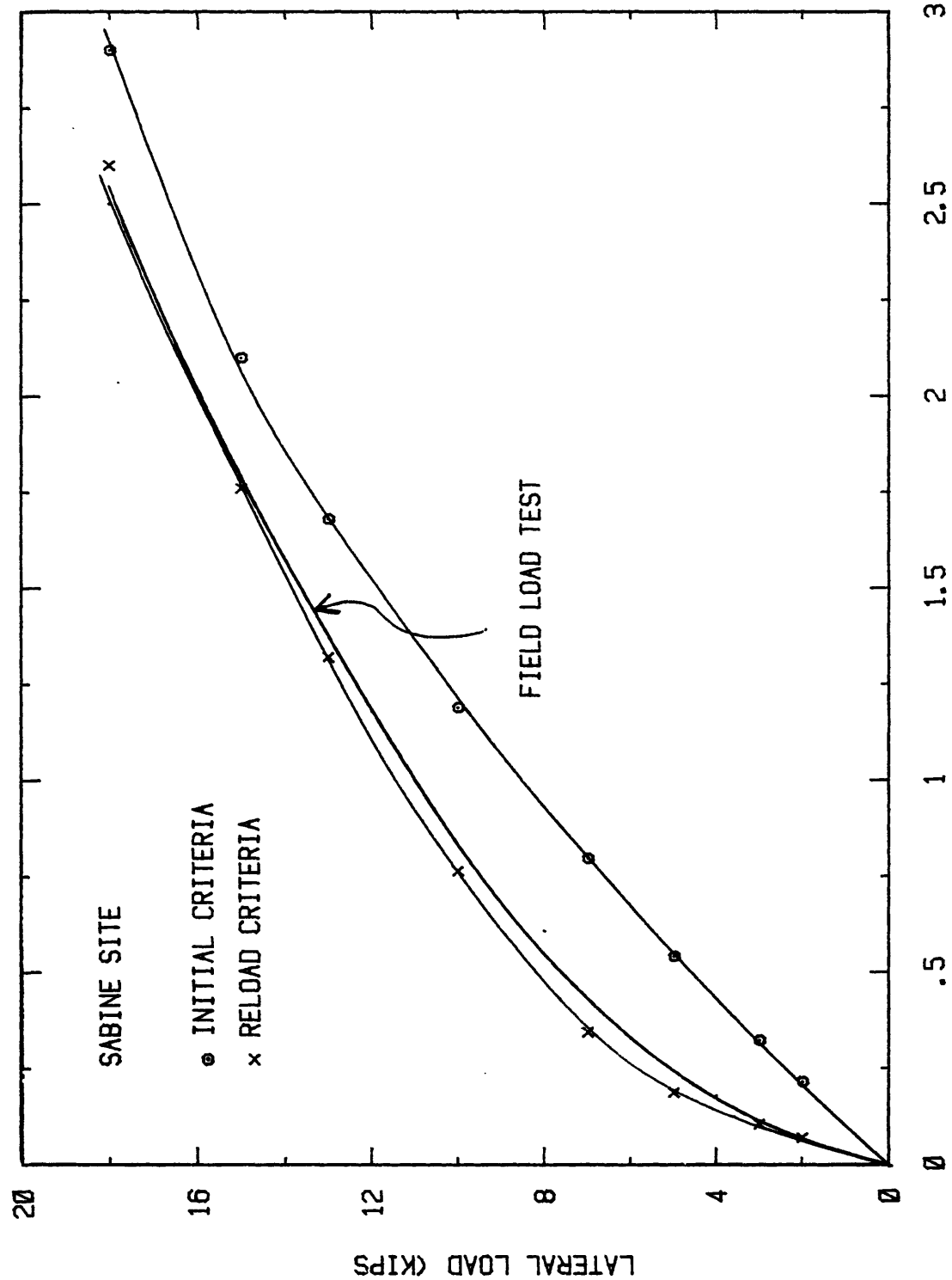

FIG. 100 - Sabine Site: Comparison of Groundline Deflection

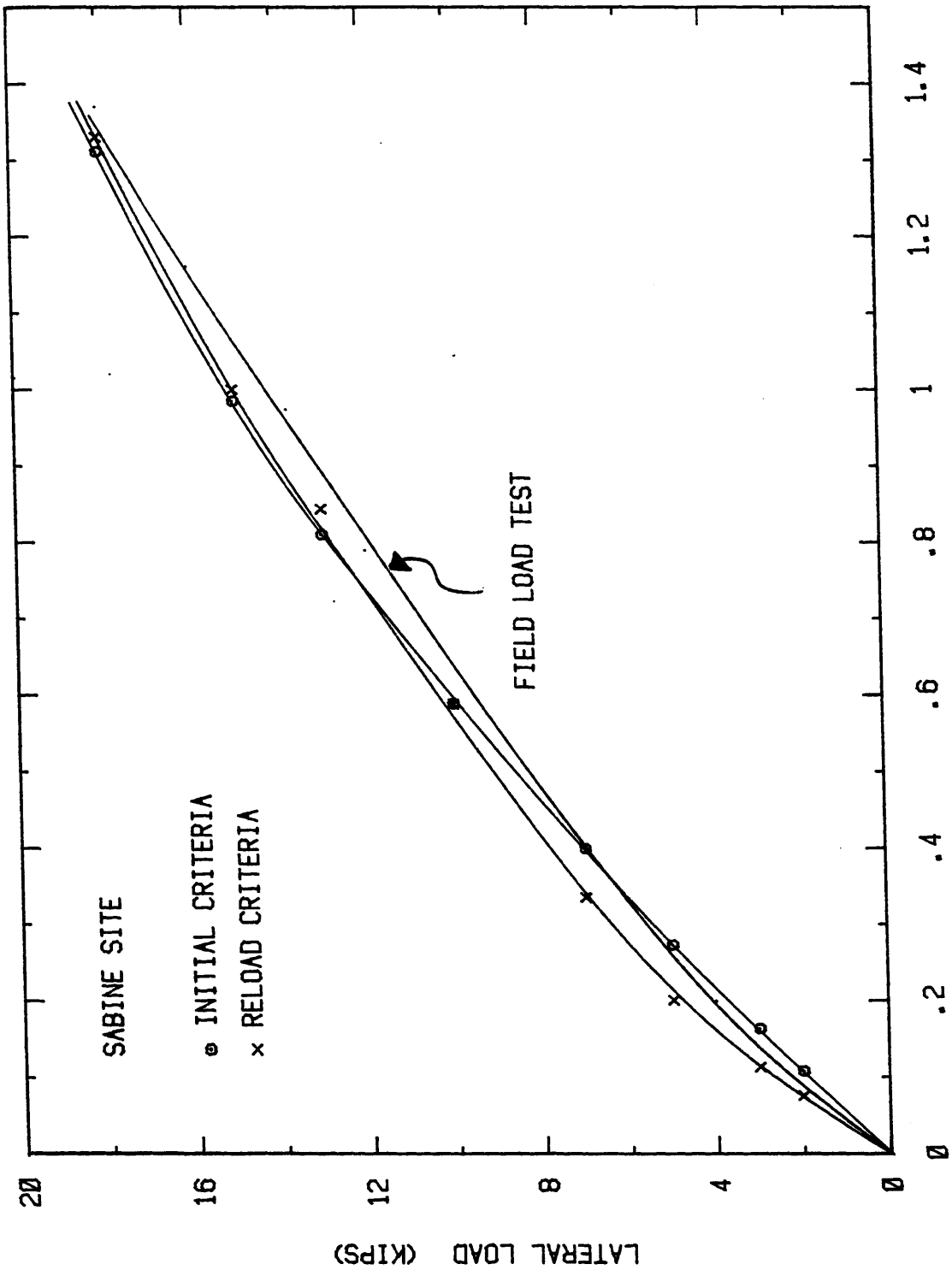

FIG. 101 - Sabine Site: Comparison of Maximum Bending Moment

derived P-y curves.

Lake Austin: Soft Clay Below the Water Table

The variations, with depth, of pressuremeter limit pressure, initial modulus and reload modulus, together with undrained shear strength, are given on Fig. 102 for the Lake Austin site. In general, the variations of soil stiffness shown on Fig. 102 are in good agreement. The increase for 2 ft (610 mm) test, is expected due to the slight overconsolidation from repeated drawdown of the lake. This test depth is, however, above the test mudline and is not used in the construction of the P-y curves. All pressuremeter test results are considered valid.

To determine horizontal earth pressures, a K_o value of 1.0 is taken by consideration of the light O.C. Pressuremeter tests were conducted using the PAV unit in a hand augered borehole results are shown in Appendix IV. The derived P-y curves at depths of 1 ft (305 mm) and 4 ft (1.2 m) are compared to the 'measured' P-y curves from 2 ft (610 mm) and 4 ft (1.2 m) in Fig.103 and Fig. 104 respectively. The 'measured' P-y curve at depth of 2 ft (610 mm) was the only one to reach an ultimate reaction for the static load test.

The initial criteria is shown to overpredict the soil reaction by 150% and the reload criterion by 400%. Both criteria fail to exhibit the degree of nonlinearity shown by the 'measured' P-y curves. The initial criteria generates shear stresses in excess of 10 times the undrained shear strength and the reload 2 times the shear strength.

In an attempt to remove the influence of the excess mobilized

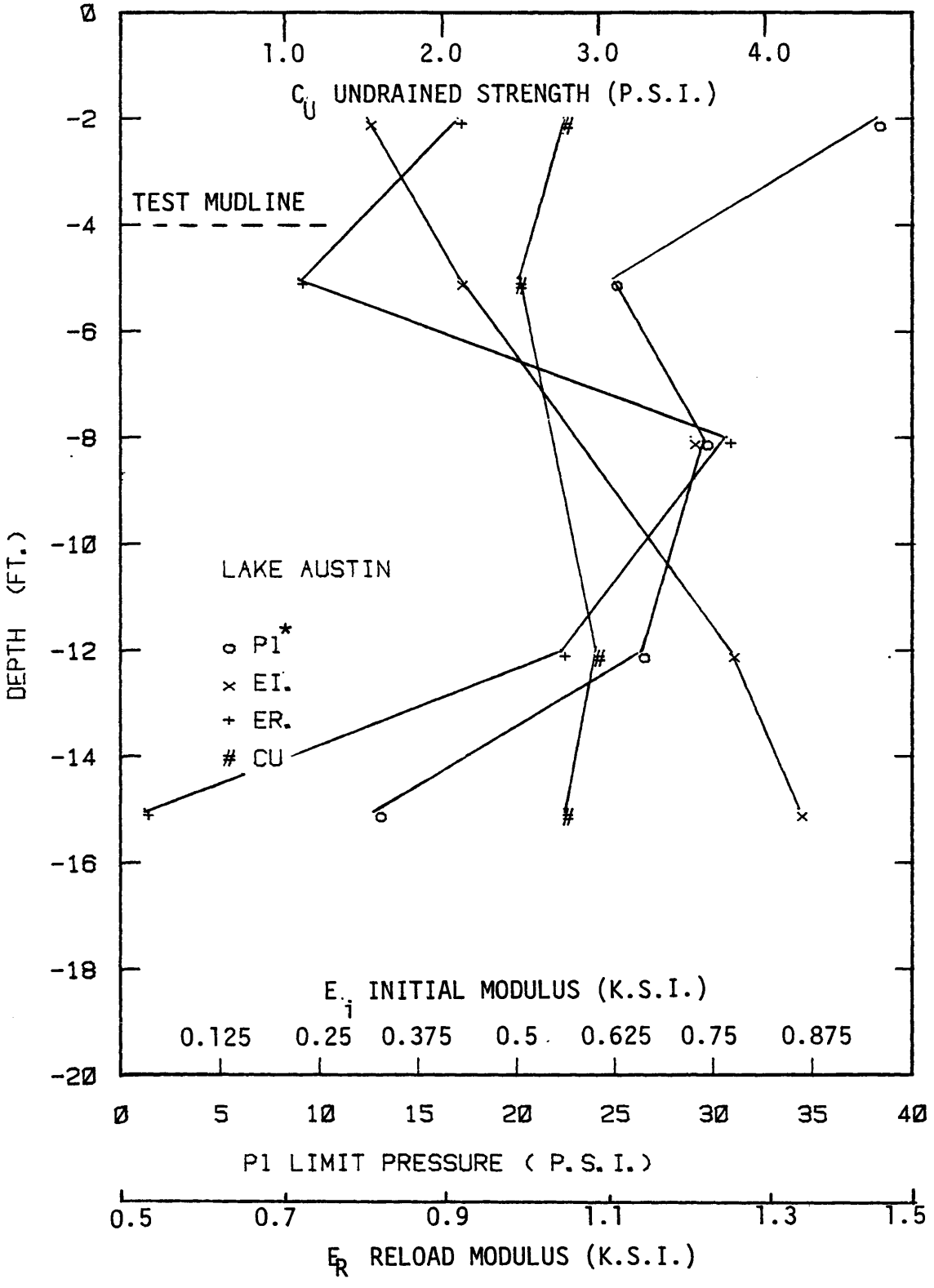

FIG. 102 - Pressuremeter Test Results and Undrained Shear Strength for Lake Austin Site

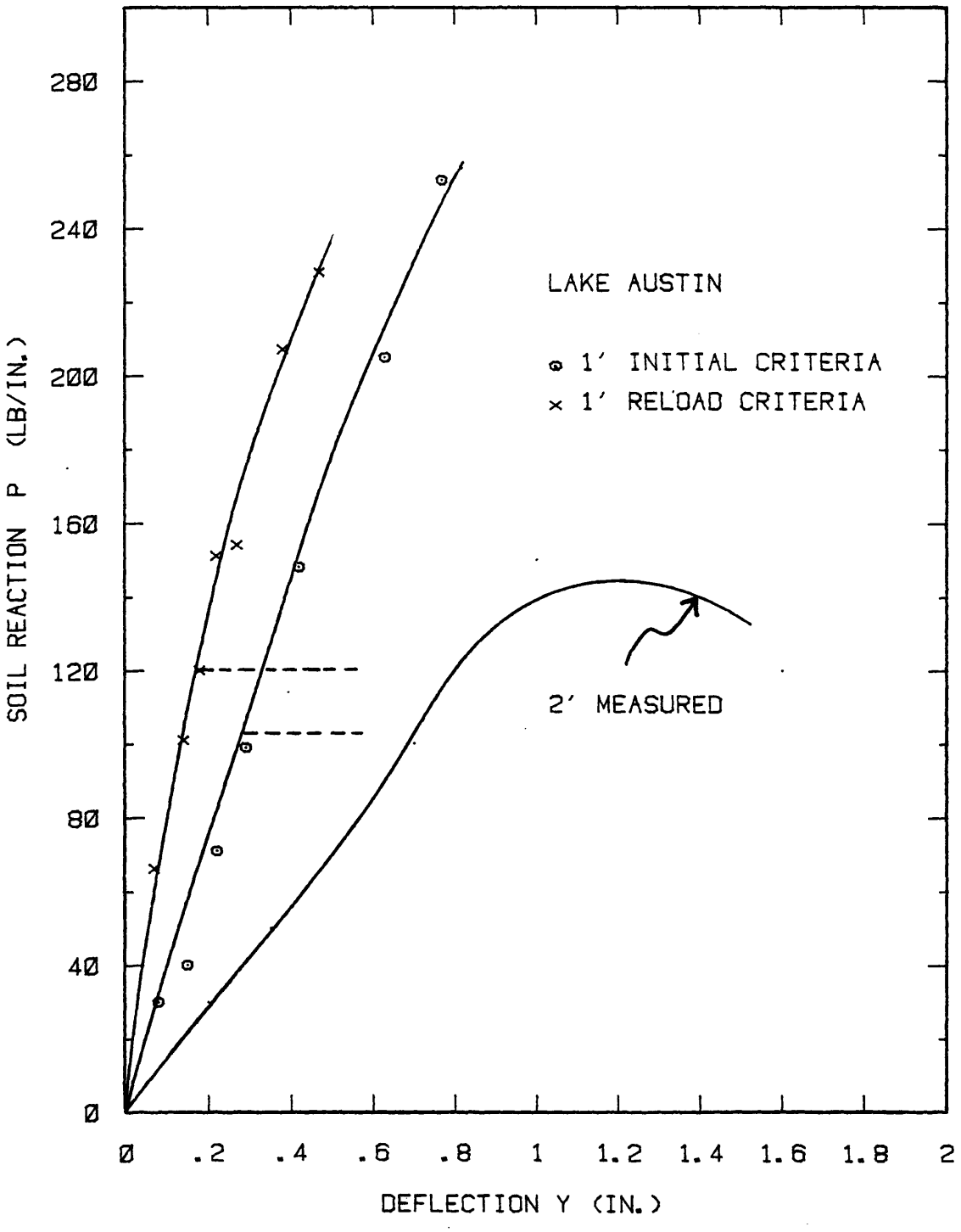

FIG. 103 - Lake Austin Site: P-y Curve Comparison at 2 ft Deep

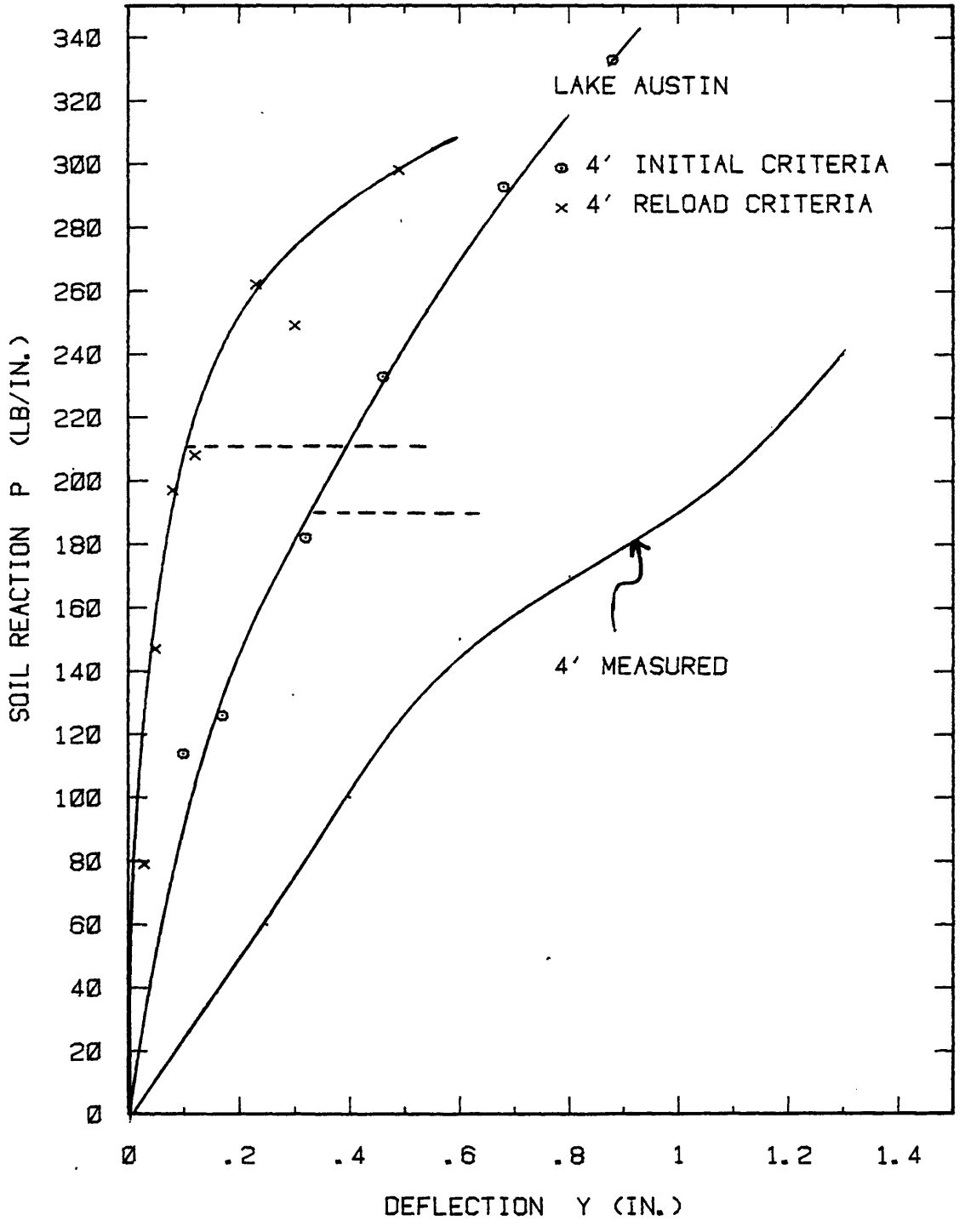

FIG. 104 - Lake Austin Site: P-y Curve Comparison for 4 ft Deep

shear stress from the pressuremeter tests, an elastic plastic curve is proposed. When the calculated shear stress exceeds a reasonable maximum, at that depth, the reaction, P, is held constant for all increasing deflections. With this modification the predicted lateral load and maximum bending moment versus surface deflection are shown on Fig. 105 and Fig. 106.

As expected, both initial and reload criteria are unconservative in the working load range and, due to the elastic-plastic modification, conservative in the ultimate load range. Good agreement is fround for the prediction of bending moments.

Manor: Stiff Clay Below the Water Table

Two steel pipe piles, an 6 in. (150 mm) and 25 in. (660 mm) were tested in a pit dug to a total depth of 6 ft (1.8 m). The test pit was excavated over a period of 6 months in three separate operations.

After each excavation, local ponding was completed to simulate a marine environment. The results of soil borings taken before the final 3 ft (914 mm) excavation showed that ponding had severely reduced the undrained strength accompanied by an increase in water content within the top 3 ft (914 mm). Final excavation of 6 in. (150 mm), and installation of test piles, took place within a period of 1 week. The reported final shear strength profile from the test mudline gave an increase to 1.0 t.s.f. (96 kPa) at 1 ft (305 mm) depth and 4.0 t.s.f. (384 kPa) at 12 ft (3.6 m) depth. The wide scatter of results, assessment of the local ponding effects with time and the rapid increase in strength with depth, are difficult to interpret. Further, it is

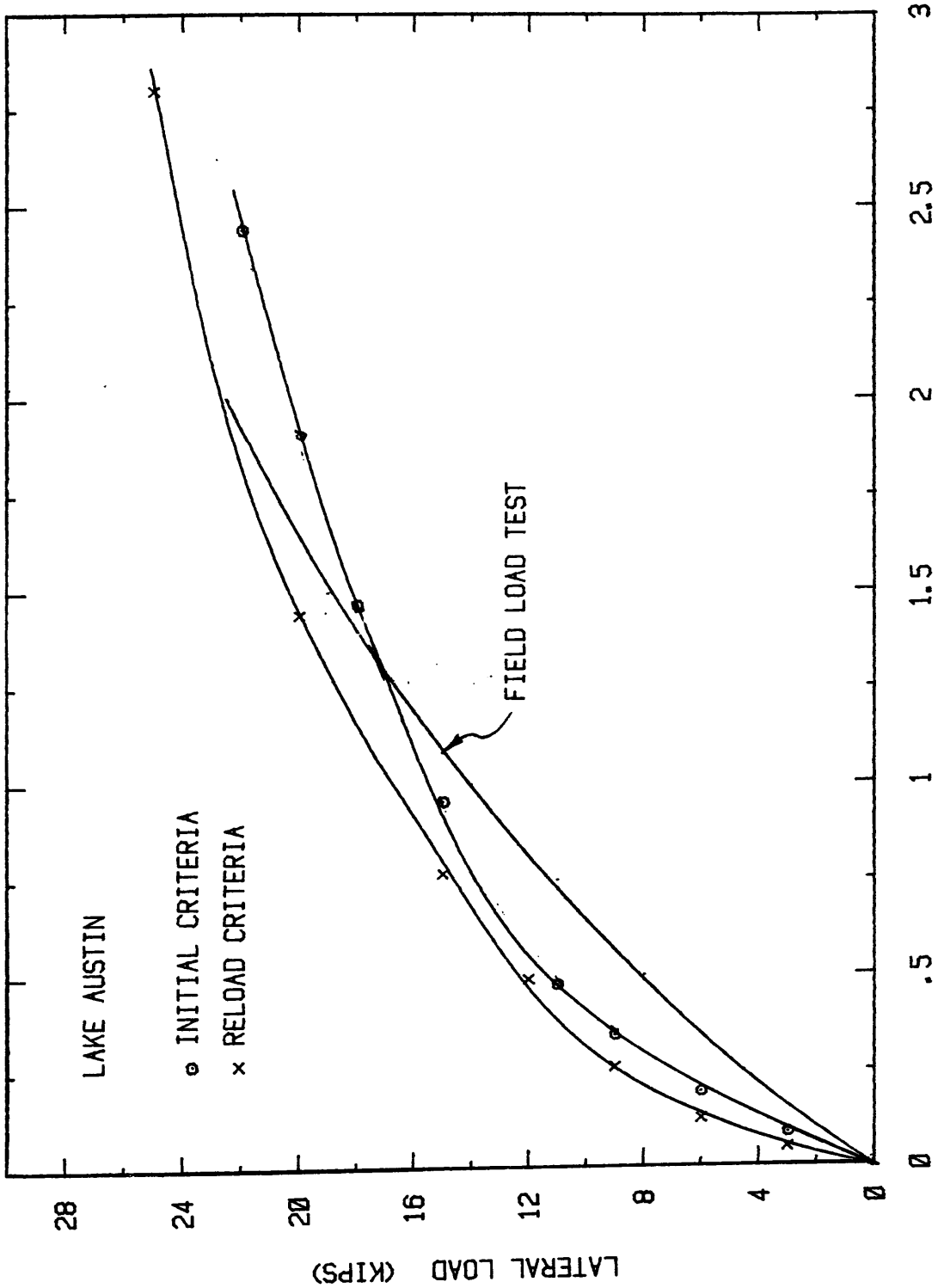

FIG. 105 - Lake Austin Site: Comparison of Groundline Deflection

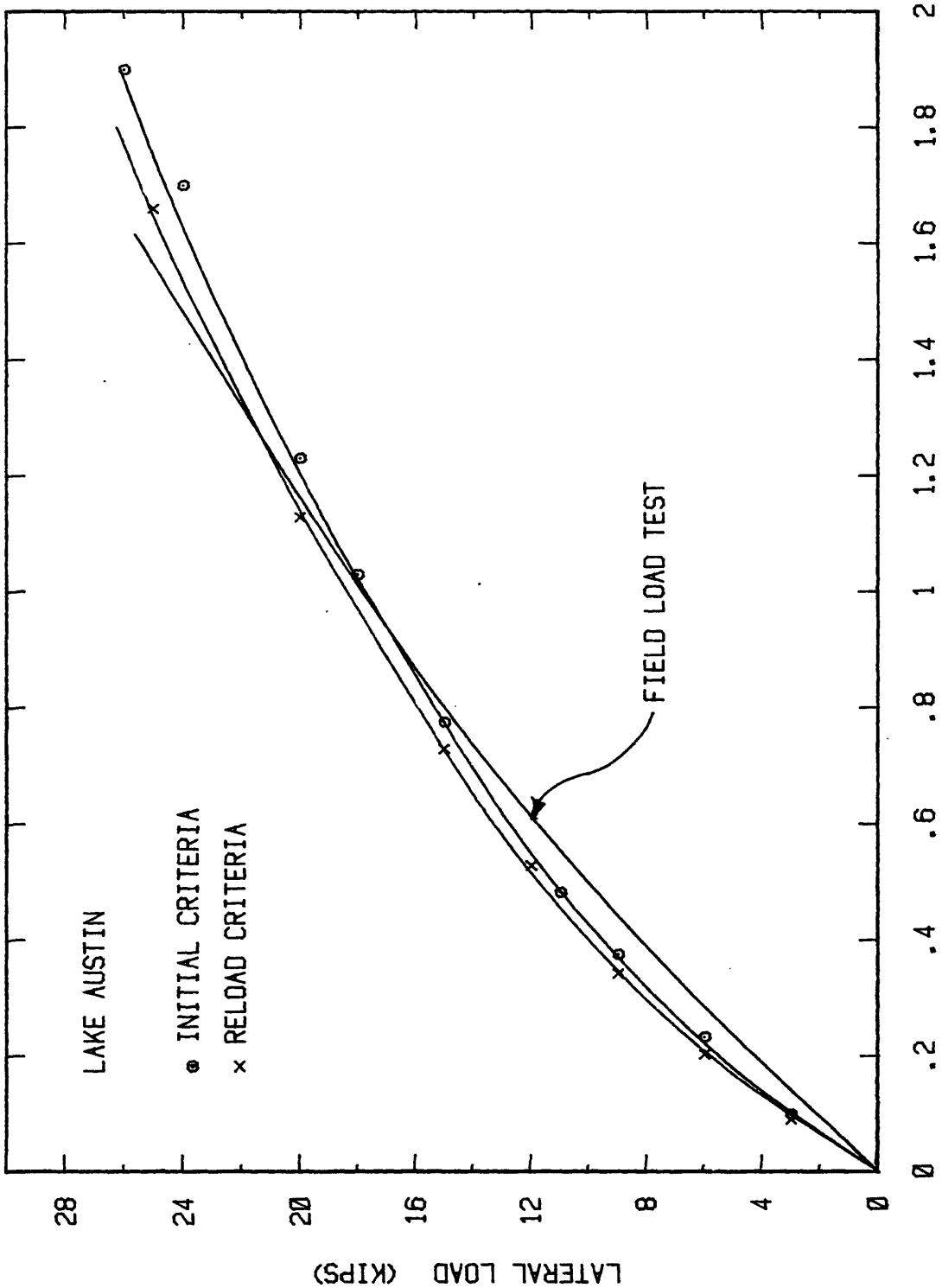

FIG. 106 - Lake Austin Site: Comparison of Maximum Bending Moment

reported that approximately 6 ft (1.8 m) of soft fill has been placed since the load test.

The variations of limit pressure, initial modulus, reload modulus and undrained shear strength, prior to the load test, are given on Fig. 107 A rapid increase in the soil stiffness beyond the 7 ft (2.1 m) pressuremeter test identifies the recent fill. The increase in stiffness beyond 11 ft (3.35 m) is well represented by the pressuremeter tests.

All pressuremeter tests are given in Appendix IV, with horizontal earth pressure at rest calculated on the basis of an O.C.R. of 2. The PAV unit was employed in dry, hand augered, holes. At the time of the load test the water table is considered at the mudline line. Test results at 11 ft (3.35 m) and 15.3 ft (4.66 m) are used, with appropriate depth reduction factors, to derive the P-y curves.

P-y curve comparison is made on Fig.108 for the 25 in. (660 m) pile reference 1, and Fig.109 for the 6 in (150 m) pile reference 3. Both initial and reload criteria are shown to give a very poor approximation to the 'measured' curves.

The generated shear strengths from the pressuremeter curves are approximately 50%-100% too high and the resulting P-y curves are limited to the undrained shear strength. For the 25 in. (660 m) pile, both criteria are of the order 5 times too unconservative and for the 6 in. (150 mm) pile, 3 times too unconservative. No comparisons are available at the depths unaffected by ponding since the pile is displaced only a very small distance.

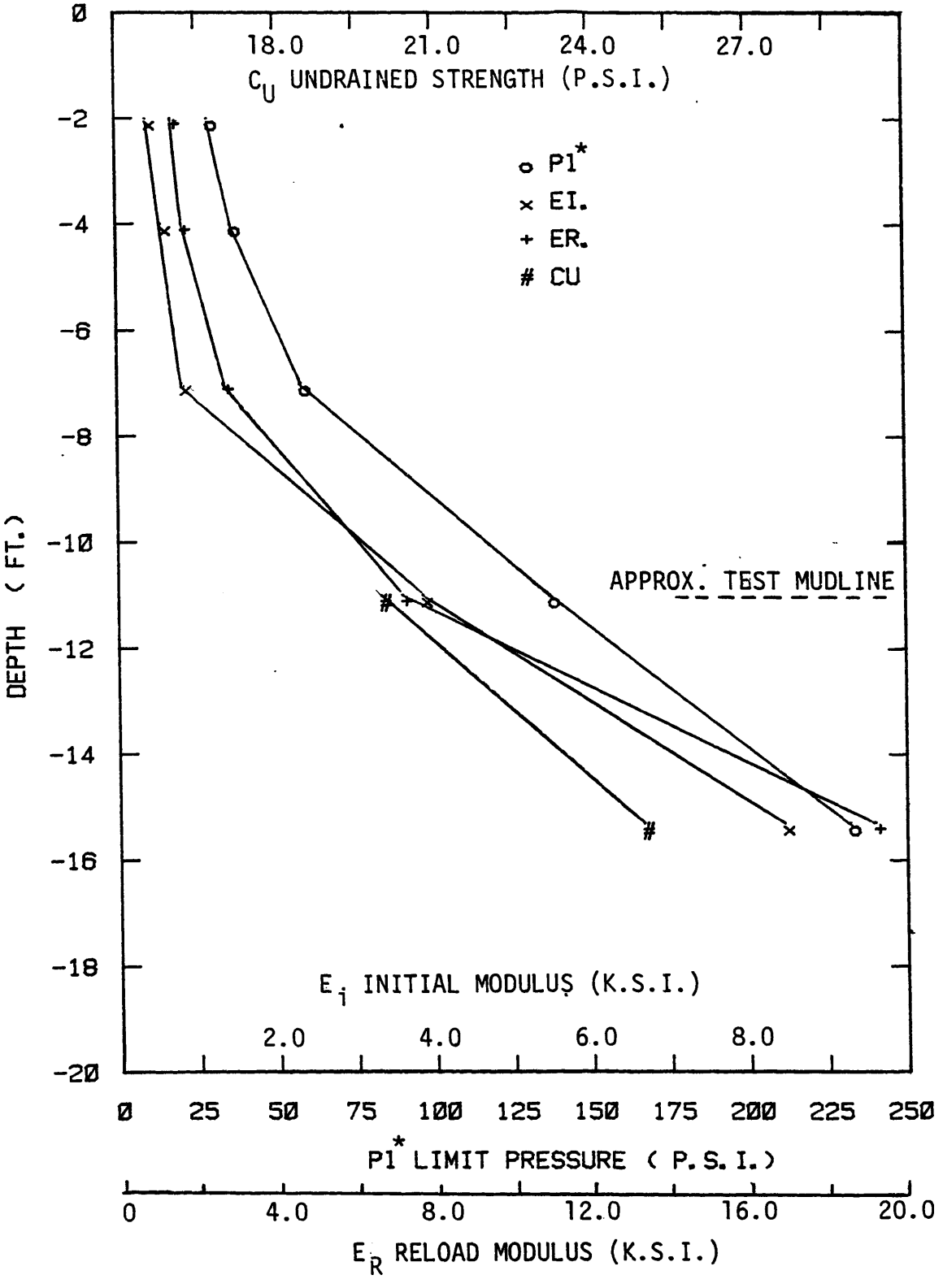

FIG. 107 - Pressuremeter Test Results and Undrained Shear Strength for Manor Site

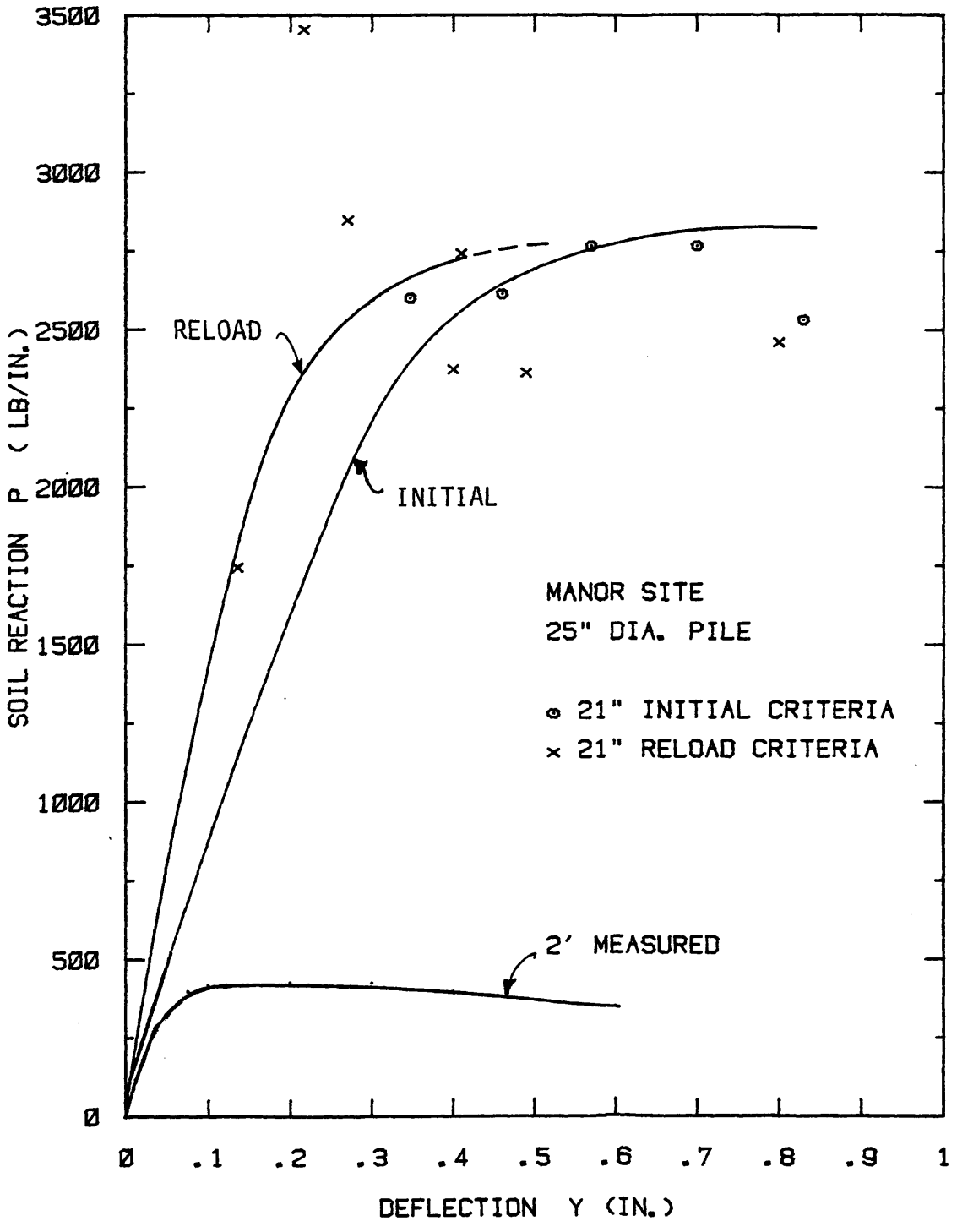

FIG. 108 - Manor Site: P-y Curve Comparison at 2 ft Deep for 25 in. Pile

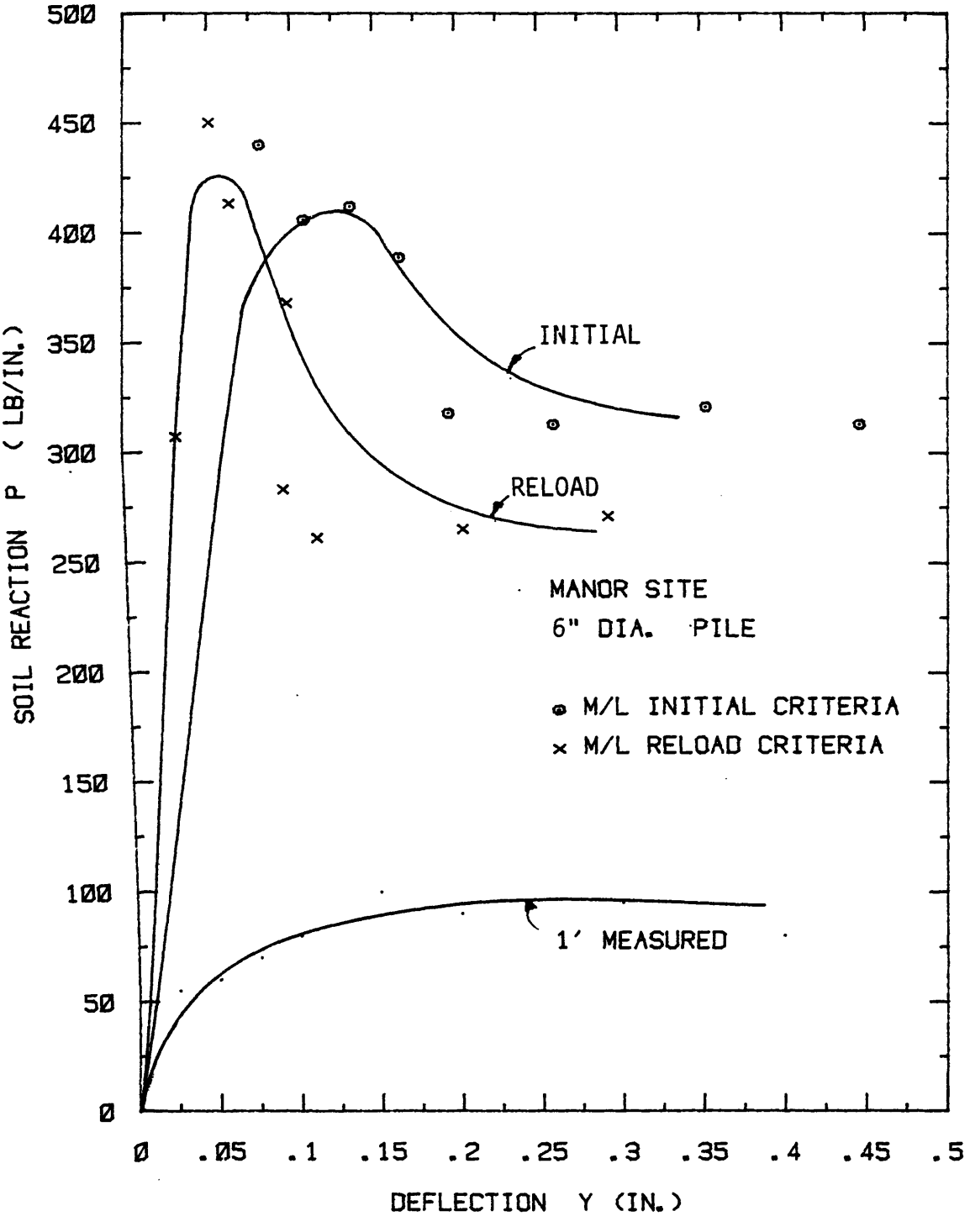

FIG. 109 - Manor Site: P-y Curve Comparison at 1 ft Deep for 6 in. Pile

At the time of the pressuremeter tests no flooded pit existed and the ponding effects are difficult to quantify. As a result the comparison shown on Fig. 110 and Fig. 111 for head deflections for each pile, is poor.

Mustang Island: Sand Below the Water Table

The variations of limit pressure, initial modulus and reload modulus with depth, based on pressuremeter tests taken in a borehole approximately 230 ft (70 m) to the north, are given on Fig. 112. Fig. 113 shows the variation of SPT blow count from the time of the load test and the present investigation.

The load test was conducted inside a 5.5 ft (1.7 m) deep pit from below which a layer 2.5 ft (770 mm) deep comprising a mixture of clay, fine sand and shell fragments had been replaced with a uniform clean sand. The ground datum for the pressuremeter tests is believed to be approximately 5 ft (1.5 m) higher than ground level for the pile test. The variation of blow count, shown on Fig. 113, indicates beyond the top 10.0 ft (2.05 m) a uniform increase with depth until approximately 19.0 ft (5.8 m) and thus the different datum elevation is ignored. A comparison of the grading curves from the load test and the present investigation is made on Fig. 114.

Penetrometer readings taken adjacent to the test pile before and after driving, showed a substantial increase in sand density. The increase was reported to be a maximum of 200% at the mudline to an increase of 50% at 10.0 ft (3.05 m) deep, thereafter remaining constant. This indicates severe disturbance through vibration, with

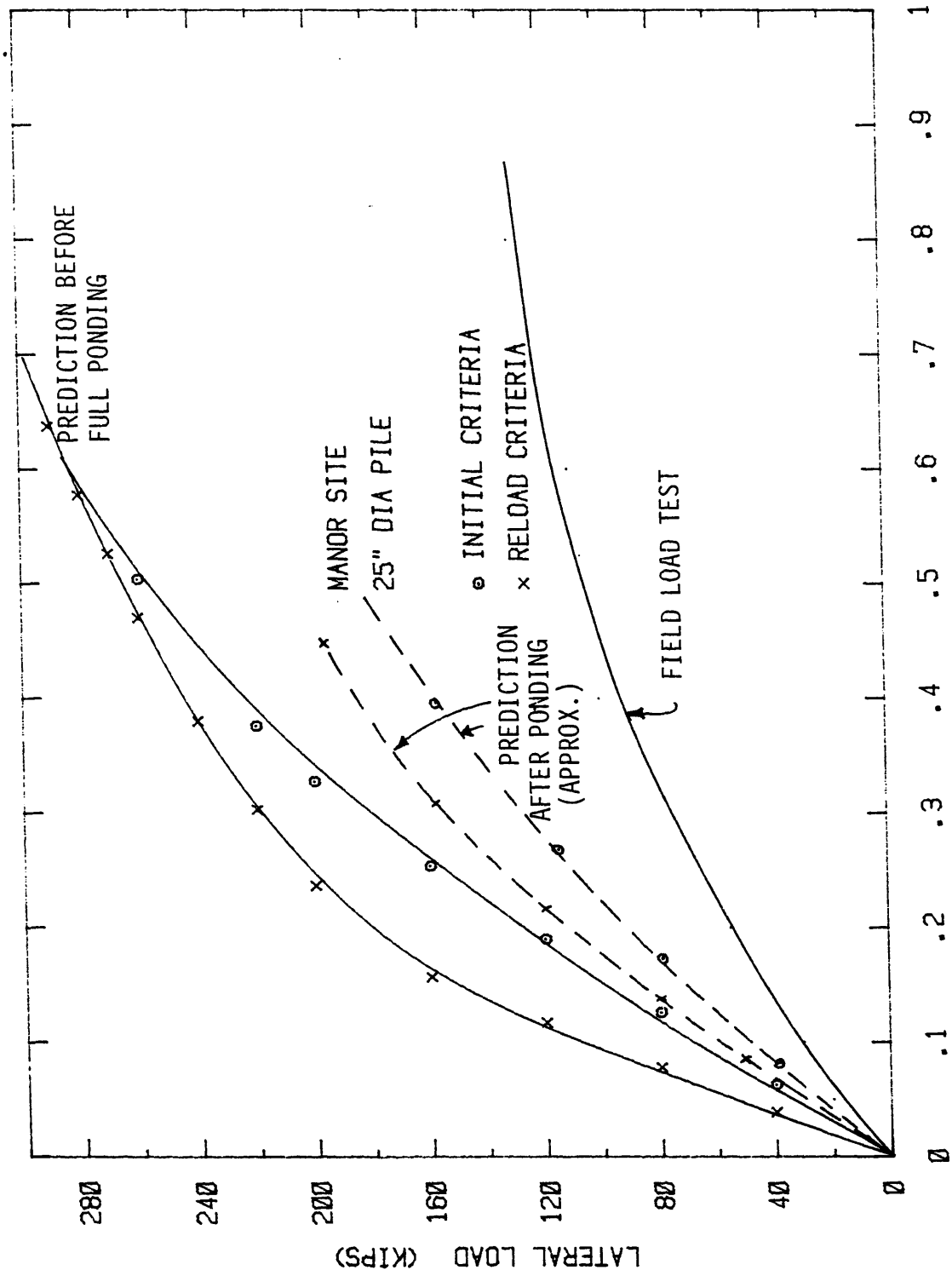

FIG. 110 - Manor Site: Comparison of Groundline Deflection for 25 in. Pile

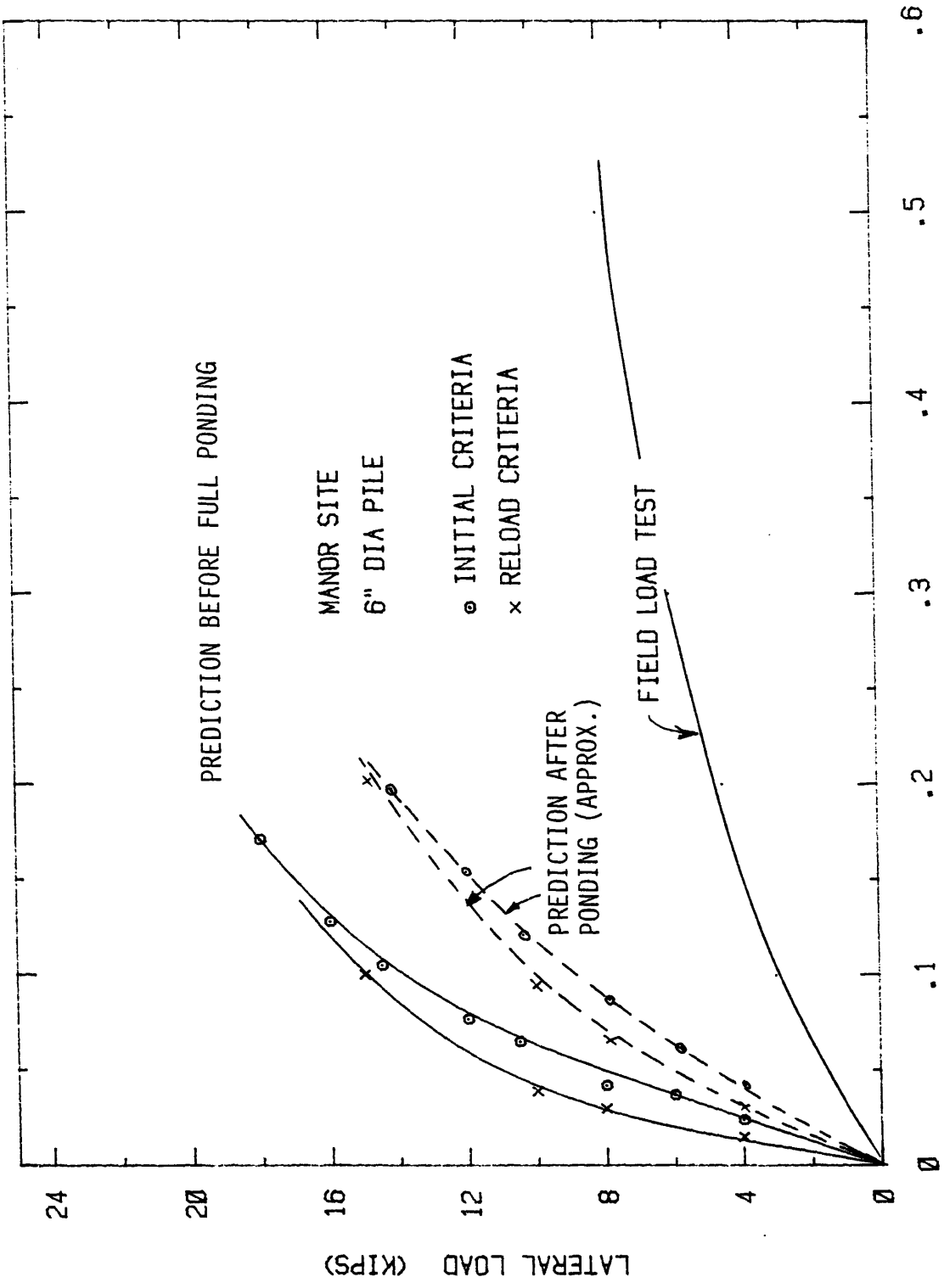

FIG. 111 - Manor Site: Comparison of Groundline Deflection for 6 in. Pile

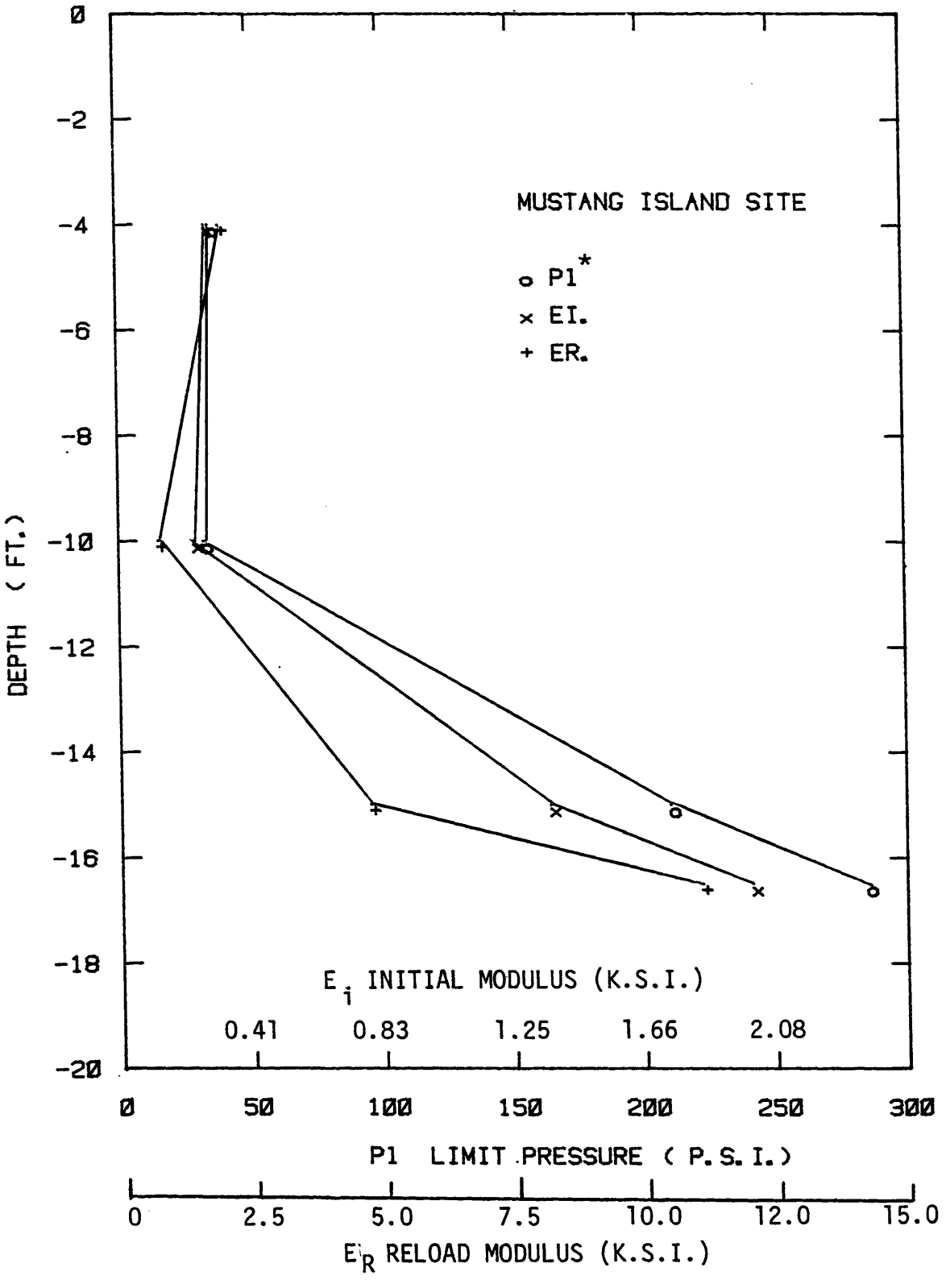

FIG. 112 - Pressuremeter Test Results for Mustang Island Site

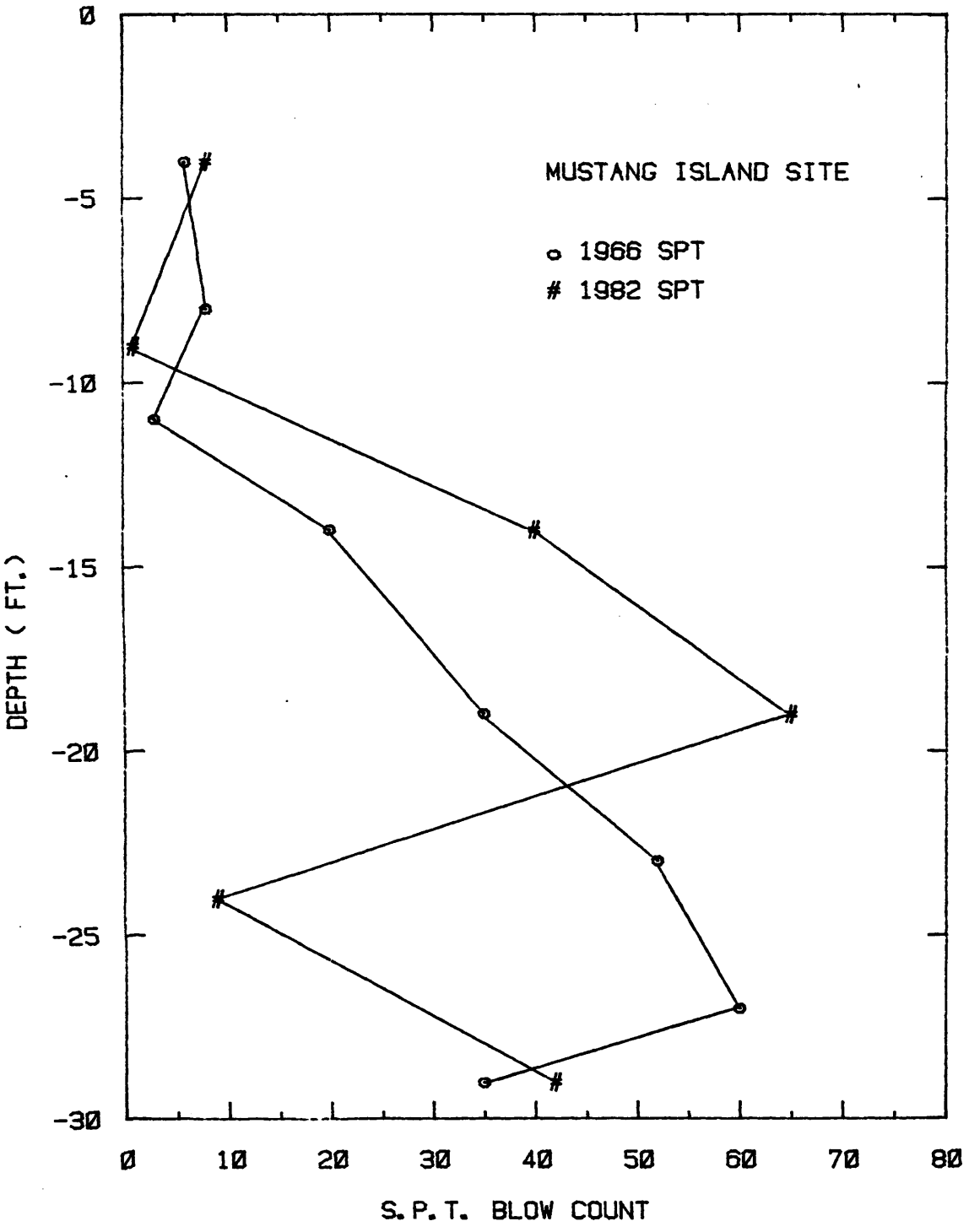

FIG. 113 - Mustang Island Site: Comparison of S.P.T. Blow Counts

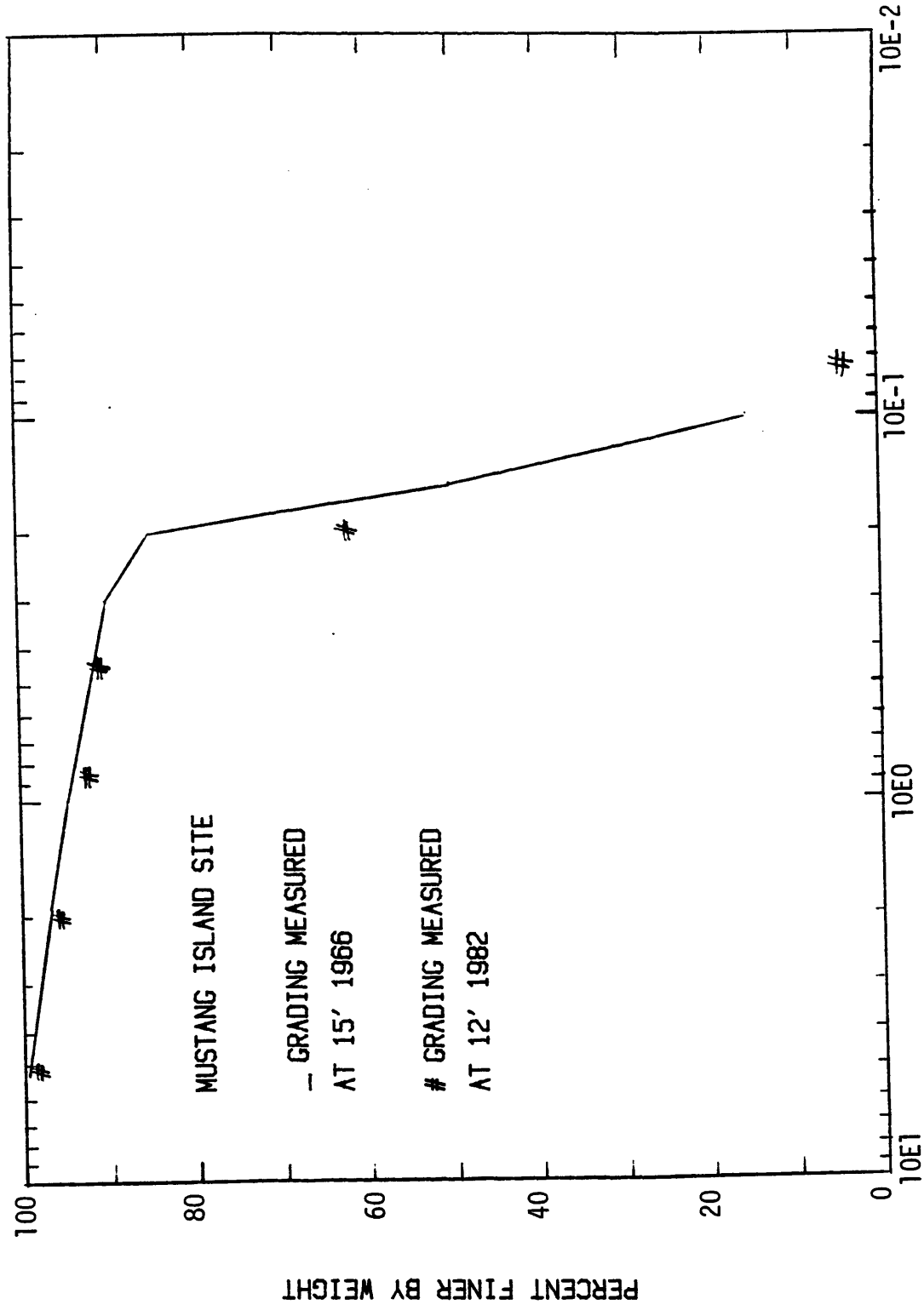

FIG. 114 - Mustang Island Site: Comparison of Grading Curves

possible fracture of the weak shell fragments within the sand. Ground settlements around the pile circumference reached 4.0 in. (100 mm).

Pressuremeter results for depths 4.0 ft (1.22 m) to 24.0 ft (7.3 m) are all given in Appendix IV. The 4.1 ft (1.22 m) test was conducted with the PAV probe 2.0 ft (610 mm) deep in a dry hard augered hole at a surface level 2.0 ft (610 mm) below the general ground datum. Shallow tests conducted with the TEXAM probe gave excess disturbance and are not shown. For all remaining tests the borehole was prepared by slow rotary drilling with circulation of drilling mud to ground level. The 10 ft (3.05 m) and 15 ft (4.57 m) tests were drilled with 2.25 in. (57 mm) and 2.0 in. (51 mm) bits respectively. The remainder of the borehole was advanced with open drill pipe and prepare mud circulation at low pressures. Both the 15.0 ft (4.57 m) and 16.5 ft (5.0 m) pressuremeter tests show oversized holes. The limit pressures for these two tests shown on Fig.112 (p. 235) are taken from p^*_ℓ / E_I correlations.

The derived P-y curves from the pressuremeter tests, without realignment of ground datums, is given in Fig. 115 and Fig.116 for 4.0 ft (1.22 m) and 10.0 ft (3.05 m) respectively.

Comparison is made to the 'measured' P-y curves from the static loading of pile number 1. The initial criterion shows little nonlinearity and drastically underestimates the 'measured' response. The small deflection response of the reload criteria is in good agreement with the 'measured' response. At both depths the reload criteria is extrapolated to the higher reaction values predicted by the initial criterion.

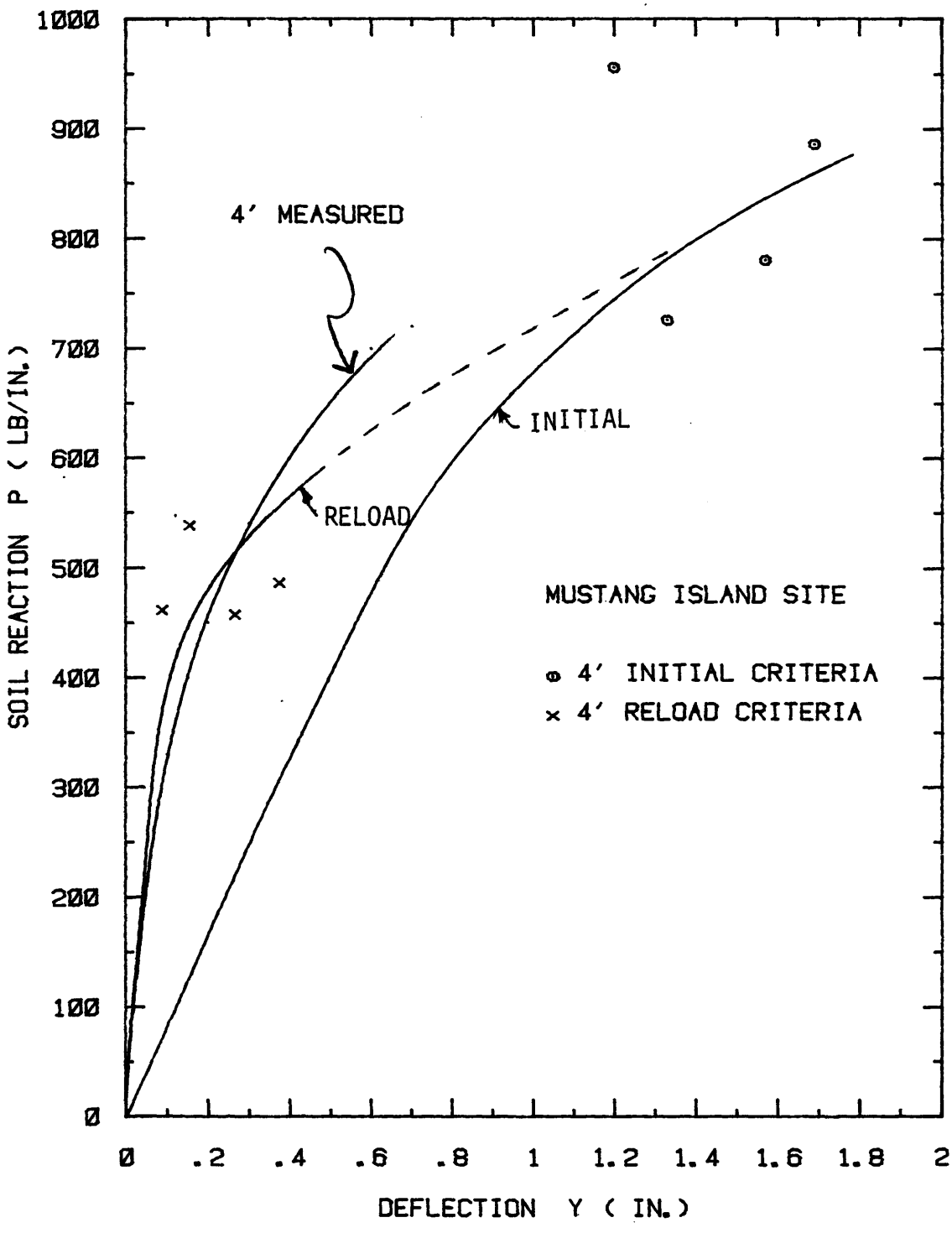

FIG. 115 - Mustang Island Site: P-y Curve Comparison at 4ft Deep

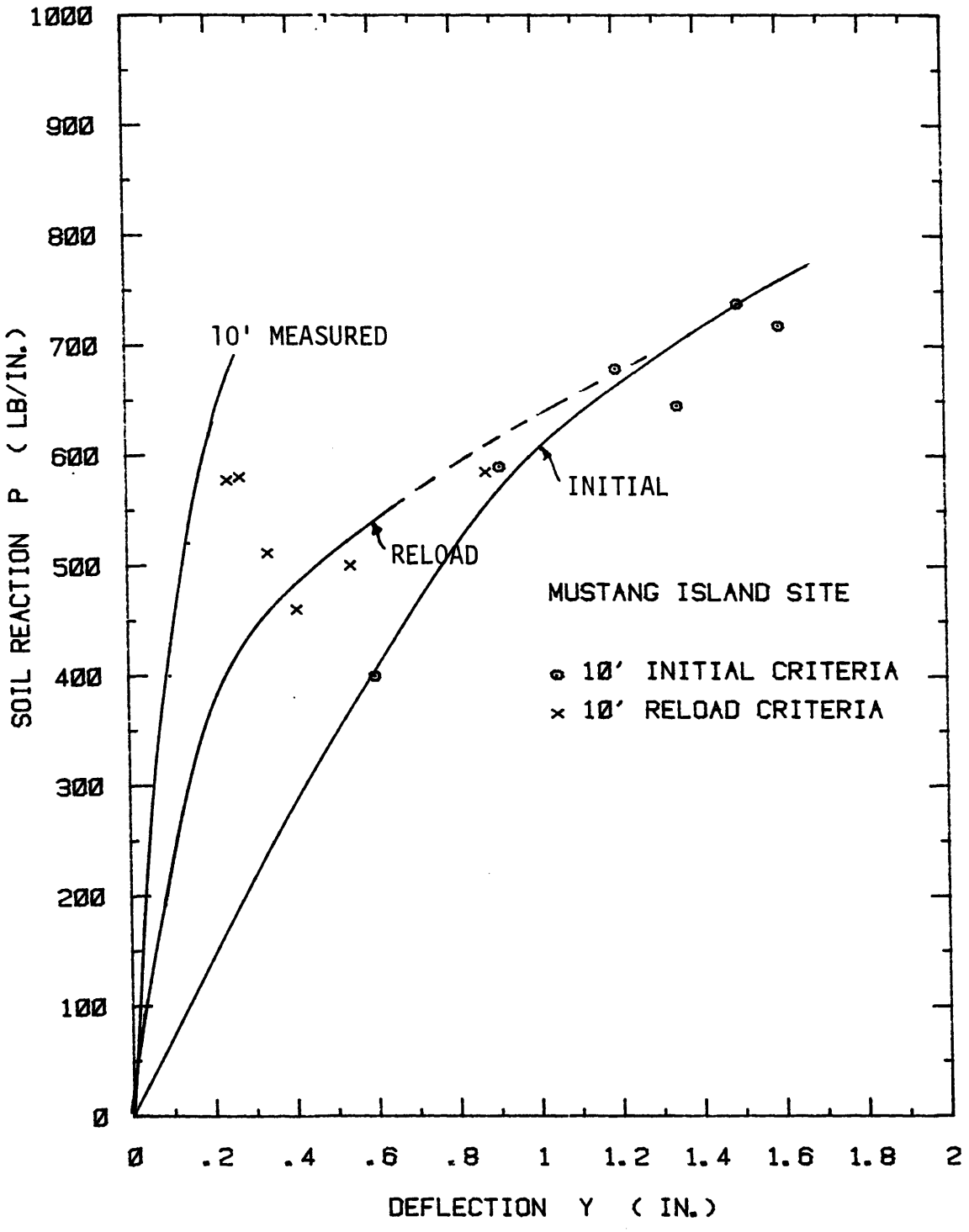

FIG.116 - Mustang Island Site: P-y Curve Comparison at 10 ft Deep

At the 4.0 ft (1.22 m) depth pressuremeter test, mobilized shear stresses reached a maximum of 15.0 lb/in.^{2} (103 kPa) and 8.0lb/in.^{2} (55 kPa) for the initial and reload cycles. These stresses correspond to coefficients of horizontal earth pressure values between 3 and 8 at 4 ft (1.22 m) depth and between 1.5 and 3 at 10 ft (3.04 m) depth. Therefore both sets of shear stresses may be considered high. However the increase in horizontal stress due to pile driving also gives an increase in the available friction between the soil and pile wall.

The prediction of lateral load versus ground deflection, and maximum bending moment, are given on Fig. 117 and 118 respectively. Good agreement is found for the reload criterion in particular over the working load range. Initial criterion predictions are 200% conservative at predicting deflections. Bending moment is shown to be insensitive to either criteria.

Sites Chosen: 'Measured' P-y Not Available

Texas A&M

The variations of limit pressure, initial modulus and reload modulus, together with undrained shear strength are given on Fig. 119 The change in soil stiffness is well represented. The exception may be the result from 15.0 ft (4.57 m) where the shear strength decreased locally together with both pressuremeter moduli, however, the limit pressure showed an increase. This depth is outside the controlling surface layer and within the vicinity of the point of rotation for these semi-rigid shafts.

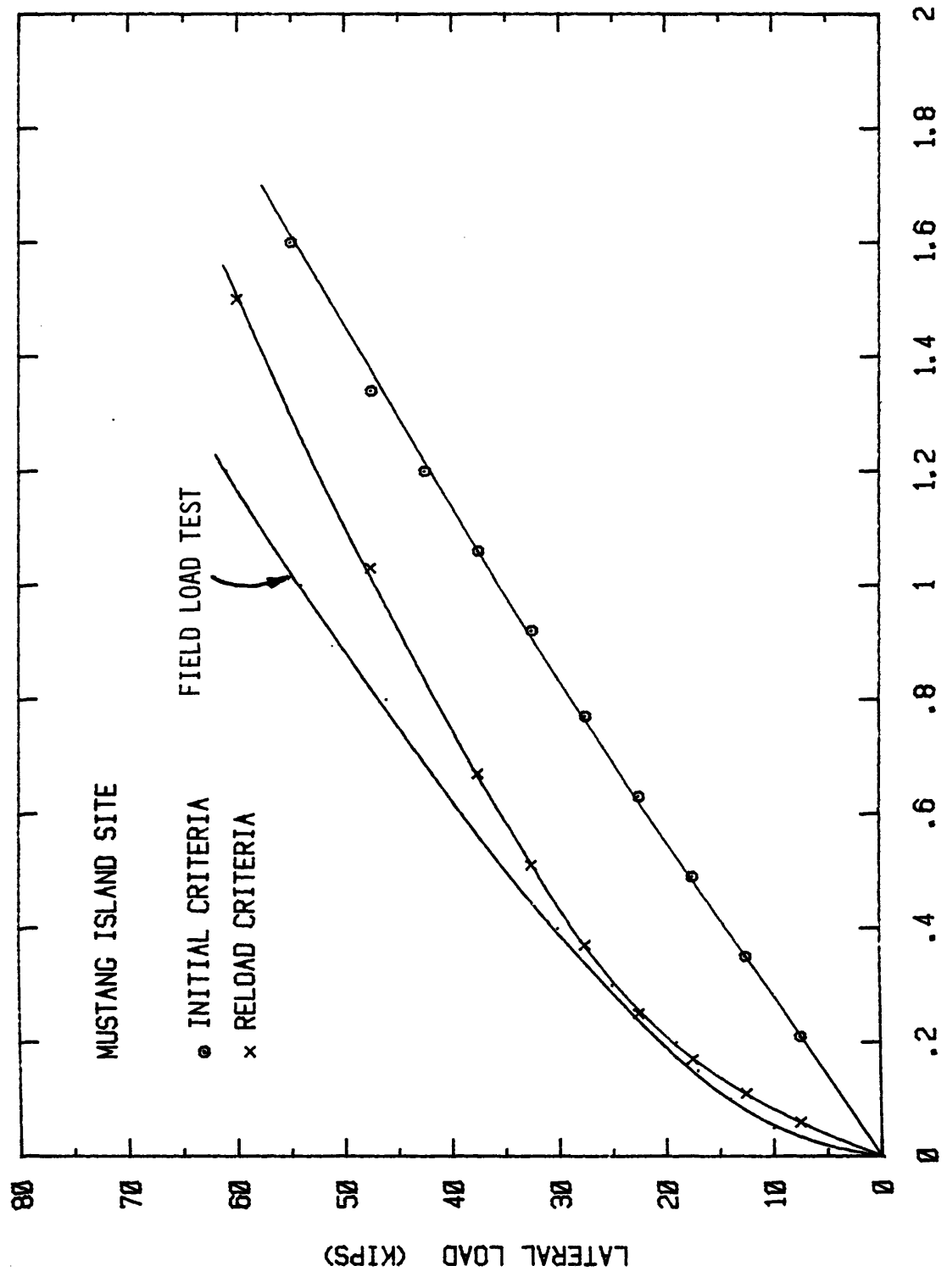

FIG. 117 - Mustang Island Site: Comparison of Groundline Deflection

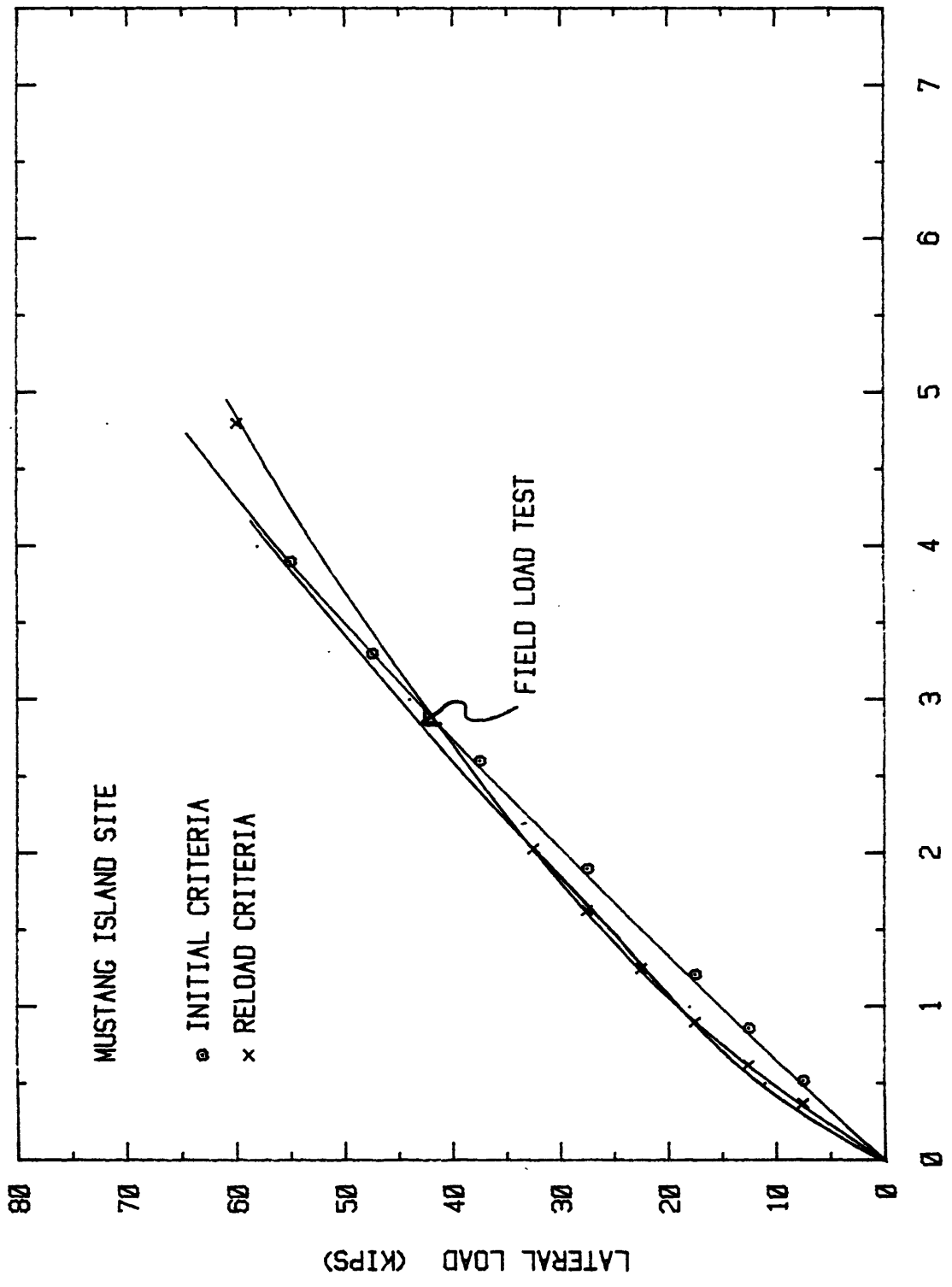

FIG. 118 - Mustang Island Site: Comparison of Maximum Bending Moment

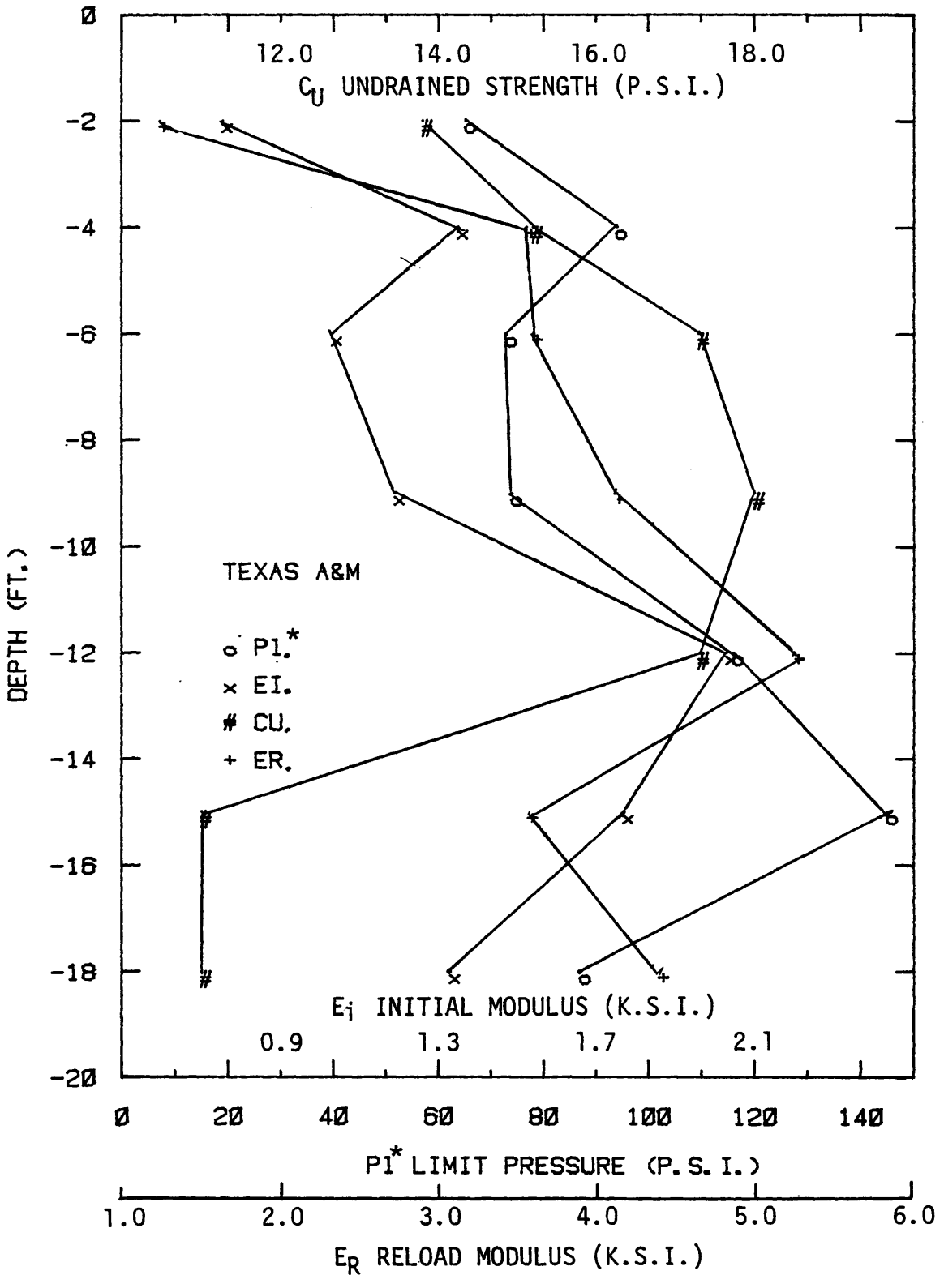

FIG. 119 - Pressuremeter Test Results and Undrained Shear Strength at Texas A&M Site

To determine the initial horizontal ground stresses, a K_o of 2 is considered for these fissured O.C. stiff clays. The water table was located 16 ft (4.87 m) below ground level. Ground level datum for the load test and pressuremeter tests were equal. During the lateral load test, increased surcharge loading was imposed at ground level to simulate backfill height. Therefore no critical depth is considered to exist for the 1977 shaft.

Due to the semi-rigid nature of the shafts a mobilized base resistance is generated and maximum undrained shear strength is assumed to be mobilized, on the base P-y curve, after a translation of 0.1 in. (2.5 mm). Appendix IV will give details of the pressuremeter tests conducted between 2.0 ft (610 mm) and 12.0 ft (3.65 m) by the PAV unit in a dry, hand augered, hole. Both the initial and reload criteria are in general agreement with respect to mobilized shear strengths, but both are 50% higher than measured. For the fissured O.C. material, it is to be expected that unconfined compressive strengths are below the measured in situ value and therefore, no attempt is made to reduce the pressuremeter P-y curves. Reload criteria P-y curves are extrapolated to the initial criteria curves at higher deflections.

The lateral load versus ground line deflection results are given on Fig. 120, Fig. 121 and Fig. 122, for 1977, 1978 and 1979 shafts respectively. Very good agreement is found for the three shafts for the reload criteria, whereas the initial criteria, in the working load range, overpredicts deflections by approximately an average of 150%.

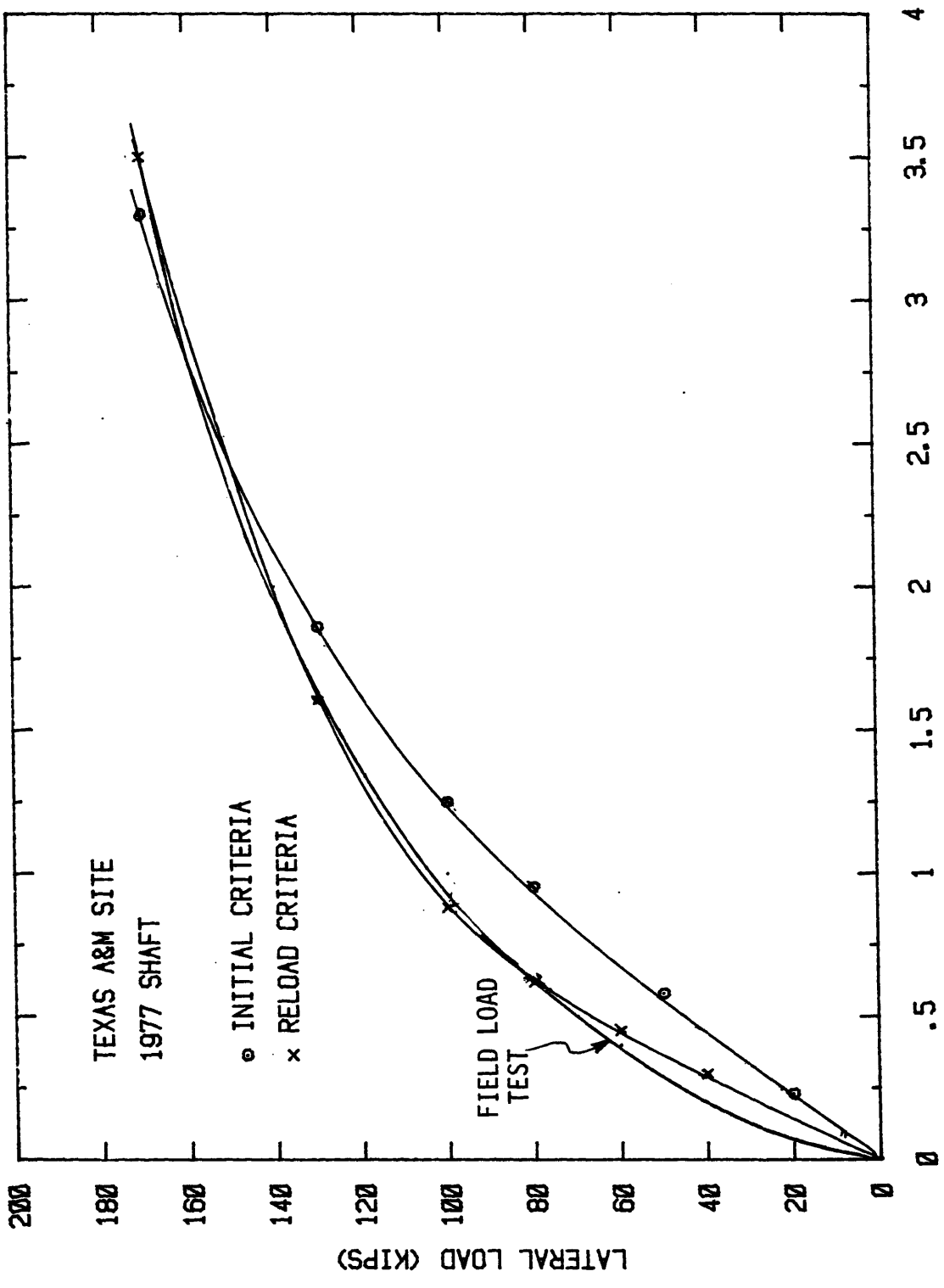

FIG. 120 - Texas A&M 1977 Shaft: Comparison of Groundline Deflection

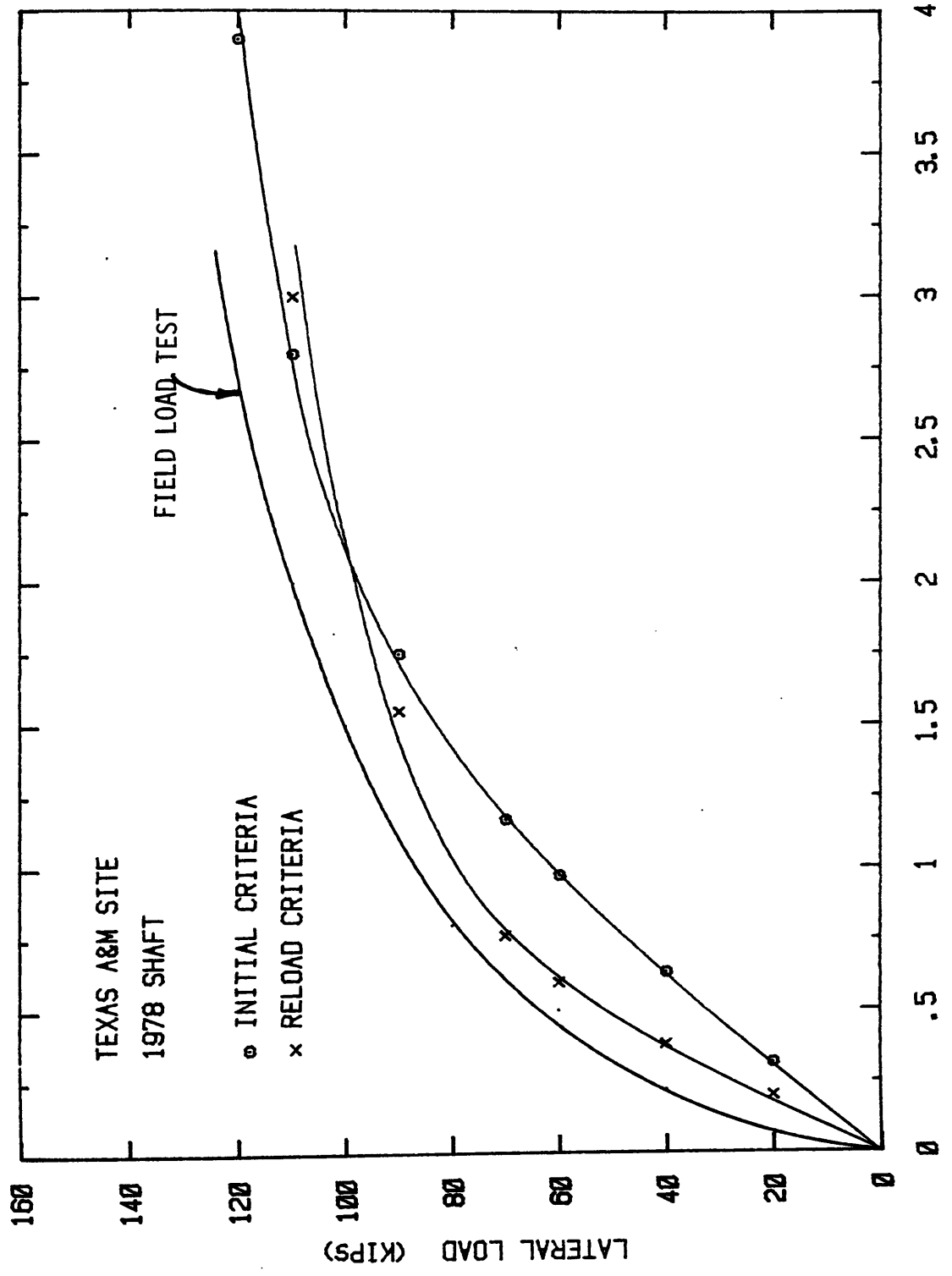

FIG. 121 - Texas A&M 1978 Shaft: Comparison of Groundline Deflection

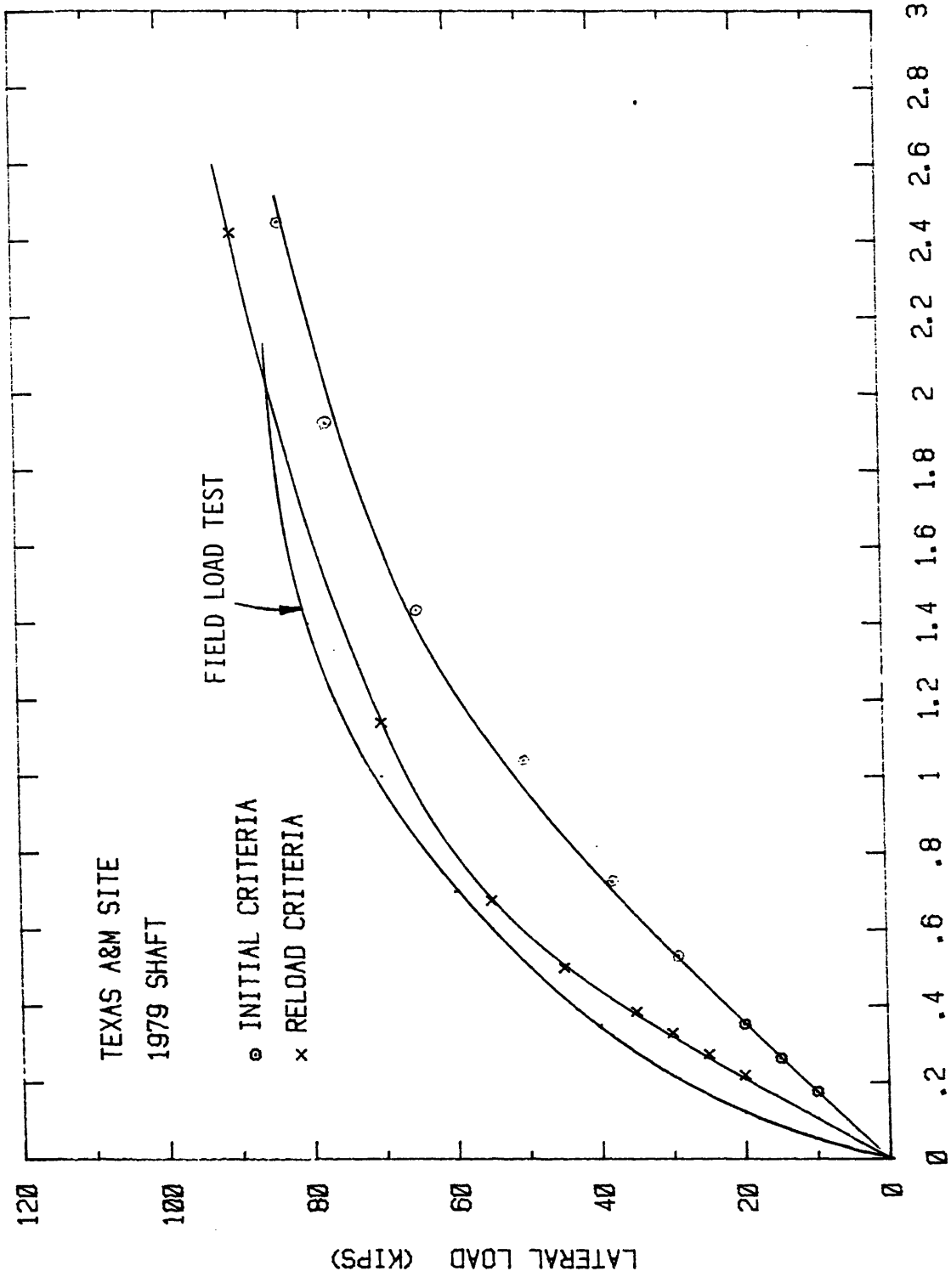

FIG. 122 - Texas A&M 1979 Shaft: Comparison of Groundline Deflection

The reported point of rotation for the 1977 shaft, based on pressure cell readings, was 14.0 ft (4.26 m) compared to 15.3 ft (4.66 m) predicted by using pressuremeter P-y curves. The same trend is noted for the 1978 and 1979 shafts where predicted points of rotation are approximately 1.0 ft (305 m) too deep. This leads to the conclusion that the mobilized base resistance curve is too high.

Lackland

A free head lateral load test performed on a reinforced concrete drilled shaft, 16 years after construction was reported by Johnson, Briaud and Stroman (47).

The site was located at Lackland Air Force Base near San Antonio, Texas. The soil consisted of 7.8 ft (2.4 m) of expansive black high plasticity clay underlain by 4-5 ft (1.2-1.5 m) of clayey gravel below which is a fissured clay shale. Average undrained shear strength of the black clay was reported as 11.0 lb/in.^{2} (77 kPa), and for the fissured clay shale 21.0 lb/in.^{2} (144 kPa).

The pile, shown on Fig. 123 , had a reported flexural stiffness of 1.52×10^{10} lb.in.^{2} (4.4×10^4 kN.M^2) and ultimate yield moment of 1.4×10^6 lb-in. (2.45×10^5 kN.M). The loading test consisted of applying a lateral load at the ground line and measuring head displacements. Fourteen of a total of twenty one strain gages were not functioning at the time of the test and no bending moment distributions are available.

The variation of limit pressure, initial modulus and reload modulus together with undrained shear strength is given on Fig. 124. A

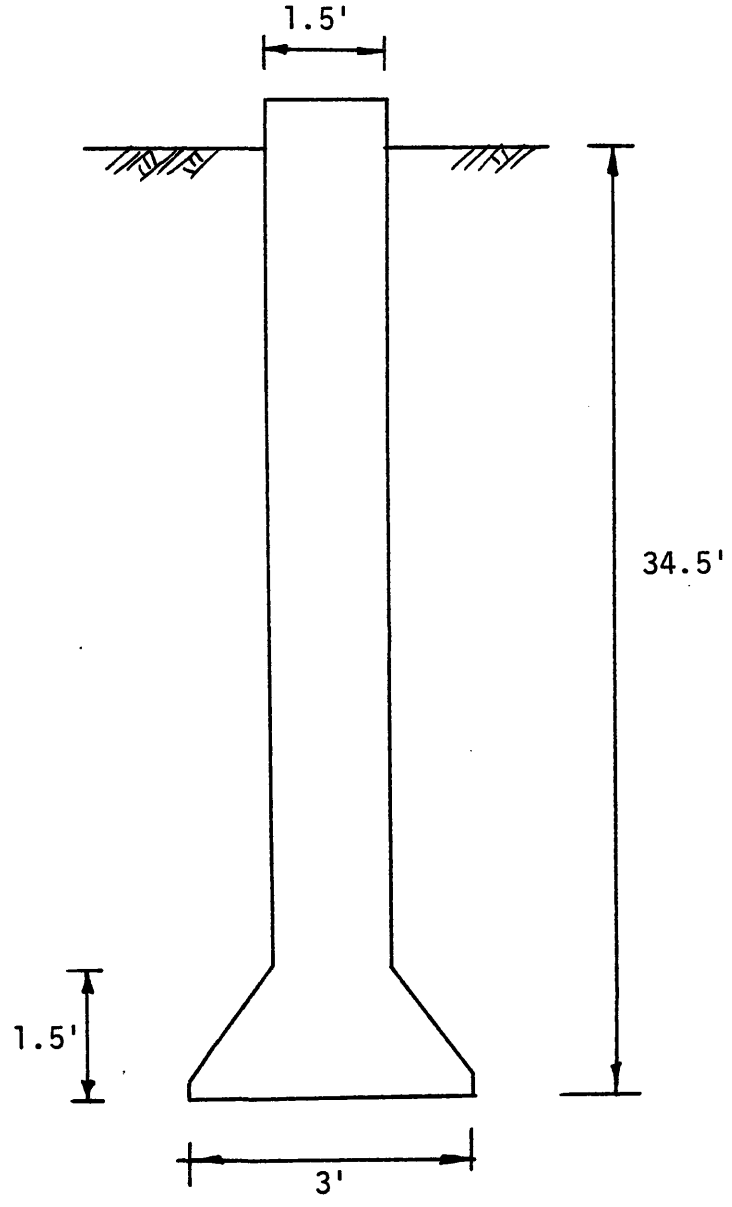

FIG. 123 - Lackland Site: Details of the Pile

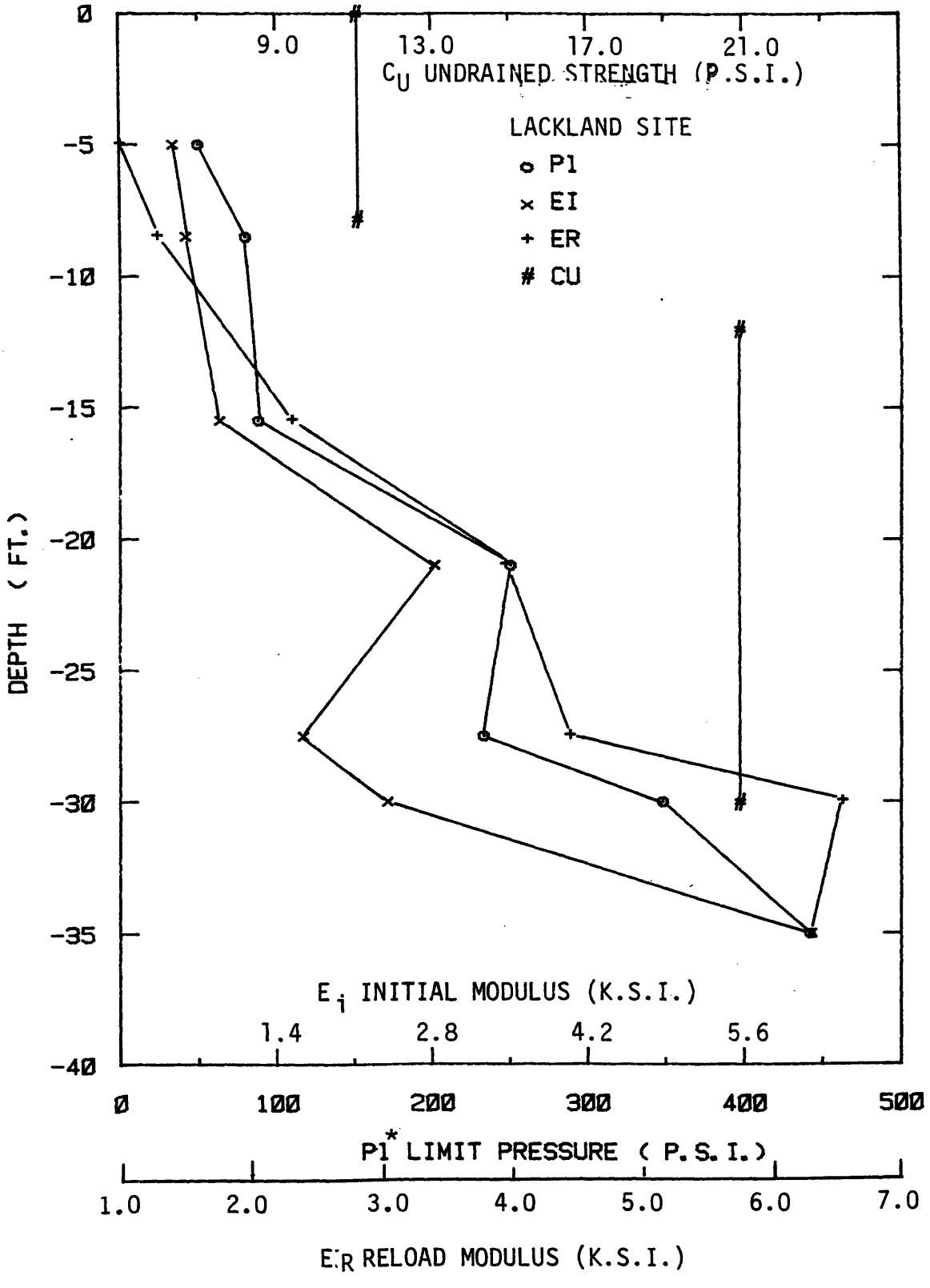

FIG. 124 - Pressuremeter Test Results and Undrained Shear Strength at Lackland Site

rapid increase, with depth, in soil stiffness is observed which is in general agreement with the reported undrained shear strength. Pressuremeter tests were conducted with the TEXAM unit, in a borehole drilled with 2.375 in. (60 mm) drill bit at low mud pressures. Tests between 5.0 ft (1.5 m) and 21.0 ft (6.4 m) are shown later in Appendix IV. No reliable tests were available from the clayey gravel. A summary of the derived P-y curves is given on Fig.125.

Lateral load versus groundline deflection predictions, together with the measured field response, is given on Fig.126. Premature failure of the test shaft was reported at approximately 30 kips (133 kN) by excess bending stresses. From the output of COM622 the ultimate bending moment is reached at a lateral load of 35 kips (155 kN).

Both initial and reload criteria show an unconservative prediction of deflection. With allowance for the reported failure of the test shaft in flexural bending, the degree of nonlinearity from the field load test is also due to changes in shaft stiffness.

Baytown

A free head lateral load test was performed at a location on the Exxon Olefins Plant at Baytown, Houston, Texas, Bigham (14). The drilled shaft was 2.0 ft (610 mm) in diameter and embedment depth 39.0 ft (11.9 m). Lateral loads were applied at the ground surface, in a free head restraint condition, and the shaft was reported tested to ultimate deflection in an undrained manner. No structural damage or

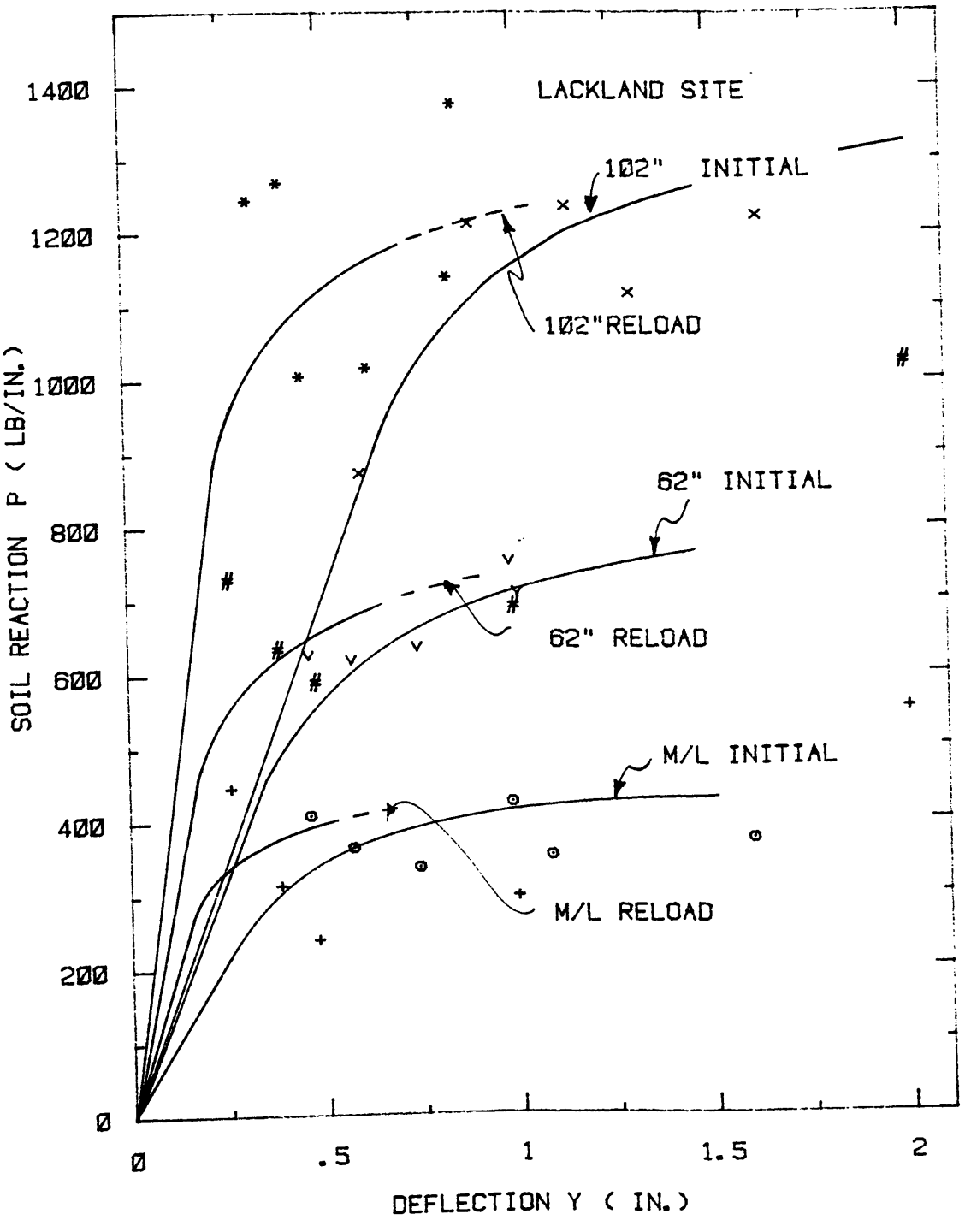

FIG. 125 - Lackland Site: Derived P-y Curves

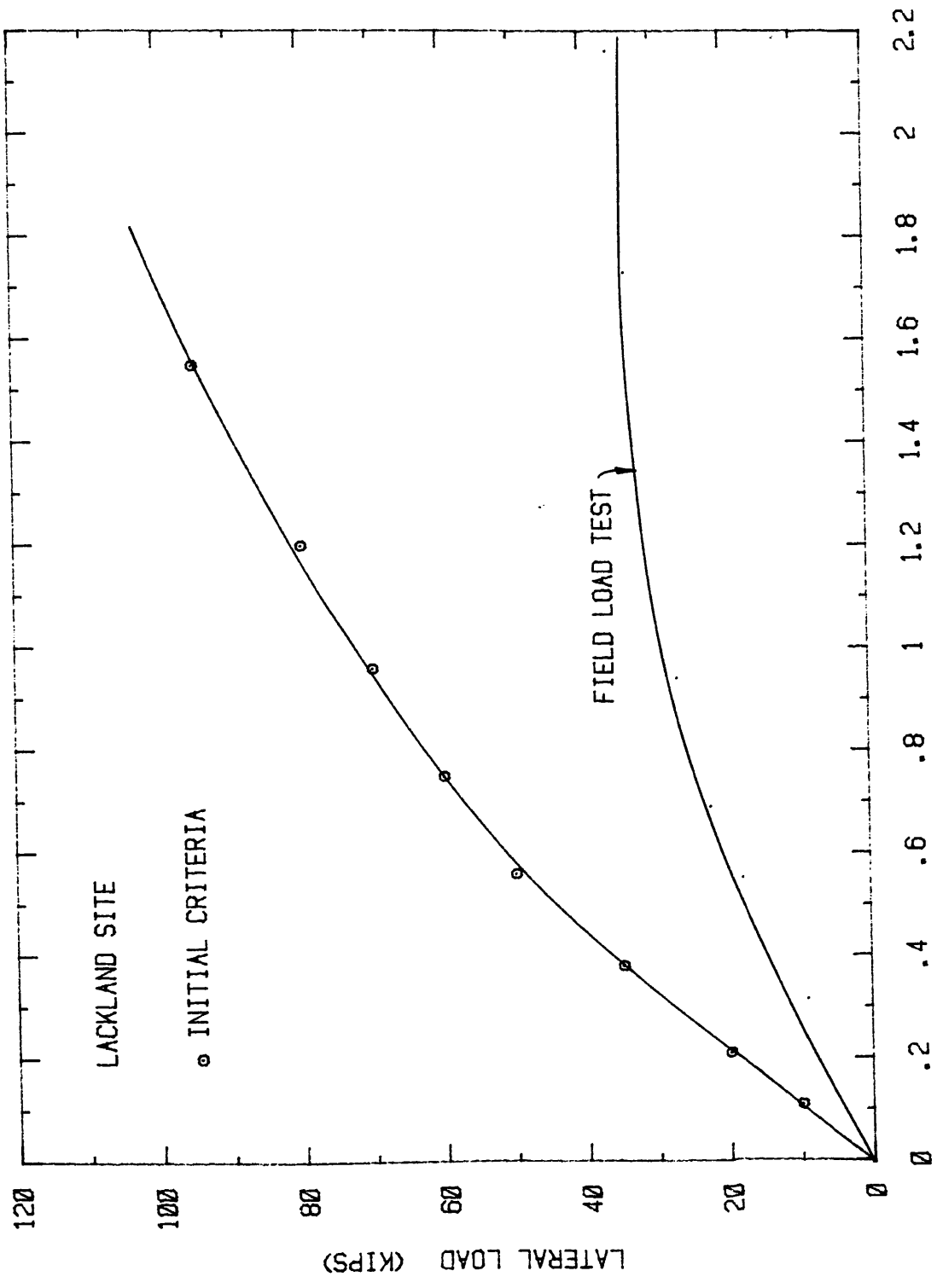

FIG. 126 - Lackland Site: Comparison of Groundline Deflection

fatigue to the pile was reported. The load test was conducted at a mudline datum 6.0 ft (1.8 m) below existing ground level. Flexural stiffness of the shaft by calculation, was 4.5×10^{10} lb.in.^{2} (1.3×10^5 kN.M^2).

The soil is a uniform slickensided tan gray clay with a slight increase in undrained shear strength beyond 9.0 ft (2.74 m) deep. Fig. 127 shows the variation of limit pressure and initial modulus, together with undrained shear strengths, with depth. The increase in soil stiffness is well represented by the pressuremeter tests and the material is considered uniform below 12.0 ft (3.65 m).

Pressuremeter tests were conducted with the PAV unit in dry, hand augered holes. The water table was not located. Pressuremeter tests at 7.0 ft (2.1 m), 9.0 ft (2.7 m) and 12.0 ft (3.6 m) are shown later on in Appendix IV. The generated shear stresses from the initial criteria are found to be between 50%-100% higher than the reported unconfined shear strengths. Since premature failure of fissured samples in an unconfined triaxial compression test the generated shear stresses from the pressuremeter results are considered valid.

The lateral load versus mudline deflection prediction, together with the measured field load test, is given on Fig. 128. The initial criteria is shown to be unconservative at predicting deflections at all load levels.

LADWP Project

To determine the suitability of drilled concrete piers for electric

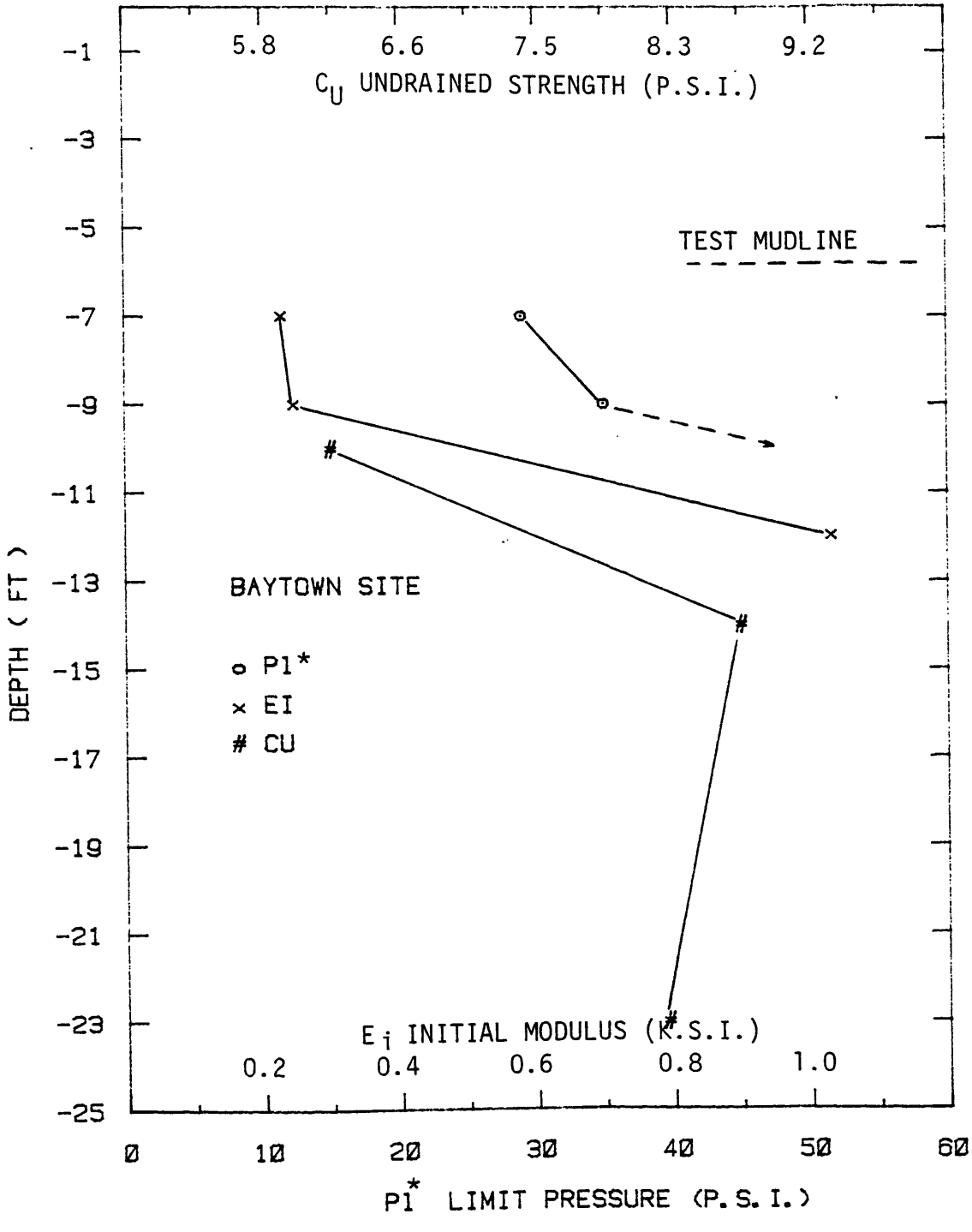

FIG. 127 - Pressuremeter Test Results and Undrained Shear Strengths at Baytown Site

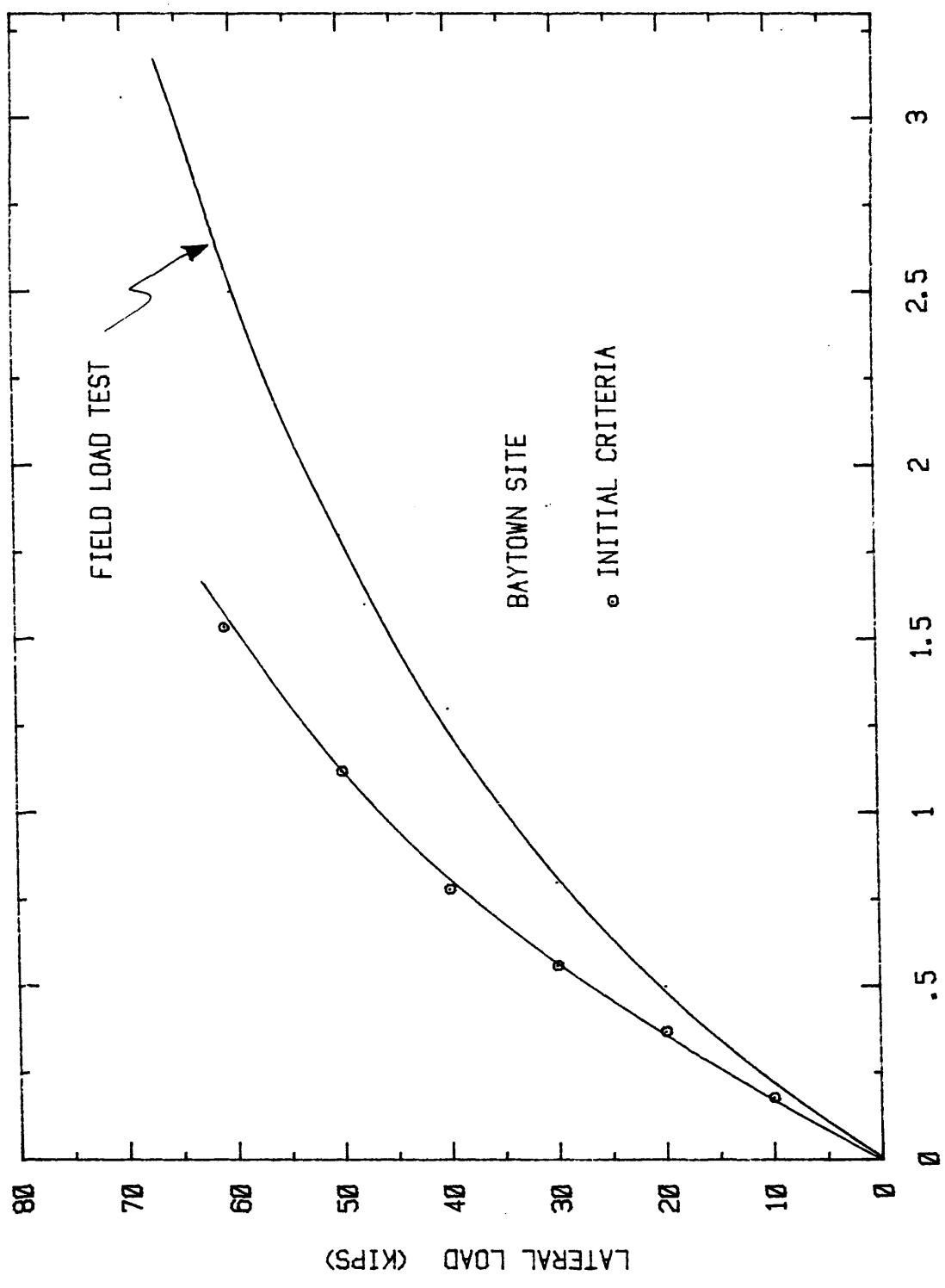

FIG. 128 - Baytown Site: Comparison of Groundline Deflections

power line pylon support, three piers were load tested at Alamo, Caliente and Delta sites and are reported by Pacal and Shively (72). Subsurface investigation details are contained in a report by Briaud (17).

At the Delta site a 26.0 in. (660 mm) diameter, 11.0 ft (3.35 m) deep, reinforced concrete shaft was load tested in a free head condition. The soil conditions consisted of 6.0 ft (1.8 m) of low plasticity silty sandy clay with undrained shear strength of 8.0 lb/in.^{2} (55.0 dPa). Below 6.0 ft (1.8 m) the soil was a silty clay with undrained shear strength of 4.8 lb/in.^{2} (33 kPa). Flexural stiffness, by calculations, is approximately 5.0 x 10^{10} lb.in.^{2} (1.45 x 10^5 kN.M^2) and the pile behaved rigid.

Pressuremeter tests were conducted at depths between 2.0 ft (610 m) and 13.0 ft (3.96 m) and the variation of limit pressure, initial modulus and reload modulus is given in Fig. 129. Pressuremeter tests were conducted with the TEXAM unit in a dry, hand augered borehole, and the results are given in Appendix IV.

The generated P-y curves from the pressuremeter, with the initial criterion overestimates shear strengths by 50%. The reload criterion is found to give between 10%-20% overestimation of shear strength. At the higher deflections reload criteria P-y curves are extrapolated to the initial criteria predictions. This generally gives an elastic-plastic relationship with little nonlinearity.

The lateral load versus head deflection is given on Fig. 130 for pier number 4. The reload criteria is shown to give good agreement in the working load range but becomes increasingly unconservative. No

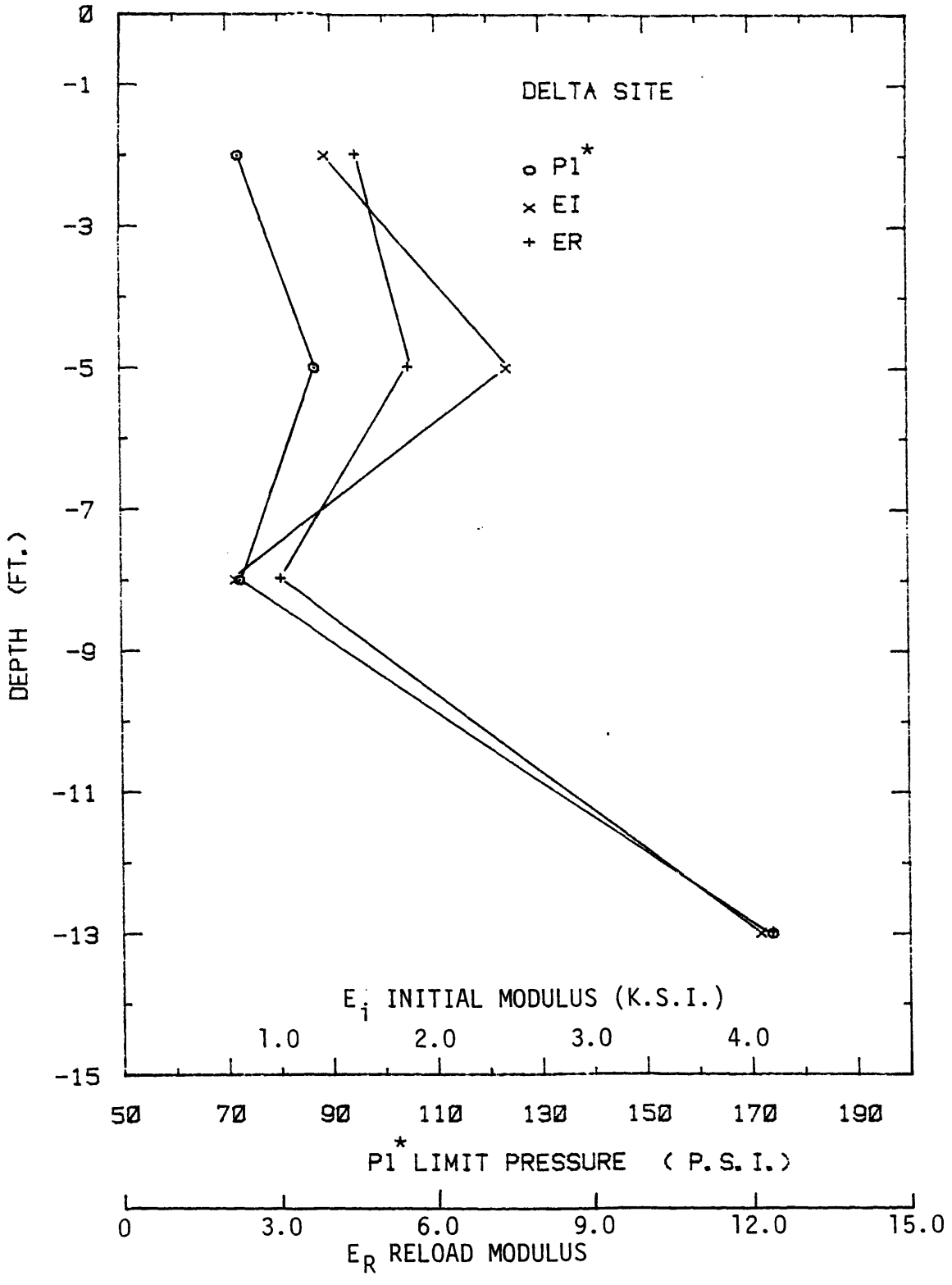

FIG.129 - Pressuremeter Test Results at Delta Site

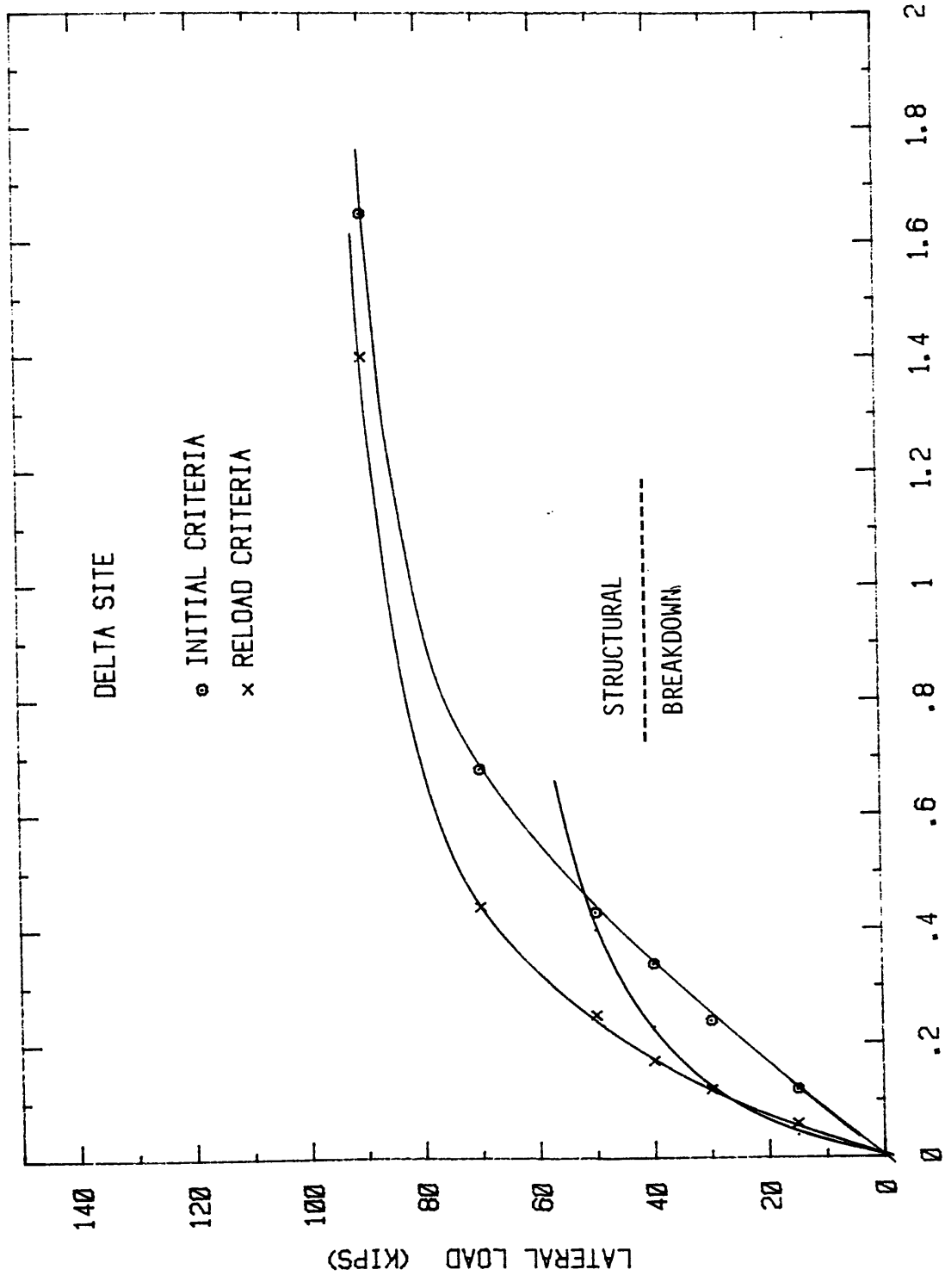

FIG. 130 - Delta Site: Comparison of Groundline Deflection

information is available with respect to the structural condition of the shaft after testing.

At the Caliente site a 28.0 in. (711 mm) diameter, 11.0 ft (3.35 m) deep, reinforced concrete shaft was tested in a free head restraint condition. The soil conditions consisted of uniform dense silty sand, ϕ 48°, with a weak cemented 1.0 ft (610 m) layer at 4.0 ft (1.22 m) deep. Flexural stiffness of the shaft, by calculation, was 5.1×10^6 lb.in.^{2} (1.45×10^5 kN.M^2).

Pressuremeter tests were conducted in two boreholes with the TEXAM unit and the variation of limit pressures, initial modulus and reload modulus is given in Fig. 131. The variation of soil stiffness highlights the weakly cemented layer at 4.0 ft (1.22 m) deep. Beyond this depth stiffness continues to increase. The two highest quality shallow tests, at 2.0 ft (610 mm) and 7.5 ft (2.36 m) deep, are given later on in Appendix IV. The 2.0 ft (610 mm) test was performed in a borehole drilled with 2.375 in. (60 mm) diameter bit with air circulation. The 7.5 ft (2.36 m) test borehole was achieved with open 1.675 in. (43 mm) diameter drill rods with full mud circulation.

The predicted lateral load behavior for pier number 4 is shown on Fig. 132 together with the observed behavior. The initial criteria and reload criteria are both in poor agreement with the field result. The degree of nonlinearity evident in the governing pressuremeter curves (and hence the resulting P-y curve) give an almost linear response in the lateral load behavior. For reasons not stated in the load test report, the test was aborted at a radial movement of 1.4%.

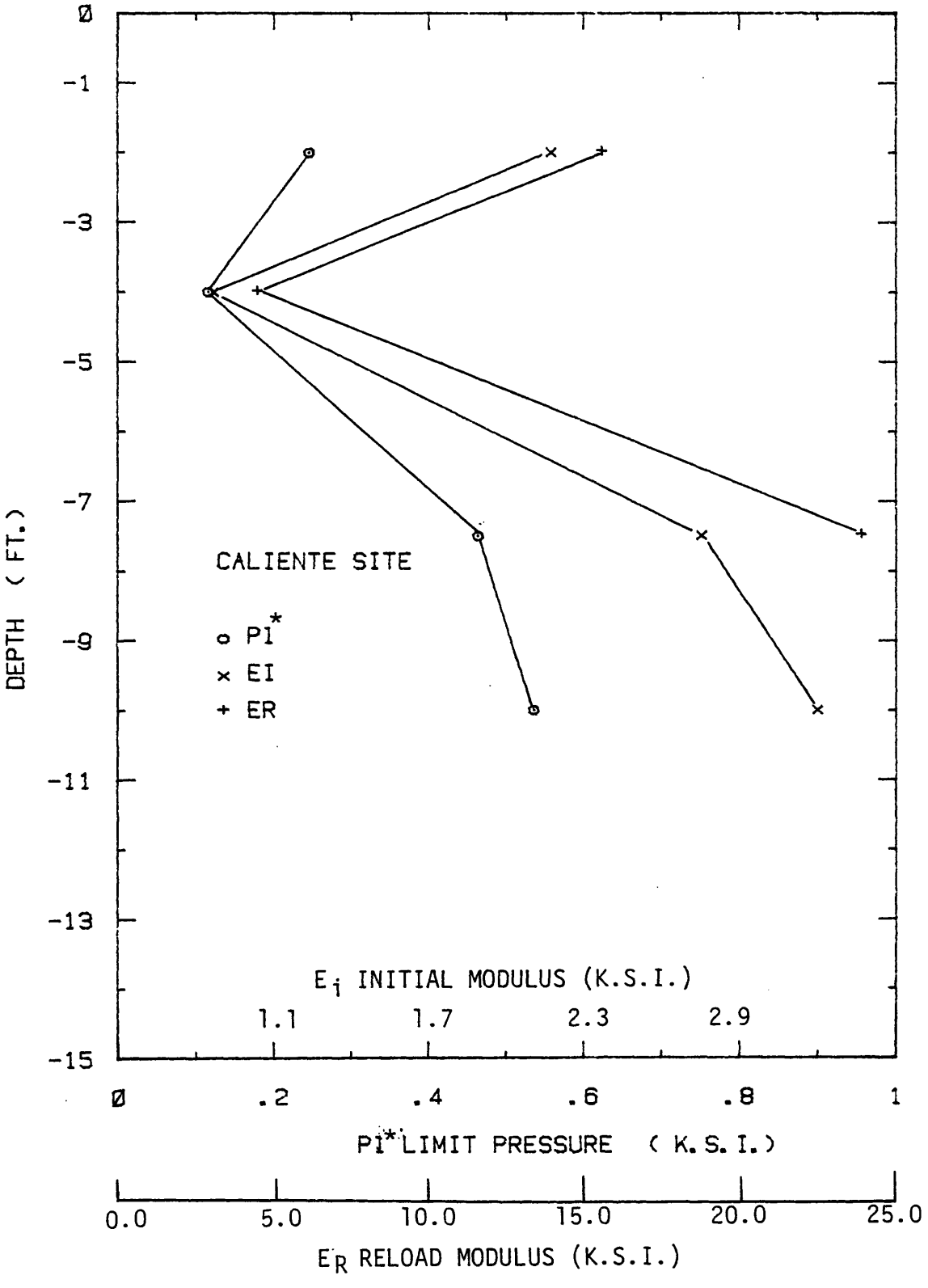

FIG. 131 - Pressuremeter Test Results at Caliente Site

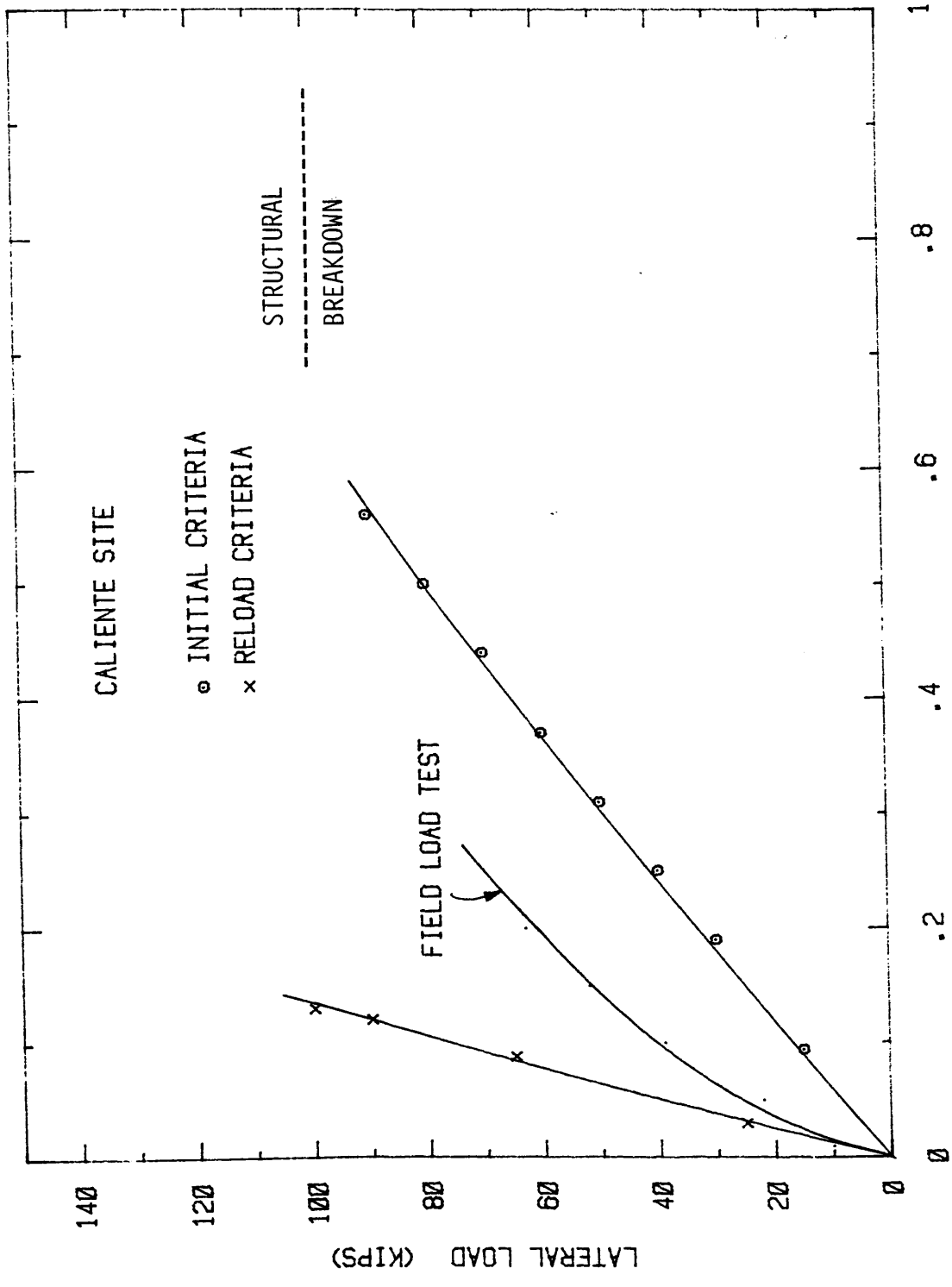

FIG. 132 - Caliente Site: Comparison of Groundline Deflection

At the Alamo site a 26 in. (660 mm) diameter, 11.0 ft (3.35 m) deep reinforced concrete shaft was load tested in a free head condition. The soil was a low plasticity uniform silty sandy clay with an average undrained shear strength 7.0 lb./n.^{2} (48.0 kPa). Flexural stiffness, by calculation, is approximately 5.0 x 10^{10} lb.in.^{2} (1.45 x 10^5 kN.M^2) and the pile is subject to rigid behavior.

Pressuremeter tests were conducted between 2.0 ft (610 mm) and 13.0 ft (3.96 m) with a TEXAM unit. The summary of limit pressures, initial modulus and reload modulus is given on Fig. 133. This shows a relatively uniform increase with depth in soil stiffness characteristics of a predominately granular material. All tests were conducted in a single borehole drilled with 2.375 in. (60 mm) diameter auger bit with air circulation only.

Test results at 2.0 ft (610 mm), 5.0 ft (1.52 m) and 8.5 ft (2.6 m) are given in Appendix IV.

The lateral load versus head deflections prediction for pier number 4 is plotted on Fig. 134 together with the measured field response. Both initial and reload criteria are shown to be increasingly unconservative with increasing defletion. However the small strain load deflection modulus from the reload criteria is a good approximation.

In summary, for the three sites , Delta, Caliente and Alamo there is no reported information concerning the structural integrity of the piers, after the load test. If an approximate yield moment of 1.26 x 10^6 lb.in. (2.2 x 10^5 kN.M) is taken, then the lateral load at which structural breakdown occurs, can be estimated. This is indicated

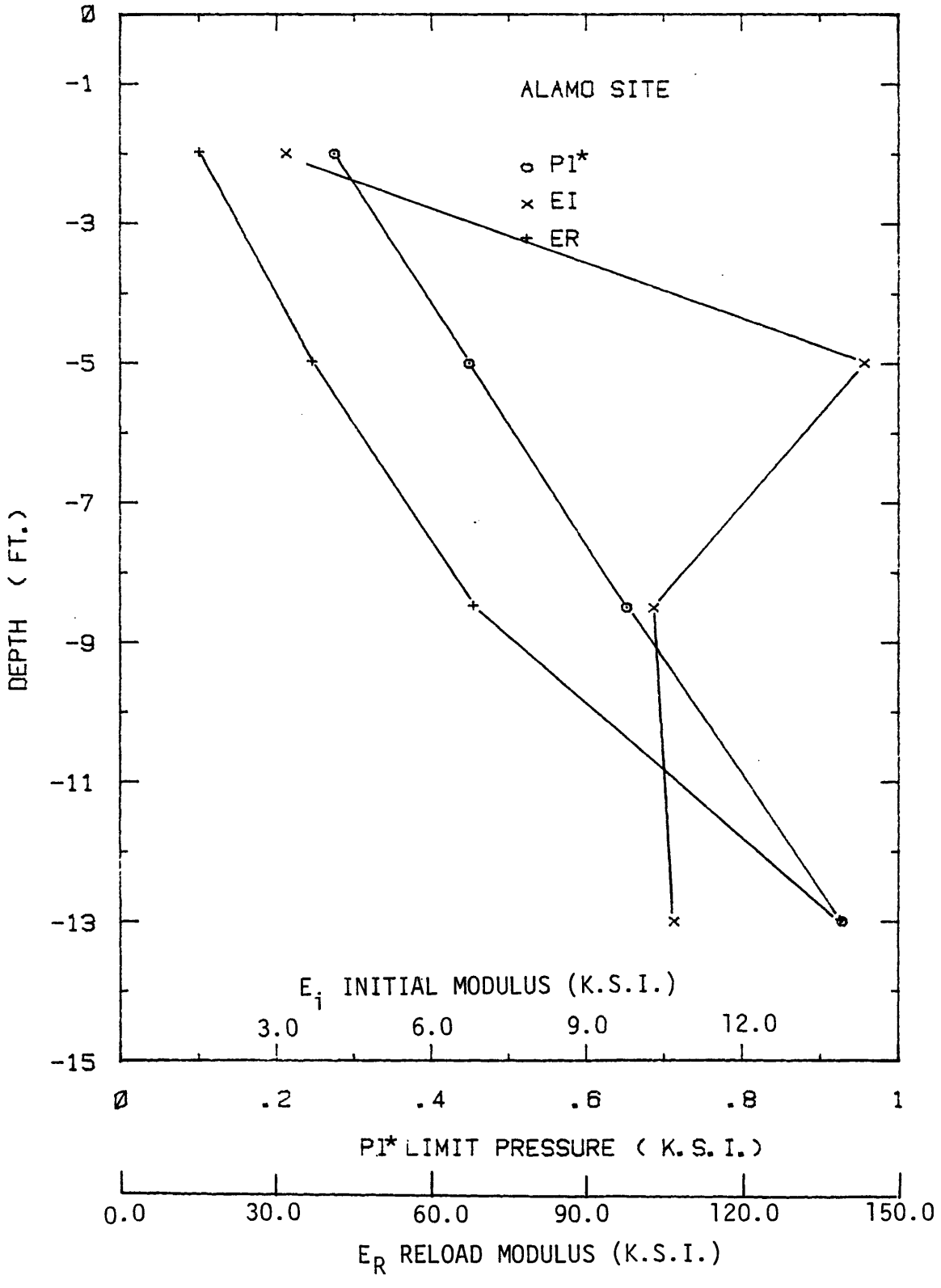

FIG. 133 - Pressuremeter Test Results for Alamo Site

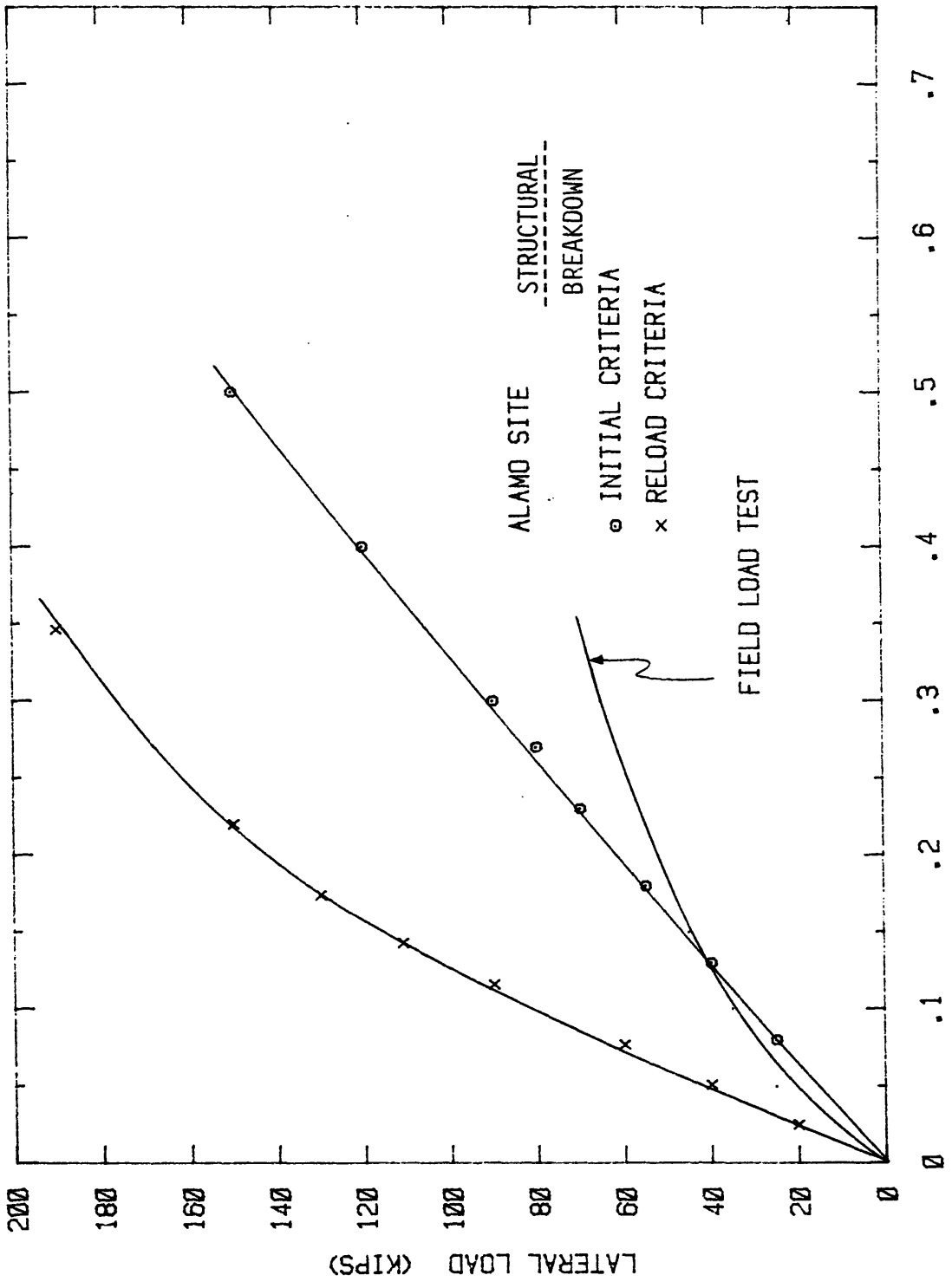

FIG. 134 - Alamo Site: Comparison of Groundline Deflection

on Fig. 130 (p. 262), Fig. 132 (p. 265)and Fig. 134 (p. 268) for Delta, Caliente and Alamo sites respectively.

Summary

The predicted results of a total of fourteen laterally loaded piles, at nine different sites, are given in a wide variety of material and soil conditions. These piles include a range of diameters from 6 in. (150 mm) to 3.0 ft (914 mm) and include tubular steel and reinforced concrete construction as well as rigid to flexible pile behavior.

At the sites reprsenting the most complete and comprehensive lateral load tests, presented in the first part of the section, the prediction by the reload criteria is generally superior to the initial criterion. For these sites, at which a 'measured' P-y curve is available, the mobilized shear stress, as a result of applying Eq. 78 and subsequent differentiation,is less erratic and closer to the measured shear strength.

This is in agreement with the comments made previously reload cycle of a prebored pressuremeter test is a good approximation to an undisturbed, selfboring, derived shear stress-circumferential strain curve. At small displacements the contribution of the friction curve, F, forms the majority of the mobilized soil reaction, P.

At the Manor site, at which both predictions are unconservative, the effects of softening by water ponding is difficult to evaluate.

Attempts to correlate moduli and limit pressures to undrained shear strength require better measured shear strengths than are available. Structural breakdown of the reinforced concrete pile at the Houston site is suspected where both criteria were unconservative.

Frequently, the pressuremeter field drilling technique must be continuously monitored, by evaluating the test quality, hole size, etc, and modified if required. The surface layers are shown to control the lateral load behavior and the poor information available at the Manor and Baytown sites gives less confidence in the output. For soft N.C. clays with low limit pressures, and shallow heavily O.C. clay, evaluation of the at rest horizontal earth pressure is of paramount importance for predicting large deformation.

For six of the nine sites, the lateral load test mudline datum and the existing ground level are different. Evaluation of critical depth effects based on Fig. 57 (p.150), for sand, and Fig. 58 (p.151) for clay, are inappropriate. The net effects for the pressuremeter and for the pile have been evaluated independently for these piles. At Sabine, Lake Austin, Mustang Island and Manor sites, the exact location of the original pile load test was difficult to establish accurately but it is believed the pressuremeter borehole is in representative soil conditions. In all investigations, with the exceptions of Lackland and LADWP study, a number of years had passed since the lateral load test. The effect of time upon the soil conditions is impossible to establish without a thorough site investigation, but is believed to be small. The variation of soil stiffness, however, is in general agreement with the results of the original site investigation.

No account is made by COM622 in modeling the structural conditions of the pile. For the piles at Houston, Texas A&M, Lackland and, to a lesser degree of certainty, the LADWP study, there is evidence that serious structural decay commenced through excess flexural stresses. The behavior of a pile under lateral load is a classical soil-structure interaction phenomenom but only the effects of increasing load by the nonlinearity upon the soil response, is made. To model the complete problem the structural behavior of the pile should be incorporated. This accounts for some of the poor comparisons evident at these sites. It also implies that the effects of structural behavior are present within a 'measured' P-y curve, but are impossible to separate.

EXAMINATION OF REPORTED CASE HISTORIES

Lock and Dam 26

From the extensive series of lateral load tests conducted at the proposed site of Lock and Dam 26, conducted during November 1978 (103), on the Mississippi river, test references T3 and T4 have been detailed in previously The 'H' section pile T3 and pipe pile T4 were driven 50.0 ft (15.2 m) into fine to coarse sand and gravels of glacial outwash origin. Both piles had diameter, or projected width, of 14.0 in. (355.0 mm) and were loaded in a free head condition. Pressuremeter tests are reported, using a BX size probe, and only a single initial loading cycle is available. P-y curves, developed from the procedure detailed previously are made from the initial criterion.

The lateral load versus groundline deflection predictions, and the measured field results, are shown on Fig. 135 and Fig.136 for piles T3 and T4 respectively. For both piles, the working range prediction is generally satisfactory, being slightly conservative for the pipe pile and increasingly unconservative for the square 'H' pile. In the ultimate range of behavior the initial criteria predictions are unconservative. In general the predictions for the circular pile section are satisfactory whereas no laboratory or field information is available to confirm pile shape factors on square piles.

The measured field response between the piles show the square pile, of the same projected width as the circular pile, had a 40%

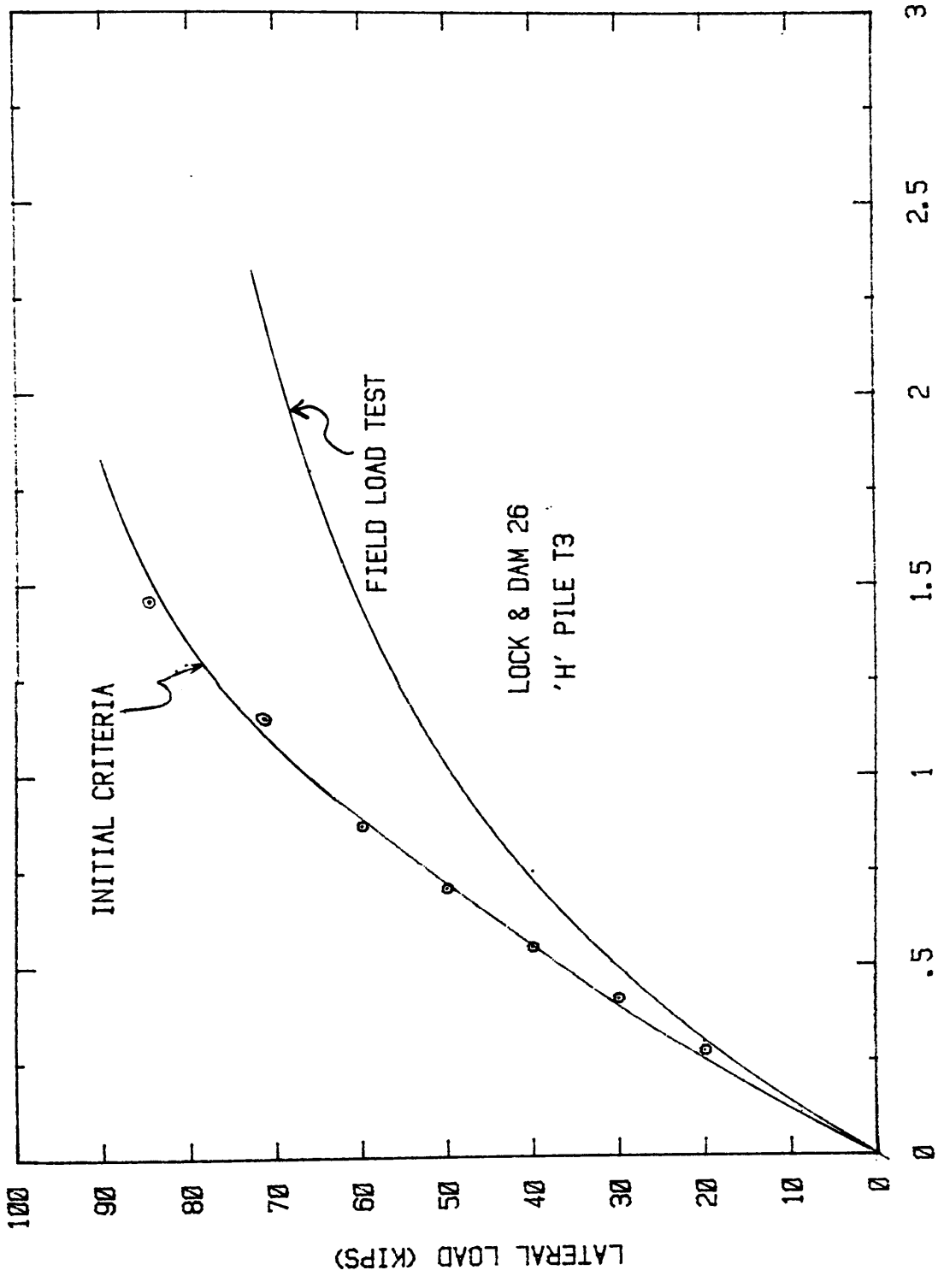

FIG. 135 - Lock and Dam 26, Pile T3: Comparison of Groundline Deflection

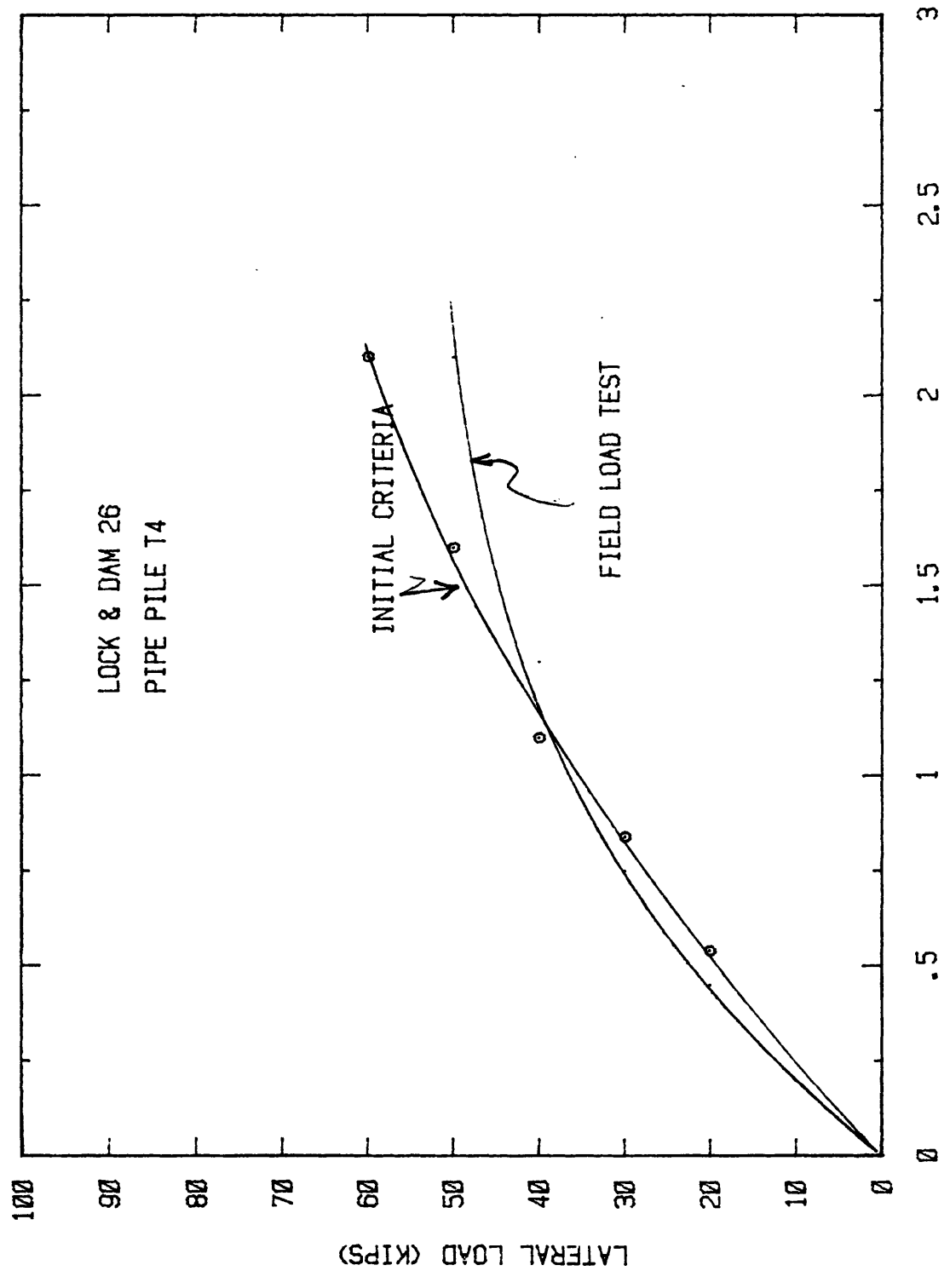

FIG. 136 - Lock and Dam 26, Pile T4: Comparison of Groundline Deflection

increase in load bearing capacity. Application of the existing criteria, discussed in previous Sections would result in equal P-y curves for both piles.

Electric Power Research Institute (E.P.R.I.) Study

An extensive series of load tests were performed by GAI Consultants, (34), on behalf of the Electric Power Research Institute (E.P.R.I.) to improve design procedures for short, rigid, concrete piers supporting power line towers. The dimensions of nine of the tested piers and the sponsoring companies are shown in Table 6.

The loads were applied to the piers from a loading cable, inclined 22^{o} to the horizontal, attached to the top of a 80.0 ft (24.3 m) steel pole bolted to the foundation pier. From this arrangement the applied loads on the pier are vertical, horizontal and moments at the groundline.

Pressuremeter tests were conducted during the investigation, at each site, with an NX size probe. No reload cycles were performed.

The reported pier sizes, and their rigid behavior, are very different from the instrumented piles detailed previously which were used to develop the existing State of the Art criteria. To compare the pressuremeter P-y criteria with the existing techniques, both methods are used to solve for the load versus deflection behavior of each pier. The pressuremeter P-y predictions are from the initial criterion and from the existing available techniques the predictions are termed existing criteria.

Table 6 - Details of Piers from the E.P.R.I. Study

SPONSOR	DIAMETER (feet)	DEPTH (feet)	FLEXURAL STIFFNESS (pounds square inch)
Test Pier 1	4.5	14.0	1.5
Virginia Electric Power Company	4.5	11.5	1.4
Allegheny Power Systems	4.5	16.0	1.8
Jersey Power and Light	5.0	21.0	2.2
Carolina Power and Light	4.5	14.9	1.5
Oklahoma Gas and Electric	5.0	12.5	2.6
Southern California Edison Company	5.0	20.3	2.6
Utah Power and Light Company	5.0	20.0	2.6
Iowa Public Service Company	4.5	15.0	1.5

Test Pier 1

The drilled reinforced concrete shaft was placed in the dry, in predominately cohesive soil underlain by granualr material. The ground deflection versus applied groundline bending moment is shown in Fig. 137.

Virginia Electric Power Company

The drilled reinforced concrete shaft was placed in the dry in cohesive material with rock at the base. The groundline deflection versus applied groundline bending moment is shown in Fig. 138.

Allegheny Power System

A drilled reinforced concrete shaft placed in wet conditions in stiff clay. The ground deflection versus applied groundline bending moment is shown in Fig. 139.

Jersey Central Power and Light

The drilled reinforced concrete shaft was placed in medium sand, with the use of casing, in the dry. The ground deflection versus applied groundline bending moment is shown on Fig. 140.

Carolina Power and Light Company

The drilled reinforced concrete shaft was placed with the use of drilling mud in silty sand underlain by clayey silt. The ground deflection versus applied groundline moment is shown on Fig. 141.

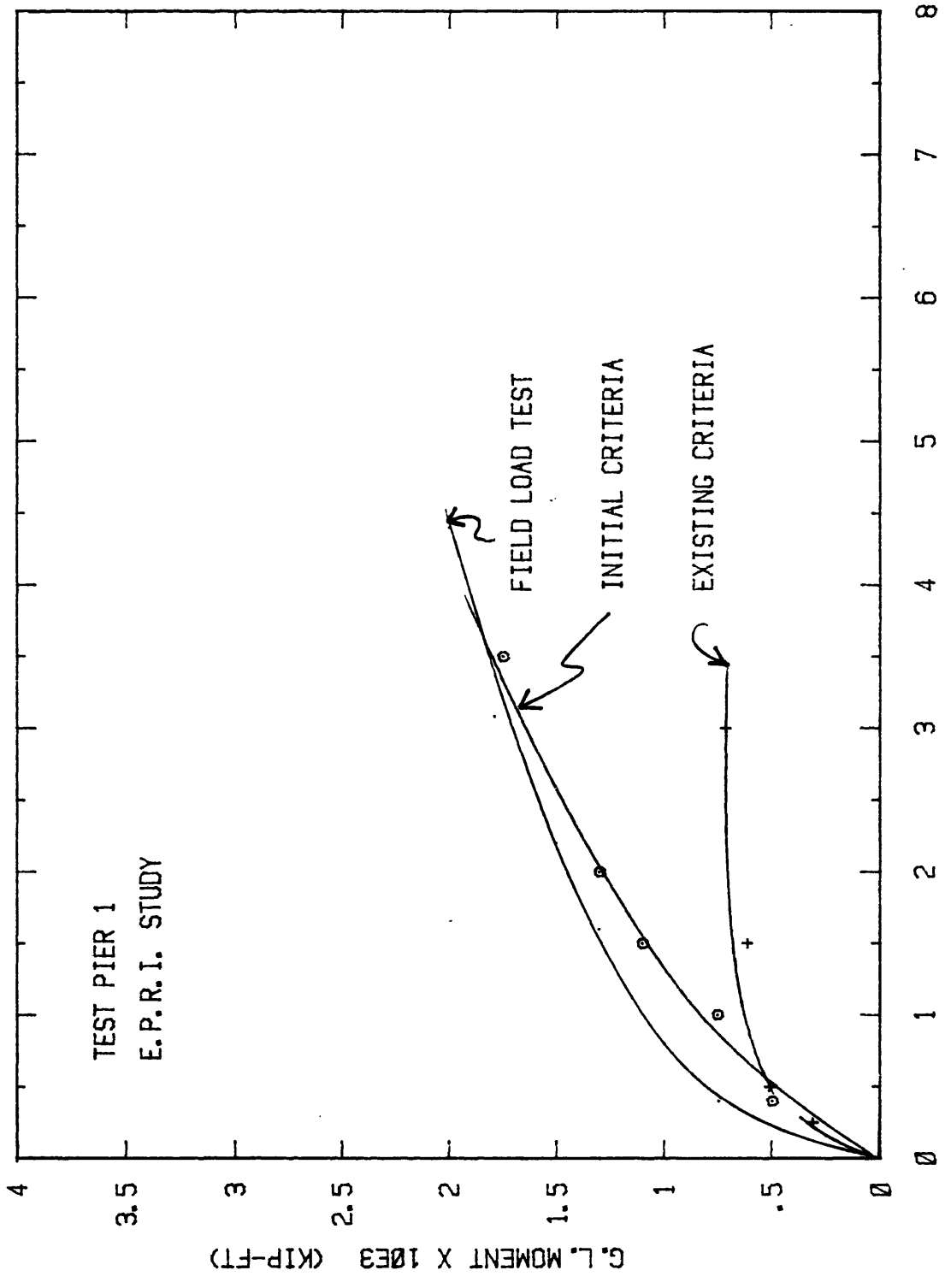

FIG. 137 - Test Pier 1: Comparison of Groundline Deflection

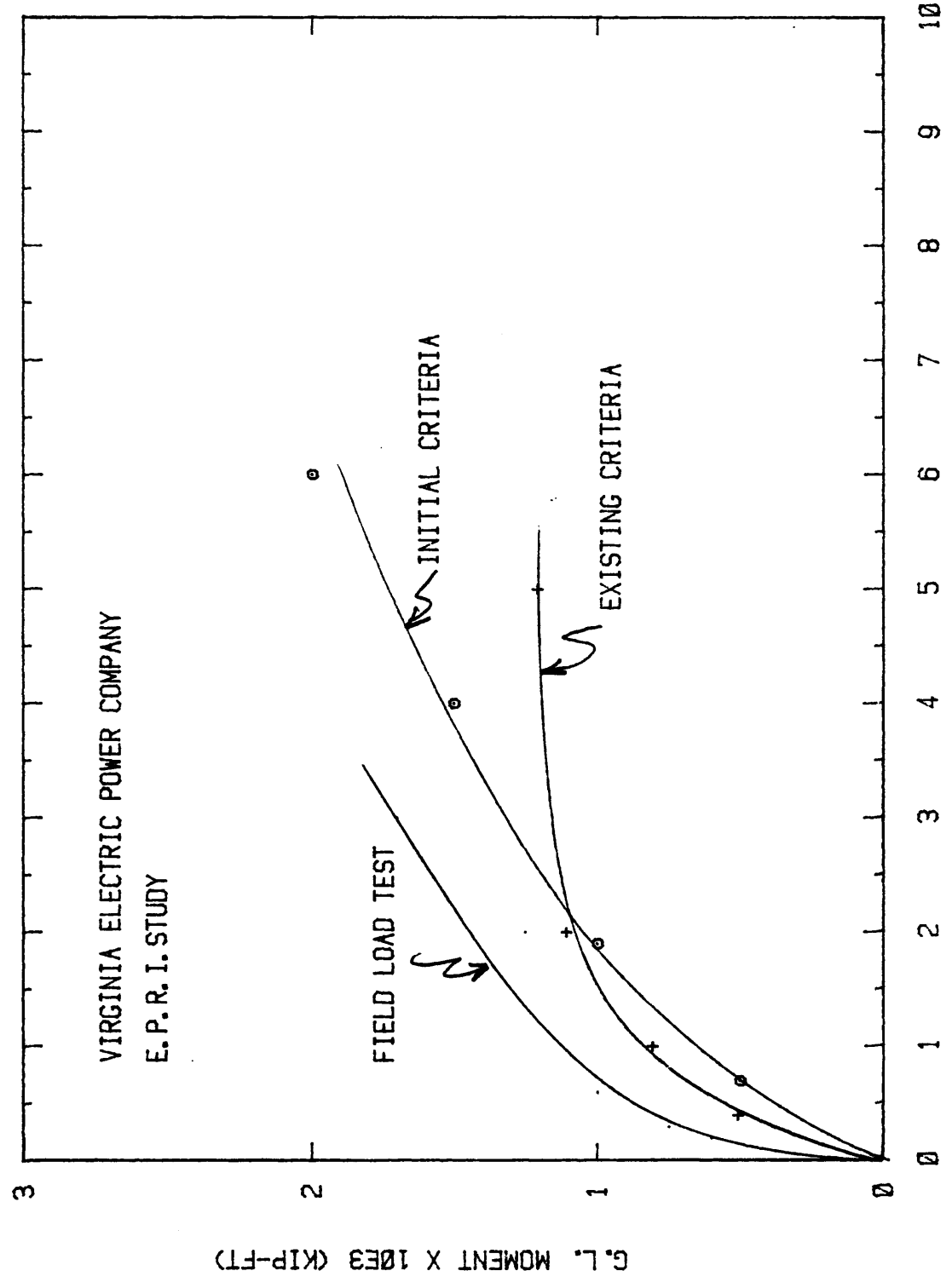

FIG. 138 - Virginia Electric Power Company Pier: Comparison of Groundline Deflection

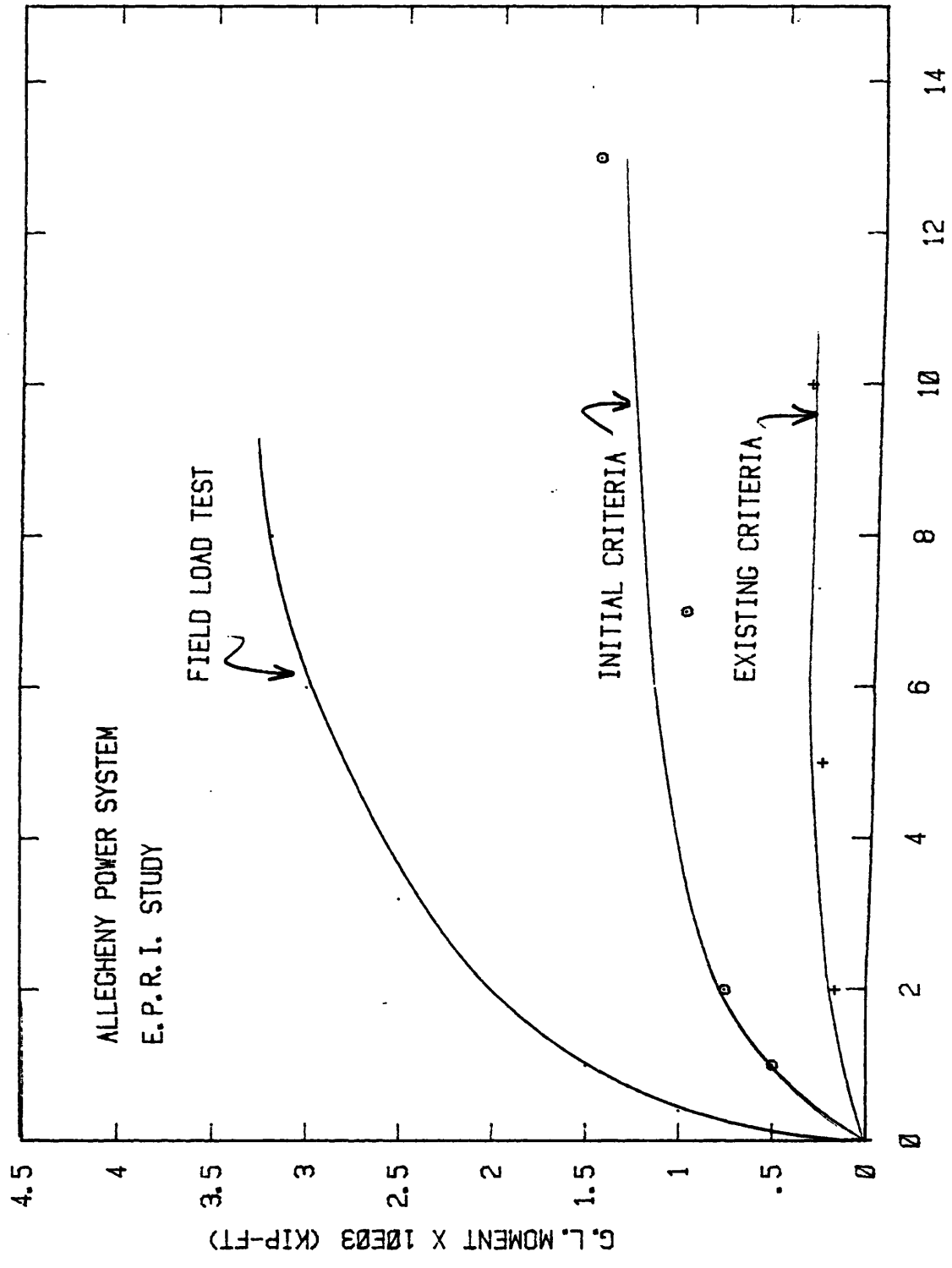

FIG. 139 - Allegheny Power System: Comparison of Groundline Deflection

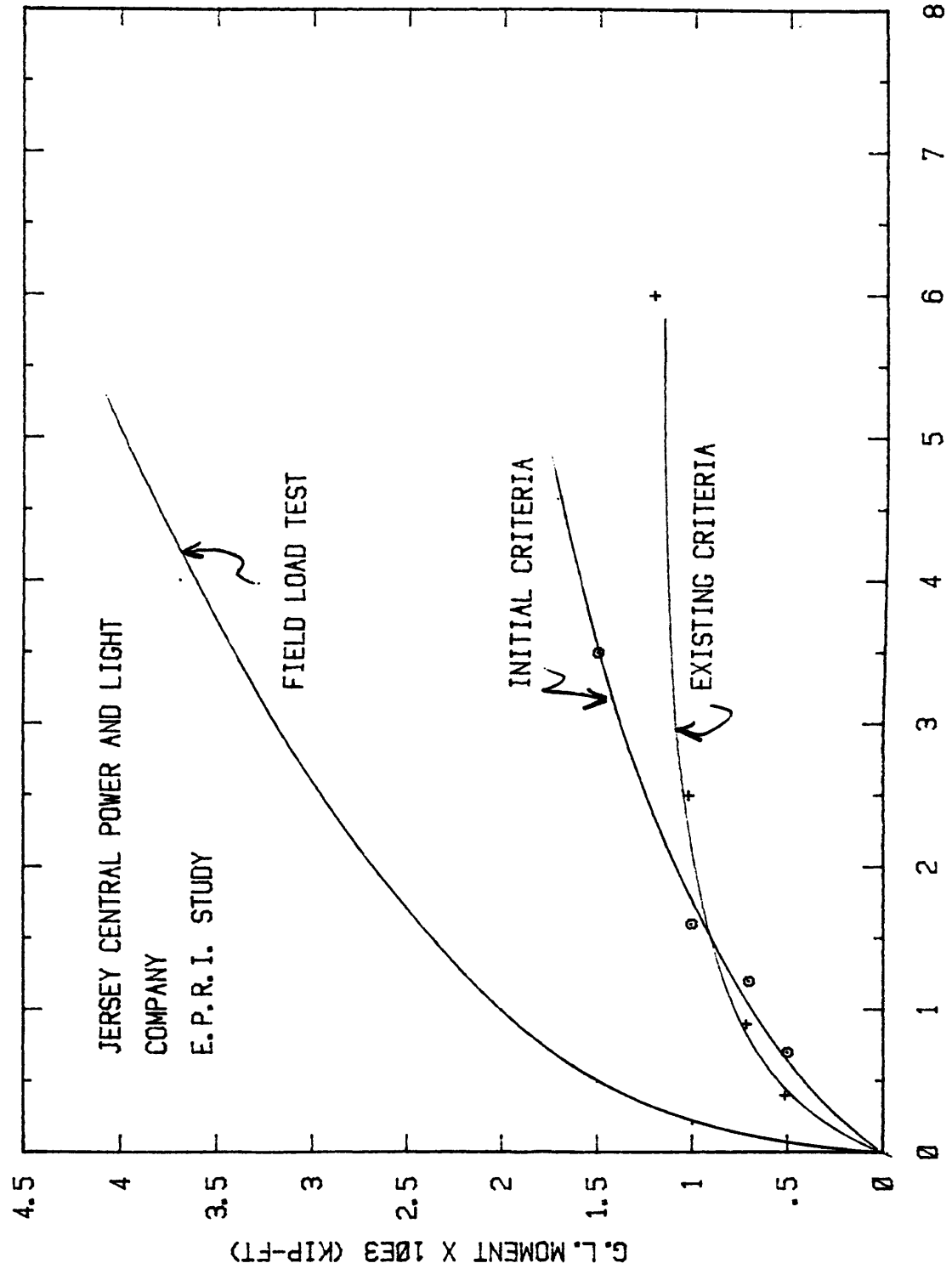

FIG. 140 - Jersey Central Power and Light: Comparison of Groundline Deflection

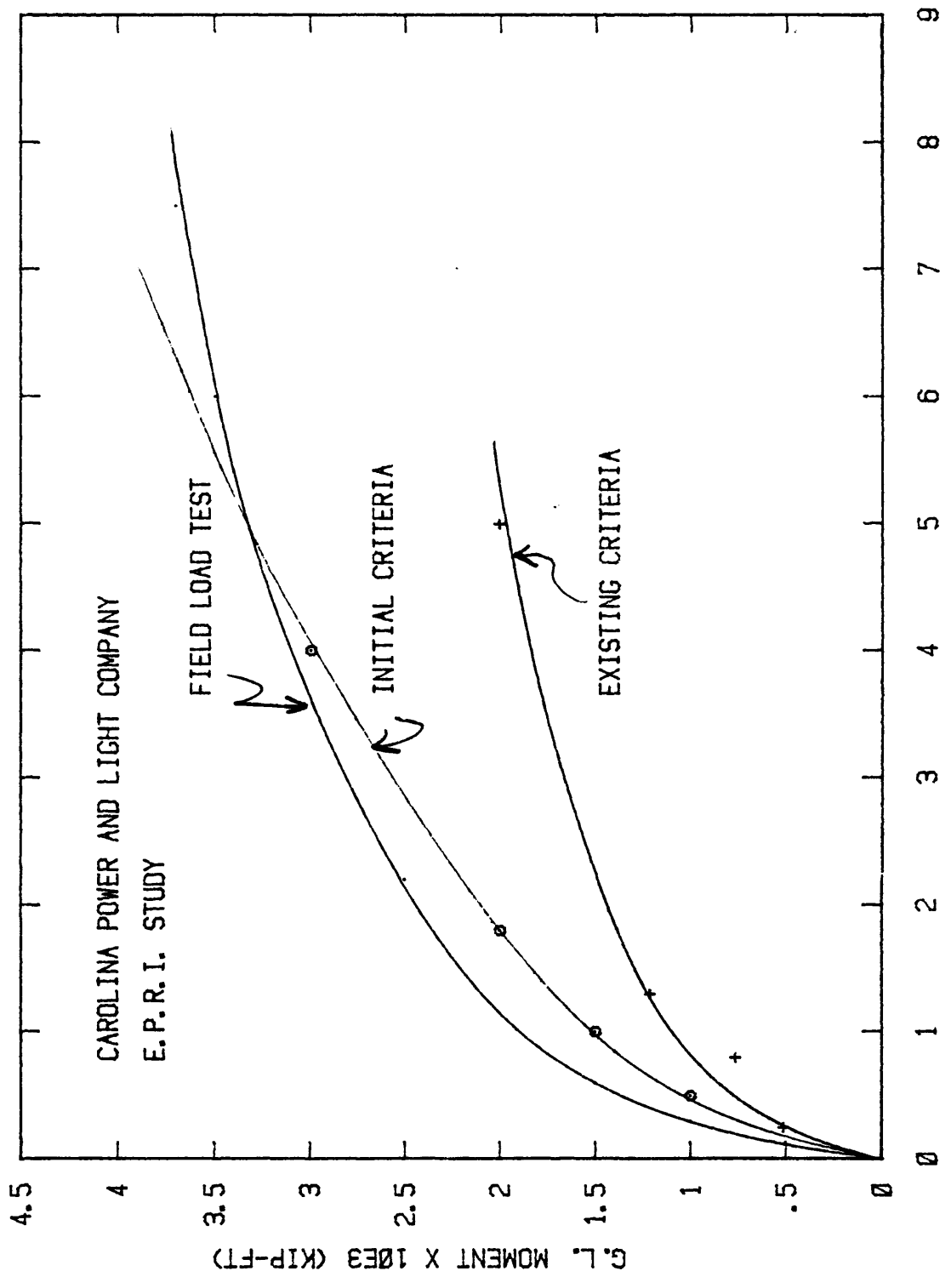

FIG. 141 - Carolina Power and Light Company: Comparison of Groundline Deflection

Oklahoma Gas and Electric Company

The drilled reinforced concrete shaft was placed dry, into clay underlain by rock. The groundline deflection versus applied groundline moment is shown on Fig.142.

Southern California Edison Company

The drilled reinforced concrete shaft was placed, with the use of casing, into medium dense sand. The groundline deflection versus applied groundline movement is shown on Fig. 143.

Utah Power and Light Company

The drilled reinforced concrete shaft was placed, with the assistance of drilling mud, into a medium clay underlain by sand. The ground deflection versus applied groundline moment is shown on Fig. 144.

Iowa Public Service Company

The reinforced concrete shaft was placed dry, into a clayey silt underlain by a silty clay. The ground deflection versus applied groundline moment is shown on Fig. 145.

Summary

In general, the predictions from the Initial Criteria are in reasonable agreement with the measured field test results, but lack the nonlinearity evident in the field test. Predictions in the working range are all conservative and with the single exception of the

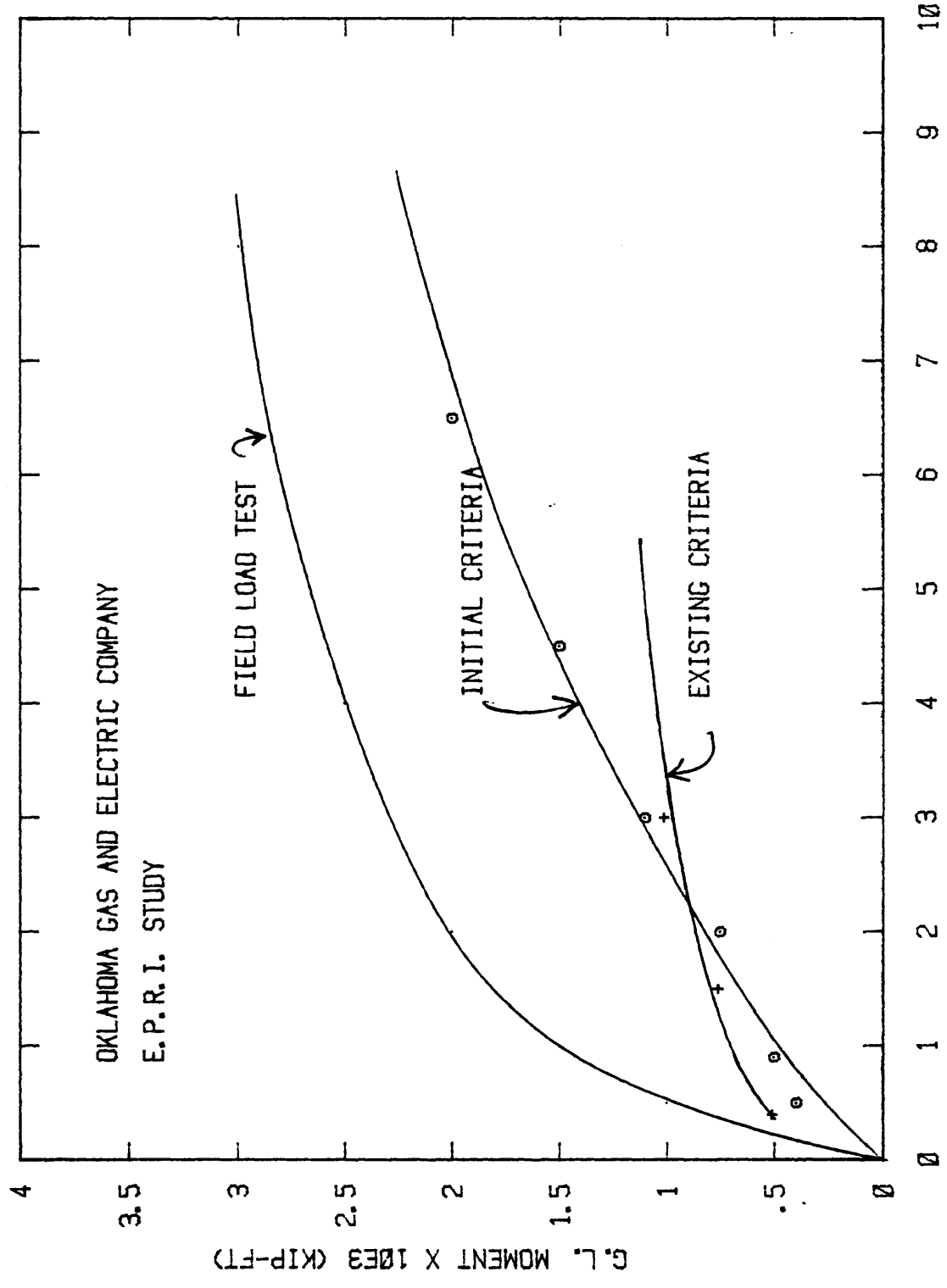

FIG. 142 - Oklahoma Gas and Electric Company: Comparison of Groundline Deflection

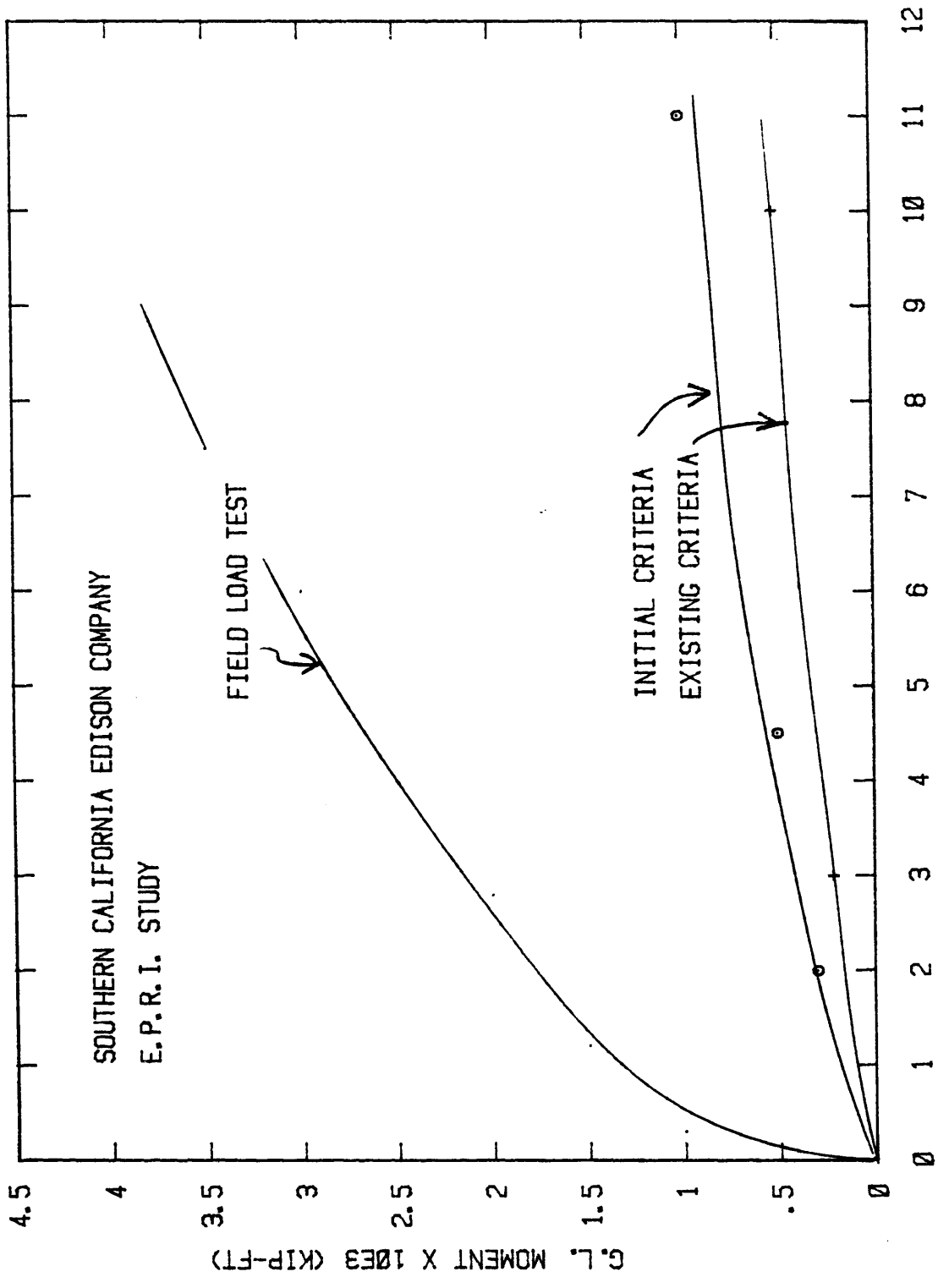

FIG. 143 - Southern California Edison Company: Comparison of Groundline Deflection

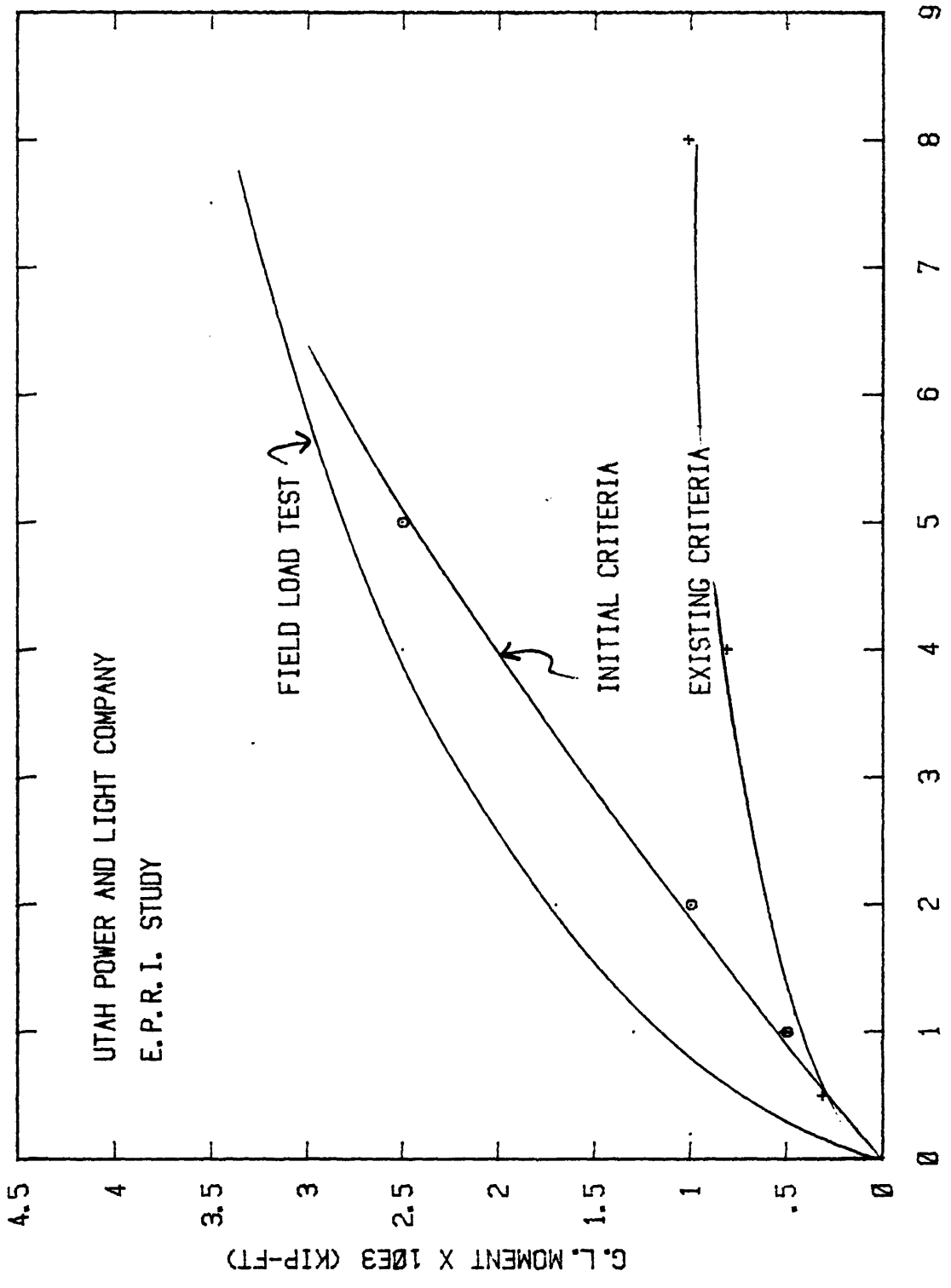

FIG. 144 - Utah Power and Light Company: Comparison of Groundline Deflection

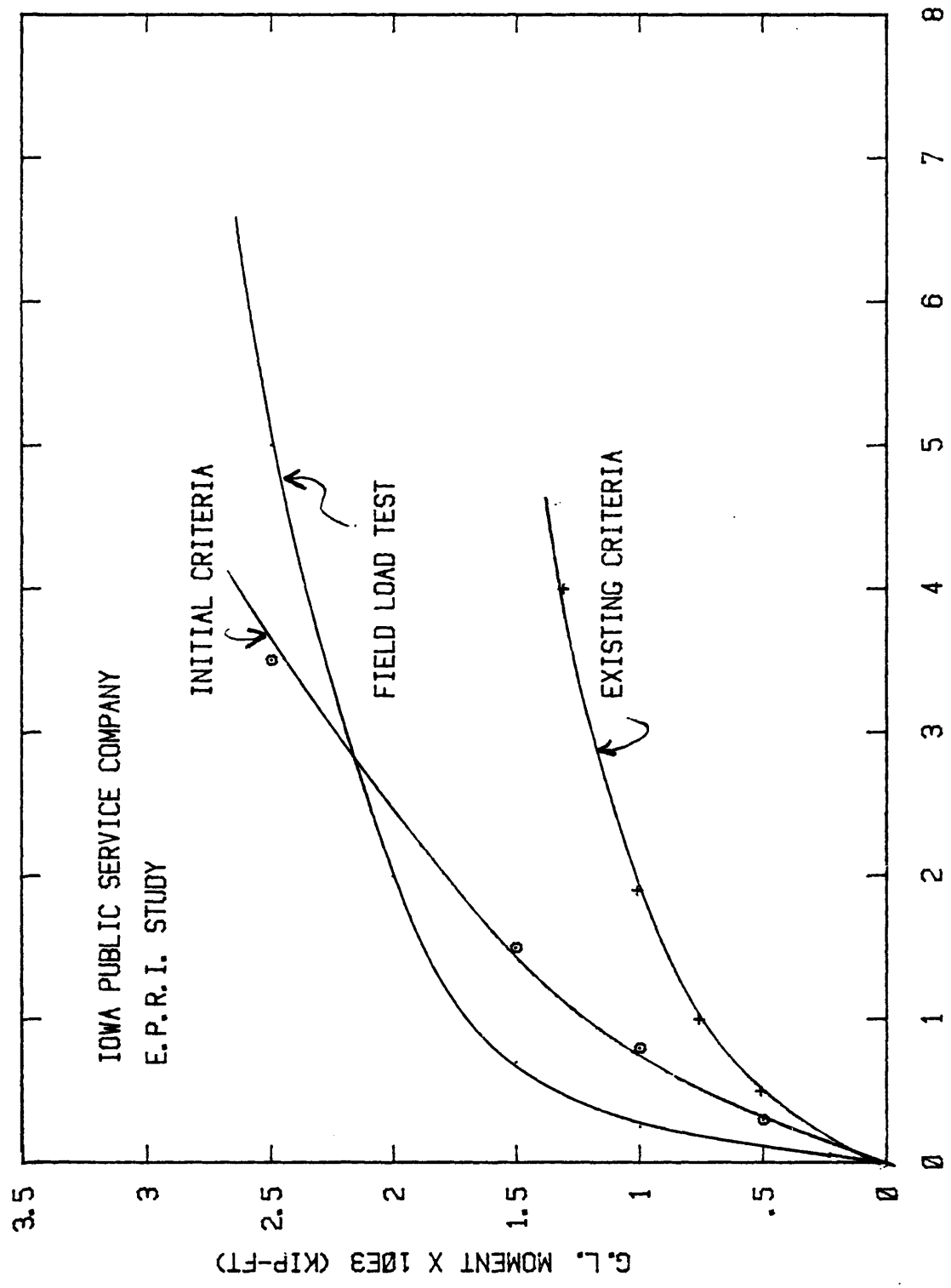

FIG. 145 - Iowa Public Service Company: Comparison of Groundline Deflection

Iowa pier conservative for the ultimate load range also. It is evident that the closest predictions are achieved in cohesive materials including the silty sands. The predictions from the Southern California test, in sand, and the Allegheny and Oklahoma piers, with bases embedded in rock, are very poor. The lack of a representative P-y curve for the pier base in rock may account for some of the difference.

The importdance of a representative shear model was emphasized in the previous section and it was found that shear derived from a reload criterion is superior to the initial criterion. The quality of the pressuremeter testing is not known and hence, disturbance effects cannot be quantified. However, based on the field studies in the previous section the shear model is expected to be improved from a reload cycle and the lack of nonlinearity in Figs. 137-145 improved.

It should be stated that these stiff rigid piers are of smaller depth/diameter ratios than is considered appropriate for solution by the finite difference scheme. Significant contributions from rotational restraint is mobilized in rigid pier behavior and the finite difference scheme approximation, contained in COM622, has no rotational soil springs.

Conparison between the field load test result and the predictions from the existing criterion highlights the inadequacy in accomodating the diameter effects. In general, the small strain prediction, up to 2% from the existing criterion is in better agreement with the field test than the initial criterion prediction. However, the ultimate range is very poor, with predictions less than 40% of the measured field moment capacity.

RECOMMENDED DESIGN PROCEDURE

Performance and Intrepretation of the Pressuremeter Test

Development of a P-y curve is shown to be sensitive to the quality of the pressuremeter test. It is imperative that the highest quality of testing be attained with well maintained, clean and reliable equipment. Particular attention should be paid to shallow pressurement tests which provide the critical, controlling, lateral load P-y curves. Quality is more important than quantity.

The prebored test is practical in all soil conditions where a borehole can be satisfactory made. The following should be observed:

1) The equipment selected to drill the hole should be chosen based on the knowledge of ground conditions prior to commencement of testing.
2) Full backup drill bit types, and sizes, should be available at all times.
3) It is advisable to drill at least one advance trial borehole and evaluate the drilling technique by checking hole size, with the probe, during early inflation.
4) Drilling should begin with a technique that is expected to give a slightly undersized hole. The technique can then be refined to give the correct hole size at that depth by reaming out. The final technique selected in the trial hole should be adopted for the test borehole.
5) Continuous monitoring of borehole size and condition should

take place before each test is performed.

6) The borehole should be advanced to the next proposed pressuremeter depth in separate increments. The time saving step of a complete single borehole before pressuremeter testing should be avoided because of increased disturbance to the hole wall.

7) If possible, either a hand augered borehole, in the dry, or with drilling fluid should be employed. A power driven auger bit with mud circulation, is acceptable but extreme care must be exercised. The lowest mud pressure required to bring up cuttings at the slowest possible rotation and penetration possible should be used.

8) A hollow pressuremeter probe is recommended to allow the passage of the borehold fluid upon insertion.

By developing a P-y curve from a highly disturbed test, the calculated mobilized shear stress is seriously overestimated. In consequence, the P-y curve will overestimate the mobilized soil reaction at a deflection corresponding to the peak shear strength and cause unconservative estimates of the pile response to be predicted. If interpretation is required for some pressuremeter test curves which are incomplete, then correlations between limit pressures and pressuremeter moduli may be used based on a correlation in the same material at that site.

To obtain accurate reload data the point of unloading for the cycle should commence at the end of the pseudo-linear response range. This point corresponds to the onset of plastic behavior in the elements

around the probe immediately adjacent to the borehole . Unloading should continue until the pressure against the borehole wall is approximately at the initial state of horizontal stress in the ground. The reload cycle then commences until the limit pressure is reached. For materials of low limit pressures, compared to the membrane stiffness, the membrane stiffness correction should also include an unload-reload cycle, because most membranes exhibit hysteresis.

To assist in test interpretation and design, a full site investigation is also recommended to supplement the information provided by the pressuremeter tests. In evaluating the initial state of horizontal stress in the ground, it is not advisable to use the commencement of the linear range from a prebored pressuremeter tests. This point is highly sensitive to the degree of disturbance at the borehole wall.

If only poor quality, highly disturbed pressuremeter test results are available, an attempt may be made to quantify the degree of disturbance. It is accepted that the initial pressuremeter modulus is more sensitive to disturbance effects than is the limit pressure. Therefore, based on field and published data, a reduction in circumferential strain to achieve the correct modulus (from correlations) can be attempted. This reduction may also apply over the full range of probe expansion. By using this procedure a better approximation to the correct P-y curve can be made.

Derivation of the P-y curve

Based on previous discussion and move together with the field test P-y predictions cited earlier the shear stress-strain relationship should be developed from a reload cycle of a prebored test. This cycle is shown to better approximate an undisturbed test and generate shear strength values in good agreement with laboratory values. The reload cycle should be used for all piles, both driven and augered. In all cases the shear stress should be compared with the measured shear strength. For augered piles, or piles driven open ended which do not plug, the front reaction curve is developed from the initial cycle of a prebored test. For full displacement piles, it may be more appropriate to use the reload cycle for the front reaction curve.

From a corrected pressuremeter test curve the recommended procedure to be followed in deriving the pile P-y curve, at the same depth, z, is as follows:

1) Calculate the initial total horizontal stress in the ground at the test depth. Perform axis translation of both pressure, p, and volume change, ΔV, axis, to form a revised origin. See Fig. 36 (p.96) and Fig. 146 .

and p_{OH} = horizontal earth pressure at rest

ΔV_o = increase in cavity to reach p_{OH}

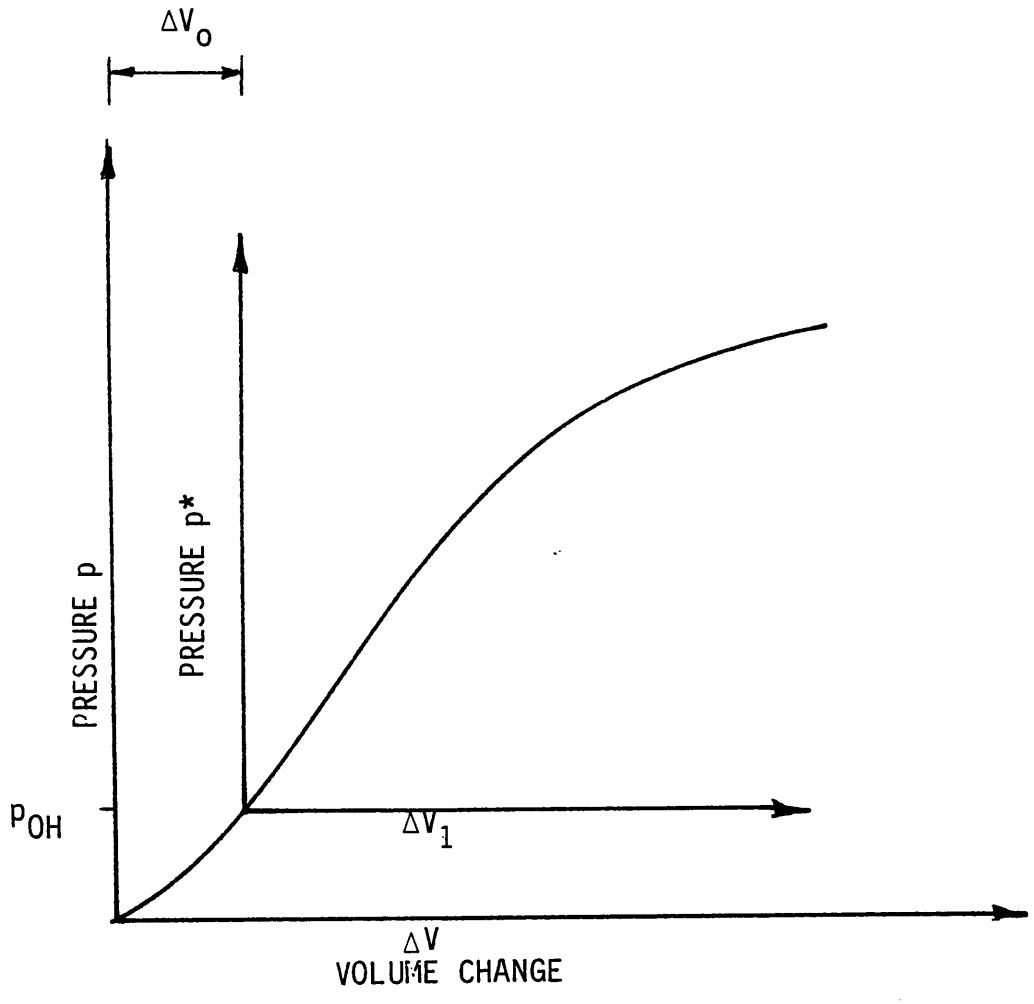

FIG. 146 - Interpretation of the Corrected Pressuremeter Curve

and recalling Eq. 89

$$p^* = p - p_{OH} \quad \text{(89)}$$

= net pressuremeter pressure

where p = pressuremeter pressure,

therefore, the initial size of the soil cavity is given by

$$V_1 = V_o + \Delta V_o \quad \text{(118)}$$

The net increase of the cavity during subsequent inflation, ΔV_1, is

$$\Delta V_1 = \Delta V - \Delta V_o \quad \text{(119)}$$

which mobilizes net pressures in excess of 'at rest' pressures, and also mobilizes shear stresses.

2) The front pressure reaction is obtained from integration of the in-line components around the pile circumference. The prebored pressuremeter test measures the mobilized front pressure at equal pile and pressuremeter radial movements. Therefore, recalling Eq. 90

$$Q = p^* \times SQ \times D \quad \text{(90)}$$

where SQ = pile shape factor for Q

= 0.75 circular piles

= 1.0 square piles

D = pile diameter or projected width

at a pile deflection, y, given by

$$y = \frac{\Delta R}{R_1} R \quad \ldots\ldots\ldots\ldots\ldots\ldots\ldots\ldots\ldots\ldots \quad (120)$$

and $$\frac{\Delta R}{R_1} = \frac{\Delta V_1}{2V_1} \quad \ldots\ldots\ldots\ldots\ldots\ldots\ldots\ldots\ldots\ldots \quad (121)$$

where R_1 = radius of soil cavity at volume V_1,

ΔR = increase in soil cavity radius from volume V_1,

and R = pile radius.

3) Calculation of the mobilization of lateral friction curve, F, proceeds using the derivation of Baguelin et al. (10). It is recommended that the reload cycle of a prebored test be used and therefore calculation of the axis translation described under 1) is required.

Recalling Eq. 78

$$\tau = x(1+x)\frac{dp}{dx} \quad \ldots\ldots\ldots\ldots\ldots\ldots\ldots\ldots\ldots\ldots \quad (78)$$

where $$x = \frac{\Delta V_1}{V_1} \quad \ldots\ldots\ldots\ldots\ldots\ldots\ldots\ldots\ldots\ldots \quad (122)$$

= volumetric strain of the cavity

and τ = mobilized shear stress at a circumferential strain given by Eq. 120.

The total shear reaction is then given by Eq. 85.

$$F = \tau \times SF \times D \quad \ldots\ldots\ldots\ldots\ldots\ldots\ldots\ldots \quad (85)$$

where SF = pile shape factor for F

= 1.0 circular piles

= 2.0 square piles

at a pile deflection given by Eq. 120

$$y = \frac{\Delta R}{R_1} R \quad \ldots\ldots\ldots\ldots\ldots\ldots\ldots\ldots \quad (120)$$

4) Final assembly of the two component curves, front pressure, Q and side friction, F is given by Eq. 38

$$P = Q + F \quad \ldots\ldots\ldots\ldots\ldots\ldots\ldots\ldots \quad (38)$$

The completed P-y curve is then obtained, and applies only at the depth of the corresponding pressuremeter test. If the pressuremeter is below the depth influenced by the surface during the loading of the

pile then the P-y curve is correct. If the curve is within the pile critical depth, the procedure in the following subsection should be followed.

Evidence was discussed previously suggesting that the lateral shear resistance to the pile side is influenced by the pile installation procedure. It is not clear what effect is felt by the front pressure reaction. It may therefore, be appropriate to introduce a pile installation factor to reduce or increase, either the mobilized front pressure or the mobilized side shear distributions.

The mobilization of shear resistance upon the base of a rigid, rotating pile, may be significant. The full shear stress is assumed to be mobilized linearly at a translation of 0.1 in. (2.5 mm), and hence

$$B = C_u \frac{A_p}{H} \quad \ldots\ldots\ldots\ldots\ldots\ldots\ldots\ldots\ldots\ldots \quad (123)$$

where B = base mobilized resistance

H = finite difference increment length

A_p = base area

and thereafter remains constant.

The units of B are therefore force/unit length, and consistent with those of Q and F. The base P-y curve only is then given by

$$P = Q + F + B \quad \ldots\ldots\ldots\ldots\ldots\ldots\ldots\ldots\ldots\ldots \quad (124)$$

This sequence of calculations is performed by a computer program, title name PYGEN written in FORTRAN IV, detailed in Appendix II.

Accounting for the Critical Depth

It is shown that both the pile and pressuremeter are subject to a reduction in the mobilized soil resistance at shallow depth. The effect of both these independent critical depths must be assessed separately. The procedure is detailed in the following steps for a single test depth.

1) For the pressuremeter, the decay in mobilized pressure, p*, for the full range of expansion within its critical depth is given on Fig. 147. This is based on superimposing, Fig. 54 (p. 145) for sand, and Fig. 55 (p.146) for clay and the ultimate critical depth is taken from the recommendations of Baguelin et al. (11) and is shown on Fig.147 . Therefore, to correct a P-y curve derived from a pressuremeter test measured within the depth of reduced resistance, the following is obtained:

$$p = \frac{1}{\beta}(Q + F) \quad \ldots\ldots\ldots\ldots\ldots\ldots \quad (125)$$

where β = reduction in mobilized pressuremeter pressure at all strains.

2) To account for the reduced soil reaction mobilized within the

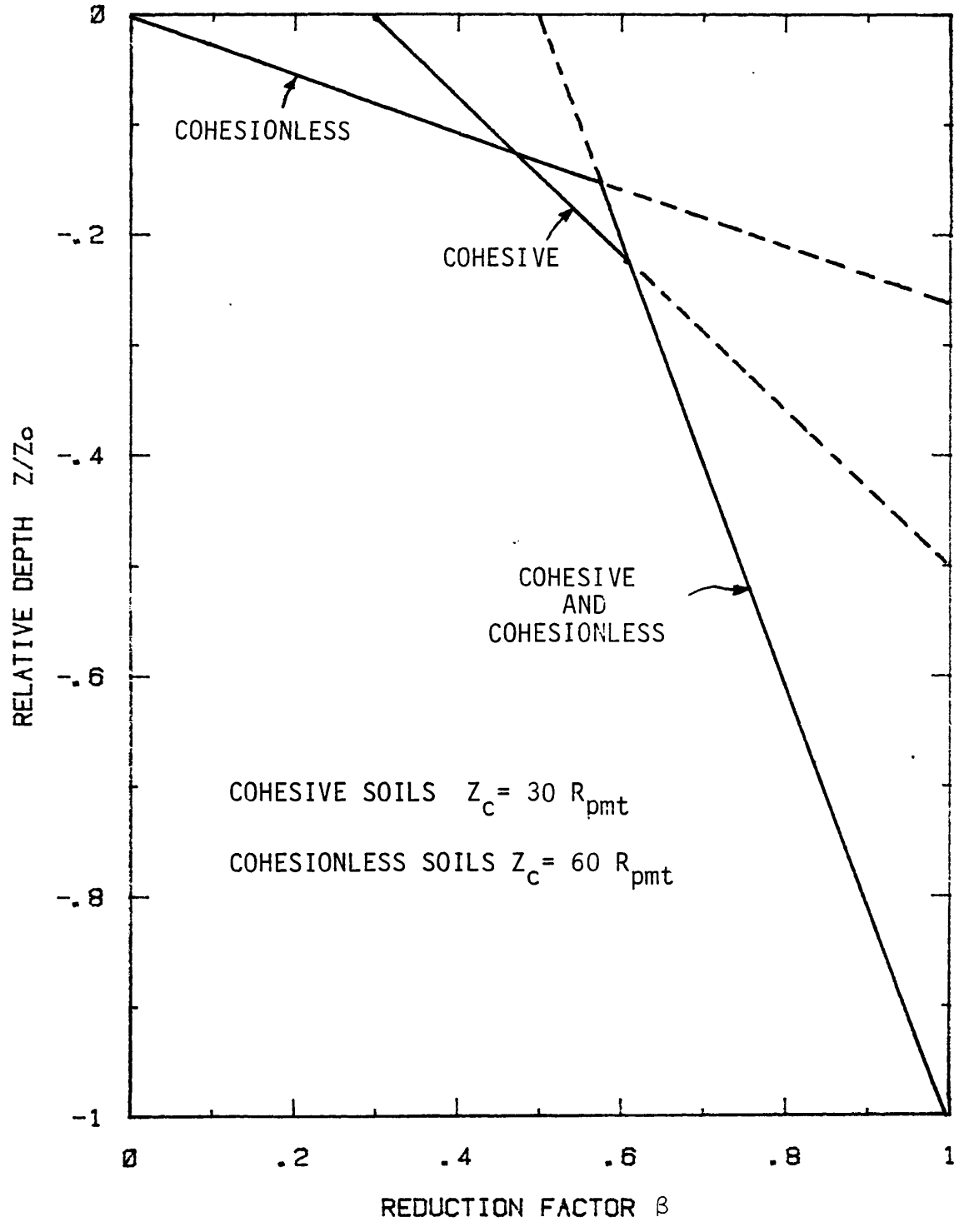

FIG. 147 - Proposed Reduction Factor for the Pressuremeter within the Critical Depth

piles critical depth, it is proposed to reduce the front reaction curve, Q, by a reduction factor, α. Therefore Eq. 90 becomes

$$Q = p^* \times SQ \times D \times \alpha \quad \ldots\ldots\ldots\ldots\ldots\ldots (126)$$

The reduction factor, α, is given on Fig. 148 by omitting the observed values from Fig. 47 (p.127). The average critical depth for the pile, $Z_{c(av)}$ is a function of the relative pile to soil stiffness and is given by Eq. 109.

$$\frac{Z_{c(av)}}{D} = \frac{\pi}{4}(RR-5) \quad \ldots\ldots\ldots\ldots\ldots\ldots (109)$$

or $Z_{c(av)}/D = 1$, whichever is greater.

The relative rigidity factor, RR, is given by Eq. 107

$$RR = \frac{1}{D}\sqrt[4]{\frac{EI}{p_l^*}} \quad \ldots\ldots\ldots\ldots\ldots\ldots (110)$$

where EI = pile flexural stiffness

p_l^* = net pressuremeter limit pressure

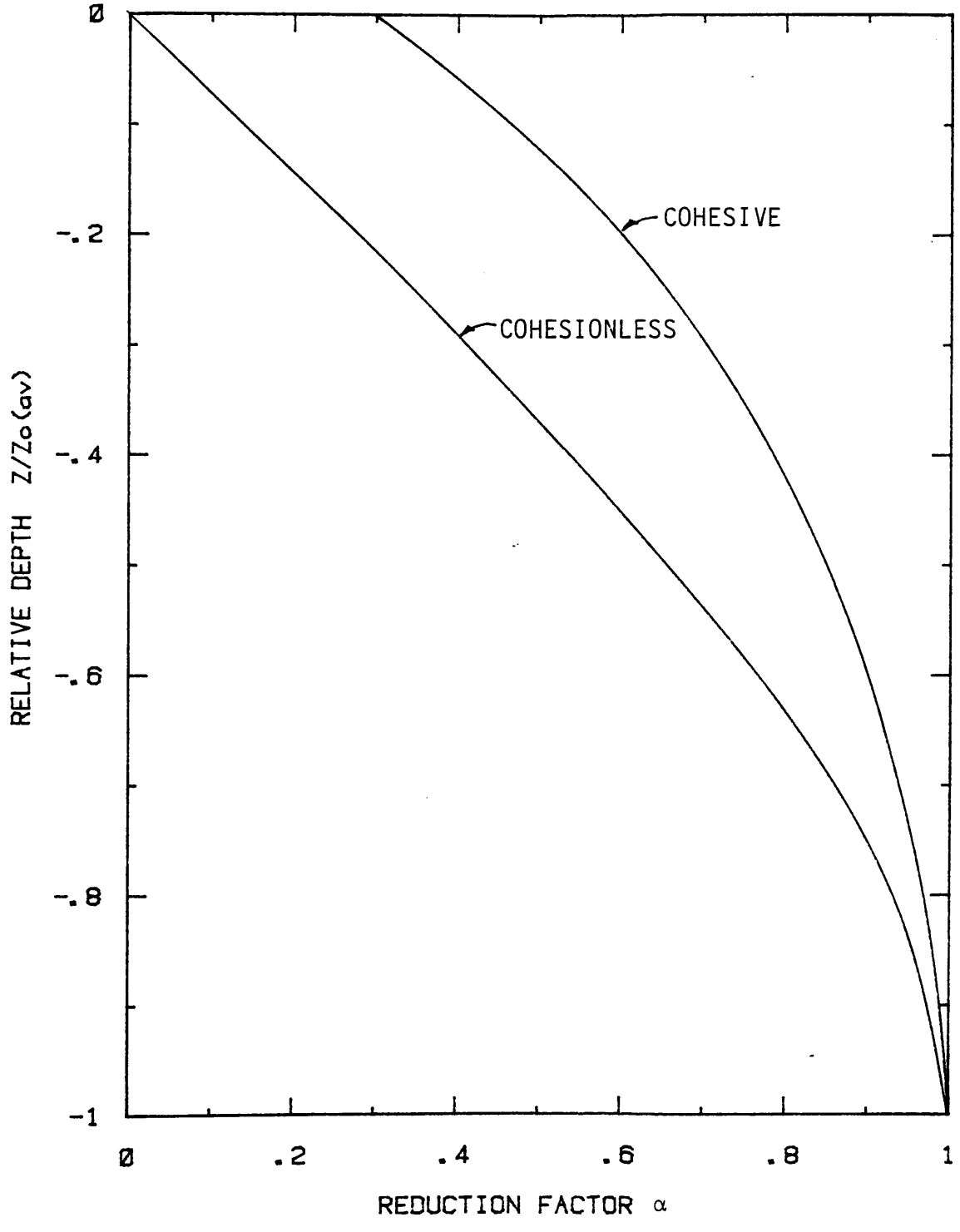

FIG. 148 - Proposed Reduction Factor for the Pile within the Critical Depth

Predicting the Pile Behavior

After compiling the necessary P-y curves to represent the non-linear soil behavior it remains to simulate, as closely as possible, the soil structure pile problem to be solved.

Typically, the finite difference scheme requires P-y input at certain discrete depths. For the soil spring response at all nodes between the input depths, linear interpolation is used. Therefore, to represent a layered soil with different P-y characteristics, it is more appropriate to input the P-y curve measured within that layer at both the top and bottom of each layer.

The ultimate yield moment of the pile section should be compared to the maximum predicted bending moment from each increasing load step. In this way the piles structural history can be closely followed. For a reinforced concrete pile, at yield, it may be appropriate to reduce the flexural stiffness locally in the region of the anticipated maximum moment. If complete structural breakdown occurs, only a small plastic flexural stiffness is expected, then the pile embedment length may require modification. In this way the behavior of a flexible pile up to yield can be predicted, together with the after yield semi-rigid behavior approximation.

Plane strain conditions may be imposed at the surface by the presence of a pile cap, or surcharge loading, then no pile critical depth should be considered.

CONCLUSIONS AND RECOMMENDATIONS

Conclusions

It is clear, from a complete review of the available methods to predict the full load deflection behavior of a pile, that the finite difference scheme, employing soil spring P-y curves as input, remains the most versatile, powerful and economic solution technique. Formidable problems remain to be solved before the application of the FEM methods can be fully exploited to solve laterally loaded pile problems.

An investigation has been carried out to explore the theoretical and empirical bases for the existing criteria used to develop lateral load P-y curves. From this investigation an appreciation of the severe limitations of the existing criteria, and their application in the finite difference numerical scheme, is given.

A theoretical relationship exists between the pressuremeter curve and the normal soil pressure response ahead of the displaced pile. In the small strain, pseudo-elastic, range of behavior the prebored pressuremeter response is in excellent agreement with the measured soil pressures. In the ultimate range of behavior the prebored response is consevative.

Two separate components exist which contribute to the P-y curve, a front pressure response, Q-y, and side friction response, F-y. For more accurate representation of the base resistance mobilized on rigid, rotating piles, a third mobilized base friction response, B-y, is

generated. The Q-y curve and F-y curve can both be derived directly from a prebored pressuremeter test, which includes a reload cycle performed at the end of the pseudo elastic phase. The mobilization of both curves is shown to be a function of radial movement, y/R, and not absolute deflection. Expressed in this form, the scale effects between the response of a small pressuremeter and a large pile are accommodated directly in the derivation. Separation of the P-y curve into these component curves enables pile installation effects and the influence of loading history to be quantified independently.

The critical depth of reduced resistance, in a zone close to the free ground surface, influences both the pile and pressuremeter results. By analysis of ten strain gage instrumented piles, the depth of reduced soil reaction is shown to be a function of displaced soil volume. The higher the pile displacement, y, the lower becomes the critical depth, Z_C. The magnitude of this depth is controlled by the relative pile/soil stiffness expressed by a relative rigidity factor, RR, given in Eq. 107. To preserve the independence of the soil reaction, P, from being a separate function of the deflection, y, the critical depth is considered stationery at an average depth.

The same critical depth phenomenon is present for the expanding pressuremeter as shown from a limited FEM study and reported test results. In small strain expansion, the cavity pressure/circumferential strain modulus is shown to be reduced within a depth of 12 cavity radii in sand and 8 cavity radii in clay.

From the laboratory study, using a driven model pile, the derived P-y curves from driven pressuremeter tests are in good agreement, or

slightly conservative, for loose sand and clay. In the clay, the effects of driving the probe, in a fully remolded material, is to increase the response over the full range of expansion. Limited laboratory evidence suggests that the derived P-y curve from a reload cycle of a prebored pressuremeter test, in a dry hole, is a conservative estimate of a driven pressuremeter P-y curve. For driven piles in dense sand, a derived P-y curve from the initial cycle of a driven pressuremeter test is unconservative.

A comprehensive field investigation, including field pressuremeter tests to predict the behavior of fourteen instrumented lateral load tests, was completed. The investigation included both rigid and flexible piles in a wide range of soil conditions at eleven sites. Very good agreement is generally found between load test 'measured' P-y curves and pressuremeter derived P-y curves. Great care should be exercised in the performance of field pressuremeter tests; however, only the highest quality data should be accepted.

The reload cycle of a prebored pressuremeter test is a closer approximation to the 'undisturbed' soil response. Generation of the mobilized shear stress from the reload cycle is preferred because of the closer approximation to measured shear strengths. The field evidence suggests the initial cycle measures the front pressure response, for in-situ piles , and piles driven open ended which do not plug.

Recommendations

Based on the results of this study the following areas warrant further investigation.

1) The application of the method should be extended from static to cyclic P-y curves. The pressuremeter is well suited to reproduce the expected frequency and magnitude of lateral load cycles applied to the pile. The effects of decay to both side friction and front pressure reactions should be quantified independently.

2) To satisfactorily reproduce cyclic behavior, at equal inflation rates, field strain controlled pressuremeters require conversion from hand cranks to a electric driven pump. In low limit pressure material a permanent pressure transducer should be installed. Continuous monitoring of pressure is also an advantage in brittle, weakly cemented materials.

3) The investigation in the laboratory with an instrumented model pile should be continued, with the use of a drilling fluid. This allows the full comparison of driven and augered piles to be made with driven or augered pressuremeter P-y predictions. This should be directed towawrds improving the understanding of the relationship between reload cycles from a prebored test and the initial cycle from a driven test.

4) The separate effects upon side friction and front pressure reactions from pile installation techniques should be studied further. The soil P-y response from cast in-situ piles may well be reduced by the local softening effects of the borehole wall from concrete placing.

5) The response of a prebored pressuremeter is sensitive to the disturbance of the borehole wall by the drilling technique. These techniques should be reviewed and improved where possible. Current drilling techniques are aimed at keeping the soil undisturbed in front of the bit, while the condition of the borehole wall is irrelevant. The requirements for a pressuremeter test are opposite. Since minimum disturbance to the borehole wall is essential, the condition of the cuttings is irrelevant. Drill bit design may require modification to achieve this aim.

6) Field measurement of the mobilization of lateral pile wall friction should be considered. This may be achieved by using instrumented piles complete with bending strain gages, and pressure cells located vertically and circumferentially. The difference between the 'measured' P-y curve and the mobilized soil front pressure reaction is the shear reaction curve.

It is suggested that the cumulative effects upon the P-y curve of such factors as cyclic loading, pile installation and radial consolidation be taken into account by simulating these effects with the corresponding insertion and loading sequence of the pressuremeter.